Utilization of Date Palm Tree Fibres as Biomass Resources for Developing Sustainable Composites for Industrial Applications

By:

Said Awad

Supervisors:

Prof. Evina Katsou

Prof. Mizi Fan

Department of Civil and Environmental Engineering

College of Engineering, Design and Physical Sciences

Brunel University London

A thesis submitted for the degree of Doctor of Philosophy

2022

Dedication:

To my Dad & Mom,

who always supported and encouraged me with every step I took in life,

especially this one!

Declaration

The work done in this thesis is based on research carried out at Brunel University London, United Kingdom. I hereby declare that the presented research is my own work except where otherwise stated, referenced to the contrary in the text, and has not been submitted elsewhere for any other degree or qualification.

Abstract

Petroleum based fibres are dominating our everyday usage of fibres, textiles, and composite development reaching an annual consumption of more than 50 million tons in 2020. Over the years, there has been a desperate need for sustainable alternatives; but unfortunately, the global production of natural fibres (NF) has reached a plateau due to the reliance on very few natural sources and lack of biodiversity. With the growing concern on climate change due to the pollution emitted from petroleum-based manufacturing products and their end life disposal, sustainable manufacturing of sustainable materials represents a primary concern for the construction industry. New technologies and materials are extensively investigated and proposed to meet sustainability guidelines imposed by governments and specifically the United Nations (UN). NF represent one of the most investigated renewable and sustainable materials. The date palm tree (DPT), Phoenix Dactylifera L., produces globally an approximate of 4.8 million tons (dry weight) where 3.6 million tons are produced in the MENA region only as by-products of pruning, regarded as agricultural waste, which are either landfilled or incinerated. This research investigates and develops novel methodologies to overcome the drawbacks of utilizing DPT by-products where DPT fibre (DPF) can be extracted from and utilized as a reinforcement in developing sustainable composites for industrial applications. An intensive literature review database was developed to highlight previous research work and investigations carried out to date on the utilization of DPF and their effect in developing sustainable composites and the drawbacks limiting their feasibility for upscaling and industrialization. This identified the problem statement in current research that must be addressed to distinguish the potential of DPF utilization and industrialization.

Various surface modification treatments as well as their conditions (soaking time and duration) effect on the characteristics of DPF (surface morphology, chemical composition, chemical structure, and crystallinity) was investigated and evaluated to develop a more hydrophobic fibre that enhances the interfacial bonding when used as a reinforcement with various matrix systems (i.e., polymers and cementitious). DPF treated with sodium hydroxide (NaOH) solution, 6%, for 3 hours showed optimal results where an increase in tensile strength of the fibre by 147%. Scanning electron microscopy (SEM) images demonstrated the effectiveness of the surface treatment showing a more porous surface where the impurities and waxes were successfully removed. Furthermore, investigations, evaluation and prediction on the effect of DPF particle size distribution, density, diameter size (unsieved, ≥1,000 µm, 500 – 1,000 µm, 250 – 500 µm, 125 – 250 µm, and ≤125 µm) and loading content (10, 20, 30, 40 wt.% of matrix) on both the mechanical, physical, fungal resistance and disintegration properties of recycled thermoplastic, recycled polyvinyl chloride (RPVC), and biodegradable thermoplastic,

polylactic acid (PLA), were evaluated. The hydrophilic nature of DPF contributed to an increase in thickness swelling (TS), moisture content (MC) and water absorption (WA) for both RPVC and PLA reinforced composites. TS, WA and MC increased by 1.57%, 1.76%, and 10.80%, respectively at 40 wt.% DPF loading content when reinforced with RPVC. Moreover, the flexural strength, tensile strength and impact strength decreased as the loading content increased showing maximum reduction at 40 wt.% loading, varying depending on DPF geometry. Furthermore, micromechanics modelling scenarios to predict the fibre orientation was investigated. To determine the effectiveness of DPF orientations in the PLA and RPVC, the rule of mixtures (ROM), modified ROM, inverse rule of mixture (IROM), modified IROM and Halpin-Tsai were applied with three possible fibre orientations in the composites. The modified ROM and modified IROM closely matches the experimental results with the DPF oriented between 0° to 45° in the direction of compression force of the DPF/PLA and DPF/RPVC composites. Also, Composites where exposed to the brown-rot fungus Irpex lacteus and white rot fungus Tyromyces palustris to evaluate its resistance to biodegradation. To evaluate their feasibility to be utilized in the construction sector as a cladding and decking composite which can act as a substitute to wood in developing wood plastic composites (WPC). Composites developed using PLA had higher weight loss (%) when compared to the same samples but reinforced with RPVC. Composites with higher DPF content showed high rates of decay when used with different polymer matrix. Also, DPF length had a significant effect on the disintegration of the composites. DPF/PLA composites did not demonstrate significant weight loss under fungal decay in 8 weeks where the composites with 40 wt.% DPF showed the highest WL% reaching 5.61% and 5.46% when exposed to Tyromyces palustris and Irpex lacteus respectively. Furthermore, a novel investigation on the biodegradation of the samples showed that DPF reinforced PLA can be implemented and developed within a circular economy scheme in which the composite was fully decomposed by earth worm within 6 weeks, developing vermicompost as manure that may be utilized as a nutrient for plants.

Furthermore, an investigation of the processing parameters effect (processing time, temperature, and pressure) on the physical and mechanical properties of DPF reinforced polyester (PES) composite is evaluated. For that, two different temperatures (90 and 110 ^{o}C) and three different pressures (1.0, 1.65, and 2.18) MPa which was achieved by varying the load applied (10, 15, and 20) ton and keeping the sample size constant are examined for three different processing durations (3, 6, and 9 min). Results showed that every processing parameter had different effects on the mechanical and physical properties of the composites developed. Moreover, investigations on the effect of varying DPF loading content (1, 2, and 3 wt.% of matrix), and length (10, 20, 30, and 40 mm) of untreated and alkali treated DPF on

the mechanical properties of DPF reinforced Ordinary Portland cement (OPC) and DPF reinforced OPC/ground-granulated blast furnace slag (GGBS) were evaluated. Two different curing conditions, water and air, effect on the mechanical strength and physical properties of the composites developed were explored. Results showed that the inclusion of 20 mm treated DPF at a loading content of 1 wt.% with OPC/GGBS as a matrix showed the greatest enhancement in strength by 57.12% and 30.97% of flexural and compressive strength respectively at 28 days of ageing in a water bath. Alkali treatment of DPF demonstrated higher mechanical properties enhancing the optimal mix designs' mechanical strength by 10% and at 28 days of water curing when compared to the untreated. Moreover, OPC as a pure matrix system had lower mechanical properties where the optimal mix design had an increase in 37.48% and 19.36% on flexural and compressive strength respectively at 28 days of curing in a water bath when compared to OPC/GGBS reinforced composites.

Overall, this thesis paves the way for developing a comprehensive foundation for utilizing DPT by-products by optimizing the parameters of surface modification, fibre geometry, fibre loading, and processing parameters for developing sustainable composites that can be industrialised for various non-structural industrial applications (i.e., construction and automotive industries).

Acknowledgments

I would like to express my deepest appreciation and gratefulness to my supervisors Prof. Mizi Fan and Prof. Evina Katsou for their supervision and invaluable motivation, help and guidance with my research. This thesis would not have come to light without their supervision.

Both supervisors did not act only as supervisors, but also as an inspiring and motivating colleague and friend that pushed me to my limits in developing my critical thinking through my research. It was an immense pleasure and honour to work with both Prof. Mizi Fan and Dr. Evina Katsou. Also, I would like to pay a special thanks to Dr. Yonghui Zhou for putting his expertise and his motivational support at the service of this research during the past three years. Moreover, I would like to express my gratefulness to Dr. Mohamad Midani and Dr. Tamer Hamouda that helped through the COVID-19 Pandemic by collaborating through using their facilities.

I also extend my thanks to the academic staff of the Civil and Environmental Engineering Department for their support and critical discussions throughout the research. A special thanks goes to the technicians of the Civil Engineering Research Centre, Mr Neil Macfadyen, Mr Michael Angelo, and Mr Charles Morrison who are highly acknowledged for their support during the experimental work. Also, I would like to thank Mr. Minal Shah for his support throughout my research programme.

I would also like to thank my friends and colleagues who have supported me throughout this long journey, namely: Akram Chwiki, Ghanimah Al-Mutairi, Mashael Al-Madi, Dr. Mazen Al-Kheetan, Nafissa Rababah, Nour Badenjki, Dr. Wasef Al Ragheb.

Finally, and uppermost “The Family”, I am indebted to my beloved parents, Mr Mosab Awad and Mrs Mouna Ibrahim, my brothers and sisters, Mohamad, Ahmad, Reema and Dana for their endless love and support. Also, I am in debt to the family that considered me as their son providing me with the support and love, The Marouf & Kayali Family, especially my work partner and brother Mahmoud Marouf that showed the greatest support at the write up phase. This work would not be possible without all of them.

Publications

Published journal articles:

1. Elseify, L.A., Midani, M., El-Badawy, A., **Awad, S.** and Jawaid, M., 2022. Comparative study of long date palm (Phoenix dactylifera L.) midrib and spadix fibers with other commercial leaf fibers. *Cellulose*, pp.1-16 DOI: 10.1007/s10570-022-04972-1
2. **Awad, S.,** Hamouda, T., Midani, M., Zhou, Y., Katsou, E., Fan, M. (2022). Polylactic Acid (PLA) Reinforced with Date Palm Sheath Fiber Bio-Composites: Evaluation of Fiber Density, Geometry, and Content on the Physical and Mechanical Properties, Journal of Natural Fibers, DOI: 10.1080/15440478.2022.2143979
3. **Awad, S.,** Hamouda, T., Midani, M., Zhou, Y., Katsou, E., Fan, M. Critical evaluation of Date Palm Sheath Fibre characteristics as a reinforcement for developing sustainable cementitious composites from waste materials. Biomass Conv. Bioref. (2022). https://doi.org/10.1007/s13399-022-02759-9
4. Al-Kheetan, M.J., Ghaffar, S.H., **Awad, S.**, Chougan, M., Byzyka, J. and Rahman, M.M., 2021. Microstructural, mechanical and physical assessment of Portland Cement Concrete pavement modified by sodium acetate under various curing conditions. Infrastructures, 6(8), p.113. https://doi.org/10.3390/infrastructures6080113
5. **Awad, S.,** Hamouda, T., Midani, M., Zhou, Y., Katsou, E., Fan, M. (2021). Date palm fibre geometry and its effect on the physical and mechanical properties of recycled polyvinyl chloride composite. Industrial Crops and Products, 174, p.114172. https://doi.org/10.1016/j.indcrop.2021.114172
6. **Awad, S.,** Zhou, Y., Katsou, E., Fan, M. (2020) A Critical Review on Date Palm Tree (*Phoenix dactylifera* L.) Fibres and Their Uses in Bio-composites. Waste Biomass Valorization. https://doi.org/10.1007/s12649-020-01105-2
7. Zhou, Y., Stanchev, P., Katsou, E., **Awad, S.** and Fan, M. (2019). A circular economy use of recovered sludge cellulose in wood plastic composite production: Recycling and eco-efficiency assessment. Waste Management, 99, pp.42-48. https://doi.org/10.1016/j.wasman.2019.08.037

Pending submission journal articles:

1. **Awad, S.**, Zhou, Y., Katsou, E. and Fan, M. Review on PHA reinforced natural plant fibre bio-composites: Physical and chemical properties, Processing parameters, Surface treatments and Functionalization (Under progress)
2. **Awad, S.**, Zhou, Y., Katsou, E. and Fan, M. The effect of different surface treatments on the strength and characteristics of date palm fibres. (Under progress)
3. **Awad, S.,** Hamouda, T., Mohareb, A., Midani, M., Katsou, E., Fan, M. Biodegradation, and disintegration evaluation of date palm fibre reinforced thermoplastic composite (under review – Journal of Polymer Degradation and Stability)

Published book chapter:

1. **Awad S.,** Zhou Y., Katsou E., Fan M. (2020) Polymer Matrix Systems Used for Date Palm Composite Reinforcement. In: Midani M., Saba N., Alothman O.Y. (eds) Date Palm Fiber Composites. Composites Science and Technology. Springer, Singapore. https://doi.org/10.1007/978-981-15-9339-0_4

Conferences:

1. **Awad, S.**, Zhou, Y., Katsou, E. and Fan, M. Processing parameters influence on DPF composite development. 2nd world conference on By-products of Palms & their Applications (ByPalma), September 2021.
2. Raad, T**.**, **Awad, S.,** Singh, H. A novel application for utilizing date palm biomass waste for VIP development. 15th International Vacuum Insulation Symposium (IVIS), April 2022.
3. **Awad, S.,** Hamouda, T., Midani, M., Zhou, Y., Katsou, E., Fan, M. Evaluation of processing parameters on the physical and mechanical properties of compression moulded unsaturated polyester resin reinforced with date palm sheath fibre. Fibre Polymer Composite in Construction (FPCC), September 2022.

Contents

List of Tables

List of Figures

List of Abbreviations

ABS	**Acrylonitrile Butadiene Styrene**
AESO	Acrylated Epoxidized Soybean Oil
AI	Artificial Intelligence
AOAD	Arab Organization for Agricultural Development
ASTM	The American Society for Testing and Materials
BS	British Standard
BS EN	British Standard European Norm
CNSL	Cashew Nut Shell liquid
CO_2	Carbon dioxide
COPU	Castor oil- based polyurethane
CR	Polychloroprene Rubber
CrI	Crystallinity Index
α_T	Coefficient of Thermal Expansion
DCP	Dicumyl Peroxide
DGEBA	Diglycidyl Ether of Bisphenol A
DPF	Date Palm Fibre
DPFPC	Date Palm Fibre Polymeric Composite
DPFCC	Date Palm Fibre Cementitious Composite
DPFRC	Date Palm Fibre Reinforced Composite
DPMF	Date Palm Mesh Fibre
DPT	Date Palm Tree
DPW	Date Palm Wood
°C	Degree Celsius
p	Density
p_c	Density of composite
p_e	Experimental density
p_f	Density of fibre
p_m	Density of matrix
p_t	Theoretical density
EDX	Energy Dispersive X-ray Analyser
ELO	Epoxidized Linseed Oil
ESO	Epoxidized Soybean Oil
FRP	Fibre Reinforced Polymer
FTIR	Fourier-transform Infrared Spectroscopy

GBP	Great British Pound
GPa	Gigapascal
T_g	Glass Transition Temperature
g	Grams
GGBS	Ground granulated blast furnace slag
GHG	Green House Gases
HCP	Hardened Cement Paste
HDPE	High Density Polyethylene
HDT	Heat Deflection Temperature
IPDA	Isophorone diamine
IRL	Irpex lacteus
IROM	Inverse Rule of Mixture
ITZ	Inter-Facial Transition Zone
K	Orientation factor
kg	Kilogram
LDPE	Low Density Polyethylene
LSF	Lime Saturation Factor
LLDPE	Linear Low-Density Polyethylene
MA	Moisture Absorption
MAPE	Maleic Anhydride-g-Polyethylene
MAPP	Maleic Anhydride-g-Polypropylene
MC	Moisture Content
MDPE	Medium Density Polyethylene
MDPSF	Male Date Palm Surface Fibres
MENA	Middle East and North Africa
MF	Melamine–Formaldehyde
MFI	Melt Flow Index
MMSO	Methacrylic Anhydride-modified Soybean Oil
mm	Millimetre
MPa	Megapascal
Tm	Melting Temperature
T:M:A	Toluene:Methanol:Acetone
TYP	Tyromyces palustris
MSO	Methacrylated Soybean Oil
µm	Micrometre
NF	Natural Fibre

NFC	Natural Fibre Composite
N.S	Not specified
OPC	Ordinary Portland cement
PA	Polyamide
PA – 4,6	Polyamide – 4,6
PA – 6,6	Polyamide – 6,6
PBD	Polybutadiene
PBP	Petroleum-based polymer
PBS	Polybutylene Succinate
PBT	Polybutylene Terephthalate
PC	Polycarbonate
PCL	Polycaprolactone
PE	Polyethylene
PET	Polyethylene Terephthalate
PGA	Polyglycolide
PHA	Polyhydroxyalkanoates
PLA	Polylactide or Poly (lactic acid)
PMMA	Polymethyl Methacrylate
POM	Polyoxy-methylene
PP	Polypropylene
PPS	Polyphenylene Sulphide
PS	Polystyrene
PTFE	Polytetrafluoroethylene
PVC	Polyvinyl Chloride
PVDC	Polyvinylidene Chloride
RLDPE	Recycled Low-Density Polyethylene
RLLDPE	Recycled Linear Low-Density Polyethylene
ROM	Rule of Mixture
RPVC	Recycled Polyvinyl Chloride
RSO	Rubber Seed Oil
RT	Room temperature
SAN	Styrene Acrylonitrile
SBR	Styrene-butadiene Rubber
SCB	Short Chain Branches
S.D	Standard Deviation
SDG	Sustainable Development Goals

SEBS	Styrene/Ethylene-Butylene Copolymer
SEM	Scanning Electron Microscope
SEPS	Styrene/Ethylene-Propylene Copolymer
SIS	Styrene/Isoprene Copolymer
SL	Starch Loading
SMA	Styrene Maleic Anhydride
TPE-A	Thermoplastic amide copolymer
TPE-E	Thermoplastic ester-ether copolymers
TPE-S	Styrene-diene block copolymers
TPS	Thermoplastic Starch
TS	Thickness Swelling
UAE	United Arab Emirates
UF	Urea-Formaldehyde
UN	United Nations
UP	Unsaturated Polyester
UPR	Unsaturated Polyester Resin
VE	Vinyl Ester
V_f	Volume fraction of fibre
V_m	Volume fraction of matrix
V_v	Volume fraction percentage of voids in composite
w/c	Water to cement ratio
Wt.%	Weight percentage
W/v. %	Weight to volume percentage
XRD	X-ray Diffractometer

Chapter 1: Introduction

1.1. Background

Globally, the rapid growth of population which is predicted by the United Nations (UN) to reach 8.5 billion by the year 2030 has a direct relation to the prodigious growth in various industries (i.e., automotive and building sectors) where the building and construction industry is expected to have significant growth trends, an increase of 85% by the year 2030. This is expected to upsurge the value of the industry to exceed 10 trillion GBP [1]. Thus, according to a recent report published by the Transparency Market Research, it is estimated that the global amount of construction waste generated annually will reach 2.2 billion tons by 2025 [2]. It can be correlated that the demand for construction composites, such as concrete and fibre reinforced polymers (FRP) will significantly increase. This significance increase has urged the UN to set 17 sustainable development goals (SDG) within their 2030 agenda [3]. Few SDG were taken into consideration while setting the path of this research study such as SDG08 (decent work and economic growth), SDG09 (industry innovation and infrastructure), SDG11 (sustainable cities and communities), SDG12 (responsible consumption and production) and SDG13 (climate action). Furthermore, considering the automotive industry perspective, the European Commission implemented a “European Guideline 2000/53/EG” that aims on improving automotive recyclability to 85% in 2005 for a vehicle by weight which was increased to 95% by 2015 [4]. These statistics and legislations are significant driving factors towards the adoption of developing sustainable composites.

Fibre reinforced composites (FRC) derived from crude oil (i.e., glass fibre and carbon fibre) have been commercially utilised intensively in several industrial applications such as aerospace, automotive and construction for the past decades owing to their enhanced properties. FRC is found to bring about significant advancements in mechanical characteristics with added advantages of high strength to weight ratio, light weight, low maintenance, low cost, excellent weathering stabilities and improved dimensional stabilities and tailor-made material behaviours [5]. Utilization of fibres with polymer matrices is found to produce enhanced strength composites with good creep and fatigue resistance, low shrinkage, and superior chemical resistance properties. Consequently, fibre reinforced cementitious matrix is found to reduce the construction costs when utilising most synthetic fibres through the replacement of traditional mesh and steel reinforcement bars [6]. Consequently, there are corresponding reductions in the labour maintenance costs. Also, due to a reduced rate of construction activities attached to synthetic fibre reinforcement as opposed to steel, the construction time can be manipulated to be lesser in comparison. Thirdly,

there are significant ameliorations with regards to energy consumption when comparing fibre reinforcement to that of traditional. This is because the volume of necessitated raw material for producing fibres is reduced as opposed to the quantity required for the manufacturing of traditional reinforcement.

Synthetic fibres utilized are various types of steel, glass, boron fibres, and aluminium oxide, etc. The production of synthetic fibres has increased drastically in the last decades where the latest published statistics showed that 76 million metric tons were produced in 2019 which is 62% increase than the amount produced in 2009 and 152% increase than the amount produced in 1999 [7]. However, the global concern on disposal issues after the end life of synthetic composites, the increase in price of synthetic polymers due to the price hike of crude oil, increased pollution and greenhouse gaseous (GHG) emitted while manufacturing (i.e. cement, polymers, and synthetic fibres), and new environmental laws and regulations has developed significant interest towards researching and utilizing more sustainable materials by replacing synthetic fibres with renewable fibres, replacing synthetic polymers with bio-based polymers and substituting ordinary Portland cement (OPC) with pozzolanic waste materials (i.e. fly ash (FA), ground granulated blast-furnace slag (GGBS), waste brick clay powder (WBCP) and waste ceramic (WC)).

Moreover, the agricultural sectors generate enormous amounts of by-products and waste (agro waste) annually. Globally, the lignocellulosic residues alone exceed 600 million tons annually and are poorly managed. Recycling agro waste by incorporating them into composites to manufacture renewable and biodegradable materials have drawn considerable attention as a biodegradable reinforcing material due to several factors such as low cost, low density, biodegradability, availability, absence of associated health hazards, and they are relatively non-abrasive [8,9] and can help in waste reduction and reduce the cost of the composites developed [10]. It is conceivable that a certain type of plant fibres are more attractive for each region. Recently, several governmental authorities in the Middle East and North Africa (MENA) region have been funding research projects for utilizing their landfill agricultural deposits. The increase of landfill deposits due to agricultural biomass waste, specifically date palm tree (DPT), which is considered the most abundant tree and agricultural biomass waste in the region has highlighted the importance of finding sustainable programmes to utilize this material. It is estimated that the global DPT fibre (DPF) accounts to 4.5 million tons (dry weight) and approximately 3.6 million tons is generated in the MENA region. However, the utilization of DPF raises difficulties, as is the case with all plant fibres. The hydrophilic polar nature of the lignocellulosic fibres makes it difficult to achieve proper adhesion to hydrophobic polymers. This is because of the abundance of hydroxyl groups that provide the fibre with a high affinity to water, hindering proper wetting of the fibres by non-

polar polymers. Several researchers have been conducted various investigations to improve the compatibility of NF with polymers. This was successfully achieved by treating the NF either physically or chemically [11–15] or by using coupling agents as reported by several researchers which increases the adhesion between NF and polymer matrix [16–19]. However, a critical aspect of understanding the geometry, length, and diameter, of NF and in specific DPF has not yet been investigated in depth and there is a lack in consistency on their effect as a reinforcement in polymeric composites.

The latest research contributed to the fabrication and development of sustainable composites with DPF reinforced with various polymeric and inorganic composites showed that there are still gaps in identifying its suitability for industrialization. Many researchers investigated the effect varying the fibre content, surface modification on developing DPF reinforced composites (DPFRC). Several researchers have developed DPF reinforced polymeric composites. Most of the outcomes were positive but not optimized, thus they will be discussed thoroughly in chapter 2. Moreover, most of the results reported demonstrated that utilization of DPF as a reinforcement for cementitious composites reduces the flexural and mechanical properties of the composites developed. Kriker et al. (2005) reported that the addition of DPF, 2% vol.%, as reinforcement in developing cementitious mortars reduced the flexural and compressive strengths by 2.67% and 6.45% respectively [20]. Also, Raut and Gomez (2016) showed a reduction of 17.39% in compressive strength with an increase on 3.10% in flexural strength when utilizing DPF with OPC at a fibre volume content of 1% [21]. Moreover, Tiou et al. (2017) showed a decrease in compressive strength when utilizing DPF with OPC at a fibre volume loading content 0.1% [22]. Thus, it is necessary to understand the physical, chemical, thermal and mechanical properties of DPF for their effective application. An optimization of DPF geometry, particle size, density, loading content, surface modification and the effect of matrix characteristics along with the processing parameters are crucial to develop DPFRC with enhanced properties that can be commercialized for various industrial application. Finally, by achieving successful utilization methodologies and techniques for DPF reinforcement in composite development which is in line with the new governmental legislation towards circular economy and sustainable production which substitutes synthetic fibre reinforcement will be considered as a contribution to research for developing sustainable composites from agricultural biomass waste.

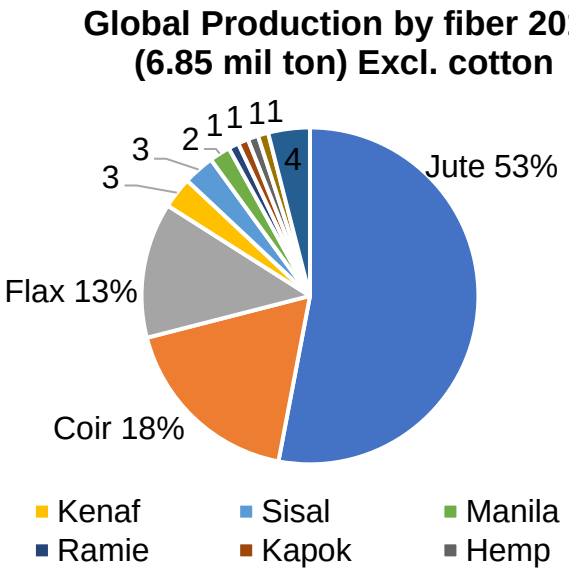

Figure 1 Global production by fibre type

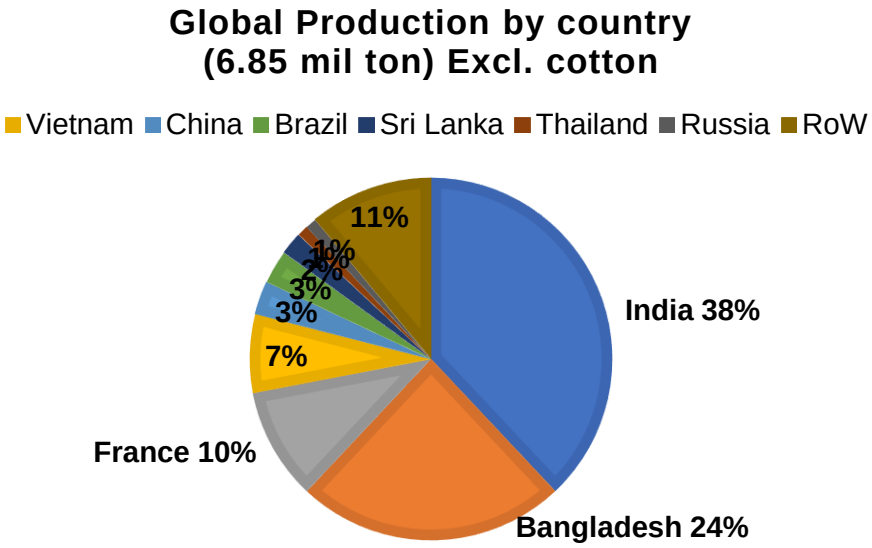

Figure 2 Global production of fibre by country

1.2. Problem statement

There is a global environmental concern due to the extensive usage of synthetic composites which are derived from petroleum-based polymers (PBP) and synthetic fibre sources. These composites are not 100% degradable, with a direct impact on the surrounding environment and human health. It has been reported that 192 countries generate more than 275 million metric tons of plastic wastage (either as in raw polymer or polymer fibres) annually, which are

either landfilled or incinerated, and 5% of the total plastic wastage are ended up in the oceans, threating the marine life and causing serious environmental issues [23]. Thus, due to the high cost of bio-based polymer which makes their utilization difficult, substituting PBP and synthetic fibres with renewable and sustainable materials decreases their negative environmental impact. Agro-waste is produced annually in enormous amounts by the agricultural sectors. Lignocellulosic residues alone amount to more than 600 million tonnes annually and are poorly managed globally. Due to several factors, including low cost, low density, biodegradability, availability, lack of associated health hazards, and relative non-abrasiveness [9,12], recycling NF by incorporating them into composites to manufacture renewable and biodegradable materials has attracted significant attention as a biodegradable reinforcing material [10]. They can also assist in waste reduction, reduction in synthetic polymer consumption and lower the cost of the composites developed. It's possible that each region prefers particular plant fibres over others.

Furthermore, the MENA region have been realising an increase in agricultural biomass wastes deposited in landfills. DPT wastes account to approximately 3.6 million tons deposited annually into landfills or incinerated; however, this can be a valuable natural source that can be utilized in developing NFC. Despite the recent research focus on utilizing DPT wastes for the development of bio-composites, there are ongoing issues that prevent their implementation at an industrial scale. As is the case with all plant fibres, the use of DPF does present challenges. It is challenging to achieve proper adhesion to hydrophobic polymers because of the hydrophilic polar nature of lignocellulosic fibres. This is due to an abundance of hydroxyl groups that give the fibre a strong affinity for water and prevent non-polar polymers from properly wetting the fibres. To increase the compatibility of natural fibres with polymers, numerous studies have been carried out. This was accomplished successfully by either physically or chemically treating the DPF [15,24,25] or by using coupling agents, as reported by several researchers, which improves the adhesion between the NF and polymer matrix [16,19].

Most of the reported research focused on the loading content effect on the mechanical properties of the composites developed and the applications of DPF reinforced composites have been limited due to the lack of enough data and knowledge. Main bottlenecks are the investigation and optimization of DPF characteristics such as geometry (i.e. particle distribution, length and diameter), density, fibre loading, surface treatments and processing parameters to achieve the optimum interfacial bonding between DPF and the matrix system which has not yet been investigated and might be the cause of the negative results achieved by researchers which reduces its feasibility for utilization. Currently, there is limited literature on achieving the optimal interfacial bonding between NF and various matrix systems as

various NF have varying microstructure and chemical composition depending on its cultivation. Thus, when researchers investigated the effect of surface modification on DPF they referred to the outcome of other researchers and took it for granted that DPF have different characteristics. Also, several assumptions are always made when analysing the data after surface modification of NF to enhance the interfacial bonding where there is no in-depth investigation and analysis to prove the scientific theories published. The prediction of the strength of the composites using micro-modelling and mechanics of material is not yet investigated. Also, the utilization of DPF for developing 100% biodegradable composite that can be part of the circular economy scheme is not yet addressed and investigated. The focus of the current research is to develop fully biodegradable composites to overcome the main environmental issues caused by PBP composites landfill deposits, and to utilize DPT agricultural biomass waste as a reinforcement for any both polymeric and cementitious matrix systems to develop sustainable bio-composites. Also, this research aims to provide DPF as a sustainable substitute to synthetic fibres that can implemented within cementitious composites to enhance its quasi-brittle characteristics. This approach was investigated by several researchers on DPF where the reinforcement failed to enhance the strength of the composite. The main reason was not utilizing the optimal DPF geometry where the aspect ratio is the optimal and the reinforcement provide the best length for stress transfer. Furthermore, this research focuses on providing scientific knowledge for future research to build their research programmes.

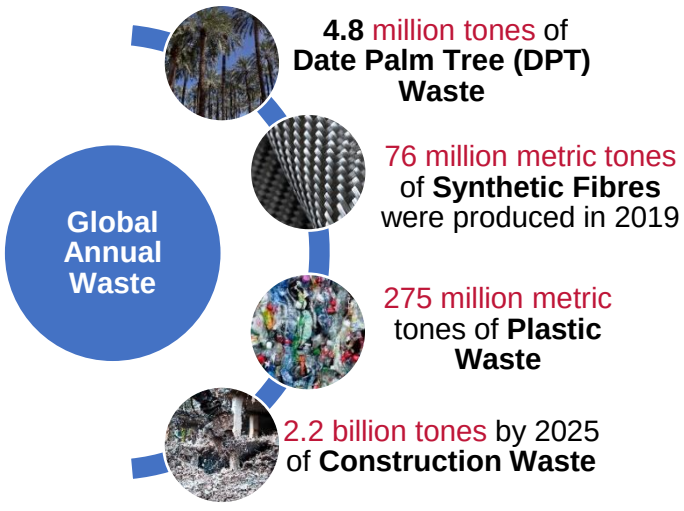

Figure 3 Global annual waste

1.3. Aims and objectives of the research

The main aim of this research is to better understand the DPF characteristics and their correlations with various matrix systems, processing conditions, parameters and develop functional sustainable bio-composites that can reduce both DPF agricultural biomass waste and PBP consumption which complies with the UN SGD and EU legislations towards sustainable development. The research work is to tackle and address the major limitations of utilizing DPF which are mentioned in Section 1.2 to develop sustainable composites that can be implemented in the construction industry for non-structural load application (i.e. cladding panels, decking panels, internal block work and external bricks) and in the automotive industry (i.e. door panels, back of seats, etc.) as a replacement of synthetic fibre. Therefore, this research has the following objectives to fulfil its aims:

1) To evaluate the research done to date through an extensive review of literature on DPF reinforced composites and to identify critical information on the physical, mechanical, and chemical characteristics of DPF from various parts of DPT and determine their reinforcement in various applications, thus establishing and achieving an in-depth understanding of DPFRC and their characteristics which will aim towards developing a database consisting of DPF characteristics and their composites.
2) To optimize and evaluate new technologies for DPF surface modification and investigate the effect of treatments on the tensile, physical and microstructure properties of the fibres.
3) To investigate and evaluate the effect of DPF geometry, density, particle distribution, and loading content on recycled polyvinyl chloride (RPVC) and polylactic acid (PLA) composites and establish their optimization parameters and correlate the findings with the physical, mechanical and biodegradability properties of the developed composites. Also, a micromechanical model was evaluated to investigate the difference between the experimental and theoretical strength of the composite developed.
4) To develop DPFRC and their processing technologies. This will evaluate and investigate the effect of various processing parameters (i.e. processing time, processing temperature and processing pressure) on the physical and mechanical properties of polyester (UPR) composites.
5) To investigate and evaluate the effect of DPF geometry and loading content on OPC and GGBS composites and establish their optimization and correlation with the physical and mechanical properties of the developed composites to develop optimal DPF geometry formulation that can be utilized with any cementitious matrix system. Also, non-fibre characteristics effect (i.e. matrix characteristics and curing conditions)

on the physical and mechanical properties will be evaluated to understand its effect on the overall strength of the composite developed.

1.4. Thesis outline

This thesis consists of eight chapters. Chapter 1 describes the research gap, the problem statement, the research aims and objectives, the scope of the present research, summary of the thesis outline and discusses the novelty of the research programme. Chapter 2 consists of a critical literature review analysis, discussing the research done to date and developing a comprehensive database of DPF characteristics and composite development. Chapter 3 presents the materials utilized in this research study, the sample preparation and fabrication, the testing procedures and characterization techniques. Chapter 4 evaluates the effect of optimizing different surface treatments and conditions (soaking time and duration) on the mechanical and structural properties of DPF. Chapter 5 evaluates the effect of DPF geometry and loading content on the physical and mechanical properties of RPVC and PLA composites. Also, a mathematical and micromechanical model that predicts the strength of the composites developed is explored. Chapter 6 investigates the effect of DPF loading content and the processing parameters (temperature, pressure, and time) on the physical and mechanical properties of DPF reinforced UPR composites. Moreover, Chapter 7 presents the evaluation and discussion of optimizing DPF length, loading content, effect of surface treatment, and the effect of curing conditions on the mechanical and physical properties of OPC and OPC/GGBS composites. Chapter 8 contains a concise summary and conclusions established within this research work providing recommendations for future research.

1.5. Novelty of research work

The research demonstrates a comprehensive study in utilizing DPF and developing DPFRC that delivers solutions for overcoming main drawbacks related with DPF composites which are mainly due to DPF's hydrophilic nature, non-uniform needle like shape, density, particle distribution and geometry. The investigation presented in this research study allows for the development and implementation of DPFRC as an effective material that can be utilised in the construction industry for non-structural applications. The effect and optimization of DPF geometry when utilised as a reinforcement with thermoplastics, thermoset and cementitious matrix systems highlighted the behaviour and effect of the matrix system and the processing conditions on the physical and mechanical properties of the developed composites. The development of 100% bio-degradable bio-composite by utilizing DPF as a reinforcement for PLA which can be degraded by earth worm to develop vermicompost from its manure induces the circular economy of DPF utilization that has not been investigated or discussed previously.

Also, understanding the different densities and particle distribution of DPF highlighted its feasibility for utilization as a core material in developing vacuum insulation panels (VIP). Furthermore, the evaluation and prediction of DPF geometry and processing conditions of the strength of polymeric composite produced a clear effect on developing optimization protocols to produce composite with ultimate characteristics. The compressive and flexural strength of the developed cementitious composites reinforced with optimal DPF characteristics and processing parameters exceeded any reported DPF reinforced cementitious composites developed by other researchers. Also, the outcomes compete successfully for substituting synthetic fibres (i.e., glass fibres) when comparing the results achieved to other researchers' outcomes that utilized synthetic fibres reinforced cementitious composites.

With the developed DPFRC and their processing techniques, the commercial viability of DPF composites as a sustainable composite for the construction and automotive industries was demonstrated, substituting synthetic fibres with natural agricultural biomass waste that is a sustainable and cost-effective material.

The significance of this study is summarized below:

- The research established an extensive database of knowledge and data related to DPF characteristics and composites and identified the gaps and future perspectives in research area by highlighting the limitations of DPF utilization as a reinforcement in composites for industrial applications.
- The study provides an optimization of chemical treatment and new bio-surface treatments of DPF to provide a better surface area and topography to increase the interfacial bonding when utilized as a reinforcement in hydrophobic matrix systems.
- The research provides an in-depth analysis of DPF geometry and density and its effect on the particle distribution of the utilized fibres on the physical and mechanical properties of RPVC and PLA composites. Developing DPF reinforced PLA composites develops a composite that is 100% bio-degradable where an investigation of DPF geometry on the biodegradation rate is evaluated. Also, the feasibility and compliance of composites reinforced with DPF to withstand environmental conditions by investigating its biodegradation was evaluated and achieved the standard regulations. Having all this experimental work done allowed us to obtain a good sized set of data that was used in evaluating micromechanical and mathematical models to predict the strengths of the composites developed which was the first approach to be conducted on DPF composites and will help future researchers to predict the strength of DPF composites developed using compression moulding techniques. Moreover, two novel applications have been deduced from this investigation. A state of art application of

DPF reinforced PLA composite where the biodegradation process can be completely done within 6 weeks by using it as a feedstock for earthworm which will produce vermicompost once it completely feeds on the DPF/PLA composite which highlights DPF within circular economy research program. Also, investigations on DPF geometry highlighted the different densities and characterise for each sieve size. This helped in highlighting the potential of utilizing DPF as a core material in vacuum insulation panel (VIP) development.

- The influence of processing parameters of DPF reinforced polyester composites leading to a better understanding of the mechanisms formulating the mechanical and physical characteristics of the composites developed.
- The research provides an in-depth and comprehensive investigations on the effect of DPF length and loading content correlated with surface modification and curing condition on the physical and mechanical properties of DPF reinforced cementitious composites.

Figure 4 Depicts the schematic flow diagram of experimental research work.

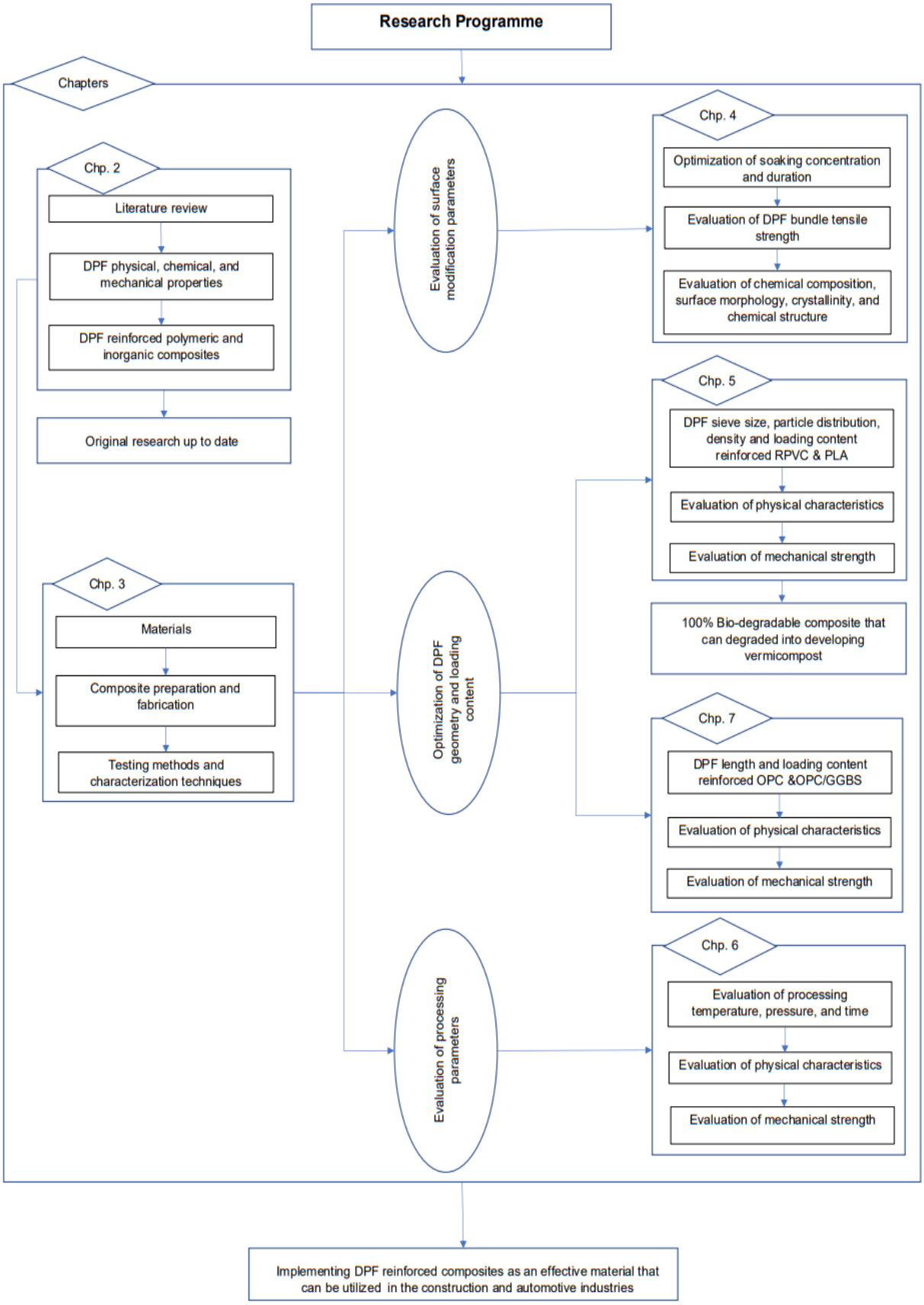

Figure 4 Schematic flow diagram of experimental research work

Chapter 2: Literature Review

The aim of this literature review is to develop a database that can be used by industries and researchers by presenting the work done and key terminologies relevant to the experimental research analysis of matrix systems reinforced with DPF. DPF history of cultivation and resources, production, structure, physical, chemical, and mechanical properties are discussed along with the up-to-date research investigations and activities. The current and future uses for DPFRC in industrial applications are discussed. Developing this database of information and data assisted in identifying the gap in research of utilization DPF and helped in developing the experimental design of this research study.

2.1. Natural fibres (NF)

A wide variety of NF exists in nature which are classified depending on their origin, coming from animals, plants, or minerals. Fibres obtained from animals mainly consists of proteins while plant fibres (NPF) are mainly composed of cellulose, 40 – 90 %, thus they are referred to lignocellulosic fibres. However, NFs are pre-treated and processed with different chemical, biological, physical, and mechanical ways to achieve specific requirements of the composite industry, but still distinguished as 'natural'. NFs can be classified as shown in Figure 5.

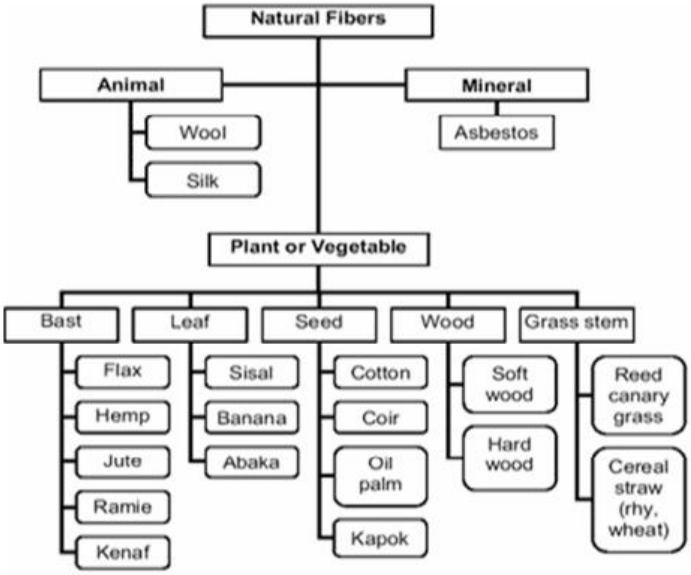

Figure 5 Natural fibres classification according to their origin [26]

The structure, microfibrillar angle, cell dimensions, defects, and the chemical composition of NF are the most important variables that determine their properties. The chemical composition varies between the plants, but also within the same plant. Also, it depends on the geographical region, climate, ages and soil conditions. The chemical properties are influenced by the fibres

growth time, stalk height and botanical classification. The cellulose in NPF is resistant to oxidizing agents and strong alkali but is easily hydrolyzed by acid to water-soluble sugars. Hemicellulose is very hydrophilic, soluble in alkali and easily hydrolyzed in acids. However, lignin is not hydrolyzed by acids, but soluble in hot alkali, readily oxidized, and easily condensable with phenol. Moreover, mechanical properties, tensile strength and Young's modulus of fibres increases with increasing cellulose content. The microfibrillar angle determines the stiffness of the fibres. NPF are more ductile if the microfibrils have a spiral orientation to the fibres axis. If the microfibrils are oriented parallel to the fibres axis, the fibres will be rigid, inflexible and have high tensile strength. Furthermore, more detailed description on the chemical composition of NF is given in Section 2.1.1. On the other hand, the hydrophilic nature of NPF is a major drawback when used as a reinforcement in plastic. It is dependent on the void content of the fibres and the non-crystalline parts and a certain humidity it affects the biological performance of the composite. Thus, the applications of NPF are often limited to interior applications due to their poor moisture resistance, but this can be improved using different chemical and physical surface treatments.

2.1.1. Physical and mechanical properties of natural fibres

The physical and mechanical properties of NF vary depending on several factors, such as the chemical structure, chemical composition, structural arrangement of cellular fibrils, crop production, soil condition, temperature, and weather conditions in which the plants are growing [27]. The extracted fibre area from the plant can also influence the fibres properties and the fibre extraction method [28]. Moreover, NFs tend to be stiffer and stronger than animal fibres which makes them suitable as a reinforcement material to produce cementitious and polymeric composites. NF possess several advantages when compared to animal fibre, such as lower cost, easy processing, and abundant availability worldwide. The specific modulus of NF is considered almost comparable to glass fibre. However, NFRC possess lower tensile strength compared to glass fibre reinforced composites although the modulus is of similar magnitude [29]. NF selection plays a crucial role in achieving specified composite requirements. The advantage on using NF and at high content in developing composites is the cost saving and the ease of processing of the developed composite which qualifies NF to be a very good reinforcer and a substitute to synthetic fibres in developing composites that could be implemented in several industries for various applications including automotive, building, household appliances and many others. Table 1 shows the physical and mechanical properties of NFs and synthetic fibres obtained from various reported literature. Few presented data might be misleading such Ramie's Young's Modulus reported, inaccuracy of price reported for fibres as they are not valued at an industrial scale, date palm and pineapple tensile strength. Also, the methods techniques of obtaining those properties must be investigated

under approved standards such as the British Standards (BS) and the American Society for Testing and Materials (ASTM). Few researches have reported their investigated results without an explanation on the standard used for testing which might present misleading results.

Table 1 Physical and mechanical properties of natural plant fibres and synthetic fibres [12,28,30–36]

Fibre type	Density (g/cm^3)	Diameter (μm)	Length (mm)	Tensile Strength (MPa)	Young's Modulus (GPa)	Elongation (%)	Poisson's Ratio	Moisture content (%)	Price ($/kg)
Abaca	1.5	100 – 200	-	400 – 980	12 – 32	3 - 10	-	5 – 15	0.36
Agave	1.2	126 – 344	-	-	-	-	-	-	-
Alfa	0.9 – 1.4	-	350	188 - 350	18 - 25	5.8	0.34	-	-
Bagasse	1.25	-	-	290	17	-	-	8.8	-
Bamboo	0.6 – 1.4	-	-	140 - 740	11 - 50	2	0.28	8.9	-
Banana	1.35	80 – 250	-	500 - 754	7.7 - 20	3 – 10.35	0.30	-	-
Coir	1.15 - 1.25	100 – 650	20 -150	106 - 220	4 – 6	15 - 47	0.18	8 - 10	0.25 – 0.50
Cotton	1.2	-	-	150- 180	4 – 6	20 - 40	0.48	-	2.1 – 4.2
Curaua	1.5 – 1.6	-	10 - 60	287 – 800	5.5 - 13	3 – 12.4	-	33 - 34	-
Date palm	0.9-1.4	100 - 1,000	20-150	158 – 1,150	11.8	3.7 – 4.3	0.17	-	0.03
Elephant grass	0.9 – 1.2	-	-	58 – 309	2.5 – 11.32	2 – 4.5	-	-	-
Flax	0.82	70 – 400	-	185	7.4	2.5	0.45	-	2.1 – 4.2
Hemp	1.4 – 1.5	19	5 – 900	345 – 1,500	27 - 80	1.16 - 4	0.39	7 – 10	1.55
Henequen	1.14 – 1.5	-	5 – 55	350 – 1,110	30 - 70	1.6 - 8.1	-	9 - 10.8	-

Fibre type	Density (g/cm^3)	Diameter (μm)	Length (mm)	Tensile Strength (MPa)	Young's Modulus (GPa)	Elongation (%)	Poisson's Ratio	Moisture content (%)	Price ($/kg)
Isora	1.2	-	-	430 – 570	10.1 – 16.3	3.7 – 5.9	-	-	-
Jute	1.2 – 1.3	-	-	500 - 600		5 – 6	0.11 – 0.36	-	0.925
Kenaf	1.3 – 1.5	20 - 200	1.5 - 120	300 – 800	10 - 55	1.2 - 3	0.41	12 – 13.7	0.378
Pineapple	0.8 – 1.6	20 – 80	900 – 1,500	180 - 1,627	1.44 – 82.51	1.6 – 14.5	0.33	11.8-13.0	-
Palymyrah	1.09	70 – 1,300	-	180 – 215	7.4 - 604	7 – 15	-	-	-
Petiole bark	0.69	250 - 650	-	185.52	4 - 6	2.10	-	-	-
Piassava	1.4	-	-	134 – 143	1.07 – 4.59	7.8 – 21.9	-	-	-
Ramie	1.5	20 - 80	900 – 1,200	220 – 1000	24.5 - 128	1.2 – 4	0.38	7.5-17.0	2.0
Sisal	1.3 -1.5	8 – 300	1 – 900	300 – 700	9 – 38	2 - 15	0.32	10.0-22.0	0.60 – 0.70
E-glass	2.55	-	-	-	-	-	0.20 – 0.30	-	1.60 – 3.50
Carbon	1.8	-	-	-	-	-	0.26 – 0.28	-	124 – 166

2.1.2. Chemical composition of natural plant fibre

NF structure as well as their chemical composition are influenced by several factors, such as the growing and climate conditions of the harvest area, age of the plant, type of species of the plant and the method of extraction (e.g. biological, chemical and mechanical) process of the fibres [32]. NF consists of single fibres with diameters ranging from 10 – 650 µm and chemical components such as cellulose, hemicellulose, lignin and pectin which contributes between 80 to 90% of the structure of NF, classifying a single NF as a composite. Additionally, NF structure contains waxes, minerals and other extractives [37]. The main chemical compositions of various NF are summarised in Table 2.

Table 2 Chemical composition of several natural fibres [12,28,30–34]

NF Type	Cellulose (%)	Hemicellulose (%)	Lignin (%)
Abaca	56 - 63	20 – 25	7 – 9
Alfa	45.4	38.5	14.90
Bagasse	55.2	16.8	25.30
Bamboo	26 – 43	30.0	21 – 31
Banana	54 – 66	19.0	5
Coir	32 – 43	0.15 – 0.30	40 – 45
Cotton	82.7 – 90	5.70	0.7 – 1.6
Curaua	73.60	9.90	7.50
Date palm	41.10	24.66	26.91
Flax	64 - 71	18.6 – 20.6	2.0 – 2.2
Hemp	68.0 – 74.4	15.0 – 22.4	3.7 – 10.0
Henequen	60	28	8
Isora	74	-	23
Jute	59 – 72	13.6-20.4	11.8 -13
Kenaf	31 - 72	20.3 -21.5	8 - 19
Palymyrah	40 – 52	29 – 32	42 – 43
Petiole bark	46	20	12
Piassava	28.6	25.8	45

NF Type	Cellulose (%)	Hemicellulose (%)	Lignin (%)
Pineapple	70 – 83	-	5 – 12.7
Ramie	68.6 – 85	13 – 16.7	0.5 – 0.7
Sisal	60 – 78	10 – 14.2	8 – 14

Moreover, the structure of the NF consists of primary wall, secondary wall, and a lumen. The inner cell wall contains rigid cellulose component, which is embedded in a soft lignin and hemicellulose matrix in the secondary wall of the fibre materials [28,38]. Lignin located in the secondary cell wall acts as a binding material for cellulose and hemicellulose. Also, pectin is another binding material that helps cellulose in binding to other components. However, when comparing pectin and lignin to cellulose, they are considered as weak amorphous polymers [39]. Furthermore, the structural arrangement of NF cell wall is demonstrated in Figure 6.

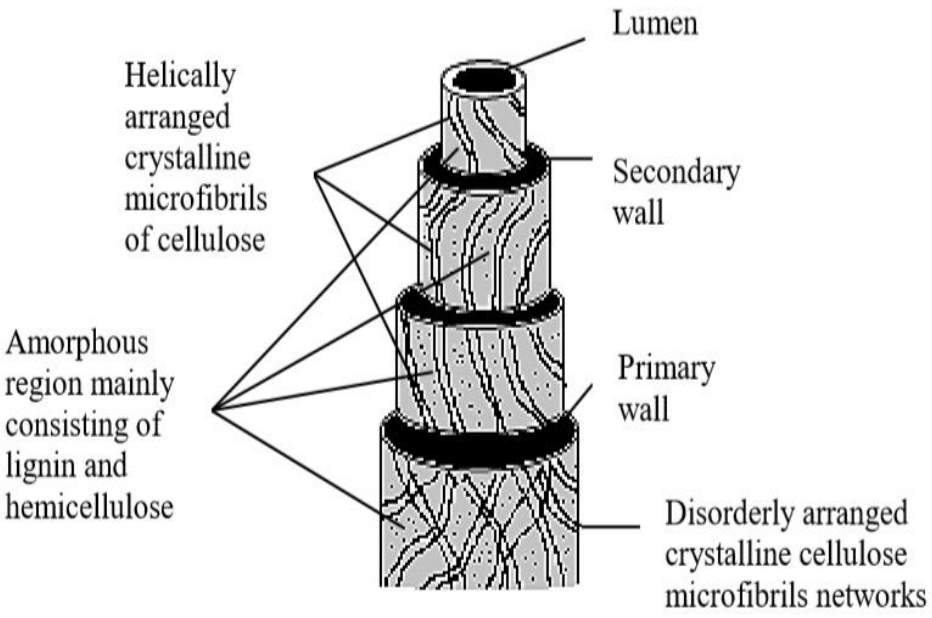

Figure 6 Structural arrangement of natural fibres [40]

2.1.2.1 Cellulose

Cellulose, a linear semi-crystalline polysaccharide, is one of the primary cell wall components of NF and considered as the most abundant polymer available on earth which is commercially exploited in the form of wood. Cellulose accounts as the main structural component in NF, where the crystalline cellulose gives the strength to the plants stem, thus the percentage of cellulose can be directly related to the mechanical properties of the NF [37]. Moreover,

cellulose polymer chains consist of a repetitive units of anhydro-glucose linked via 1,4-β-D-glycosidic linkages which are called cellobiose, as shown in Figure 7 [41].

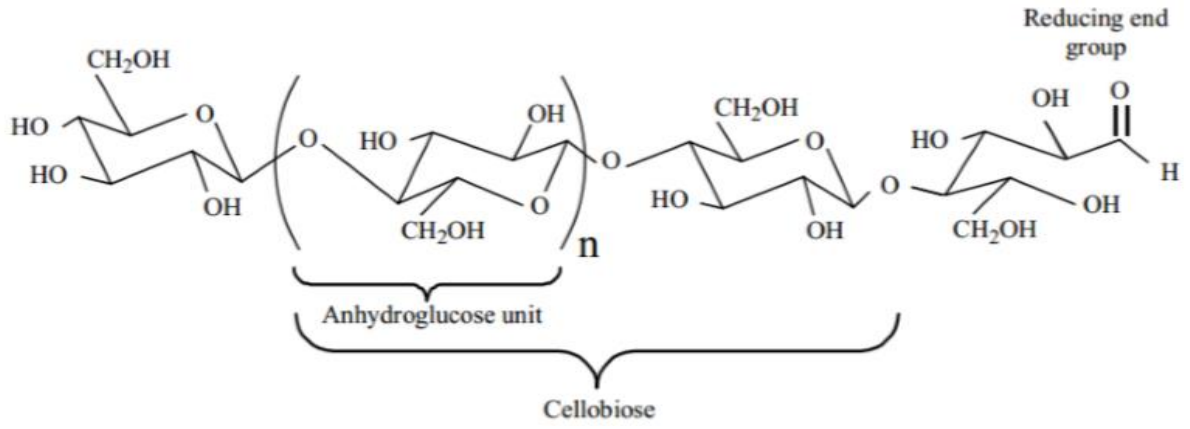

Figure 7 Haworth projection formula of cellulose [41]

2.1.2.2 Hemicellulose

Hemicellulose is not a form of cellulose at all, and the name is an unfortunate one. They comprise a group of polysaccharides (excluding pectin) that remains associated with the cellulose after lignin has been removed. In three essential ways, hemicellulose varies from cellulose. To begin with, they contain a variety of sugar units, whereas cellulose only contains 1,4-b-d-glucopyranose units. Second, they have a lot of branching in their chains, whereas cellulose is a completely linear polymer. Third, native cellulose has a ten to one hundred times higher degree of polymerization than hemicellulose.

2.1.2.3 Lignin

Lignin is a complex hydrocarbon polymer which consists of both aromatic and aliphatic constituents and is considered the second most abundant organic polymer found in NF after cellulose. Lignin binds the fibres of the plants together to form a stiff structure which provides the compression strength to the plant [42].

2.1.2.4 Pectin

Pectin is a structural component of acidic polysaccharides with a complex branched structure located in the primary cell of plants. Pectin partially consists of residues of methylated poly-β-(1-4)-D-galacturonic acid and primarily homopolymeric acid as shown in Figure 8. Exposing pectin to an alkali solution allows it to be water soluble after partial neutralisation [42]. Moreover, pectin binds the cellulose, hemicellulose, and lignin along with pectin itself forming bundles and is found in high concentrations in the middle lamella and the primary cell wall of NF [43]. During the retting process of NF, majority of the pectin is removed, which

enhances the interfacial bonding between the NF and the matrix system used to develop bio-composites [44].

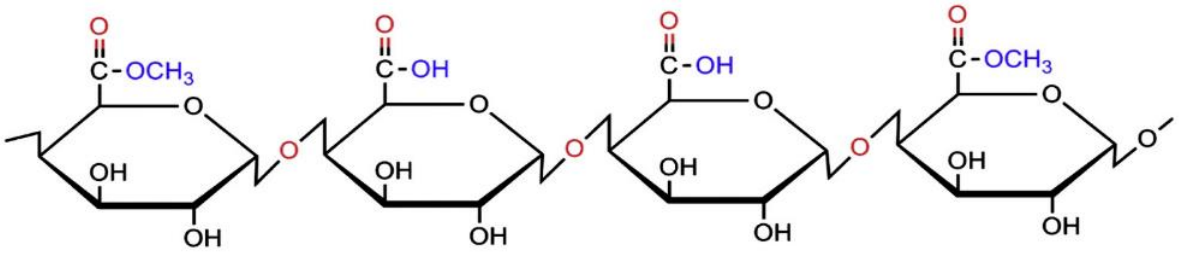

Figure 8 Chemical structure of pectin [44]

2.2. Date palm fibres (DPF)

2.2.1. Date palm tree cultivation and resources

The date palm tree (DPT), which belongs to the Palmae (Arecaceae) family, is cultivated in subtropical and tropical areas since the ancient era for its edible sweet fruits known as dates. Although its exact place of origin is still uncertain, it is assumed that it originated from a region straddling between Egypt and Western Asia [45–48]. The species is cultivated across five continents but widely across the Middle East and North Africa (MENA) region and mainly in countries like Saudi Arabia, Iraq, Pakistan, Algeria, United Arab Emirates (UAE), Egypt, Sudan, Oman, Iran, and Tunisia. The total number of DPT cultivated in the Arab countries based on a count done by Arab Organization for Agricultural Development (AOAD) in 2014, is shown in Table 3. The amount of dates produced in the top 20 countries in 2017 is given in Table 4 which reports considerable improvement in industrialization of dates, worldwide production and its utilization [47].

Table 3 Number of DPTs cultivated in the MENA region

Country	Number of trees (x 1,000)	Country	Number of trees (x 1,000)
Egypt	12,830	Libya	2,100
Algeria	15,090.93	Morocco	4,954.13
Saudi Arabia	12,000	Kuwait	312.21
Iraq	10,475	Yemen	4,623
UAE	16,757.94	Sudan	2,646
Oman	6,100	Qatar	484.97
Tunisia	3,335.80	Jordan	184.80

Country	Number of trees (x 1,000)	Country	Number of trees (x 1,000)
Bahrain	376.70	Mauritania	600
Syria	68.60	Palestine Territories	301.20

Table 4 Number of dates cultivated reported by the top 20 countries worldwide

Country	Production (tonnes)	Country	Production (tonnes)
Egypt	1,590,414	Libya	174,583
Iran	1,185,165	China	162,041
Algeria	1,058,559	Morocco	129,562
Saudi Arabia	754,761	Kuwait	87,391
Iraq	618,818	Yemen	47,615
Pakistan	524,041	Israel	43,967
UAE	475,286	USA	39,300
Sudan	439,355	Turkey	38,535
Oman	360,917	Qatar	29,404
Tunisia	260,000	Jordan	25,222

Moreover, the world's date palm biodiversity accounts to approximately 5,000 date palm cultivars [48]. Based on botanical descriptions done by several researchers, about 26 cultivars can be found in Egypt, 400 in Iran, 1,000 in Algeria, 370 in Iraq, 400 in Sudan, 250 in Tunisia, 196 in the USA and 244 in Morocco as well as plenty more cultivars in other states [49,50]. Phoenix Dactylifera L., is considered as the most cultivated species of DPT, which is considered to be the tallest from among its species with heights exceeding 30 metres and fruits size reaching 100 mm x 40 mm [51]. DPT can thrive through various growing conditions. They grow in areas characterized by hot, dry, low humidity, particularly during fruit development. DPT can be planted in a wide range of soils with varying amounts of organic and mineral nutrients. They grow well in sand and in soil where water is close to the surface due to the air spaces in their roots. However, they are not xerophyte and requires abundant amount of water [46]. In addition, moisture adversely affects the quality of fruit, as high humidity leads to fruit cracking and checking. DPT is also known to tolerate salinity more than any other cultivated fruit crop.

DPT structure is distinguished by several offshoots produced at its trunk's base. The trunk of the date palm tree is covered with persistent brownish leaf bases. It is overcome by an array of pinnate divided long leaves and needle-sharp fronds. Usually, around 10–20 new leaves are produced yearly. The leaves of the date palm are subtended by a cylindrical mesh mat of reticulate mass of tough, fibrous material, at their bases. These together form a tight protective cover for the terminal bud [52,53]. A young actively bearing DPT showing its general structure and morphological traits of date palm parts is shown in Figure 9.

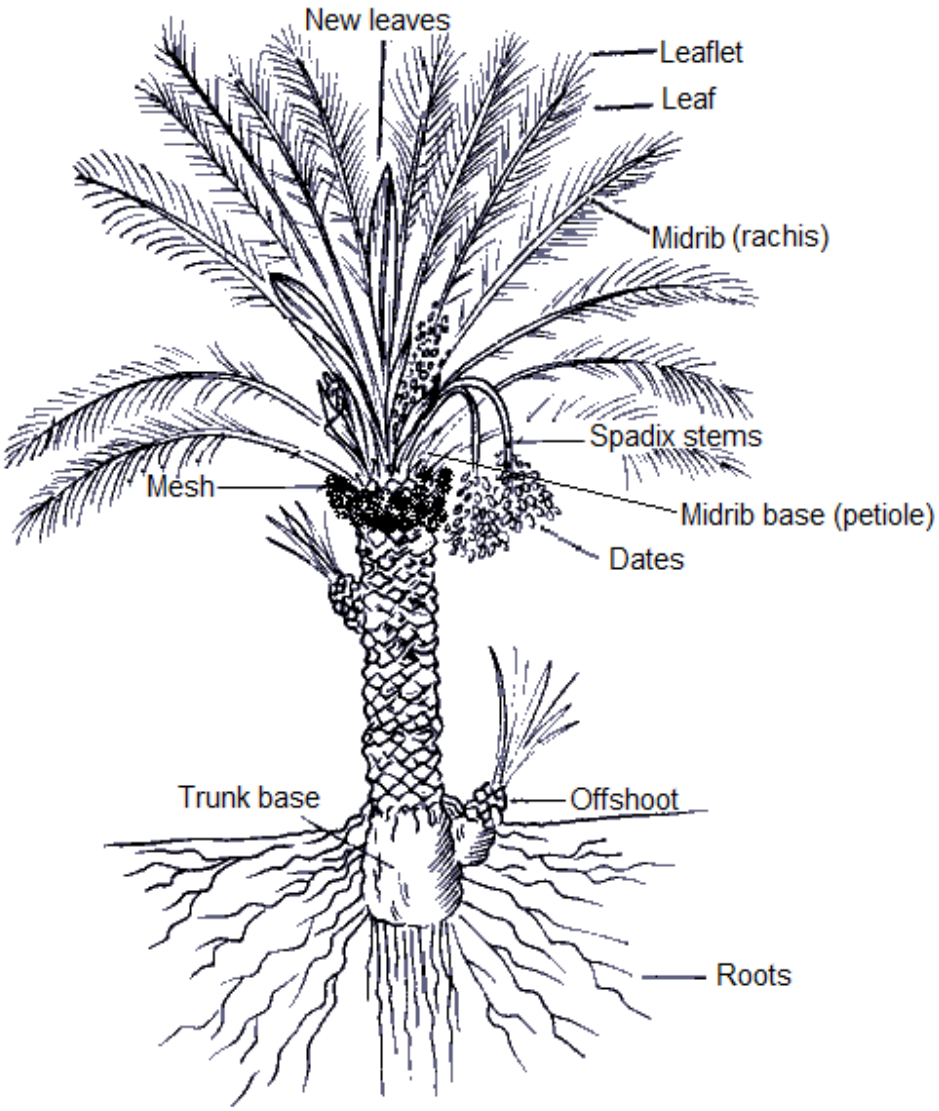

Figure 9 Date palm tree [12]

Once the date fruits are harvested, annually, large quantities of agricultural wastes from DPTs are accumulated every year in agricultural lands of different countries. These amounts of valuable biomass wastes are of potential interest in different countries since they can be considered as new cellulosic fibre sources. A single DPT annually produces approximately 26

kg of waste from various parts of DPT. For instance, DPT waste accounts for 9.8 kg midribs, 8 kg of leaflets, 7 kg of spadix stems and 1.3 kg of mesh as an agricultural waste biomass [54]. Additionally, DPTs produces another type of wastes as date pits resulting as a residue product after eating the date fruit, which are considered to be approximately 10 % of the date fruits [55]. Furthermore, Nasser et al. [52] reported that an average of 35 kg of date palm tree waste is produced annually. Unfortunately, these agriculture wastes are not accurately calculated and not properly utilized in any biological process or industrial applications in most of countries, despite of their contents of potential amount of cellulose, hemicelluloses, lignin, and other compounds. Thus, according to [54], and based on the data given in Table 5 and Table 6 the amount of agricultural waste per country produced by various parts of DPT can be estimated (Table 5). The total amount of agricultural waste produced annually in the MENA region can vary from 2.6 – 2.8 million tonnes. Therefore, innovative ways of valorising this abundant renewable resource should be found [56]. One of the solutions that has been implemented on research scale is to extract DPFs from the agricultural waste (midribs, leaflets, spadix stems, and mesh) using different fibre extraction techniques and to utilize the fibres in developing composites that are suitable and applicable for different industrial applications.

Table 5 The amount of agricultural waste from DPT in the MENA region [12]

Country	**Amount of agricultural waste from DPT (tons)**				
	Midribs	**Leaflets**	**Spadix stems**	**Mesh**	**Date Palm Pits**
Egypt	125.734	102.64	89.81	15.396	2,202.9
Algeria	147,891.1	120,727	105,636.51	18,109.1	159,041.4
Saudi Arabia	117,600	96,000	84,000	14,400	105,855.9
Iraq	102,655	83,800	73,325	12,570	75,476.1
UAE	164,227.8	134,064	117,305.58	20,109.5	61,881.8
Oman	59,780	48,800	42,700	7,320	47,528.6
Tunisia	32,690.84	26,686.4	23,350.6	4,002.96	36,091.7
Bahrain	3,691.66	3,013.6	2,636.9	452.04	26,000.0
Syria	672.28	548.8	480.2	82.32	1,050.1
Libya	20,580	16,800	14,700	2,520	430.9
Morocco	48,550.47	39,633	34,678.91	5,944.96	210.0
Kuwait	3,059.658	2,497.68	2,185.47	374.652	12,956.2

Country	Amount of agricultural waste from DPT (tons)				
	Midribs	**Leaflets**	**Spadix stems**	**Mesh**	**Date Palm Pits**
Yemen	45,305.4	36,984	32,361	5,547.6	8,739.1
Sudan	25,930.8	21,168	18,522	3,175.2	4,761.5
Qatar	4,752.706	3,879.76	3,394.79	581.964	43,935.5
Jordan	1,811.04	1,478.4	1,293.6	221.76	2,940.4
Mauritania	5,880	4,800	4,200	720	2,522.2
Palestine Territories	2,951.76	2,409.6	2,108.4	361.44	4,396.7
Total	**788,156.3**	**643,393**	**562,968.77**	**96,508.9**	**596,021**

Furthermore, the cost per kilogram (kg) of DPF and its availability worldwide are considered as the main parameters for its applications in different industrial sectors. DPFs are among the most cost effective and mostly abundant NF due to the large amount of DPT available world-wide. Based on the data reported by Al-Oqla and Sapuan, (2014) Figure 10 and Figure 11 are developed to show the difference in price per kg and availability comparing DPF and other NFs respectively [51,57]. It can be estimated that DPF price is approximately 0.03$ which is significantly cheaper than coir, hemp, bamboo, and sisal which are estimated to be 0.25$, 1.20$, 1.75$ and 0.90$ respectively. It is crucial to consider that the reported DPF is based on assumption that the waste is available locally and there is not extraction and transportation cost added to it as there is no commercial or industrial DPF production plant.

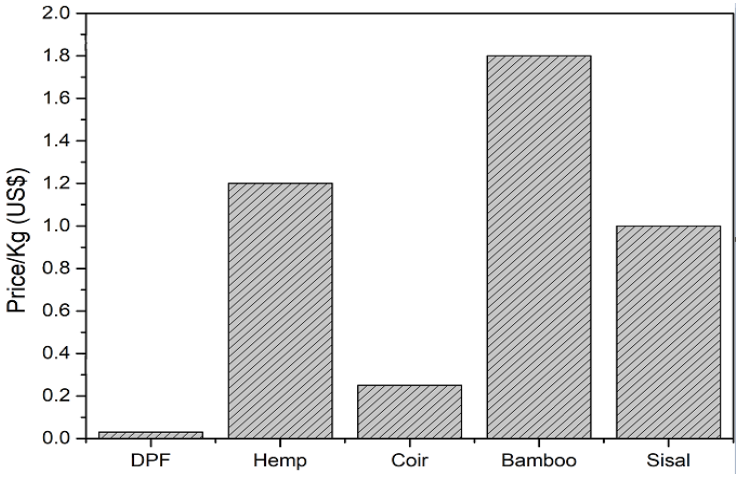

Figure 10 Prices of DPFs compared to other NFs [51]

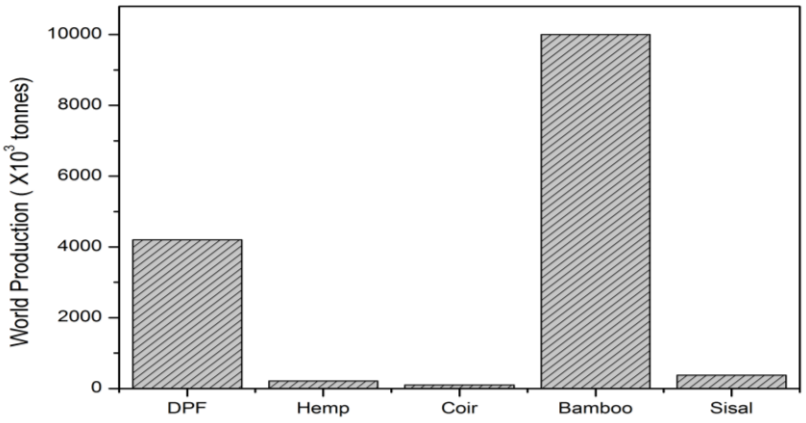

Figure 11 World production of DPF compared to other NFs [51,57]

2.2.2. Characterization of date palm fibre

Utilizing DPF for industrial applications as a reinforcement in polymeric matrices is a relatively new application. Thus, it is necessary to comprehend the chemical, physical, mechanical, and thermal properties of DPF to identify the limitations and strengths of DPF reinforced composites. Research investigations on DPF and their composites have started in 2004, however, these properties are not yet well established and an inconsistency in literature is well noticed. Previous DPF investigations conducted and reported concerning the chemical, physical, mechanical, and thermal properties is accordingly reviewed and discussed in the following Sections.

2.2.2.1 Chemical composition and structure of date palm fibre

The climate and geographical conditions have an influence on the chemical composition and structure of NF [58]. Therefore, DPF chemical composition varies from one country to the other as shown in Table 6, which also summarizes the chemical composition of different parts of DPT investigated by previous researchers. Also, it is observed from previous work done in determining the chemical composition of natural fibres, that the sum of all constituents stated might not sum up to 100%. Some constituents within the fibres were not traced to a measurable quantity. Furthermore, understanding the chemical composition of DPF is crucial for determining their applicability for different industrial applications particularly in developing date palm fibre reinforced composites (DPFRC). Thus, some characteristics of these DPFRC, such as weather resistance, recyclability and degradability, tensile and flexural strength, strongly depend on the chemical composition and structure of the fibre [51,59].

The cell structure and chemical composition of DPF are quite complex, where a single fibre itself is a composite material made up of cellulose, hemicelluloses lignin and other constituents, such as wax, starch proteins and sugar. The latter are influenced by several factors, such as the variation in the cross-sectional area of the fibre, fibre extraction and processing parameters, and fibre treatment conditions [28].

DPF consist mainly of cellulose fibrils that are embedded in lignin matrix which are considered the most crucial structural components. Cellulose is usually found as a slender rod like crystalline micro-fibrils and aligned along the fibres length [59]. The nature of cellulose and its crystallinity which is determined by the hydrogen bonding in it regulates the physical properties of DPF. Thus, cellulose is the main constituent that provides DPFs with stiffness, strength and stability [60,61]. Moreover, cellulose is resistant to oxidizing agents, hydrolysis, and strong alkali. It degrades to some extent when exposed to chemical treatments for long durations [59]. Hemicelluloses are polysaccharides bonded together in relatively short branching chains which are intimately associated with cellulose microfibrils, embedding the cellulose in a matrix. They are very hydrophilic in nature with molecular weights lower than that of cellulose [58]. While lignin is a complex aromatic hydrocarbon polymer that provides rigidity to plants and assists in water transportation. It is hydrophobic, resists most of microorganisms attacks as well as acid hydrolysis, it is usually soluble in hot alkali, readily oxidized, and easily condensable with phenol [60]. Lignin, oils and waxes should be removed for better adhesion between the DPF and the matrix, thus achieving an effective composite reinforcement [28].

Table 6 Chemical Composition of DPF from various parts of DPT [12]

Origin	DPT Part	Cellulose (%)	Hemicelluloses (%)	Lignin (%)	Ash (%)	Moisture Content (%)	Reference
Egypt	Rachis	-	-	25.80	3.40	-	[62]
India	Leaflets	58.00	-	15.30	-	-	[63]
UAE	Mesh	46.00	18.00	20.00	-	5.00	[64]
Sudan	Rachis	43.10	-	23.80	5.60	-	[65]
	Leaflets	30.30	-	31.20	9.60	-	
Morocco	Leaf	33.90	26.10	27.70	6.90	-	[66]
Egypt	Mesh	48.00	19.00	24.00	-	-	[13]
N.S	Rachis	44.00	-	14.00	2.50	-	[67]
	Leaflets	33.50	-	27.00	6.50	-	

Origin	DPT Part	Cellulose (%)	Hemicelluloses (%)	Lignin (%)	Ash (%)	Moisture Content (%)	Reference
Morocco	Leaflets	35.00	28.00	27.00	-	-	[68,69]
	Oxidized Leaflets	46.00	34.00	12.00	-	-	
Iran	Petiole	23.00	-	31.00	-	-	[70]
	Rachis	32.00	-	37.00	-	-	
	Trunk	27.00	-	38.14	-	-	
Tunisia	Rachis	45.00	29.80	29.80	3.00	-	[71]
Saudi Arabia	Midrib	46.41	25.89	-	7.91	-	[72]
Morocco	Leaflets	35.00	28.00	27.00	-	-	[69]
Algeria	Rachis	35.87	28.58	26.89	-	-	[15]
	Trunk	43.70	38.14	16.94	-	-	
	N.S	45.00	26.00	5.00	-	-	
Morocco	Rachis	39.80	31.40	14.00	9.20	10.00	[73]
	Leaflets	29.70	23.30	11.6	9.20	6.30	
	Mesh	50.60	8.10	31.9	6.80	8.80	
	Trunk	34.00	28.90	18.2	12.30	7.90	
Iran	Leaflets	40.21	12.80	32.2	10.54	-	[74]
	Rachis	38.26	28.17	22.53	5.96	-	
India	Leaflets	54.75	20.00	15.30	-	-	[75]
Saudi Arabia	Frond base midrib	40.74	33.84	25.45	7.64	-	[52]
	Midrib-base	44.92	26.77	28.30	4.02	-	
	Midrib-middle	46.14	24.59	29.27	3.40	-	
	Midrib-top	43.71	26.30	29.99	3.37	-	
Algeria	Petiole	33.79	20.44	26.03	3.70	-	[76]
	Rachis	41.42	19.35	33.00	4.00	-	

Origin	DPT Part	Cellulose (%)	Hemicelluloses (%)	Lignin (%)	Ash (%)	Moisture Content (%)	Reference
	Leaflets	38.58	20.05	28.57	2.62	-	
	Mesh	43.94	21.68	27.80	1.55	-	
Saudi Arabia	Midribs from different cultivars	47.84	23.10	29.60	-	-	[77]
		48.86	19.86	31.28	-	-	
		47.17	22.30	30.19	-	-	
China	Mesh	28.16	20.60	44.07	-	-	[78]
Saudi Arabia	Trunk	39.37	30.31	30.32	-	-	[52]
	Frond base	43.05	31.34	25.61	-	-	
	Frond midrib	45.16	28.16	26.68	-	-	
	Leaflet	47.14	16.13	36.73	-	-	
	Fruit stalk	43.05	27.48	29.47	-	-	
	Fruit empty bunch	44.40	24.30	31.30	-	-	
	Stone	32.77	30.20	37.03	-	-	
	Mesh	47.50	12.64	39.86	-	-	
Algeria	Mesh	43.00	8.00	35.00	-	-	[79]
Saudi Arabia	Mesh	45.10	27.70	16.90	1.70	-	[80]
Egypt	Mesh	57.06	16.97	13.09	-	-	[81]
Algeria	Mesh	43.00	8.00	35.00	1.20	9.00 – 10.00	[22]
Egypt	Mesh	42.66	-	20.74	1.37	-	[82]
Saudi Arabia	Leaf stalk	35.00	15.40	20.10	-	-	[83]
	Fruit bunk	44.00	26.00	11.00	-	-	
	Mesh	43.50	24.00	18.00	-	-	
	Trunk	40.00	9.75	29.50	-	-	
Saudi Arabia	Mesh	26.92	43.21	27.42	-	6.00 – 8.00	[84]

Origin	DPT Part	Cellulose (%)	Hemicelluloses (%)	Lignin (%)	Ash (%)	Moisture Content (%)	Reference
Oman	Midrib	64.00	4.00	19.00	-	-	[85]
Tunis	Various	39.34	22.95	27.81	8.12	-	[86]
UAE	Mesh	44.80	22.50	30.50	-	-	[87]

Furthermore, it can be noticed in Table 7 that there are variations in the chemical compositions of DPT due to parameters discussed previously. Thus, summarized tabled data, Table 7 shows the minimum to maximum values, and Table 8 shows an average value of chemical compositions for different parts of DPT fibres is developed respectively based on the results reported in Table 6, which will support the comparison of DPF with other natural fibres. A comparison and evaluation between the average values of the chemical composition can demonstrate the viability, competitiveness, and appropriateness of DPF for being a potential type of reinforcements for NFC compared to other NFs. It can be deduced from the comparison shown in Figure 12 that DPF has an added value over abaca, sisal, kenaf and hemp due to its lower cellulose content which may reduce the ability of DPF to absorb water comparing to other NFs [51,59]. In contrast, bamboo and coir have lower cellulose content than DPF but their hemicellulose or lignin are higher which may not make it suitable as a reinforcement compared to DPF.

Table 7 Chemical composition for different parts of date palm tree [12]

DPT Part	Cellulose (%)	Hemicelluloses (%)	Lignin (%)	Ash (%)	Moisture (%)
Mesh	26.9 – 55.1	8.0 – 43.2	13.1 – 39.9	1.6 – 6.8	5.0 – 8.8
Rachis	32.0 – 44.0	19.8 – 29.8	14.0 – 33.0	2.5 – 9.2	10.0
Leaflets	29.7 – 58.0	12.8 – 28.0	11.6 – 36.7	2.6 – 10.5	6.3
Midribs	40.7 – 48.9	19.8 – 33.8	25.5 – 31.1	3.3 – 7.6	-
Trunk	27.0 – 39.8	30.3 – 38.1	18.2 – 38.1	12.3	7.9

Table 8 Average chemical composition range for different parts of date palm tree [12]

DPT Part	Cellulose (%)	Hemicelluloses (%)	Lignin (%)	Ash (%)	Moisture (%)
Mesh	43.71	18.66	29.43	4.18	6.93
Rachis	39.93	26.48	25.20	4.81	10.00

Leaflets	40.21	20.05	25.19	7.69	6.30
Midribs	45.66	25.65	28.85	5.27	-
Trunk	36.02	32.45	25.90	12.3	7.90
Average DPF	***41.1***	***24.66***	***26.91***	***6.85***	***7.76***

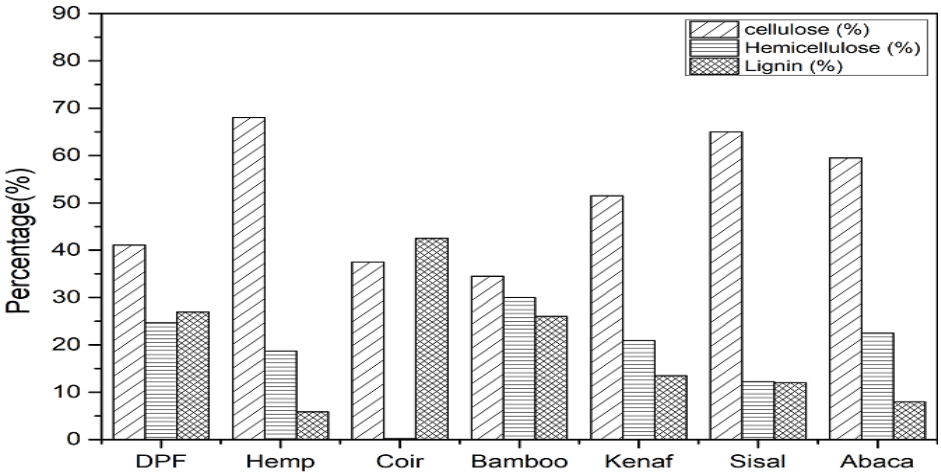

Figure 12 Average chemical composition of date palm fibre and other natural fibres [51,59]

2.2.2.2 Physical properties of date palm fibres

Physical properties of DPFs are critical in determining their eligibility for various industrial applications in addition to developing DPFRCs. DPF's diameter, length, density, and aspect ratio are considered key physical properties [51,88,89]. DPF average bulk density ranges from 0.199 – 1.98 (g/cm^3) based on literature data [12,51] which is lower than the respective one of NF such as hemp, sisal and coir. However, the moisture content of the fibres measured were not taken into consideration while measuring the densities. The latter can have an added value in the field of NFRC development [51,54,70,89], especially in developing light weight DPFRC that may be suitable for space and automotive applications [53]. The physical properties vary depending on the fibre type and the fibre extraction technique. DPF extracted mechanically accounts for having higher diameters and lengths [54]. However, previous research studies have not indicated whether the reported physical properties correspond to a single or bundle DPF, thus it is very crucial to understand and differentiate between the different properties and characteristics of single and bundle DPF. A summary of the reported physical properties of DPF is given in Table 9. Also, a comparison between DPF with other NFs regarding their average physical properties is demonstrated in Table 10.

Table 9 Physical properties of DPF reported by different authors [12]

Origin	Fibre Type	Bulk Density (g/cm^3)	Length (mm)	Diameter (µm)	Aspect Ratio	Reference
	Midribs	-	1.5 – 2.5	8 – 16	150 – 190	[63]
Saudi Arabia	Leaflets	-	4.70	435.2	10.80	[90]
UAE	Mesh	0.91	-	-	-	[64]
Sudan	Midribs	-	1.10 – 1.30	13.7 – 16.6	66.30 – 95.00	[65]
Algeria	Mesh	0.51 – 1.09	15 – 60	200 – 800	18.75 – 300	[20,91]
N.S	Leaf	0.99	-	-	-	[92]
	Mesh	0.96	100 - 300			
Iran	Petiole	-	1.00	12.50	80.00	[70]
	Rachis	-	1.19	17.00	70.00	
	Trunk	-	1.30	40.00	33.00	
N.S	Mesh	-	-	200 – 800	-	[93]
Morocco	Fibrillum	0.241	-	389	-	[73]
	Leaflet	0.316	-	316	-	
	Rachis	0.289	-	289	-	
	Mesh	0.199	-	199	-	
Egypt	Spadix stems	-	0.61 – 0.81	23.4	26.0 – 34.6	[94]
Iran	Leaflet	-	1.41	15.18	93.00	[74]
	Rachis	-	1.39	18.10	77.00	
N.S	Mesh	-	80	450 – 550	145 – 160	[95]
Algeria	Petiole	0.86	-	400 – 1,000	-	[76]
	Rachis	0.75	-	600 – 750	-	
	Leaflets	0.83	-	350 – 900	-	
	Mesh	0.79	-	500 – 800	-	
N.S	Mesh	0.92	-	408	-	[96]
Iraq	Mesh	1.00 – 1.98	-	-	-	[97]
N.S	Mesh	0.6 – 0.7	50 – 300	100 – 2,000	150 – 500	[98]

Origin	Fibre Type	Bulk Density (g/cm^3)	Length (mm)	Diameter (µm)	Aspect Ratio	Reference
Morocco	Mesh	0.70	50 – 60	71.4 – 85.7	-	[99]
Algeria	Mesh	0.51 - 1.09	20, 60, 100	100 – 800	12.5 – 300	[22]
Oman	Midrib	1.40	-	150 – 500	-	[85]

Table 10 Average physical properties of date palm fibres and other natural fibres adopted from [12,51].

Fibre Type	Average Density (g/cm^3)	Length (mm)	Diameter (µm)	Specific Modulus (approx.)	Thermal Conductivity (W/m K)
DPF	0.93	20 – 150	100 – 1,000	7.00	0.083
Hemp	1.45	5 – 55	25 – 500	40.00	0.115
Coir	1.20	20 – 150	10 – 650	4.00	0.047
Sisal	1.40	1 – 900	8 – 200	17.00	0.070

2.2.2.3 Mechanical properties of date palm fibres

The mechanical properties of DPF are determined and affected by several parameters such as the cell structure and dimensions, chemical composition, microfibrillar angle, and defects [28,53,59,100]. Mentioning previously the importance of the chemical composition and the cell structure and dimension on the strength of DPF, the microfibrillar angle is highlighted in this Section for its importance of the mechanical properties of DPF. It can be stated that NFs with higher mechanical strength possess higher cellulose content, longer cell length, higher degree of polymerization of cellulose, and lower microfibrillar angle. DPF mechanical properties, such as tensile strength, tensile strain at failure and Young's modulus usually increase as cellulose content and cell length increases [61,101]. Moreover, the microfibrillar angle plays an important role in determining the strength of NFs. It has been reported that the smaller the angle the higher stiffness and strength of DPF while larger angles leads to higher ductility. The mechanical properties of DPF and other NF are shown in Table 11 [76,91].

Table 11 Average Mechanical properties of DPF and other NFs adopted from [76,91]

Fibre Type	Tensile Strength (MPa)	Elongation at break (%)	Young's Modulus (GPa)
DPF	58 – 309	5.0 – 19.0	2.0 – 7.5

Fibre Type	Tensile Strength (MPa)	Elongation at break (%)	Young's Modulus (GPa)
Hemp	350 – 1,100	1.6 – 8.1	30.0 – 70.0
Coir	106 – 220	15.0 – 47.0	4.0 – 6.0
Bamboo	140 – 740	2.0	11.0 – 50.0
Kenaf	250 – 930	1.2 – 7.5	4.3 – 53.0
Sisal	300 – 700	2.0 – 15.0	9.0 – 38.0
Abaca	400	3.0 – 10.0	12.0

2.2.3. Surface treatments of date palm fibre

The characteristics of DPFRC depend mainly on DPF and the matrix interfacial bonding which has a vital role in determining final mechanical properties of the composites [93,102]. DPF are generally hydrophilic due to the presence of hydroxyl groups within its chemical structure [89], on the other hand, most of the thermosets and thermoplastics polymers are hydrophobic. Thus, to improve the characteristics of DPFRC, it is necessary to impart hydrophobicity into the DPF by treating the fibres either chemically, physically or mechanically, in order to improve the interfacial bonding between the DPF and polymer matrix [53]. It is worth noting that only one work has been found on physical treatment of DPF which used corona treatment [15]. The main surface treatments that were reported by several studies on DPF are chemical treatments, discussed in Table 13. In addition, Table 14 summarizes the mechanical properties including the testing parameters of the treated DPF.

2.3.3.1 Water retting

Water retting technique is a process that is used in the last 50 years which employs the action of moisture and micro-organisms on NFs to rot away or dissolve the cellular tissues and impurities from the surface of NFs [103]. However, it has not been widely used as a treatment or pre-treatment method for DPFs. This may be due to the long treatment period, 7 – 14 days, to allow water penetration into the NFs stalk and break the outermost layer which provokes the development of a bacterial community and increase the moisture absorption [104]. Also, the duration of treatment depends on several parameters, such as the type of bacterial inoculum, water type and water temperature. Nevertheless, water retting treating is environmentally friendly and cheap compared to other treatment techniques [103,105]. To date few authors reported soaking DPFs in water bath for few days as a pre-treatment before any further chemical treatment. The water retting process helped in partially removing lignin, hemicelluloses and other constituents from DPF [106,107]. However, more research should

be done on water retting process since the effect of this process on DPF physical mechanical and chemical characteristics has not been investigated.

2.3.3.2 Alkali treatment

Alkaline treatment, also known as mercerization, is one of the most widely adopted chemical treatment process used for treating DPF when used as a reinforcement for composite making due to its low cost and effectiveness in surface modification. Alkaline treatment cleans the surface of the fibre by removing certain amount of lignin, oils and wax that covers the external surface of the fibre cell wall, depolymerizes cellulose and exposes the short length crystallites. In addition, certain amount of hemicellulose is removed which forms a less dense and less rigid interfibrillar region increasing the ability of the fibrils to rearrange themselves in the direction of tensile deformation. Thus, the surface roughness of the fibre increases which improves the matrix/fibre adhesion. Moreover, alkaline treatment disrupts the hydrogen bonding in the structure of the fibre, promotes ionization of the hydroxyl group to the alkoxide, and thus increases its aspect ratio and surface roughness which increases the sites of mechanical interlocking of the fibre, promoting more resin/fibre interpenetration at the surface [43,108]. However, when DPF are exposed to an excess amount of alkaline solution, the fibres start to degrade leading to a damaged and weaker fibres, which leads to a decrease in the mechanical characteristics of DPF.

The optimum efficiency of the alkali treatment on the properties of the DPF and their composites developed depends on several parameters such as alkali solution type and concentration, treatment temperature and time. Following the alkaline treatment, DPF is further washed with acetic acid for few minutes to neutralise the DPF and remove any excess alkali. Equation 1 shows chemical reaction between NaOH and DPF.

$$Fibre - OH + NaOH \rightarrow Fibre - O - Na + H_2O + Surface\ Impurities \qquad \text{Equation 1}$$

The treatment parameters and effect of alkaline treatment on various part of DPT fibres is summarized in Table 12.

2.3.3.3 Soxhlet extraction

Soxhlet extraction is a classic method for solid sample extraction where pure organic solvents, such as dichloromethane and hexane, or mixture of solvents, such as hexane with acetone or dichloromethane are used in different proportions. Major limitations with Soxhlet extraction are the large solvent volumes used and generally long extraction times, more than 24 hours [13,90]. Soxhlet extraction for treating DPF surface has been studied in the work Taha et al., 2006. The treatment lasted 24 hours without specifying the temperature of the solution. DPF

treated with Soxhlet extraction technique using toluene, methanol and acetone at 4:1:1 weight ratio respectively showed positive results regarding the mechanical properties of DPF. The tensile strength and the elongation at break increased by approximately 28% [13]. Furthermore, Sbiai et al. (2008) used Soxhlet extraction technique for treating DPF as a filler for epoxy resin composites. Results showed improved mechanical properties with an increased glass transition temperature that resulted in a lower molecular mobility and water absorption level [68].

2.3.3.4 Silane treatment

Silane are a group of compounds with a chemical formula SiH_4 for inorganic-silane and a chemical formula of $R(CH_2)_n\ Si(OR)_3$ (where n = 0, 1, 1, 3…) for organ-silanes which is used as a coupling agent to increase the interfacial bonding between DPFs and the matrix. Silane coupling agents reduce the number of cellulose hydroxyl groups in the DPF – matrix interface [109,110]. In the presence of water and alcohol, the hydrolysis of the alkoxy group leads to the formation of silanols that reacts with the hydroxyl groups of DPF, forming stable covalent bonds to the cell wall that are physically absorbed onto the DPF surface. Thus, the hydrocarbon chains produced from the silane treatment prevent the swelling of DPF by creating crosslink network due to the covalent bonding between DPF and the matrix [43,108]. The reactions are described in Equation 2 and Equation 3.

$$CH_2CHSi(OC_2H_5)_3 + H_2O + Alcohol \rightarrow CH_2CHSi(OH)_3 + 3C_2H_5OH \qquad \text{Equation 2}$$

$$CH_2CHSi(OH)_3 + Fibre - OH \rightarrow CH_2CHSi(OH)_2O - Fibre + H_2O \qquad \text{Equation 3}$$

2.3.3.5 Maleated coupling agents

Maleated coupling agents are widely used as a compatibilizer that acts as a bonding agent to strengthen composites containing natural fibres and different thermoset and thermoplastic matrices [111]. Maleic anhydride is the most widely used coupling agent being grafted to either polyethylene or polypropylene to produce maleic anhydride-g-polyethylene (MAPE) or maleic anhydride-g-polypropylene (MAPP). The grafting reaction has been debated in the literature. Several studies suggest that the grafting utilizes the carbon–carbon unsaturation of the maleic anhydride group to form the bond to the polymer chain thus leaving the anhydride group free to react as an anhydride in the newly formed polymer [111,112]. The chemical bonding of maleated coupling agents with NF can be illustrated in Figure 13.

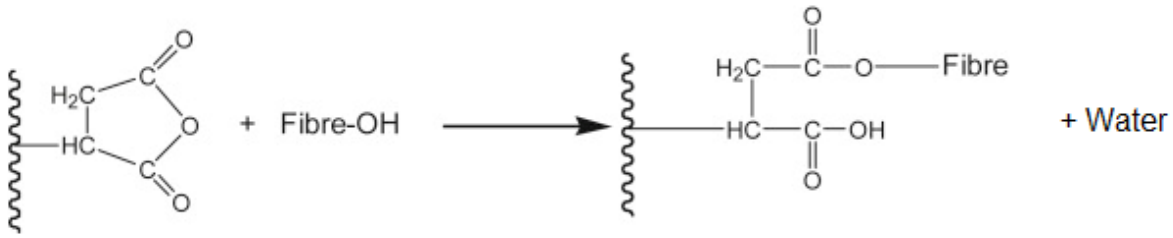

Figure 13 Chemical bonding of maleated coupling agents with natural fibre [112]

2.3.3.6 Peroxide treatment

Peroxide is a specific functional group or a molecule with the functional group RO – OR containing the divalent ion O–O. Organic peroxides tend to decompose easily to free radicals of the form RO.. RO. reacts with the hydrogen group of the matrix and NF. For example, the peroxide initiated free radical reaction between polymer matrix and NF is shown from Equation 4 to Equation 7 [112];

$$RO - OR \rightarrow 2\,RO^{\cdot} \qquad \text{Equation 4}$$

$$RO^{\cdot} + Polymer - H \rightarrow ROH + Polymer^{\cdot} \qquad \text{Equation 5}$$

$$RO^{\cdot} + Fibre - H \rightarrow ROH + Fibre^{\cdot} \qquad \text{Equation 6}$$

$$Polymer + Fibre^{\cdot} \rightarrow Polymer^{\cdot} - Fibre \qquad \text{Equation 7}$$

Dicumyl Peroxide (DCP) belongs to the organic peroxide family that has been used by AlMaadeed and his colleagues as a compatibilizer, not for surface treatment, of DPF [113]. The authors investigated the effect of adding 1%, 2%, and 3% DCP (wt.%) to different composition of date palm wood (DPW) reinforced recycled linear low-density polyethylene (RLLDPE). The addition of DCP was done when both DPW and RLLDPE were melt mixed together. Results showed that the addition of small percentage of DCP increased the mechanical properties of the developed composites [114].

Table 12 Effect of alkaline treatment of DPF and its composites

Fibre	Alkali Solution	Alkali Solution Concentration (wt. %)	Soaking Time (hrs)	Soaking Temperature (ºC)	Results	Reference
Leaf	NaOH	8, 12	2,3	100	Increasing the NaOH concentration along with the soaking time increased the removal of lignin and other surface impurities.	[62]
Mesh		5	2	100	Bonded with polyester polymer matrix, the treatment increased the flexural strength by 24% and the impact properties by 71% of the developed composite.	[64]
Mesh		2	24	-	The mechanical properties of DPF increased where the Young's Modulus, tensile strength and tensile strain increased by approximately 32%, 47% and 25% respectively.	[13]
N.S		2	1	25	Combination of both alkaline solution and silane coupling agent, improved the stress transfer efficiency at the interface by more than 40%.	[109]
Spadix Stems		2,5	2,4,6,24	23	Results contradicts El-Morsy (1980) showing that optimum mechanical properties were achieved at relatively short treatment times of 2 h and 4 h at NaOH solution concentrations of 2% and 5% respectively.	[115]
Mesh		0.5,1,1.5,2.5, 5	1	100	The results revealed that NaOH treatment had a positive effect on the mechanical properties of DPF, where 1% NaOH treatment was the optimum condition to increase the tensile strength of DPF up to 400%.	[116]
Mesh		6	3	95	Increase of both tensile strength and elongation at break by 57% and 2.6% respectively. Also, the effect of alkaline treatment on smaller diameter DPF was greater	[93]
Mesh		3,6,9	24	RT	Results showed that 6% was the optimum concentration, where 3% NaOH solution	[8]

Fibre	Alkali Solution	Alkali Solution Concentration (wt. %)	Soaking Time (hrs)	Soaking Temperature (ºC)	Results	Reference
					exhibited less influence on the mechanical properties of the DPF while 9% NaOH solution weakened and damaged the DPF	
Mesh		1	1	100	Increase in Weibull modulus, which describes the variability in brittleness and strength of DPF, by 15%	[102]
Mesh		6	24	RT	Reduction of the porosity and enhance the interfacial bonding between the epoxy matrix/DPF.	[117]
Mesh		1	24	100	-	[118]

Table 13 Surface treatment conditions of DPF

Fibre	Treatment Type	Additives	Solution (wt. %)	Procedure Notes	Soaking Time (hrs)	Soaking Temp (ºC)	Drying Temp (ºC)	Drying Duration (hrs)	Reference
Leaf (Rachis)	Alkali	NaOH	8, 12	-	2, 3	100	-	-	[62]
		$Ca(OH)_2$	12						
Leaf	Soxhlent Extraction	Ethanol: Toluene	1:2 (v/v)	Fibre extraction not treated for developing the composite	24	-	105	24	[90]
Mesh	-	Commercial detergent	-	-	2	100	-	-	[64]
	Alkali	NaOH	5						

Fibre	Treatment Type	Additives	Solution (wt. %)	Procedure Notes	Soaking Time (hrs)	Soaking Temp (ºC)	Drying Temp (ºC)	Drying Duration (hrs)	Reference
		Dioxin solution	-	This was done on the NaOH treated fibres	24	-			
Leaf	Soxhlent Extraction	Acetone: Ethanol	75:25	-	24	-	80	2	[66]
		Acetic anhydride and Maleic anhydride	-	-	0.5	-	60	24	
Mesh	Soxhlent Extraction	Toluene: Methanol: Acetone:	4:1:1 (T:M:A)	After each treatment the fibres were rinsed with tap water then with diethyl ether and left to dry in air for 24 hrs before placed in the oven for further drying	24	-	60	24	[13]
	Chlorination	Carbon tetrachloride	-						
	Alkali	NaOH	2						
	Alkali	Sodium lauryl sulphate	2						
N.S	Alkali	NaOH	2	-	1	25	60	24	[109]
	Silane	Silane	1	Made in a solution with 0.5% DCP, 90% methanol, 10% water	1	-			
Mesh	Retting in water	Water	-	After retting the fibres are removed and scraped with a sharp knife to remove any foreign matter	72	RT	-	-	[92]
Leaf									
Spadix stems	Alkali	NaOH	2, 5	After treating the fibres with NaOH they are neutralised with dilute acetic acid	2, 4, 6, 24	23	RT	24	[115]
	Acid	Acetic acid	-		-	-			

Fibre	Treatment Type	Additives	Solution (wt. %)	Procedure Notes	Soaking Time (hrs)	Soaking Temp (°C)	Drying Temp (°C)	Drying Duration (hrs)	Reference
Leaf	Soxhlet Extraction	Acetone: Methanol	75:25 (A:M)	-	24	-	-	-	[68]
	Catalytic Oxidation	TEMPO, Sodium Bromide, Sodium Hypochlorite	-	Aqueous HCl is added to adjust the pH and maintaining the pH by adding 0.5 M NaOH. (This was done in a Thermo – controlled bath)	-	-	30	18	
Mesh	Alkali	NaOH	0.5, 1, 1.5 2.5, 5	-	1	100	60	24	[116]
	Acid	NaCl	0.3, 0.9, 1.6						
Mesh	Water	Hot water	-	Before immersing the fibres in hot water, they were washed with tap water to remove sand, dust and other deposits	0.5	50	70	24	[93]
	Alkali	NaOH	6	Solution to fibre ratio 1:40	3	95	Hot air oven	24	
Mesh	Alklai	NaOH	-	Rinsed with fresh water after treatment	24	RT	RT	24	[119]
Leaf	Alkali	NaOH	0.5, 1, 2, 5	-	2	100	70	3	[120]
Mesh	Alkali	NaOH	3, 6, 9	Tried different ratios and the optimal was 6 %	24	RT	RT	24	[8]

Fibre	Treatment Type	Additives	Solution (wt. %)	Procedure Notes	Soaking Time (hrs)	Soaking Temp (°C)	Drying Temp (°C)	Drying Duration (hrs)	Reference
Frond	Alkali	NaOH	0.5 mol/L	Silane treatment applied to NaOH treated fibres	2	-	Air dried	-	[121]
	Silane	Phenlysilane	2		24	-	60	-	
Leaf	Alkali	NaOH	5	-	1	100	60	24	[122]
Rachis	Soxhlet Extraction	Acetone: Ethanol	75:25 (A:E)	-	-	-	80	2	[123]
Mesh	Alkali	NaOH	1	-	1	100	100	1.5	[102]
Spadix stems	Water	Water	-	-	48	RT	-	-	[106]
	Alkali	NaOH	5	Stirred in home-use mixer for 30 min between 80 – 90 °C	3	90	-		
	Acid	Acetic acid	5	Done for treated fibres to remove excess NaOH then washed with cold water (neutralize the fibre)	-	-	120	3	
Leaf	Alkali	NaOH	5	-	1	80	60	24	[75]
		Water: Benzene			0.25	85	-	-	
	Acid	Acrylic acid	0.3 M		-	-	80	24	
Mesh	Alkali	NaOH	6	Before treating the fibres were washed with water & 2% detergent then dried for 48 hours at room temp	24	RT	RT	24	[117]

Fibre	Treatment Type	Additives	Solution (wt. %)	Procedure Notes	Soaking Time (hrs)	Soaking Temp (°C)	Drying Temp (°C)	Drying Duration (hrs)	Reference
Spadix stems	Alkali	NaOH	0.5, 1, 2, 3	Sulphuric acid is applied to the NaOH treated fibres then the fibres are dried	12, 24, 48 72, 96	23	-	-	[124]
	Acid	Sulphuric acid	1		-	0.25	70	5	
Mesh	Salt Water	NaCl	3.5	-	48	-	50	-	[125]
	Acid	Maleic acid	5	-	20	-	-	-	
Leaf	Acid	Acrylic acid	0.3M	Fibres were first washed with alkaline solution (1 g/l NaOH and 6 g/l NaCl) for 15 min	-	-	80	24	[75]
	Alkali	NaOH	5	-	1	80	60	24	
Mesh	Alkali	NaOH	1	-	1	100	70	24	[118]
Leaf	Alkali	NaOH	1	Washed and dried before treatment. Neutralized with acetic acid	12	RT	Air drying	72	[126]
Mesh	Alkali	NaOH	5	After NaOH treatment fibres were washed in HCL solution to neutralize the fibres then distilled water	1	-	65 – 70	3	[127]
Leaf	Water	Water	-	It was left to rot afterward cleaned and dried	480	-	100	24	[128]
Mesh/	Alkali	NaOH	5	Water	-	-	-	-	[129]

Fibre	Treatment Type	Additives	Solution (wt. %)	Procedure Notes	Soaking Time (hrs)	Soaking Temp (°C)	Drying Temp (°C)	Drying Duration (hrs)	Reference
Bunch/ Leaflet		NaOH	1	Ultrasound	-	-	-		
		NaOH + Enzyme	1	Enzymatic treatment followed NaOH in water and ultrasound	-	-	-	-	
Frond	Alkali	NaOH	1	-	2	-	-	-	[130]
Spadix stems	Water	Water	-	-	48	RT	-	-	[107]
	Alkali	NaOH	5	-	3	80 – 90	-	-	
Rachis	Soxhlet extraction	Toluene: Ethanol	38:62 (T:E)	-	-	-	80	2	[131]
N.S	Alkali	NaOH	2, 5, 10	-	1	25	80	24	[110]
Mesh	Water	Water	-	NaOH treated fibres were dipped in the acetic acid solution then washed and dried	48	-	120	3	[81]
	Alkali	NaOH	5		3	90	-	-	
	Acid	Acetic acid	5		-	-	120	3	
Leaf	Alkali	NaOH	1	-	1	80	60	24	[132]
Petiole/Trunk	Water	Water	-	The fibre was treated with NaOH directly after water retting then cleaned under acid solution for 10 minutes	24	-	-	-	[133]
	Alkali	NaOH	5		24, 48, 72	-	-	-	
N.S	Alkali	NaOH	1	-	1	100	60	24	[134]

Fibre	Treatment Type	Additives	Solution (wt. %)	Procedure Notes	Soaking Time (hrs)	Soaking Temp (ºC)	Drying Temp (ºC)	Drying Duration (hrs)	Reference
-	Alkali	NaOH	5	-	1	RT	80	24	[110]
	Silane	3-mercatopropyl-trimethoxysilane & 3-aminopropyl-trimethoxysilane	0.1, 0.5, 1, 2	Done for alkali treated DPF and prepared using methanol/water (80/20: wt/wt) stirred for 30 min	24	RT	80	-	
Mesh	Alkali	NaOH	1	Just washed	-	-	RT	24	[135]
		Acetone: Ethanol	3:1						
Mesh	Natural	Gum Arabic	-	A solution is made by dissolving Gum Arabic in water	-	-	Outdoor Environment	Few days	[136]
Midrib	Alkali	NaOH	10	Neutralized with dilute acid	6	-	70	3	[85]

Table 14 Mechanical properties and testing parameters of single DPF testing and DPF pull-out testing

Fibre	Template & Dimensions (mm)	Window Dimensions (mm)	Gauge Length (mm)	Glue Type	Crosshead Speed (mm/min)	Treatment Technique	Tensile Strength (MPa)	Young's Modulus (GPa)	Tensile Strain (%)	Reference
Mesh	Sheet of paper 50 x 20	20 x 10	20	Epoxy resin	1	Untreated	178.20	5.36	11.44	[13]
						NaOH	262.60	7.07	14.34	
						$NaC_{12}H_{25}SO_4$	204.70	4.43	16.48	
						CCl_4	180.60	5.24	10.31	

Fibre	Template & Dimensions (mm)	Window Dimensions (mm)	Gauge Length (mm)	Glue Type	Crosshead Speed (mm/min)	Treatment Technique	Tensile Strength (MPa)	Young's Modulus (GPa)	Tensile Strain (%)	Reference
						Toluene/ Methanol/ Acetone	227.00	4.46	14.66	
Mesh	ASTM-D3379-75					Retting in water	459.00	1.910	24.00	[92]
Leaflets							309.00	11.32	1.40	
Spadix stems	-	-	20	-	1	NaOH (2 %)	680.00	15.50	5.30	[115]
						NaOH (5 %)	600.00	19.50	5.00	
Spadix stems	Stiff galvanic steel 50 x 15 x 1	20 x 10	50	-	1	Untreated	200.00	9.50	-	[116]
						NaOH (0.5%)	450.00	161.00	-	
						NaOH (1 %)	850.00	150.00	-	
						NaOH (2.5%)	375.00	140.00	-	
						NaOH (5%)	210.00	65.00	-	
Mesh	ASTM C1557-03				1	Untreated	233.00	7.10	10.30	[93]
						NaOH (6%)	366.00	5.45	12.80	
Leaflet	ASTM D 638-02 & ASTM D 3822-07		100	ASTM D 638-02 & ASTM D 3822-07	5	Untreated	95.00	6.10		[120]
						NaOH (0.5%)	82.00	4.90	-	
						NaOH (1%)	72.00	5.30	-	
						NaOH (2%)	70.00	4.90	-	

Fibre	Template & Dimensions (mm)	Window Dimensions (mm)	Gauge Length (mm)	Glue Type	Crosshead Speed (mm/min)	Treatment Technique	Tensile Strength (MPa)	Young's Modulus (GPa)	Tensile Strain (%)	Reference
						NaOH (5%)	58.00	5.90	-	
Mesh	ASTM STP 452				1	NaOH (3%)	425.00	-	16.00	[8]
						NaOH (6%)	345.00	-	20.00	
						NaOH (9%)	119.00	-	6.00	
Mesh	N.S					Untreated	190.00	5.50	-	[102]
						Water	191.00	6.00	-	
						Heat	200.00	7.50	-	
						NaOH (1%)	300.00	10.00	-	
Leaflets	ASTM-D-638					Untreated	32.43	6.48	4.33	[75]
						NaOH (5%)	33.33	9.70	5.03	
						Acrylic acid (0.3M)	70.27	16.34	5.84	
Mesh	ASTM-D638-10					NaOH (6%)	450.00	2.75	-	[117]
Spadix Stems	ASTM-D-3822-01				1	Untreated	117.00	4.30	3.13	[124]
						NaOH (0.5%) 12 – 96 hrs	178 – 328	5.2 – 11.6	3.26 – 3.98	
						NaOH (1%) 12 – 96 hrs	222 – 276	6.70 – 9.50	3.13 – 3.88	
						NaOH (2%) 12 – 96 hrs	220 – 235	7.20 – 8.20	3.33 – 4.19	

Fibre	Template & Dimensions (mm)	Window Dimensions (mm)	Gauge Length (mm)	Glue Type	Crosshead Speed (mm/min)	Treatment Technique	Tensile Strength (MPa)	Young's Modulus (GPa)	Tensile Strain (%)	Reference
						NaOH (3%) 12 – 96 hrs	224 – 292	7.10 – 10.10	3.67 – 4.04	
Bunch	XP T 25-501-3				5	NaOH (1%) + Enzyme	215.80	5.10	-	[129]
Mesh							246.70	26.10	-	
Leaflet							-	-	-	

2.3. Fibre geometry affecting natural fibre composite properties

Certain characteristics of the NF, as well as the processing techniques used to achieve the desired properties of the fibre reinforced composite, should be considered when selecting a specific NF for composite development. When using NF as a reinforcement in various matrix systems for developing composites with specific engineering properties, several factors such as fibre orientation, fibre dispersion, fibre aspect ratio, fibre loading or volume of fibre, and certain NF characteristics should be considered.

2.3.1. Fibre orientation

NF orientation or direction is a crucial factor that should be considered for achieving specific engineering properties of NFRC. The mechanical properties are superior for unidirectional long NFRPC compared to short randomly orientated NFC. It is very rare to achieve a specified orientation in short fibre reinforced composites. Geethamma et al. (1998) investigated the effect of coir fibre orientation on the mechanical properties of natural rubber composites. The results showed that the performance of any short-fibre-reinforced polymer composite is dependent upon the angle between the directions of fibre orientation and the applied force or, in other words, the extent of fibre orientation. The efficiency of stress transfer is higher if fibres are aligned parallel to the direction of application of force. Thus, processing techniques aim to orient the fibres in the preferred direction to meet the anticipated loads on fabricated products [137].

2.3.2. Fibre dispersion

Filler dispersion is one of the key factors, which affects the mechanical properties of the fibre reinforced polymer composites specifically in the short fibre reinforced composites. It is well reported in the literature that a significant reduction in the tensile and impact properties occurs due to poor dispersion of fibres across the composites. Poor fibre dispersion causes the fibre agglomeration in the composites which creates stress concentration points and leads to sudden mechanical failure. Compatibility between NF (hydrophilic nature) and polymer matrices (hydrophobic) is the major reason for the poor dispersion of the fibres. Compatibility between natural fibres and the polymer matrices can be improved by subjecting to a suitable surface treatment of either natural fibres or polymer matrices. Another important reason which causes the poor dispersion is mixing time during the processing of composites. Higher mixing time gives better dispersion of the fibres across the polymer matrix [138].

2.3.3. Fibre aspect ratio

NF's aspect ratio is defined as the ratio between the length and the width of the fibre. It plays a crucial role in affecting the mechanical properties of the NFRC especially when a polymeric matrix system is used. Ashori and Nourbakhsh (2010) studied the effect of particle size of pine and oak wood reinforced PP composites in the overall mechanical strength of the composite. Results showed that with the increase in the aspect ratio the interfacial bonding between the fibre and the polymer matrix increased which led to an increase in the flexural and tensile strength of the composite [139].

2.3.4. Fibre volume fraction

The amount of fibre loaded into the matrix system plays a crucial role in determining the overall mechanical and thermal properties of the composite developed. Several researchers have reported that the mechanical properties of NFRC decreased significantly with low volume fraction of NF added due to the creation of flaws between the matrix system and the fibre which led to a mechanical failure [38]. Also, at a high fibre volume fraction, short fibres cause agglomeration within the matrix system creating stress concentration points which reduced the overall mechanical properties of the composite [38]. Thus, optimization of fibre volume fraction or fibre loading is very essential to achieve the optimum mechanical properties. Geethamma et al. (1998) stated that the tensile strength of NFC initially drops up to a certain amount of fibre and then increases. This minimum volume of fibre is known as the critical volume above which the fibre reinforces the matrix. The critical volume varies with the nature of both fibre and matrix, fibre aspect ratio, fibre/ matrix interfacial adhesion, etc [137].

2.4. Processing parameters

2.4.1. Drying conditions of date palm fibres

Prior to processing of DPFRC, DPF must be sufficiently dried to prevent hydrolysis which may lead to a lower physical property, such as tensile strength. NF has the tendency to absorb water due to the presence of hemicellulose that give the hydrophilic nature and makes them less compatible with matrix with hydrophobicity properties. Thus, drying natural fibres ensure there is no moisture in the fibre and provides between interfacial bonding. Based on previous applications and research it is recommended to have a moisture level ranging between 1% and 2% for DPFs. This may be achieved by using a vacuum oven then placing the dried DPF and dried polymers in dry sealed bags ready for further processes. Table 15 summarizes the drying conditions for DPF used in DPFRC development. DPF dried in a vacuum oven at 60 – 70^{o}C for 24 hours could reduce the moisture content to the desired range [64,93,122,128,132,140,141]. However, using higher temperature, 95 – 105^{o}C, for 24 hours

might damage the fibre, thus it is advised to dry it for a very short time at high temperatures [102,142]. Still there are no reports that indicate the optimal drying conditions and the effect of the different drying conditions of DPF on the properties of their developed composites.

Table 15 Drying parameters of DPF [12]

DPF Type	Temperature (ºC)	Duration (hrs)	Reference
Mesh	60	24	[64]
Mesh	70	24	[93]
DPWF	65	24	[140]
N.S	70	24	[141]
Leaf	60	24	[122]
Mesh	100	1.5	[102]
DPWF from leaflet, leaf and rachis	100	24	[74]
Leaf	80	1	[142]
Leaf	70	24	[75]
Leaf	50	24	[128]
Leaf	60	24	[132]
Mesh	105	24	[87]

2.4.2. Melt mixing/ compounding parameters for date palm fibre composites fabrication

Before processing DPFRC, the polymer matrix and DPF are usually blended by melt-mixing using a compounder to ensure a homogenous mix of the polymer and the DPF. Additives such as plasticizers and coupling agents are added at that stage. Afterwards, the product is grinded and is ready to be used for the different types of processing techniques, single screw extruder or hot press, compression moulding. Table 16 summarizes the melt-mixing parameters for polymer matrices along with DPF reinforcements and their additives to increases the interfacial bonding between the polymer matrix and the DPF.

Table 16 Melt-mixing parameters of date palm fibre [12]

Polymer Blend	Additives	Mixing Temperature (ºC)	Mixing Speed (rpm)	Mixing Time (min)	Reference

PP/Rachis	MAPP	-	40	10	[123]
LLDPR/DPWP	DCP	140	35	10	[113]
PVP/Leaf fibre	Surface treatment of fibres	160	100	5	[75]

2.4.3. Extrusion processing parameters for date palm fibre composites fabrication

Extrusion is a core process in processing composites which transforms polymer pellets from solid to liquid stage in an extruder. The temperature at different zones of the extruder and the die have a crucial role in extruding DPFRC. This is because polymers degrade at high temperatures and at low temperatures they shear with poor homogeneity. Consequently, DPF degrade, at high temperatures, thus the zone temperature is critical. At the inlet of the extruder, the highest temperature is normally used to ensure the melting of the polymer without degrading. Along the extrusion process, at different zones the temperature either decreases or remains the same, while the temperature decreases reaching its lowest at the die, where composite mix is extracted. Thus, to achieve an ideal melt viscosity, and ensure that all the crystalline domains of the semi-crystalline polymers are melted, the temperature of the extruder zones is usually set near its melting temperature.

The proportion of flight length of the screw to its external width, L/D ratio, decides the shear and residence arrangement time of the polymer melting. Screws with an extensive L/D ratio give more prominent shear heating, longer melting time, and better mixing in the extruder. The reported research on DPFRC was processed by using conventional screws equipped with unspecified L/D ratio. Another critical screw parameter is the pressure compression ratio, which is the proportion of the flight depth in the feed segment to the flight depth in the metering segment. The more significant the pressure proportion a screw has, the greater the shear warming it gives [143]. The speed of the screw determines how fast the polymer is extracted from the extruder. Table 17 summarizes the extrusion parameters for DPFRC reported to date by different researchers.

Results show a very wide range of temperature at different zones which has an impact on the degradation of DPF. It has been reported by Abu-Sharkh and Hamid that no deterioration of properties is noticed when processing temperatures of the extruders temperature zones are kept under 200°C [90]. However, few research works have given the zone temperature higher than 200°C but did not mention its effect on DPF properties.

Table 17 Extrusion processing parameters of date palm fibre [12]

Polymer Blend	Additives	Zones Temp (°C)	Screw Speed (rpm)	Screw Length (mm)	L/D Ratio	Reference
HDPE/Petiole	MAPE	170	30	-		[70]
HDPE/Rachis						
HDPE/Trunk						
RPP/DPWF	-	190 – 230		-		[140]
PP-EPDM/	MAPP	160 – 200	60	-		[141]
PLA/N.S DPF	-	175 – 200	63	-		[15]
PC/Leaf		120 – 240	25 – 55	750	30	[144]
PVC/Leaf		100 – 220	25 – 50			
PS/Leaf		120 – 180	70			
RPET/Leaf	-	225 – 245	55	-		[122]
LDPE/Leaflet Flour	MAPE	145 – 150	7	-	21	[74]
Leaf Flour						
Rachis Flour						
RHPE/RLDPE/RPP/ Leaf	MAPE	180 – 220	60	-		[132]
PP/N.S	MAPP	100 – 200	-		40	[134]
PCL/Mesh	-	-	100 & 400	1,018	36	[145]
PHB/Mesh	-	175	200	-	-	[146]

2.4.4. Injection moulding processing technique

Injection moulding is the most regularly utilized strategy being portrayed by precisely dimensioned items and by high creation rates. An extruder and injection moulding machine are nearly the same, however the distinction between the two methods is their screw choices and the injection nozzle. Injection moulding procedure includes softening the DPF/polymer by an extruder having a reciprocate screw that rotates and moves forward and in reverse, to infuse the liquid DPF/polymer matrix into a mould. The procedure is described as that at first the polymer pellets are extruded by inserting the pellets at the inlet and warming them up till their liquefying melting temperature in the barrel. Afterwards, the moulds close, nozzle opens, and the screw moves by injecting the molten polymer/DPF matrix through the nozzle into the

mould. The mould is outfitted with a cooling framework giving controlled hardening and cooling of the DPF/polymer matrix, and the screw is maintained at the infusion position by keeping pressure steady since polymer/DPF matrix shrinks among cooling. Finally, while the DPF/polymer matrix remains to cool in the mould, the nozzle is shut off, and the screw starts to reverse backwards under a control back pressure to ensure it is dimensionally stable to withstand the opening stroke of the moulds.

Injection moulded DPFRC might be subjected to several limitations such as torque, if the screw has a high compression ratio. Also, the cycle time is often minimized to maximize the production. This can be achieved by minimizing the duration of the non-process events such as mould closing and opening time, and by transferring the partially cooled injected mould to a post cooling machine, to provide enhanced cooling by forced air or by direct contact on a cooled surface. Moreover, a decrease in moulds temperature has a crucial role in increasing the heat extraction rate from the composite. Thus, it is crucial to understand the effect of each parameter of the processing process and try to optimise its parameters.

2.4.5. Compression moulding/ Hot-press moulding parameters for date palm fibre composite fabrication

Compression moulding is a process where a preheated polymer is compressed into a heated mould cavity under specified pressure for a certain period, usually couple of minutes. This process can produce objects with different lengths, thickness and complexities depending on the mould specifications. Compression pressure, temperature and time of compressions are the important parameters that affect the characteristics of the produced composite. Finally, cooling after the heating compression is crucial.

The most crucial parameter that should be considered is initial determination of the correct amount of material required to fill the mould which could also determine the sufficient temperature to melt the polymer and not degrade the DPF processed. Meanwhile, the minimum time required to heat the material is very important to avoid the degradation of the material. Table 18 summarizes the processing conditions from literature using hot press/compression moulding technique.

Table 18 Hot-Press/Compression moulding processing parameters of DPF

Polymer Blend	Temperature (ºC)	Weight (Tons)	Pressure (MPa)	Duration (min)	Thickness of composite (mm)	Reference
HDPE/Petiole	170	-	14.71	-	-	[70]
HDPE/Rachis						

Polymer Blend	Temperature (ºC)	Weight (Tons)	Pressure (MPa)	Duration (min)	Thickness of composite (mm)	Reference
HDPE/Trunk						
PC/Leaf	185	118	-	-	10 ± 0.5	[144]
PVC/Leaf	185	119				
PS/Leaf	160	119				
PLA/DPF	165	-	0.30	-	-	[15]
Rachis	130	5	-	8	-	[123]
TPS/ Spadix Stems	160	-	5.00	30	-	[106]
LLDPR/DPWP	140	-	-	1	1	[114]
Leaflet Flour	160	-	0.30 – 0.35	6	5	[74]
Leaf Flour						
Rachis Flour						
TPS/Spadix stems	160	-	5.00	30	2	[107]
TPS/Mesh	130	5	-	60	3	[81]
EPS/Leaflet	-	-	1.00	10	30, 40	[147]
Mesh powder/ RLLDPE	190	-	-	-	-	[136]

2.5. Polymer composites reinforced with date palm fibres

2.5.1. DPF/Thermoplastic composites

Research on DPF reinforced thermoplastic composite was initially done by Al-Sulaiman and his colleagues fabricated panels of date palm leave reinforced composites, were two types of matrix were selected. The authors have found that all panels exhibit a very low thermal conductivity [148]. Abu-Sharkh and Hamid [90], investigated the degradation and stabilization of DPF/PP composite under artificial and natural weathering conditions showed that DPF/PP reinforced composite possessed higher stability than PP itself under both accelerated and weathering exposures, and the compatibilized DPF/PP reinforced composite showed substantial degradation compared to un-compatibilized DPF/PP reinforced composites The effect of DPF rachis, trunk and petiole, at different loading concentrations, 20%, 30% and 40%, on the mechanical properties of high density PE (HDPE) reinforced composites was also investigated, and the results showed that the addition of more than 20 wt.% of DPF from the different parts of DPF produced better mechanical properties than pure HDPE. The optimal fibre content that attained the highest strengths was 40 wt.% for the trunk DPF, increasing

both the tensile and flexural strength by 17% and 37% respectively. On the other hand, 30 wt.% was the optimal fibre loading for both rachis and petiole DPFs, increasing the tensile strength by 15.5% and 6%, and the flexural strength by 8.5% and 60% respectively [70]. Additionally, AlMaadeed and his colleagues investigated the mechanical and thermal properties of recycled PP (RPP) based hybrid composites of date palm wood flour (DPWF)/glass fibre although only one composite was made from RPP reinforced with 30% DPWF and concluded that RPP reinforced DPWF composite has 10% higher tensile strength than pure RPP, where the tensile strength increased from 14.8 MPa to 16.5 MPa. However, the melt flow index (MFI) decreased by 45%, from 1.78 g/10min to 1.23 g/10min [140]. The addition of the treated DPF with 5% NaOH aqueous solution to reinforce recycled PET matrix was reported to increase both the tensile and flexural strength with the increase of the concentration of DPF, 5%, 10% and 15% in the composite. The incorporation of DPF lowered the thermal stability, but increased the overall degree of crystallinity of the composites [149]. AlMaadeed and his fellow researcher (2014) also investigated the mechanical properties of date palm wood powder (DPWP) as a filler for recycled linear low-density PE (LLDPE) composite with filler concentration ranging between 10 – 70 % at 10% increment. The Young's modulus of the composites increased significantly with increasing DPWP concentration, reaching 645% (308 MPa to 1,989 MPa) higher at 70% filler than that for the neat RLLDPE. The stress at break of the composites decreased sharply with increasing DPWP concentration and the composite became brittle when filled with more than 10 wt. % DPWP [113].

Research done on thermoplastic starch (TPS) as a source of biodegradable matrices to develop hybrid composites with DPF reinforcement showed that the thermal stability increased as the DPF content increases. Also, results showed that the tensile strength and modulus increased by 760% (4.8 MPa to 36.48 MPa) and 350% (0.8 GPa to 2.8 GPa) respectively for 50 wt.% DPF reinforcement compared to pure TPS with no DPF reinforcement added. Flexural strength and modulus showed similar behavior. At 60 wt.% fiber content and above, the mechanical properties started to deteriorate as a result of the increase in the composites porosity [106]. Afterwards, Saleh et al. [81] reported similar results as Ibrahim et al. (2014) that DPF reinforced TPS matrices had the highest fatigue and flexural strengths at 50 wt.% DPF content. Furthermore, using a mixture of recycled HDPE, LDPE, and PP with 1 % maleic anhydride as a compatibilizing agent was effective for chemical modification of the DPFRC which promoted dispersion and better interfacial adhesion between the polymer matrices and DPF. Thus, the mechanical properties of the composites were improved where results showed a noticeable increase in both tensile strain and modulus but a large decrease in the percentage of elongation at break. The physical properties of the composites showed good resistance to alkalis and acids. The polymer melting and crystallization temperature were not affected by

the addition of DPF or maleic anhydride, indicating that the additives did not affect the thermal behavior of the polymer matrices.

During the latest study reported by Alshabanat, the biodegradation of linear low-density PE (LLDPE) reinforced with powder DPF composites is affected by the fibre treatment, UV stabilizers, antiblock additives and polymer additives. Results showed that the composite containing UV stabilizer degraded faster than the composite containing antiblock additive which is due to the difference in the chemical additives within them [136]. More comprehensive summary on mechanical properties of DPF reinforced thermoplastic composites is demonstrated in Table 19.

Table 19 Mechanical properties of DPF/Thermoplastic composites

Polymer Matrix	Filler Type	Fibre Loading Wt.%	Processing Technique	Chemical Treatment	Compatibilizing agent	Optimal Additive Wt.%	Optimal Fibre Wt.%	Optimal Fibre dimension (mm)	Ts (MPa)	Tm (GPa)	Fs (MPa)	Fm (GPa)	Reference
PP	Leaf	27.39, 29.19	Extrusion & Injection Moulding	Ethanol: Toluene	-	-	-	4.70 (length)	-	-	-	-	[90]
HDPE	Petiole	20, 30, 40	Extrusion & Compression Moulding	Not Treated	MAPE	2	30	40.00 (length)	17.00	1.01	37.00	1.85	[70]
	Rachis						30		20.00	1.05	30.00	1.58	
	Trunk						40		19.80	1.50	33.00	1.58	
RPP	DPWF	30	Extrusion & Injection Moulding	Not Treated	-	-	30	-	16.50	1.10	-	-	[140]
PP-EPDM	N.S	5, 10, 20, 30	Extrusion & Injection Moulding	Not Treated	MAPP	2	20	-	-	-	-	-	[141]
R-HDPE	Mesh	6	Compression Molding	NaOH	-	-	6	-	38	-	-	-	[119]
PLA	N.S	30, 40	Extrusion & Compression Molding	Not Treated	-	-	30	(1.5 – 2.0 diameter)	48.45	-	-	-	[15]
				Corona Treatment					57.35	-	-	-	
R-PET	Leaf	5, 10, 15	Extrusion & Injection Moulding	5% NaOH	SEBS-g-MA	10 (phr)	15	-	30.00	20	51.00	2.25	[122]
PP	Rachis	5, 10, 15, 20, 25, 30	Melt Mixing & Compression Moulding	Soxhlet Extraction	MAPP	2	25	10 (length) (0.5 diameter)	31.00	1.30	-	-	[123]
RLLDPE	Wood powder	10, 20, 30 40, 50, 60 70	Melt Mixing & Compression Moulding	Not Treated	DCP	2	70	0.25 – 1.00 (length)	-	-	-	-	[113]
TPS	Spadix stems	20, 40, 60, 80	Compression Moulding	5% NaOH	-	-	50	13.80	31.00	2.80	73.60	5.00	[106]

Polymer Matrix	Filler Type	Fibre Loading Wt.%	Processing Technique	Chemical Treatment	Compatibilizing agent	Optimal Additive Wt.%	Optimal Fibre Wt.%	Optimal Fibre dimension (mm)	Ts (MPa)	Tm (GPa)	Fs (MPa)	Fm (GPa)	Reference
				+ 5% Acetic acid									
RHDPE+ RLDPE+ RPP	Leaf	20	Extrusion & Injection Moulding	Not Treated	MAPE	1	20	20.00 (length)	21.00	0.81	-	-	[150]
LLDPE	Leaflet Flour	45, 60, 75	Extrusion & Compression Moulding	Not Treated	MAPE	2	45	1.69 – 3.42 (length)	13.00	-	29.50	2.80	[74]
	Leaf Flour								12.50	-	27.00	0.80	
	Rachis Flour								12.50	-	26.00	0.75	
PVP	Leaf	10,20,26 30,40	Melt Mixing & Injection moulding	Acrylic acid	-	-	26	5.00 (length)	21.77	-	31.70	3.35	[75]
PVP	Leaf	10, 20, 26 30, 40	Injection Moulding	Acrylic acid	-	-	26	-	-	-	-	-	[75]
PP-EPDM	Mesh	5, 10, 20, 30	Extrusion & Injection Molding	NaOH	MAPP	2							[118]
PP/Flax	Leaf	10, 20, 30		NaOH	-	-	20	-	24	-	-	-	[126]
ABS	Leaf	5, 10, 20	Injection molding	Water retting	-	-	-	-	-	-	-	-	[128]
LDPE	Frond	20	Hand lay-up, Oven, and Compression Moulding	2% NaOH	-	-	20	1250 (length)	8.2	-	-	-	[130]
TPS	Spadix stems	50	Compression Moulding	5% NaOH	-	-	50	-	28.20	3.85	-	-	[107]
TPS	Mesh	20, 50 70	Compression Moulding	5% NaOH	-	-	50	20 – 30 (length)	-	-	78.00	3.10	[81]

Polymer Matrix	Filler Type	Fibre Loading Wt.%	Processing Technique	Chemical Treatment	Compatibilizing agent	Optimal Additive Wt.%	Optimal Fibre Wt.%	Optimal Fibre dimension (mm)	Ts (MPa)	Tm (GPa)	Fs (MPa)	Fm (GPa)	Reference
HDPE + LDPE + RPP	Leaf	10, 20, 30	Extrusion & Injection Moulding	1% NaOH	MAPE	1	10	-	25.00	0.58	-	-	[132]
PCL	Mesh	20	Extrusion	Not Treated	-	-	20	10.00 (length)	25.70	0.28	-	-	[145]
EPS	Leaflets	70, 75, 80	Compression Moulding	Not Treated	-	-	70	0.1 – 0.315 (length)	-	-	2.90	0.76	[147]
								0.315 – 0.5 (length)	-	-	2.45	0.78	
								0.5 – 1.0 (length)	-	-	1.30	0.3	
RLLDPE	Mesh powder	5	Compression Moulding	Gum Arabic	-	-	-	-	-	-	-	-	[136]
PP	Various	20, 40, 60	Melt Mixing & Injection moulding	Not Treated	MAPP	5	60	-	35.35	4.99	62.30	4.99	[86]
PHB	Mesh	10, 20, 30, 40, 50	Extrusion & Compression moulding	Not Treated	-	-	-	0.212 (length)	-	-	-	-	[146]
PP	Leaflets	10, 20, 30	Extrusion & Compression moulding	4% & 8% NaOH	-	-	10	10.4 (aspect ratio)	19.85	0.72	23.5	0.60	[151]

2.5.2. DPF/Thermoset composites

Research on DPF reinforced thermoset composites was firstly done by Al Kaabi and his colleagues in investigating different DPF loading, 6 – 10%, treated with three different chemicals. They also investigated the effect of DPF length on the mechanical properties of the composite. Their results showed that the optimal fibre loading was 9% treated with 5% NaOH solution for 2 hours. Where the DPFRC had higher flexural strength, flexural modulus and impact strength than the thermoset polymer by approximately by 66%, 50%, 475% respectively [64]. The effect of a higher fibre loading, 20 – 60%, and the fibres orientation, woven or unidirectional, on the mechanical properties of DPFRC without any prior treatment of the DPF was also reported, showing that both unidirectional and woven orientation DPF reinforced polyester resin had greater mechanical properties than neat polyester resin, however unidirectional orientation had higher mechanical properties than woven orientation reinforced DPF where the flexural strength and elongation increased with the increase of fibre loading. On the other hand, the impact strength decreased with the increase of DPF loading. The flexural strength and elongation of the optimum unidirectional orientation DPF (60% loading) reinforced polyester composites increased approximately by 55% and 10% respectively compared to neat polyester composites. However, the inter-laminar failure and delamination always occurred along the fibre/matrix interface [152]. Using poly epoxy as a matrix with varying DPF loadings, 5 %, 10 %, and 15%, subjected to oxidation using soxhlent extraction, was also investigated and the results showed that there is a slight increase in flexural modulus of the reinforced composites with the increase of DPF loading by 19% and a decrease in the stress at break or elongation and impact strength with the increase of DPF loading by 71% and 87% respectively [153].

The effect of various diameters of DPF treated in 6% NaOH solution on the strength of reinforced epoxy composites was reported that the mechanical properties increased with the decrease in diameter of treated DPF. DPF with diameter size ranging from 200 – 400 micrometres has 120% and 13% higher tensile strength and Young's Modulus respectively than DPF diameter size ranging between 600 – 800 µm. The elongation strain of untreated DPFRC is higher than the treated DPFRC by 65%, 77%, and 15% for DPF diameters ranging between 200 – 400, 400 – 600, and 600 – 800 micrometres respectively [93]. A recent investigation on the effect of different DPFs from different parts of DPT on epoxy matrix composites showed an increase in mechanical properties of epoxy composites, with the tensile strength, tensile modulus, flexural strength, flexural modulus and impact strength showing an increase using different types of DPTF. The highest increase was with the reinforcement of date palm fruit bunch stalk, having higher tensile strength, tensile modulus, flexural strength, flexural modulus and impact strength than neat epoxy resin by 95%, 405%,

243%, 179% and 119% respectively. However, the incorporation of DPF in epoxy resins resulted in an increase in the water absorption with time which can be explained due to the hydrophilic nature of DPF [83]. Likewise, different DPF loadings, 45%, 50%, and 60% showed the epoxy DPF composites resulted in an increase in flexural strength and flexural modules by approximately 25% when loaded with 50% DPF [84]. More comprehensive summary on mechanical properties of DPF reinforced thermoset composites is given in Table 20.

Table 20 Mechanical Properties of DPF/Thermoset composites

Polymer	Fibre Type	Fibre Loading Wt%	Processing Technique	Optimal Fibre Treatment	Optimal Treatment Wt.%	Optimal Fibre Wt.%	Optimal Fibre L & D (mm)	Ts (MPa)	Fs (MPa)	Fm (GPa)	Is (KJ/m^2)	Reference
Polyester resin (8120TEC)	Mesh	6,7,8,9,10	Compression Moulding	NaOH	5	9	2	-	70.00	6.30	11.80	[64]
Polyester resin (8420-P) Hardned (MEKP)	N.S	20, 40, 60	Resin Transfer Moulding	No Treatment	-	60	-	86.00	-	4.25	0.21	[152]
Epoxy Resin	Leaf	17	Contact Method	Soxhlet Extraction	-	17	15 length (1.0 diameter)	-	-	1.92	-	[66]
				Anhydrides						2.49		
Unsaturated polyester resin (G154TB)				Soxhlet Extraction						1.92		
				Anhydrides						1.71		
Polyepoxy (epoxy with amine curing agent)	Leaf	5, 10, 15	Resin Transfer Moulding	Soxhlet Extraction	-	15	2 – 10 length (0.2 – 0.8 diameter)	-	-	3.25	2.10	[153]
Epoxy Resin (YD-128) Hardend (D-230)	Mesh	10	Hand lay-up technique	NaOH	6	10	10	366.00	-	-	-	[93]
Polyester resin (Siropol 7440)	Frond	10, 20, 30, 40, 50, 60, 70	Hand lay-up technique	NaOH & Silane	2	20	-	-	-	-	-	[121]
Epoxy Resin (R246TX) Kinetix (H160)	Mesh	35	Compression Moulding	NaOH	6	35	0.3 (diameter)	65.00	-	-	-	[117]
Polyester Resin Hardened (Methyl Ethyl	Mesh	40	Hand lay-up technique	Alkali and Acid	-	40	-	-	-	-	-	[125]

Polymer	Fibre Type	Fibre Loading Wt%	Processing Technique	Optimal Fibre Treatment	Optimal Treatment Wt.%	Optimal Fibre Wt.%	Optimal Fibre L & D (mm)	Ts (MPa)	Fs (MPa)	Fm (GPa)	Is (KJ/m^2)	Reference
Keton Peroxide Mekp)												
Epoxy Resin (R246TX) Kinetix (H160)	Mesh	35	Hand lay-up technique	-	-	35	80 length (0.5 diameter)	66.2	-	-	-	[95]
Epoxy Resin (A – B)	Leaf	31.4	Compression Moulding	No Treatment	-	31.4	-	-	-	-	-	[142]
Polyester Resin	Date palm seed powder											[154]
Epoxy Resin	-	50	Hand lay-up technique	NaOH Treatment	5	50	3	21.29	35.28	-	2.63	[127]
							6	23.12	39.36	-	3.05	
							9	24.98	47.67	-	3.52	
							12	27.22	81.75	-	4.11	
							15	25.86	48.24	-	6.41	
Epoxy Resin	Stem	5, 10, 15	Hand lay-up technique	-	-	-	-	12.5	29.03	-	-	[155]
Polyester Resin	-	30	-	-	-	-	-	-	-	-	-	[156]
Epoxy Resin (LY 556) Hanrdend (HY951) + E-Glass fibre	Mesh	10, 20, 30	Hand lay-up technique	Washed with aceton, ethanol and NaOH	-	20	2 Length	74.00	42.72	3.98	48.5	[135]

Polymer	Fibre Type	Fibre Loading Wt%	Processing Technique	Optimal Fibre Treatment	Optimal Treatment Wt.%	Optimal Fibre Wt.%	Optimal Fibre L & D (mm)	Ts (MPa)	Fs (MPa)	Fm (GPa)	Is (KJ/m^2)	Reference
Epoxy Resin Hardened Jointmine 905-3S	Leaf	50	Hand lay-up technique	No Treatment	-	50	0.8 – 1.0 (diameter)	26.45	77.65	4.55	62.65 (J/m)	[83]
	Bunch							40.12	110.16	6.43	99.45 (J/m)	
	Mesh							36.17	98.46	5.54	87.34 (J/m)	
	Trunk							28.44	89.43	5.12	71.07 (J/m)	
Epoxy Resin (Jointmine 905-3S)	Mesh	40, 50, 60	Hand lay-up technique	Not Treated	-	50	N.S (0.8 – 1.0 mm diameter)	-	32.5	3.30	-	[84]
Polyester Resin	Midrib	50	-	NaOH	10	50	10 (length)	14.34	43.2	-	11.23 (J/mm)	[85]
Epoxy Resin (D.E.R 331) Hardened Jointmine 905-3S	Stems	40, 50, 60	Mechanical stirring	-	-	50	-	25.77	-	-	98.71 (J/m)	[157]
Phenolic Resin (Grade PH-4055)	-	40, 50, 60	Compression Moulding	Not Treated	-	50	1	15.03	-	-	5.5	[158]
Biophenolic Resin (Grade PH-4055)	-	40, 50, 60	Compression Moulding	NaOH	6	50	1	19.50	37.21	4.52	-	[159]

2.6. Inorganic matrix reinforced with date palm fibres composites

2.6.1. DPF/Cementitious material composites

Kriker et al. (2005) reported that water curing condition has a better effect on the ductile behaviour of concrete but not on the first crack strength compared to air curing. Also, it was reported that in dry-hot environment, the first crack strength of fibre-concretes decreases with time and with increasing fibre reinforcement percentage and length. By observing the micro-structure of the fibre–matrix interface cured in hot-dry and water environments, it can be seen that the voids around the fibres are large for the dry environment, thus affecting the mechanical properties of the composites developed [20]. Afterwards, Kriker et al. (2008) also investigated the durability of concrete cured under different conditions against its resistance to high alkaline solutions. Results showed that after six months in $Ca(OH)_2$ solution the MDPSF retained about 69%, 40% and less than 10%, and in NaOH solution they retained about 76%, 46%, and 16% of their original strength, for the diameters, 0.8, 0.6, and 0.4 mm, respectively. Also, the DPF extracted from concrete in the hot dry conditions and are slightly more effected than that cured under wet conditions [91]. Moreover, another research reported on Ozerkan et al. (2013), DPF loading content greater than 2%, showed poor workability as well as difficulty in preparing and obtaining monolithic compacted samples due to excessive separation of mortar components was encountered. Hence, it is recommended that such DPF inclusion in mortars to be limited to less than 2% by weight. DPF treated with 0.173% $Ca(OH)_2$ displayed better tensile strengths and stiffness properties than those treated with NaOH and hence, the former was chosen as preferred pre-treatment for the bundled fibres used in the mortar mixes. The setting time of the mortar pastes was observed to be prolonged with the increase in the fibre content. Water absorption rate and capacity decreased with increasing weight percent of palm fibre in the mixes. Results also indicated that inclusion of fibres improves the flexural strengths. However, compressive strengths decreased with the increase in treated fibre content [11]. Afterwards, Benmasnour and his colleagues [160] investigated the thermophysical and mechanical properties of the mortar reinforced with DPF. The experimental investigations indicated that the increase of DPF content allows lightens the mortar by decreasing its density and increases the insulating capacity of mortar by decreasing its thermal conductivity. The thermal conductivity of composites is strongly influenced by water absorption which showed a rapid increase of thermal conductivity with water absorption. Moreover, the increase in DPF content reduces the mechanical strength of mortar [160]. Additionally, Abani et al., (2015) investigated the effect of DPF on the thermal conductivity and specific heat of reinforced plaster cementitious mortars. Results showed that the specific heat and the thermal conductivity decrease as the fibre loading percentage increase, concluding that DPF are beneficial in

developing composites that possess better thermal conductivity characteristics [161]. Furthermore, according to the latest study done by Vantadori et al. (2019) investigating the effect of DPF content on the mechanical properties of cementitious mortar showed that, with the increase in DPF the decrease in density is not significant and the flexural strength and fracture toughness decreased by 47% and 58% for DPF content 4% and 6% respectively [162]. A summary of the fibre type, fibre properties, fibre treatment, mix design, and curing conditions are shown in Table 21.

Table 21 DPF/Cementitious mortar and concrete composites [12]

Fibre type	Binder (B)	Mix Design		Fibre loading	Fibre length (mm)	Fibre diameter (mm)	Fibre treatment	Curing conditions	Reference
		B:S:A	W/B						
Mesh	Cement	1:1.88:2.5	0.6	2, 3 Vol. %	15, 60	-	No Treatment	Water bath, ambient atmosphere uncontrolled hot-dry climate, steam room (T = 32 ± 2 ^{o}C, HR = 28 ± 2%)	[20]
Mesh	Cement	1:1.88:2.5	0.675	2 Vol.% of aggregate	15, 60	-	No Treatment	Wet Curing and Hot dry curing	[91]
			0.725	3 Vol.% of aggregate					
Midribs	Cement	1:0:0	0.45	7.5 Wt.% of cement	-	(20 – 40 mesh)	Cold and hot water	-	[72]
Leaflet	Plaster	-	-	-	-	-	NaOH	-	[163]
Leaves	Cement	1:2.93:0	0.515	0.5 Wt.% from sand	100	0.7 – 4.0	NaOH and $Ca(OH)_2$	Water bath	[11]
		1:2.89:0	0.540	1.0 Wt.% from sand					
		1:2.82:0	0.550	2.0 Wt.% from sand					
Petiole & Rachis	Cement	7:3:0	0.5	5, 10, 15, 20, 25, 30 Wt.% from the mass of the mortar	-	3.0 & 6.0	No Treatment	Open air	[160]
Mesh	Plaster & Cement	1:3:0	0.5	1, 2, 3, 4, 5 Wt.% from the mass of the mortar	300 – 500	200 – 300	No Treatment	RT (T = 27 ± 2 ^{o}C, HR = 55%)	[161]
Mesh	Cement	1:3:0	0.6	0.6 Wt.% of cement	20 – 100	0.1 – 1.0	No Treatment	-	[164]

Fibre type	Binder (B)	Mix Design		Fibre loading	Fibre length (mm)	Fibre diameter (mm)	Fibre treatment	Curing conditions	Reference
		B:S:A	W/B						
Mesh	Cement	1:1.8:2.8	0.6	0.5, 1, 1.5, 2, 2.5 Wt.%	50, 60, 70	0.04 – 1.00	No Treatment	Water Curing	[165]
Mesh	Cement	1:3:0	0.6	21, 31, 41, 51 Wt.%	50 – 60	0.0 – 0.7	No Treatment	Water bath 20 ± 1 ^{o}C	[99]
Mesh	Cement	1:3:0	0.6	21, 27, 31, 35, 48, 51 Vol. %	20 – 50	>0.7	High pressure water	Water bath 20 ± 1 ^{o}C	[166]
Mesh	Cement	1:2:2.25	0.59	0.1, 0.2 Vol. %	20	-	Heat treatment	climatic chamber (T = 40 °C, RH = 25 ± 5%), Room Temp. (T = 20 ± 2 °C, RH = 50 ± 5%)	[22]
Mesh	Cement	1:3:0	0.55	2, 4, 6, 8, 10 Vol. %	7 – 10	-	No Treatment	Water bath at RT	[167]
Petiole & Rachis	Cement	1:2.7:0	0.68	15 Wt.% from the mass of sample	50	3.0	No Treatment	RT (T = 21 ^{o}C, HR = 45%)	[168]
Mesh	Cement	1:3:0	0.55	2, 4, 6, 8, 10 Vol. %	7 – 10	-	Water treatment	-	[169]
Petiole & Rachis	Cement	1:0.38	0.42	5 Wt.%	50	3.0	No Treatment	Open air for 48 hours then room temperature till testing	[170]
		1:0.36	0.54	10 Wt.%					
		1:0.37	0.68	15 Wt.%					
Mesh	Cement	1:3	0.55	2, 4, 6, 8, 10 Vol. %	200 – 500	0.1 – 0.8	Water treatment	Saturated condition & RT.	[162]

2.6.2. DPF/Clay composites

In the process of developing composites and materials from cheap local resources to achieve sustainable development in the construction industry, especially in undeveloped countries to improve the thermal comfort, researchers in the MENA region have been attracted to investigate DPFs clay mortars for brick production with better thermal conductivity and heat resistance by virtue of good thermal property of DPFs. Chaib and his colleagues [171] investigated the effect of DPF as a reinforcement for clay brick to achieve better thermophysical properties in hot and dry climates. Their results showed that as the content of DPF increased, 3 wt.%, the density, thermal conductivity and specific heat decreased by about 28%, 32%, 10% respectively, and the heat resistance of the bricks developed showed an increase of 45%. On the other hand, Mekhermeche and his colleagues [79] investigated the same parameters as Chaib et al. (2015) using the same fibre characteristics but without using sand in developing their composite. Their results showed that as the content of DPF increased, 3 Wt.%, the density, thermal conductivity and specific heat decrease by about 6%, 57%, 6% respectively, and the heat resistance of the bricks developed showed a significant increase of 133% [79]. These results showed that the inclusion of DPF gave rise to a great enhancement to the thermophysical properties of clay brick. It may also be interpreted that developing clay brick with the inclusion of sand and DPF, compared to clay bricks without sand, lead to lower density, thermal conductivity and heat resistance composites. Furthermore, Hakkoum et al. (2017) reported similar results to Chaib et al. (2015) and Mekhermeche et al. (2016), but also stated that the inclusion of DPF in clay matrix had a negative effect on the compressive and bending resistances [172]. A summary of the fibre type, fibre properties, fibre treatment, mix design, and curing conditions is given in Table 22.

Table 22 DPF/Clay composites [12]

Fibre type	**Binder (B)**	**Mix Design**		**Fibre loading**	**Fibre length (mm)**	**Fibre diameter (mm)**	**Fibre treatment**	**Curing conditions**	**Reference**
		B:S:A	**W/B**						
Mesh	Clay	7:3:0	-	1,2,3 Wt.%	20 – 100	0.1 – 1.0	No Treatment	-	[171]
		4:1:0							
Mesh	Clay	1:0:0	N.S	1, 2, 3 Wt.%	20 – 100	0.1 – 1.0	No Treatment	-	[79]
Mesh	Clay	7:3:0	0.36	1 Wt.%	-	0.1 – 1.0	No Treatment	Open air drying for 4 days then placing the samples in stove for 12 hours @ 700 °C	[172]
			0.37	2 Wt.%					
			0.40	3 Wt.%					

2.6.3. DPF/Gypsum composites

DPF was investigated by several researchers on its impact as a reinforcement in gypsum plaster as DPF has very interesting thermophysical, mechanical and acoustic properties. Chikhi and his colleagues [173] developed a DPF-gypsum bio-composite that can be used in building as thermal insulation panels. Their results revealed that the flexural strength, compressive strength, density and thermal conductivity decreased with the increase of the DPF fibre content. Also, the water absorption of the developed composite increased with the increase in DPF content. Moreover, Chikhi (2016) investigated the effect of fibre size, content and porosity on the Young's modulus of DPF-gypsum bio-composite. Results showed that the addition of DPF resulted in an increase in the stress-strain and stiffness of DPF composites, and prevented the brittle fracture of DPF gypsum composites, which can be attributed to the high strength rupture parameter of DPF. DPF is applicable as a reinforcement for gypsum material in order to develop bio-composite materials for thermal insulation applications in building [174]. Furthermore, a remarkable improvement of thermal properties, a decrease in thermal conductivity with increasing the DPF fibre content, of DPF-gypsum bio-composite was also reported by Braiek and his colleagues [175]. Results showed that the addition of 20% DPF produced composite with thermal conductivity 0.17 $Wm^{-1}K^{-1}$ and density 0.74 g/cm^3 which were lower or close to several insulating materials used in buildings. A summary of the fibre type, fibre properties, fibre treatment, mix design, and curing conditions is given in Table 23.

Table 23 DPF/Gypsum composites [12]

Fibre type	Water/Gypsum Ratio	Fibre loading	Fibre length (mm)	Fibre diameter (mm)	Fibre treatment	Curing conditions	Reference
Petiole and rachis	0.6	1, 2, 3, 4, 5, 7, 10 Wt.%	-	3.0 & 6.0	No Treatment	-	[173]
Mesh	0.4, 0.6, 0.8	2, 4, 6, 8, 10 Vol. %	50 – 300	0.1 – 2.0	No Treatment	15 days @ 31 ^oC	[98]
Petiole, bunch and rachis	0.6	1, 2, 3, 4, 5, 7, 10 Wt.%	-	3.0 & 6.0	No Treatment	-	[174]
N.S	0.6	5, 10, 15, 20 Wt.%	-	2.0	No Treatment	Ambient temperature	[175]

2.6.4. DPF/Asphalt composites

Permanent deteriorations encountered on the surface layers of bituminous pavements due to the elevated temperatures, up to 60 ^{o}C during summer, and the drastic traffic loadings in the MENA region have triggered researchers to find solutions in modifying bitumen to enhance the properties and service life of the pavements developed. Several approaches have been reported in using polymers, fibres, additives, recycled tires and other materials [176]. However, the addition of fibres showed better performance than other types of additives [177]. Considering DPF, to date there has been limited research reported for utilizing DPF in modifying bitumen for pavement development. Al-Otaibi and his colleagues [177] investigated the effect of DPF size and content on the characteristics of fibre modified asphalt. Results showed that asphalt reinforced with DPF had higher softening point and less penetration compared to the samples without DPF reinforcement. Moreover, Bellatrache et al. (2020) recently reported that DPF can be suitable for modifying bitumen binder for various reasons. DPF does not degrade thermally at manufacturing temperatures, the use of bituminous mixtures and melting of bitumen which occurs at below 200 ^{o}C, thus it can be blended with bitumen mixture without any modification or treatment. Also, an improved thermomechanical behaviour was reported by the inclusion of DPF where the developed composite was harder in terms of penetration and softening point at service life temperature along with improving the viscosity and rutting resistance. This enhancement can be justified by the presence of semi-amorphous fibre network which acts as a mechanical reinforcement in the bituminous matrix [176]. A summary of the results and experimental approach is listed in Table 24.

Table 24 DPF/Asphalt composites [12]

Fibre type	**Binder (B)**	**Fibre loading**	**Fibre length (mm)**	**Fibre diameter (mm)**	**Fibre treatment**	**Reference**
N.S	Asphalt	0.075, 0.150, 0.225, 0.300, 0.375 Wt.% from the mass of the asphalt binder	-	-	No Treatment	[178]
Bunches	Asphalt	1.5, 3, 4.5, 6, 7.5 Wt.% from the mass of the asphalt binder	-	0.15	No Treatment	[177]

Fibre type	Binder (B)	Fibre loading	Fibre length (mm)	Fibre diameter (mm)	Fibre treatment	Reference
Leaf	Bitumen	1, 2, 3, 4, 5, 6 Wt.% from mass of bitumen	≤ 1	<1	No Treatment	[176]

2.7. Natural fibre composites industrial applications

Several industries such as construction, aerospace, and automotive are being challenged by governmental legislations and society's environmental requirements to produce greener products that can reduce the utilization of crude oil and end life deposits [27].

The main objective of this research investigation, as aforementioned in the introduction is the development of DPFC and assessing its properties for its applications in various industrial applications, mainly the construction sector. To date there has not yet been reported that DPF is upscaled into an industrial scale and is used for suppling the construction market with their derived products, unlike many other NF that are used in various industrial applications. Thus, developing composites with enhanced properties at research scale could bring to light the feasibility of upscaling into pilot scale which can be industrialized.

2.8. Summary of literature review

Utilizing DPT agricultural wastes could develop very valuable composites due to their competitive physical, mechanical, thermal and environmentally friendly properties and other characteristics. DPT agricultural wastes have different mechanical, physical and chemical characteristics depending on their country of origin, in which DPF could be extracted from various parts of the DPT. The existence of very large quantities of DPT produces millions of tons of waste annually, especially in the MENA region, China, Pakistan and United States, which could lead to using DPT agricultural waste as an alternative low-cost material that in turn reduce the environmental pollution and enhance the industrial sustainability. Many studies demonstrated the capability of DPFs to produce various composites using different matrix systems, i.e., organic, and inorganic matrices, along with various surface treatments of DPF to increase its interfacial surface bonding with the various matrix systems used to develop bio-composites. However, there is an inconsistency with the data reported to date by previous researchers on the physical, chemical, and mechanical properties as they varied from one to another region and varied due to different cultivars. Also, various chemical treatments mainly treating DPF with alkali solutions have been explored but not yet upscaled to study its

feasibility on an industrial scale. Additionally, there is one physical treatment reported by the application of corona treatment on DPF, but there are several other physical treatments that are applied on other types of natural fibres, i.e., gamma and plasma, which showed positive results that could also be investigated. Another treatment that should be taken into consideration is bio-treatments that are environmentally friendly and sustainable. Factors, such as the efficiency of the treatment, cost and industrially feasible treatment/modifications are yet to be developed to achieve optimum interfacial bonding when reinforced with different matrices to develop high thermophysical and mechanical bio-composites.

Several investigations have been carried out to utilize DPF in developing construction materials using various matrix systems. DPF used as a reinforcement in polymeric composites showed positive results in enhancing the mechanical and physical properties with the amount of fibre content up to 60%; using DPF as a reinforcement for cementitious composites, clay, gypsum, and asphalt mortars for developing building components has not yet been explored widely. Moreover, low DPF content has been attempted for reinforcing cementitious composites, clay, gypsum, and asphalt mortars, but the thermophysical properties of the developed composites greatly improved which could be potential in building application for increasing thermal comfort. Nevertheless, the DPF geometry, i.e., DPF length, treatment and loading in composites are yet optimised and tested for their feasibility to be upscaled into an industrial scale.

Chapter 3: Materials and Methods

In this chapter, a detailed description of the materials and methods are discussed, i.e., selection of materials, manufacturing procedure for DPFRC development, sampling, and testing. DPF were selected based on the chemical, physical and mechanical properties, market significance in terms of availability and price.

3.1. Materials

3.1.1. Date palm fibre (DPF)

DPF collected from the surrounding of the date palm trees stems which are known as DPF mesh or sheath, were obtained from a local farm on the outskirts of Cairo city in Egypt. DPF mesh shown in Figure 14 (B) was converted into a rope format as shown in Figure 14 (A) for controlling DPF length when cut for reinforcement in cementitious matrices. DPF were washed and cleaned from dust and dirt because of their exposure to the natural growing environment and then packed in cardboard boxes until utilized.

Figure 14 A) DPF raw material turned into rope; B) DPF mesh in nature form

The natural format of DPF was grinded using a Retsch cutting mill (SM 100, Germany) to achieve small fibre size, as demonstrated in Figure 15, that can be processed with thermoplastic polymer matrices, RPVC and PLA, during melt-mixing and thermoset, UPR, matrices by hand-layup technique. However, the rope format was used when investigating the effect of DPF length on cementitious matrices, OPC and OPC/GGBS, composites where four different DPF length was cut, 10 mm, 20 mm, 30 mm, and 40 mm as shown in Figure 16.

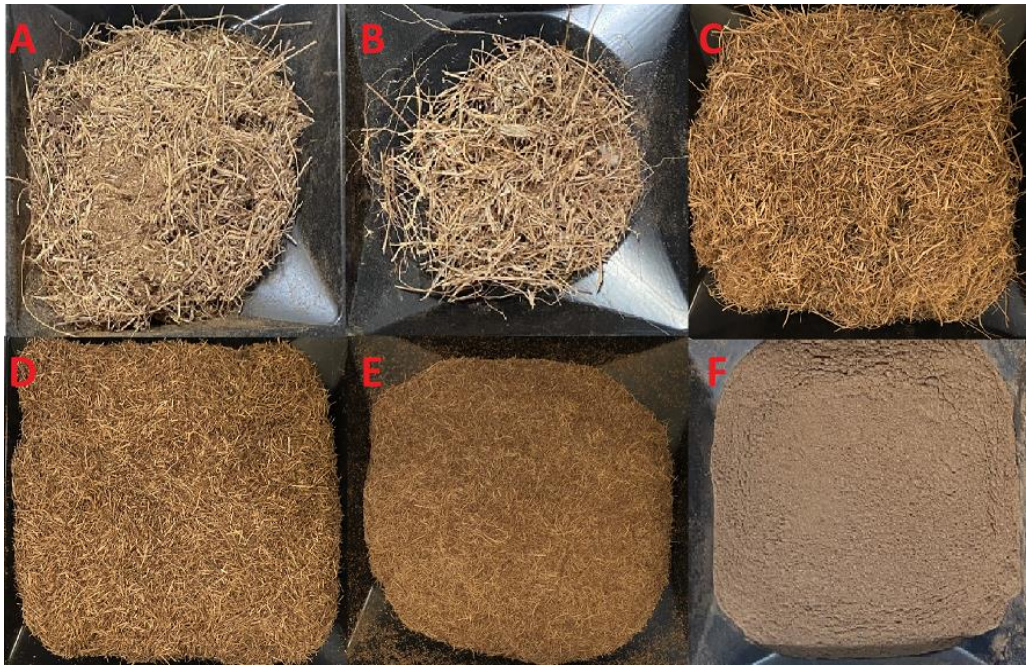

Figure 15 Shows different sieved size of DPF - A) Unsieved DPF, B) ≥1000 µm DPF, C) 500 - 1,000 µm DPF, D) 250 – 500 µm, E) 125 – 250 µm DPF, F) ≤125 µm DPF

Figure 16 DPF mesh after cleaning (left) and DPF cut into different length (right)

3.1.2. Polymer matrix

Thermoplastic polymers, RPVC and PLA were supplied by Ecodeck Ltd in powder form and as pellets respectively. The density of RPVC was 1.41 g/cm^3 and the MFI was 7.12 g/10 min. PLA had a MFI of 9.89 g/10 min and density of 1.23 g/cm^3. Moreover, thermoset matrix system, unsaturated polyester resin, was purchased from CFS Ltd, UK. The resin has 1.09 g/cm^3 density, 2.3 – 2.7 dPa.S rotothiner viscosity at 25 ^{o}C and 42 – 46% volatile content. ENCORE 30 was used as a catalyst.

3.1.3. Inorganic matrix

For the purposes of this research, two cementitious binders were used, OPC and GGBS. Standard CEM II Portland-limestone (~ 6 – 20 %) cement (Class 32,5 R), complying with BS EN 197-1, was acquired from Crescent Building Supplies, UK; whereas, the GGBS (Type II addition) complying with BS EN 15167-1:2006 Annex ZA [179] was provided by a company called LKAB Minerals, UK, working on developing sustainable materials. LKAB acquire the GGBS from a steel industry that they sell iron pellets to. Thus, LKAB Minerals recovers, reclaims and recycles the steel – making by – products whilst reducing landfill usage. Hence, as GGBS acquirement does not revolve around mineral extraction, it has ideal sustainability which makes it an ideal substitute to OPC for developing sustainable bio-composites.

Blaine fineness and specific gravity density of both OPC and GGBS used for this research were tested in compliance to BS EN 196-6:2018 [180] and the results are shown Table 25. GGBS possess lower gravity density and finest particles compared to OPC as shown in Table 30 and they both meet the physical requirements according to BS EN 196-6. Moreover, the chemical compositions of both OPC and GGBS were obtained through Energy Dispersive X-ray (EDX) incorporated within a scanning electron microscope (SEM) in terms of oxides as shown Table 26. This was done to ensure that GGBS can be used as a pozzolanic material according to the BS, where the content of MgO, CaO and SiO_2 sum up to 85.85 % by mass and their ratio by mass, (MgO + CaO)/(SiO_2), is 1.56 which satisfy the specified requirements in BS EN 15167.

Table 25 Blaine fineness and gravity density of OPC and GGBS

Cementitious material	**Blaine fineness (m^2/kg)**	**Gravity density**
OPC	449	2.93
GGBS	521	2.89

Table 26 Chemical composition (oxides) of OPC and GGBS (Wt.%)

	CaO	**SiO_2**	**Al_2O_3**	**FeO**	**TiO_2**	**MgO**	**K_2O**	**Na_2O**	**SO_3**
OPC	70.91	15.28	3.16	2.07	-	0.77	0.89	0.54	5.36
GGBS	45.44	33.60	10.43	3.10	0.58	6.81	0.33	0.38	2.64

3.1.4. Fine aggregate

The fine aggregate utilised was more specifically sharp sand with 2 mm nominal maximum grain size purchased from Crescent Building Supplies, UK, with origins tracing to a quarry in Leighton Buzzard. Therefore, the fine aggregate used for the purposes of this research study was washed sand in nature indicating a prolonged history of water erosion and can also be referred to as the Leighton Buzzard Sand. Thus, prior to the mortar manufacturing, it is crucial to note that the aggregates were oven dried according to BS EN 1097-2008 where a ventilated drying oven housed the aggregates at a 105°C. The sand in its wet form and after drying has been shown in Figure 17 and Figure 18 respectively.

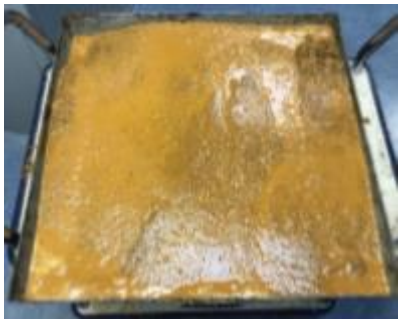

Figure 17 Wet sand prior to drying

Figure 18 Dried sand after 24 hours at 105 °C

3.1.5. Chemical reagents and additives

All chemicals listed in Table 27 were used carefully according to the safety guidelines provided by the supplier.

Table 27 Properties of chemical reagents and additives

Chemical	Molecular weight (g/mol)	Purity (%)
Sodium hydroxide	40.00	98.00
Acetic acid	60.05	99.00
Toluene	92.14	99.80
Acetone	59.21	98.80
Methanol	32.04	99.90

3.2. Sample preparation and fabrication

3.2.1. DPF Surface treatments

3.2.1.1 Water treatment

DPM were cut to 20 cm of length, weighing 10 grams, immersed in 2 different water baths at different temperatures. A comparison between the effects of water temperature on DPF was investigated by immersing DPF in room temperature water bath and the other at hot water bath for 24, 48, 72, 96, 120, 144 hours. Consequently, DPF were then washed several times with distilled water to ensure that the fibre surface is clean. The fibres were then oven dried at 60 ^{o}C for 24 hours.

3.2.1.2 Alkaline treatment

DPM were cut to 20 cm of length, weighing 10 grams, and were soaked in 3 different concentrations of aqueous sodium hydroxide solutions, 3%, 6% and 9% at room temperature ranging from 23 – 27 ^{o}C for 1, 3, 6, 12 and 24 hours. Afterwards, DPF were then washed several times with distilled water to remove any excess NaOH attached to the fibre surface, neutralized with acetic acid, 1% wt., and finally washed again several times with distilled water.

3.2.1.3 T:M:A treatment

A mixture of toluene/methanol/acetone with a ratio of (3:1:1 by volume) was prepared at room temperature. The solutions were mixed for 1 hour before soaking the DPF to ensure

homogenous mixing of the solution. DPF were cut to 20 cm of length, weighing 10 grams, and soaked in the solution for 1, 3, 6, 12 and 24 hours. Subsequently, DPM were then washed several times with distilled water to remove any excess solution mixture attached to the fibre surface.

3.2.1.4 Starch treatment

Starch solutions were prepared by dissolving starch powder in boiling water at 3 different concentrations, 3%, 6% and 9% wt.% and 3 different time soaking durations, 3 - 9 min. The untreated DPF were soaked at a specified concentration and duration then soaked in distilled water for few minutes to remove any excess starch from the surface. Afterwards the fibres were then oven dried at 60 ^{o}C for 24 h. The starch loading (SL) was calculated based on the weight gained by DPF after treatment using Equation 8.

$$\text{SL}\ (\%) = \frac{\text{Final Weight} - \text{Initial Weight}}{\text{Initial Weight}}\ \text{x}\ 100 \qquad \text{Equation 8}$$

Finally, after each treatment, DPF were manually extracted by hand and preserved in polyethylene bags with labels for identification to reduce the moisture content, 1% - 2%, until they were used for testing and analysis.

3.2.2. Polymeric matrix reinforced DPF composites

3.2.2.1 Thermoplastic polymer matrix reinforced DPF

The DPF were dried in an oven at 60 ^{o}C for 24 hours to ensure that the fibres have minimal moisture content. DPF were then grinded with a 2 mm sieve. The grinded DPMF were then preserved in sealed polythene bags to avoid any moisture absorption from the atmosphere. Both thermoplastic matrices, RPVC and PLA, were dried in an oven at 60 ^{o}C for 24 hours to ensure that the polymer have minimal moisture content. Afterwards, the DPF and polymer matrix were processed in a Barbender Plastograph twin-screw mixer (with Cam blades for mixer type N50EHT) at 190 ^{o}C and 170 ^{o}C for RPVC and PLA polymer matrix respectively with screws speed of 50 rpm for 6 minutes. Samples with four different mass proportions, 10 %, 20 %, 30 % and 40 %, and six different fibre diameter size, sieved through various mesh screens, ≥ 1,000 µm, 500 – 1,000 µm, 250 – 500 µm, 125 – 250 µm, ≤ 125 µm, was produced and compared to the unsieved DPF size. This was achieved by initially feeding into the mixer the required amount of thermoplastic polymer, RPVC powder or PLA pellets, for each batch allowing it to completely melt for 2 minutes, and subsequently feeding in the DPF for 4 minutes to obtain a uniform mixture. Thus, the resulted mixture was grinded to pellets equipped with a 2 mm sieve. The grinded pellets were compression moulded into a 100 mm (L) x 100 mm (W)

x 4 mm (T) mould using an electrically heated hydraulic press. Compression moulding procedure involved pre-heating at 190 ^{o}C for 10 minutes without applied load followed by 5 minutes compressing at the same temperature under 10 MPa pressure, and subsequently cooling under load until the mould reached 35 ^{o}C. The compression moulded composite was cut using bandsaw (SEALEY SM1304) to achieve specific specimen dimensions, 100 mm (L) x 10 mm (W) x 4 mm (T) compatible to the BS to evaluate the developed composite properties. Figure 19 and Figure 20 represent a schematic diagram on processing of DPF/RPVC and DPF/PLA composites respectively.

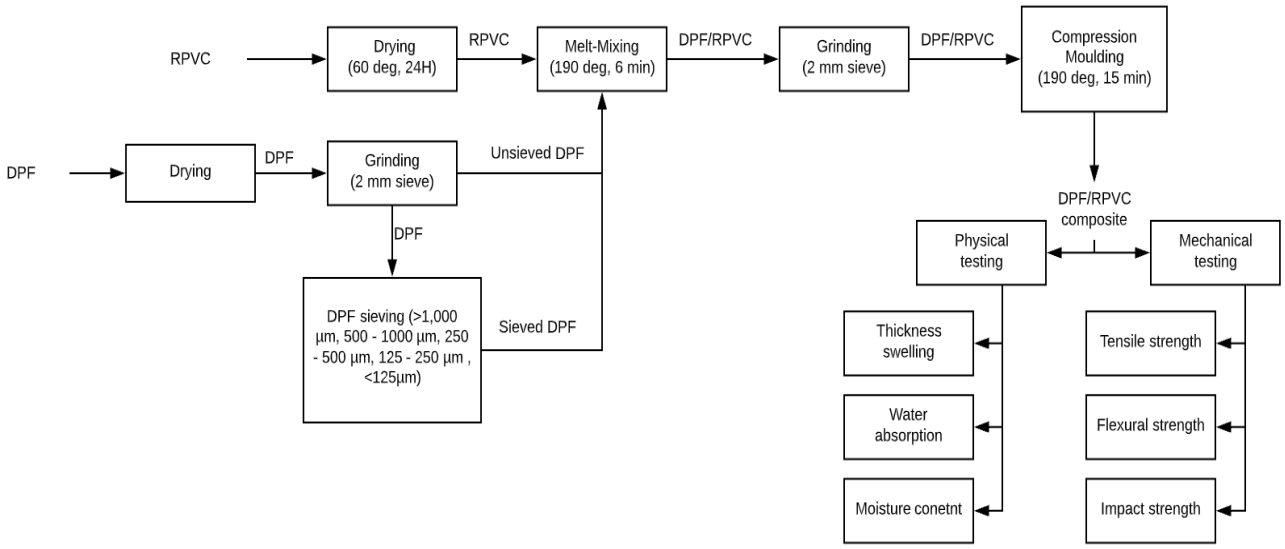

Figure 19 Schematic diagram on processing of DPF/RPVC composite

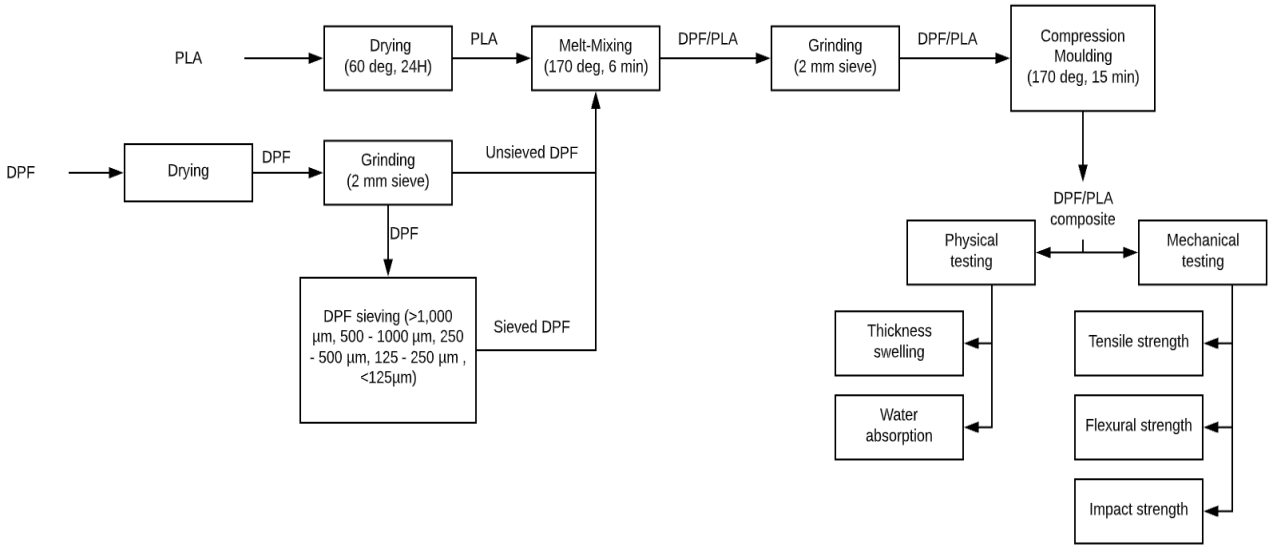

Figure 20 Schematic diagram on processing DPF/PLA bio-composite

Table 28 Composition of untreated DPF/RPVC composites

RPVC (Wt. %)	**Untreated DPF (Wt. %)**	**Untreated DPF Size (µm)**
100	0	-
90	10	Unsieved
		≥ 1,000
		500 – 1,000
		250 – 500
		125 – 250
		≤ 125
80	20	Unsieved
		≥ 1,000
		500 – 1,000
		250 – 500
		125 – 250
		≤ 125
70	30	Unsieved
		≥ 1,000
		500 – 1,000

RPVC (Wt. %)	Untreated DPF (Wt. %)	Untreated DPF Size (µm)
		250 – 500
		125 – 250
		≤ 125
60	40	Unsieved
		≥ 1,000
		500 – 1,000
		250 – 500
		125 – 250
		≤ 125

Table 29 Composition of untreated DPF/PLA composites

PLA (Wt. %)	Untreated DPF (Wt. %)	Untreated DPF Size (µm)
100	0	-
90	10	Unsieved
		≥ 1,000
		500 – 1,000
		250 – 500
		125 – 250
		≤ 125
80	20	Unsieved
		≥ 1,000
		500 – 1,000
		250 – 500
		125 – 250
		≤ 125
70	30	Unsieved
		≥ 1,000
		500 – 1,000

PLA (Wt. %)	Untreated DPF (Wt. %)	Untreated DPF Size (µm)
		250 – 500
		125 – 250
		≤ 125
60	40	Unsieved
		≥ 1,000
		500 – 1,000
		250 – 500
		125 – 250
		≤ 125

3.2.2.2 Thermoset polymer matrix reinforced with date palm fibre

The investigation and evaluation of the processing parameters on the physical and mechanical properties on DPF/thermoset resin was applied to the unsieved DPF at a loading content of 30 wt.% with UPR at various temperatures, pressure and time. The temperatures investigated are 90 and 110 ^{o}C, processing pressure investigated (10, 15 and 20 ton), compressed for different processing durations of (3, 6 and 9 min). The DPF were dried in an oven at 60 ^{o}C for 24 hours to ensure that the fibres have minimal moisture content. DPF were then grinded using Retsch cutting mill (SM 100, Germany) equipped with a 2 mm sieve. The grinded DPMF were then preserved in sealed polythene bags to avoid any moisture absorption from the atmosphere. Samples with a constant DPF loading content 30 wt.% and 70 wt.% UPR resin. DPF and UPR were mixed using hand lay-up technique to form a homogenous mix which is then compression molded into a 300 mm (L) x 300 mm (W) x 4 mm (T) mould using an electrically heated hydraulic press. Compression moulding procedure involved various processing parameters mentioned above. Post curing of the samples occurred for 24 hours at 40 ^{o}C. The compression molded composite was cut using bandsaw (SEALEY SM1304) to achieve specific specimen dimensions, 100 mm (L) x 10 mm (W) x 4 mm (T) compatible to the BS to evaluate the developed composite properties.

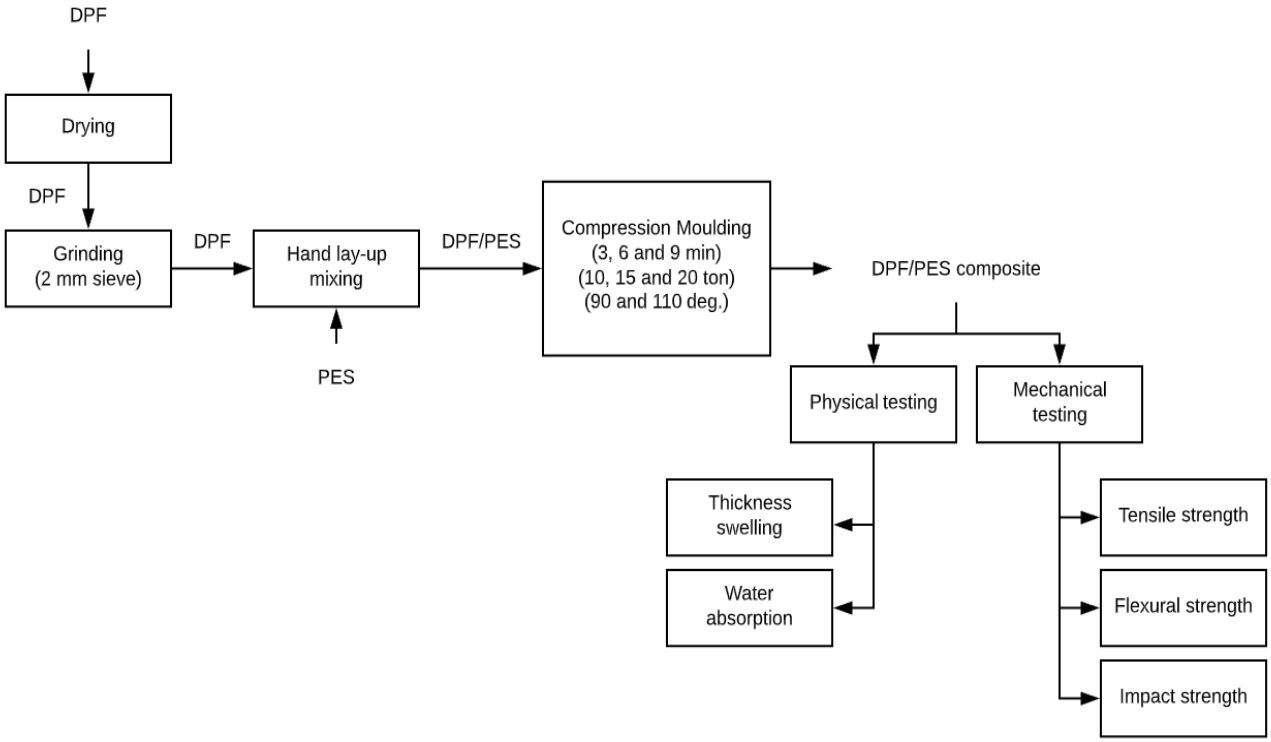

Figure 21 Schematic diagram on processing DPF/ UPR bio-composite

3.2.3. Cementitious matrix reinforced with date palm fibre

3.2.3.1 Mix design and formulations

The mix proportion ratio used for the cementitious mortars was Binder: Sand = 1:1.5 by weight with water-to-binder ratio equal to 0.45 based on several optimisation cycles of mix workability. The binders used for making the mortars consisted of OPC and GGBS which were mixed at 50%:50% based by weight. However, 100% OPC samples were produced as a benchmark for comparison. The DPF reinforced cementitious mortars had varying volume and length of DPF. DPF was added by 1%, 2%, and 3% by weight compared to the weight of the binder, and the length varied from 10 mm, 20 mm, 30 mm, and 40 mm for each varying volume as shown in Table 30 and Table 31.

Table 30 Mix design formulation for DPF reinforced OPC composites

DPF content (Wt.%)	DPF Length (mm)	DPF (g)	Sand (g)	OPC (g)	Water (g)
0	0	0	1,050	700	315
1	10	7	1,050	700	315
2	10	14	1,050	700	315

DPF content (Wt.%)	DPF Length (mm)	DPF (g)	Sand (g)	OPC (g)	Water (g)
3	10	21	1,050	700	315
1	20	7	1,050	700	315
2	20	14	1,050	700	315
3	20	21	1,050	700	315
1	30	7	1,050	700	315
2	30	14	1,050	700	315
3	30	21	1,050	700	315
1	40	7	1,050	700	315
2	40	14	1,050	700	315
3	40	21	1,050	700	315

Table 31 Mix design for DPF reinforced OPC/GGBS composites

DPF content (Wt.%)	DPF Length (mm)	DPF (g)	Sand (g)	OPC (g)	GGBS (g)	Water (g)
0	0	0	1,050	350	350	315
1	10	7	1,050	350	350	315
2	10	14	1,050	350	350	315
3	10	21	1,050	350	350	315
1	20	7	1,050	350	350	315
2	20	14	1,050	350	350	315
3	20	21	1,050	350	350	315
1	30	7	1,050	350	350	315
2	30	14	1,050	350	350	315
3	30	21	1,050	350	350	315
1	40	7	1,050	350	350	315
2	40	14	1,050	350	350	315
3	40	21	1,050	350	350	315

3.2.3.2 Mortar sample preparation of date palm fibre cementitious composites

This Section describes three different stages of mortar preparation which includes, the preparation of the mould, mixing and casting of the fresh mortar mix. The preparation was performed complying to BS EN 12390-1,2:2019, Sections 4.4.1 and 6.1 respectively. The subsection 4.4.1 mentioned in BS EN 12390 states that the dimensional requirements of prismatic moulds should have a minimum length dimension of 3.5 times of the depth and width dimensions. Thus, the prismatic moulds used for the experimental study were 40 mm x 40 mm x 160 mm (width x depth x length) as shown in Figure 144 which complies with the British Standards.

Prior to mixing the mortar mix, the inner surfaces of the prismatic moulds were coated with a thin layer of mould release oil applied using a thick applicator brush. Afterwards, having the mould ready, the mixing procedure of the mortar mix is started. The mixing process was performed in accordance to section 7.2 of BS EN 12390 – 2. KENWOOD (KVL8300S) mixer was used for the mixing of the mortar mix. The mixing parameters, i.e., time, was kept constant throughout the experimental study. Firstly, the cementitious matrix system and the fine aggregate, sand, were mixed for 2 minutes to provide a homogenous mix of the matrix system. Afterwards, DPF was added to the matrix system and were mixed for 2 minutes at a speed of 1, which is equivalent to 80 rpm. Consequently, water is added slowly into the mix and mixed for 1 minute then the mixing process is stopped, and the mixing bowl is removed from the KENWOOD mixer and then hand mixed for 30 seconds with a spatula to make sure that any sand or cementitious matrix remained or attached to the walls or at the bottom the bowl (unreachable by the mixer's blade) was properly incorporated in the mixture. Subsequently, the bowl was placed back into the KENWOOD mixer for another 2 minutes of mixing. Afterwards, pouring the fresh mortar mix into the mould was done in three pouring increments, i.e., the mortar was poured by diving it into three layers filling up third of the mould at each pouring increment. After each layer of mortar added into the mould, manual compaction by tapping the mould on a hard surface in a vertical motion was done. This required 25 taps for each layer, complying with sub-section 6.2.3 in BS EN 12390, after which an additional layer of the mortar is added. This layer experienced another subsequent 25 manual taps until the mortar mix filled two thirds of the mould. This ramming procedure was carried out one more time after the third layer was put into the mould. Upon completion of the pouring of the third layer, mechanical vibration was employed in accordance with Section of 6.2.2.1 BS EN 12390, where a vibrator was used.

Subsequently, the compaction of the mortar mix until the mould was filled, the sides of the mould were also subjected to taps courtesy of a mallet. This practice was carried out until the

existence of air bubbles on the surface was brought to a minimum. It is important to note that in this step, care is taken to remove the entrapped air whilst ensuring the entrained air is kept within the mixture. Succeeding this, the top layer of the mould was levelled by utilizing a steel trowel. Moreover, Figure 22 demonstrates schematic diagram on processing cementitious composites reinforced with DPF.

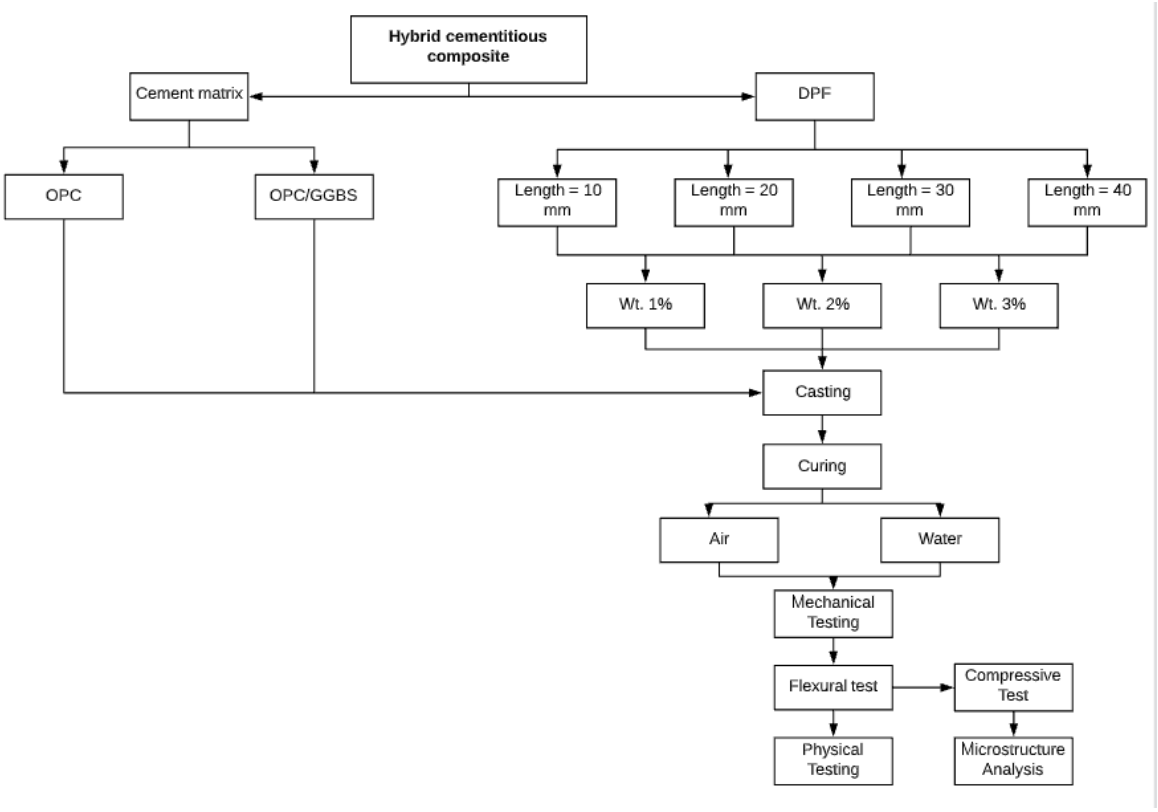

Figure 22 Schematic diagram on processing of cementitious composites reinforced with DPF

3.2.3.3 Curing conditions of date palm fibre cementitious composites

Two different curing conditions were investigated in this experimental study in which the demoulded mortar samples, demoulded after 24 hours of casting complying to BS EN 12390-2:2019, were placed either in a controlled water bath, water curing, or in a controlled environment room, air curing for two ageing durations, 7 and 28 days. The curing methodology was accomplished by complying to BS EN 12390-2:2019.

Air curing was performed complying to Section 6.5.3 of BS EN 12390 in which the samples were left in a chamber with an environment at 20 ± 2 ^{o}C for 7 and 28 days of ageing. On the contrary, water curing was performed complying to BS EN 12390, where the samples were immersed in a water tank/bath with temperature maintained at 20 ± 2 ^{o}C, ensuring that not less than 5 mm gapped space existed between the samples to ensure that water had free access to all six faces of the samples for 7 and 28 days of ageing.

3.3. Testing methods

3.3.1. Tensile test

3.3.1.1 Tensile test procedure for single DPF

Single DPF were separated manually by hand from the prepared treated fibres stored in the polythene bags and glued at both ends of a mounting card (20 x 55) with a central window (10 x 25 mm) as shown in Figure 23. The apparent diameter of single non-circular cross-section DPF was measured under an optical microscopy, Leica microsystems wetzlar GmbH type 020-518.500. The cardboard acted as a mounting attachment for single fibre from DPMF. The gauge positions of the paper were cut after gripping it in the jaws of the testing machine. Subject the test pieces to tensile strength test by using Instron 5566 at crosshead speed of 1 mm/min and with 25 mm gauge length with screw grips with a load cell capacity of 10 kN, cat number 2530-10kN, and a resolution of 1mN with calibration certificate E2655022019101521. Twenty-five samples were tested for all different condition types of treatments. The displacement and reaction force were recorded, and the strain, stress and Young's modulus were determined.

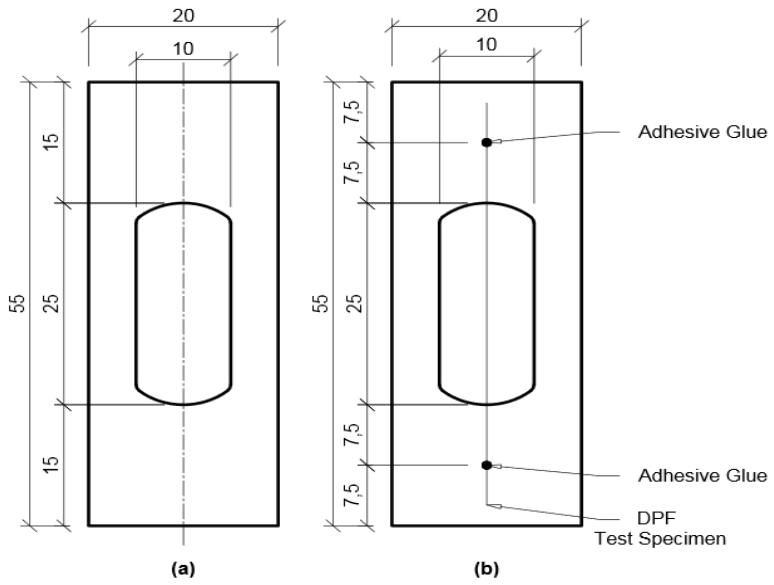

Figure 23 Set-up of single fibre test: (a) specimen mount and (b) test specimen mounted on the mount (dimensions are in mm)

3.3.1.2 Tensile test procedure for DPF reinforced polymer composite

Rectangular shaped samples were cut from the compression moulded samples of pure PLA, RPVC and unsaturated polyester, untreated and different surface treated DPF reinforced PLA, RPVC and unsaturated polyester composites to be tested using an Instron 5900 testing

machine with a load cell capacity of 30 kN, serial number 105942, calibration certificate number E2655022019101520, and speed of 1 mm/min at 25 ^{o}C and relative humidity of 60%. The dimensions of the tensile samples for the polymeric composites were 80 mm (L) x 10 mm (W) x 4 mm (T). The ratio of span length to specimen thickness is 20. Five samples were tested and at least four replicate samples have been presented as an average value of tested samples along and the standard deviation is also reported.

3.3.2. Three-point flexural test

Two different standards are applied to determine the flexural strength of DPFRC. The flexural strength of DPF reinforced polymer matrix systems were measured at 25 ^{o}C and relative humidity of 60% determined according to BS EN ISO 527-2:2012 a using an Instron 5900 testing machine with a load cell capacity of 30 kN, serial number 105942, calibration certificate number E2655022019101520, and speed of 1 mm/min. The dimensions of the flexural samples for the polymeric composites were 80 mm (L) x 10 mm (W) x 4 mm (T). The ratio of span length to specimen thickness is 16. Five samples were tested and at least four replicate samples have been presented as an average value of tested samples and the standard deviation is also reported.

Moreover, the flexural strength, 3-point flexural test, of the developed DPFCC samples was determined according to BS EN 196-1:2016 using a universal machine, Instron 5566, with a load cell of 50 kN, serial number 304044, calibration certificate number E323080321094901, applying a constant load at a rate of 50 kN/min. The prismatic samples, 40 x 40 x 160 mm^3, developed for different curing conditions were tested after 7 and 28 days of ageing. Water cured samples were taken out of the water bath on the testing day and wiped with a towel before testing. The reported results were the average of three prismatic specimens with the error reported as average deviation from the mean.

3.3.3. Impact test

Rectangular shaped samples were cut from the compression moulded samples of pure PLA, RPVC and unsaturated polyester, untreated and different surface treated DPF reinforced PLA, RPVC and unsaturated polyester composites to be tested for impact strength. Impact strength was evaluated using using CEAST Torino 6546/000, pendulum impact machine, with an edgewise impact and 2J hammer capacity according to ISO 179-1:2010. Samples with dimensions 80 mm (L) x 10 mm (W) x 4 mm (T) were cut and the impact test was performed at ambient room temperature for seven notched samples composite developed and the average value for at least five samples along with the standard deviation is reported. It was noticeable that all specimens failed by separation into two parts.

3.3.4. Compressive test

The compressive strength of the developed samples was determined according to BS EN 196-1:2016 using a universal machine, Instron 5960, with a load cell of 150 kN, cat number 2580-150KN, applying a constant load at a rate of 144 kN/min. The prismatic samples developed for different curing conditions were tested after 7 and 28 days of ageing. Water cured samples were taken out of the water bath on the testing day and wiped with a towel before testing. The reported results were the average of three prismatic specimens with the error reported as average deviation from the mean.

3.3.5. Density

The density was calculated for DPF retained on the named sieve sizes and the developed bio-composites using AccuPyc II 1340 gas pycnometer with temperature control and a 100 cm^3 chamber volume. The unsieved, ≥1,000 µm, 500 – 1,000 µm, 250 – 500 µm, 125 – 250 µm and ≤125 µm DPF were weighed directly into the chamber cup using a measuring balance with 0.01g accuracy. The same procedure was carried out for the bio-composites developed. Helium was admitted into the compartment until reaching an equilibrium rate of 0.0050 psig/min. The samples were tested for 10 purge and 10 cycles to increase the accuracy of the test. Theoretical density was calculated as shown in Equation 9 where ρ_c is the theoretical density of the composite, ρ_f is the density of fibre (DPF), V_f is the volume fraction of the fibre (DPF), ρ_m is the density of the polymer matrix (PLA or RPVC), and Vm is the volume fraction of polymer matrix. The volume fraction percentage of voids (V_v) in the composites is calculated as shown in Equation 10 where ρ_t is the theoretical density and ρ_e is the experimental density of the composite [181].

$$\rho_c = \rho_f V_f + \rho_m V_m \quad \text{Equation 9}$$

$$V_v = \frac{\rho_t - \rho_e}{\rho_t} \quad \text{Equation 10}$$

3.3.6. Thickness swelling test

Thickness swelling of the fabricated samples were determined according to BS EN 317, where samples were immersed in a water bath at (20 ± 1) ^oC for 24 hours. The samples thickness was measured before immersing it in the water bath and afterwards the thickness of the sample was measured after 24 hours. The dimensions of the specimens were 10 mm (L) x 10 mm (W) x 4 mm (T).

3.3.7. Moisture content and Moisture absorption test

The moisture absorption or water absorption of the developed samples were determined according to BS EN 322. The samples were first dried in an oven at 105 ^{o}C for 24 h to remove the moisture and then the composites were weighed using a weighing balance and immersed in a water bath. The water-soaked samples were taken out at regular intervals of time and the experiment continued till no change in mass was observed. The composite samples were dried gently with a towel after removing it from the water bath and weighed using a digital balance. A digital weighing balance with a weighing precision of 0.001 g was used to weigh the samples. The percentage of moisture absorption (W_A) was calculated using Equation 11.

$$W_A(\%) = \frac{M_w - M_d}{M_d} \text{ x } 100 \qquad \text{Equation 11}$$

Where, Mw and Md are the wet and dry weights of the composite samples respectively. Moisture absorption is a vital property in which the mechanical properties of NFRC decrease significantly with increasing the moisture absorption [182].

3.3.8. Fungal durability

A laboratory decay tests using mini block specimens 30 mm (L) x 10 mm (W) x 4 mm (T) were undertaken to assess biological resistance of the developed composites against Pinus sylvestris solid wood control samples. Sterile culture medium (20 ml), prepared from malt 40 grams and agar 20 grams in distilled water (1 L), was placed in 90 mm diameter Petri dish with a small piece of mycelium of a freshly grown culture of Tyromyces palustris (Berk. et Curt) Murr. as a brown rot fungus and Irpex lacteus HHB 7328 as a white rot fungus. The culture was incubated for 2 weeks at 27°C and 70% HR to allow full colonization of the medium by the mycelium. Samples were supported on sterile plastic mesh to prevent contact with culture medium [183]. All samples, previously oven dried at 60°C to constant weight, were sterilized with radiation and three blocks (two treated and one control) were placed in each Petri dish under sterile conditions, and all treatments were duplicated. Incubation was carried out for 8 weeks at 27°C under controlled humidity conditions of 70% RH in a climatic chamber WTB BINDER TYP KBF 240. At the end of the test period, 12 weeks, mycelia were removed, and all specimens were oven-dried to constant mass at 103°C and weighed. Weight loss (WL) was expressed as a percentage of the initial oven-dried weight of the samples according to Equation 12.

$$WL\ (\%) = \frac{M_0 - M_f}{M_0} \text{ x } 100 \qquad \text{Equation 12}$$

Where M_0 is mass of oven-dried sample prior to the test, and M_f is mass of oven-dried sample after the test.

3.3.9. Disintegration analysis

The degradation test by composting was carried out according to ISO 20200 standard. The test determines the degree of disintegration of the materials when exposed to composting at laboratory conditions. For this test, previously dried and weighed 20 mm x 20 mm specimens were buried in a compost medium. The sample weight in each reactor represents 5 % wt. of the total wet weight of compost. The compost medium consisted of 55 % wt. water and 45 % wt. of synthetic solid waste. The solid waste composition was 40 % wt. sawdust, 30 % wt. rabbit feed, 10 % wt. mature compost, 10 % corn starch, 5 % wt. saccharose, 4 % wt. cornseed oil, and 1 % wt. urea. Samples of each composition (by triplicate) were removed from reactors every 10 days, cleaned, and dried at 55 °C until constant weight. The biodegradation (degree of disintegration) was calculated using Equation 13.

$$\text{Weight loss } (\%) = \frac{W_0 - W_t}{W_0} \text{ x } 100 \qquad \text{Equation 13}$$

Where W_t is the weight of the sample after certain time into the controlled compost soil and W_0 is the initial dry weight of the sample. All tests were triplicated to ensure reliability in results.

3.3.10. Micromechanical models

Micromechanics is the analysis of materials on the level of its constituents. Micromechanical modeling of composite involves the prediction of macroscopic behavior of composite based on its microscopic constituent behavior.

Rule of Mixture (ROM): the property of the composite is equal to the sum of volume weighed property of constituent materials i.e., both phases in the material experience the same strain under the action of load. ROM provides the upper bound for the composite modulus and generally termed as ROM_P

$$E1 = (E_F V_F + E_M V_M) \qquad \text{Equation 14}$$

Where, E_1 is the Elastic modulus of the composite in fiber direction, E_F is the Elastic modulus of the fiber, E_M is the Elastic modulus of the matrix, V_M is the volume fraction of Matrix and V_F is the volume fraction of Fiber. V_F can be calculated using Equation 15:

$$V_F = \left(\frac{\frac{W_F}{\rho_F}}{\left(\frac{W_F}{\rho_F}\right) + \left(\frac{W_M}{\rho_M}\right)} \right) \quad \text{Equation 15}$$

Where W_F and W_M is the Weight Fraction of the Fiber and Matrix, ρ_F & ρ_M is the density of fiber and Matrix respectively.

In moulded composite parts, the orientation of fibre plays a very important role in the mechanical properties that can be achieved, Contribution of fibre reinforcement to the modulus of the composite depends mainly on its orientation. Fibres provide maximum stiffness when it is aligned along the direction of loading. To account for the alignment of fibres, a fibre orientation factor (K) can be introduced into ROM Equation 14 and termed Equation 16 as Modified ROM_P:

$$E1 = (K * E_F * V_F + E_M * V_M) \quad \text{Equation 16}$$

Values of K depend on the orientation of the fibre; for complete alignment and when stress is parallel to fibres (k = 1); for fibres laid in two directions at right angles (bi-directional or cross-laid fibres) and stress is in one of these directions (k = ½); for fibres in random and uniform distribution within a specific plane, and stress is in any direction in the plane of the fibres (k = 3/8) and for fibres in random and uniform distribution within three dimensions in space, and stress is in any direction (k = 1/5)

In 1929, “Reuss” predicted the lower bound of composite properties using the inverse rule. Fibres and matrix experience the same stress when the composite is loaded in the direction transverse to the fibres, later termed as Inverse Rule of Mixture (IROM) or ROM_S:

$$E2 = \left(\frac{E_F * E_M}{E_F * V_m + E_M * V_F} \right) \quad \text{Equation 17}$$

Where, E_2 is the composite modulus, in a direction transverse to the fibres.

Modified IROM models for composite modulus, in a direction transverse to the fibres, are also presented by Voyiadjis and Kattan (2005) [184]:

$$E2 = \left(\frac{V_F + \eta * V_M}{\left(\frac{V_F}{E_{F_2}}\right) + \left(\frac{\eta * V_M}{E_M}\right)} \right) \quad \text{Equation 18}$$

Where, E_{F_2} is fiber modulus in the transverse direction and η is the stress-partitioning factor. The stress-partitioning factor satisfies the condition 0 <η <1, but usually taken between 0.4 and 0.6. In this study, η values considered as 0.4, 0.5 and 0.6

"Halpin–Tsai" model demonstrates the effect of fibre reinforcement on the stiffness properties of composite as a function of filler aspect ratio and volume fraction. The elastic modulus of a composite material in Halpin–Tsai model is written as Equation 19:

$$E_C = E_M \left(\frac{1 + \zeta * \eta * V_F}{1 - \eta * V_F} \right) \quad \text{Equation 19}$$

$$\eta = \left(\frac{E_F - E_M}{E_F + \zeta * E_M} \right) \quad \text{Equation 20}$$

$$\zeta = 2 \left(\frac{L}{D} \right) \quad \text{Equation 21}$$

where ζ is a shape parameter depending on the filler geometry and loading direction. Є = 2 (L/D) for fibres [185]. For transverse direction, Є = 2 (constant) is considered for all composites.

3.3.11. Mathematical model

3.3.11.1 Finite Element Model (FEM) simulation

The simulations were performed using Polyflow software (ANSYS, USA) with the finite element method (FEM), non-Newtonian isothermal flow model and Carreau-Yasuda law for viscosity. The model consists of about 65000 uniformly distributed tetrahedral segments as shown in Figure 24. The simulation was carried on Carreau-Yasuda law as shown in Equation 25. The constants of Equation 25 were calculated from PLA material data and their values were, n = 0.35, η_0 zero shear rate viscosity= 350 Pa sec, η_∞= 100 Pa sec, κ natural time= 0.002 sec and a = 0.5 rotations.

For isothermal steady flow of generalized Newtonian fluids with inertia, the conservation laws are expressed by the following forms. The form of the momentum and continuity equations is;

$$-\nabla p + \nabla \cdot T + \rho f = \rho \frac{Dv}{Dt} \quad \text{Equation 22}$$

$$\nabla \cdot v = 0 \quad \text{Equation 23}$$

Where, p is the pressure, f is the body force, ρ is the density, v is the velocity vector, t is the time and T is the extra-stress tensor. For a generalized Newtonian fluid;

$$\mathrm{T} = 2\eta(\gamma)\mathrm{D} \qquad \text{Equation 24}$$

Where, D is the rate-of-deformation tensor and viscosity η can be function of the local shear rate γ.

The Carreau-Yasuda law for viscosity is;

$$\eta = \eta_\infty + (\eta_o - \eta_\infty)[1 + (\gamma\kappa)^a]^{(n-1)/a} \qquad \text{Equation 25}$$

Where, η_o is the zero-shear-rate viscosity, η_∞ is the infinite-shear-rate viscosity, $\boldsymbol{\kappa}$ is the natural time (which is conventionally taken as the inverse of the shear rate at which the fluid changes from Newtonian to power-law behaviour), n is the power-law index and a is the index that controls the transition from the Newtonian plateau to the power-law region. At low value of a (a < 1), the transition from Newtonian to non-Newtonian flow occurs over a wide range of shear rate. Whereas, at high value of a (a > 1) the transition from Newtonian to non-Newtonian flow occurs abruptly over a narrow range of shear rate.

3.3.11.2 Mathematical equations

Based on the principle, mathematical model was derived based on Composite mechanics approach [186–189].

Based on composite mechanics approach [187], calculation of the force sustained by the fibres crossing a scan line, i.e. an arbitrary line perpendicular to the applied load in a thin, rectangular specimen. Composite mechanics approach involves:

1. Calculating the number of fibres of length L and θ that cross the scan line of the specimen,

2. Finding the axial force in a fibre of length L and θ,

3. Obtaining the load-direction component of the axial force in a fibre of length L and θ,

4. multiplying the number of fibres that cross the scan line by the load-direction component of the axial force in a fibre of length L and θ, and

5. Integrating the above quantity over fibre length and fibre orientation distributions to find the total force sustained by all the fibres across the scan line of the investigated specimen.

The specimen is in the shape of a thin, rectangular plate of dimensions a, b and c with the dimension c parallel to the X-axis direction as shown in Figure 24. The specimen consists of

N straight fibres dispersed in and bonded to a matrix resulting in a fibre volume fraction V_f. The fibres have a circular cross-section with a radius r_f. The fibre orientation is defined as the angle between the axial direction of the fibre and the X-axis direction. A single fibre of length L and orientation θ is shown in Figure 24. The statistical variation in the length and orientation of the fibres are defined by independent probability density functions h(L) and g(θ), respectively. Load, in the form of strain $\mathcal{E}_0$, is applied to the specimen in a direction parallel to the X-axis direction.

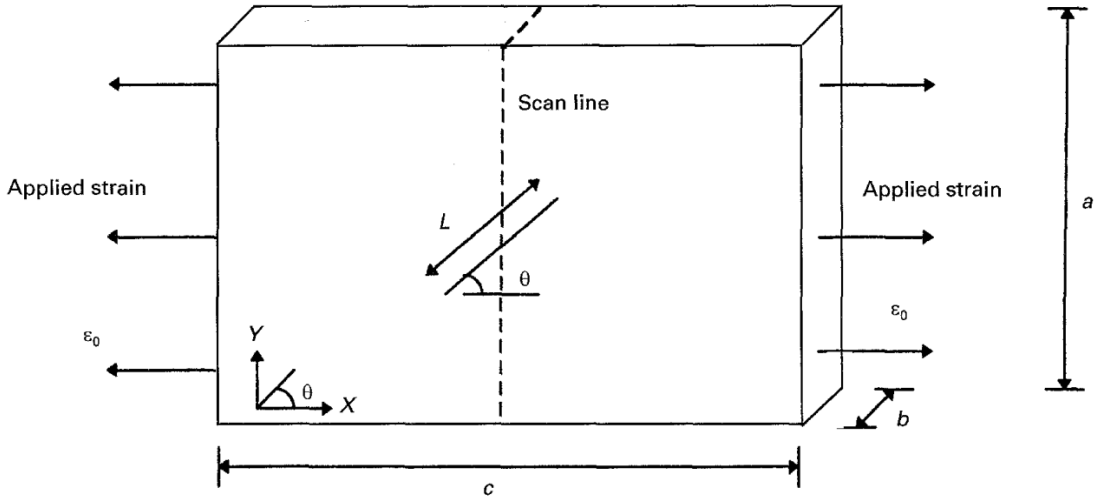

Figure 24 Schematic diagram of composite [187]

The two-dimensional probability density function of the fibre orientation distribution satisfies the following condition:

$$\int_0^{\frac{\pi}{6}} g(\theta)\, d\theta = 1 \qquad \text{Equation 26}$$

The probability density function of the fibre length distribution satisfies the following condition:

$$\int_0^{a} h(L)\, dL = 1 \qquad \text{Equation 27}$$

The average fibre length is defined as:

$$\bar{L} = \int_0^{\infty} L\, h(L)\, dL \qquad \text{Equation 28}$$

The average length of projection on the X-axis of the fibres in the specimen is given by (Jayaraman and Kortschot, 1996) [187]

$$\overline{L_X} = \int_0^{\frac{\pi}{6}} \int_0^{a} L \cos\theta \, h(L) \, dL \, g(\theta) \, d\theta \qquad \text{Equation 29}$$

Area of cross-section of the fibre is:

$$A_f = \pi {r_f}^2 \qquad \text{Equation 30}$$

The volume of the specimen is:

$$V = abc \qquad \text{Equation 31}$$

Fibre volume fraction:

$$V_f = \frac{N A_f \bar{L}}{abc} \qquad \text{Equation 32}$$

$$N = \frac{V_f abc}{A_f \bar{L}} \qquad \text{Equation 33}$$

Where N is the straight fibres dispersed in and bonded to a matrix resulting in a fibre volume fraction V_f.

The average number of fibres that cross the scan line can be found as:

$$N_{Scan} = \frac{N \overline{L_X}}{c} = \frac{V_f ab}{A_f} x \int_0^{\frac{\pi}{6}} g(\theta) \cos\theta \, d\theta \qquad \text{Equation 34}$$

The average axial force in a fibre of length L and orientation θ projected in the direction of the applied strain (X-axis direction) is:

$$F_x = \bar{F_f} \cos\theta \qquad \text{Equation 35}$$

$$\bar{F_f} = A_f * \overline{\sigma_f} \qquad \text{Equation 36}$$

The average axial stress ($\overline{\sigma_f}$) in a fibre of length L and orientation θ in the specimen is given by (Fakuda and Kawata,1974) [189] as:

$$\overline{\sigma_f} = \Phi E_f \varepsilon_0 (\cos^2\theta - \nu_s sin^2\theta) \qquad \text{Equation 37}$$

where Φ = a dimensionless function of fibre length and other fibre, matrix, and specimen properties, E_f = Young's modulus of the fibre, ε_0= strain applied to the specimen, and ν_s = Poisson's ratio of the specimen.

$$\overline{F_f} = A_f * \Phi E_f \varepsilon_0 (\cos^2\theta - \nu_s \sin^2\theta) \quad \text{Equation 38}$$

$$F_x = A_f * \Phi E_f \varepsilon_0 (\cos^2\theta - \nu_s \sin^2\theta) \cos\theta \quad \text{Equation 39}$$

The average value of the X-direction component of the axial force "for all the fibres in the specimen" can be found as

$$\overline{F_X} = \int_0^{\frac{\pi}{6}} \int_0^{a} [F_x]\, h(L)\, dL\, g(\theta)\, d\theta \quad \text{Equation 40}$$

$$\overline{F_X} = \int_0^{\frac{\pi}{6}} \int_0^{a} [A_f * \Phi E_f \varepsilon_0 (\cos^2\theta - \nu_s \sin^2\theta) \cos\theta]\, h(L)\, dL\, g(\theta)\, d\theta \quad \text{Equation 41}$$

$$\overline{F_X} = A_f E_f \varepsilon_0 \int_0^{\frac{\pi}{6}} \int_0^{a} \Phi\ h(L)\ g(\theta) (\cos^3\theta - \nu_s \sin^2\theta \cos\theta)\ dL\, d\theta \quad \text{Equation 42}$$

Total load that fibres crossing the scan line is given by (Fakuda and Kawata,1974) [189]:

$$F_T = [N_{Scan}][\overline{F_X}] \quad \text{Equation 43}$$

$$F_T = \left[\frac{V_f\, ab}{A_f} * \int_0^{\frac{\pi}{6}} g(\theta) \cos\theta\ d\theta\right]\left[A_f E_f \varepsilon_0 \int_0^{\frac{\pi}{6}} \int_0^{a} \Phi\ h(L)\ g(\theta) (\cos^3\theta - \nu_s \sin^2\theta \cos\theta)\ dL\, d\theta\right] \quad \text{Equation 44}$$

$$F_T = E_f \varepsilon_0 V_f\, ab\left[\int_0^{\frac{\pi}{6}} g(\theta) \cos\theta\ d\theta\right]\left[\int_0^{\frac{\pi}{6}} g(\theta)(\cos^3\theta - \nu_s \sin^2\theta \cos\theta)\, d\theta\right]\left[\int_0^{a} \Phi\ h(L)\, dL\right] \quad \text{Equation 45}$$

$$F_T = E_f \varepsilon_0 V_f\, ab[C_A][D] \quad \text{Equation 46}$$

$$C_A = \left[\int_0^{\frac{\pi}{6}} g(\theta)\cos\theta \; d\theta\right]\left[\int_0^{\frac{\pi}{6}} g(\theta)(\cos^3\theta - \nu_s \sin^2\theta\cos\theta)\, d\theta\right] \quad \text{Equation 47}$$

$\boldsymbol{C_A}$ is the fibre orientation factor of the composite for Compression force acting on the axial direction,

$$D = \int_0^a \Phi \; h(L)\, dL \quad \text{Equation 48}$$

D is the fibre length factor and **Φ** is given by [187] as

$$\Phi = 1 - \frac{\tanh\left(\frac{\beta L}{2}\right)}{\left(\frac{\beta L}{2}\right)} \quad \text{Equation 49}$$

$$\beta = \left[\frac{E_m}{E_f\,(1+\nu_m)\,r_f^2 * \frac{1}{2}\ln\frac{2\pi}{\sqrt{3}\,V_f}}\right] \quad \text{Equation 50}$$

Fibre length and orientation distribution factors were introduced to calculate the elastic modulus of matrix is given by [190]:

$$E = C_A * D * E_f * V_f + E_m V_m \quad \text{Equation 51}$$

For Elastic modulus at Transverse direction, IROM models developed for composite modulus [184] showed in Equation 52 provides more accurate result:

$$\mathrm{E_2} = \left(\frac{\mathrm{V_F} + \eta * \mathrm{V_M}}{\left(\frac{\mathrm{V_F}}{\mathrm{E_{F_2}}}\right) + \left(\frac{\eta * \mathrm{V_M}}{\mathrm{E_M}}\right)}\right) \quad \text{Equation 52}$$

Where, $\boldsymbol{E_{F_2}}$ fibre modulus in the transverse direction is unknown in most cases but 'η' the stress-partitioning factor can be calculated empirically. The stress-partitioning factor satisfies the condition 0 <η <1, but usually taken between 0.4 and 0.6. Though it gives accurate results, the orientation of fibres and length is not considered in Equation 52.

Therefore, Equation 47 is modified to accommodate orientation function in the Equation 51. In general, the fibre orientation is defined as the angle between the axial direction of the fibre and the X-axis direction. In Transverse direction, fibre has the probability to align between 0° to 30° in the flow with respect to Y-axis as shown in Figure 24. Therefore, for transverse

direction calculation, fibre orientation angle (***θ***) lower limit can be set between π/6 and π/2, consider the force is acting on the axial direction of the fibre.

For Compression force at Transverse direction,

$$C_T = \int_{\pi/6}^{\pi/2} g(\theta)\, cos\theta\, d\theta \int_{\pi/6}^{\pi/2} g(\theta) * (cos^3\theta - \nu_m\ sin^2\theta\, cos\theta)\, d\theta \qquad \text{Equation 53}$$

3.3.12. Analytical and microstructure techniques

3.3.12.1 Scanning Electron Microscope (SEM)

Scanning Electron Microscope (SEM) is used to examine the morphology and microstructure of the tested sample materials. This is achieved by using Zeiss Supra 35VP microscope (Figure 157) with a high field emission employed to interact with the atoms of the tested sample material producing micro-images with a very wide range and high magnifications, reaching up to 50,000X. Before loading the tested sample for SEM analysis, the sample is subjected to gold coating to increase their conductivity for better micro-images production. This is done using Polaron-SC7640 coating device, with a coating time of 100 seconds for each sample. Moreover, the atomic density of the tested sample material was assessed using an Energy Dispersive X-ray (EDX), which is incorporated within the SEM machine.

3.3.12.2 X-Ray Diffractometer (XRD)

X-Ray Diffractometer (XRD) was used to analyse the crystallinity of cellulose in DPF using X'Pert Pro MRD (PANalytical) diffractometer using CuKα (1.2405980Å) radiation Ni-filter and scintillation counter as detector at 45 kV and at 23 mA. Experiments were carried out in the continuous mode at a scan speed of 2° per min and with a step size of 0.02°. The X-ray diffracto-grams were recorded from 10 to 50° (Bragg angle). The crystallinity index and percentage of crystallinity (%Cr) of cellulose were calculated according to peak height method using Equation 54.

$$\mathrm{C_rI}\ (\%) = \frac{(\mathrm{I_{002}} - \mathrm{I_{am}})}{\mathrm{I_{002}}}\ \mathrm{x}\ 100 \qquad \text{Equation 54}$$

3.3.12.3 Fourier-transform Infrared Spectroscopy (FTIR)

Fourier-transform Infrared spectroscopy (FTIR) is an analytical technique used to identify the organic material, and in some cases inorganic, by measuring the absorption of the infrared radiation by the sample material versus wavelength. Also, the chemical bonds within the sample material, their functional groups and their interaction mechanism with the polymer or cementitious matrix can be investigated and detected through FTIR analysis. Perkin Elmer

Spectrum device, shown in Figure 158, was used to carry the FTIR analysis. Sample materials were placed on an attenuated total reflection stage with a diamond detector, where the Infrared beam penetrates through the sample material and the resultant transmitted energy is measured. Subsequently, a spectrum is produced with a wavenumber ranging from 600 cm^{-1} to 4,000 cm^{-1} with a 2 cm^{-1} resolution, 5 kHz scanning speed 30 scan count for each sample material. According to several researchers, the FTIR analysis is very accurate with high sensitivity and reliability in analysing and quantifying materials.

3.3.12.4 Optical Microscopy

Samples developed in this experimental study were examined using laboratory Stereo zoom microscope Optika Italy model SZN-6 with Parfocal achromatic zoom 0.67x – 4.5x. Image analyses were carried out on the cross Section of a 10 x 10 mm samples for the polymer reinforced composites and debris for the inorganic reinforced composites. Microstructure analyses were carried out to ensure the homogeneous mixture between the DPFs and the binder matrix system and to study the failure mechanism due to different sieving size. Also, debris resulting from DPF reinforced cementitious composites were analysed to evaluate the microstructure of the sample.

Chapter 4: The Effect of Surface Treatments on the Tensile Strength and Characteristics of Date Palm Fibres

4.1. Abstract

The increase in demand of utilizing natural fibres as a reinforcement for sustainable composite development, DPF shows a significant potential to be utilized due to its cost effectiveness and abundancy in the MENA region. DPF suffer from a low compatibility with hydrophobic matrix systems. Therefore, improving the interfacial bonding between the DPF and polymer matrices is crucial. In this chapter, DPF were modified using several treatment types and conditions with the aim of optimising the parameters of each treatment to achieve the optimum adhesion between DPF and polymer matrices. DPF modifications were characterized and analysed using Scanning Electron Microscopy (SEM), Fourier Transform Infrared analysis (FTIR) and X-Ray Diffraction analysis (XRD). The tensile strength of untreated and surface modified DPF was done to evaluate the effectiveness of the treatment and the parameters on the strength of the fibre. The chemical composition of the optimal samples from each treatment type was analysed to see enhance the results with the % change in cellulose, hemicellulose and lignin content of the fibre.

4.2. Results and discussion

4.2.1. Tensile property of DPF

The tensile testing results of DPF surface modified with different types of treatments at different conditions and concentrations are presented in this section. Each test was repeated 25 times and the average results are displayed along with the standard deviation. Initially, the effect of soaking DPF in room temperature and hot water temperature water baths on the tensile stress and strain of DPF are presented in Figure 25 and Figure 26 respectively. In general, DPF exhibits a tensile behaviour that shows that they are ductile, the elastic regions can be identified from Figure 25 to Figure 32. The scatter in standard deviations is high for the results when measuring NF diameters due to their non-uniform needle-like surface morphology, unlike synthetic fibres.

Soaking DPF in room temperature water had lower effect in comparison to soaking it in hot water, which indicates that temperature has a vital role in surface modification. Soaking DPF in both room temperature and hot water showed an increase tensile stress by 70.28 and 102.86 % respectively after 120 hours. However, DPF soaked in room temperature water showed further increase of 9.73% in tensile stress after further 24 hours of treatment but a

decrease in tensile strength of 14.93% for DPF soaked in hot water when comparing the strength at 120 and 144 hours of soaking duration. This may be due to the fibre damage at high temperature and long duration which will have a negative impact on the strength of the fibre.

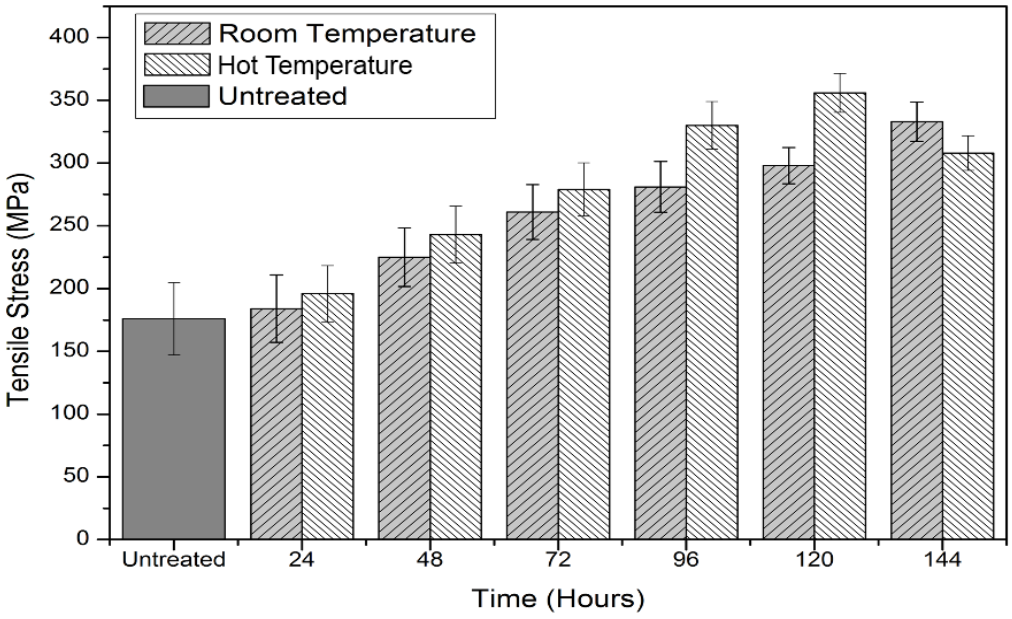

Figure 25 Tensile stress of water retting DPF treatment

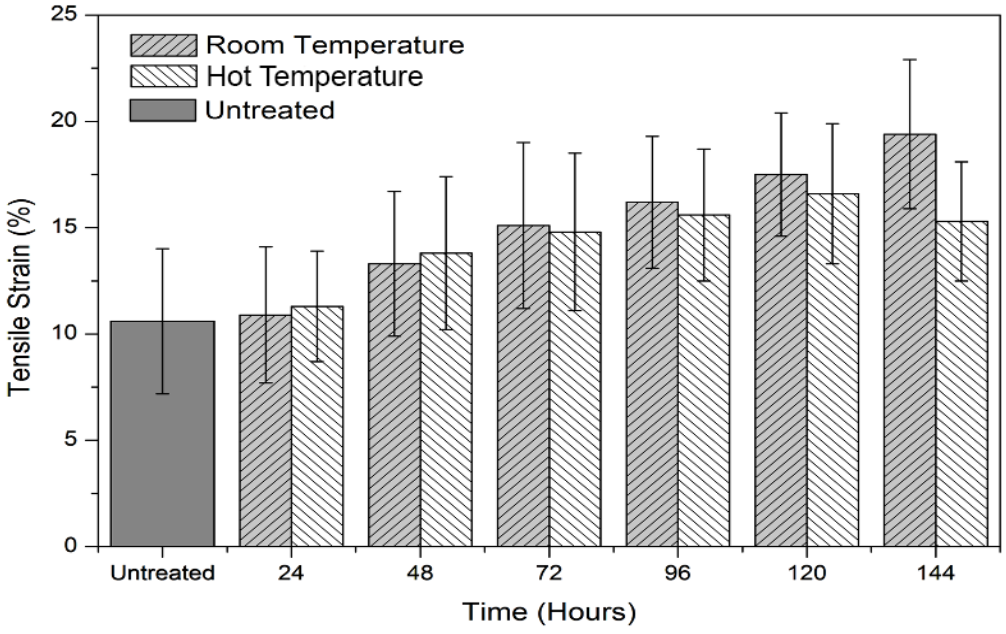

Figure 26 Tensile strain of water retting DPF treatment

Alkaline Treatment

Alkaline treatment of DPF with different concentrations (3, 6, and 9 wt.%) for different treatment durations had a great impact on the tensile strength and mechanical properties of DPF. Immersing DPF in 6% NaOH aqueous solution for 24 h at room temperature exhibited the best tensile strength of 433 MPa, which is 147% increase than untreated DPF and an increase in strain up to 18%. The lowest tensile strength, 88 MPa, was treating DPF with 9% NaOH for 24 hours which showed a reduction in tensile strength by 49.7%. Thus, from the results we can say that as the concentration of NaOH increases, the tensile properties of DPF decreases. Therefore, in alkaline treatment there are several parameters that have an important role in identifying the characteristics and properties of DPF, there is an optimum NaOH concentration, soaking duration and temperature. However, for this study we can propose that 6% NaOH at boiling temperature is the optimum concentration which provides good fibre strength.

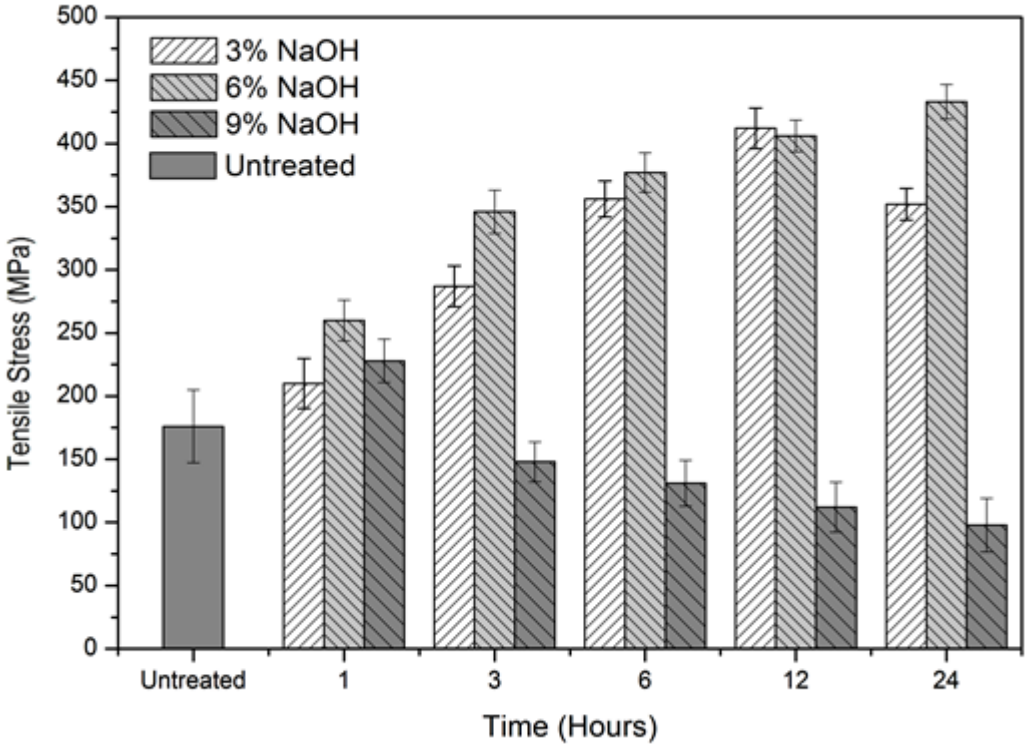

Figure 27 Tensile stress of alkaline DPF treatment

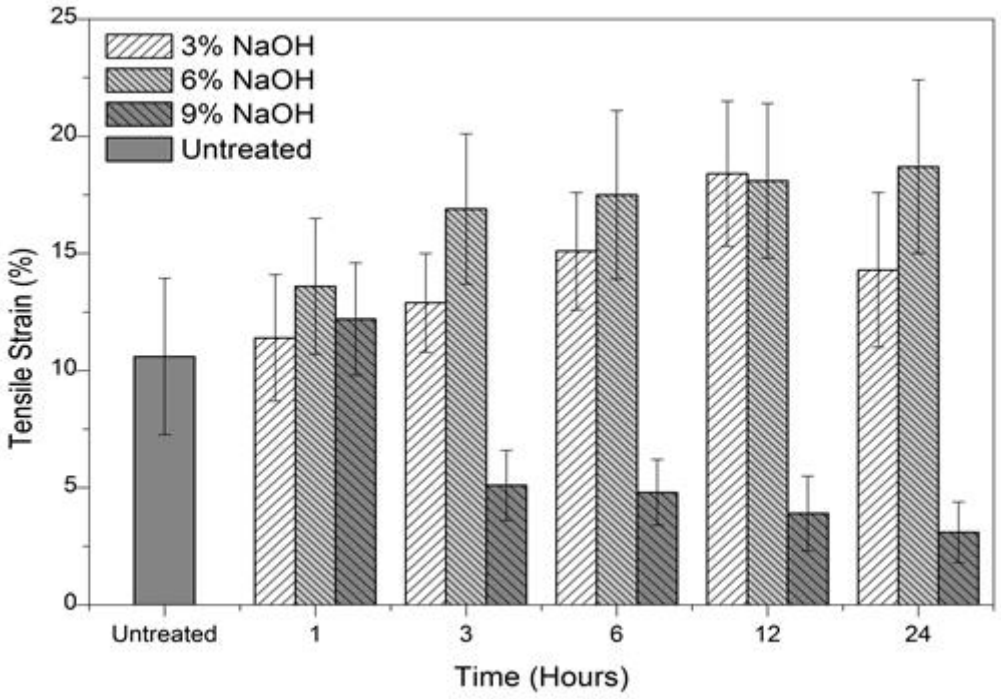

Figure 28 Tensile strain of alkaline DPF treatment

TMA Treatment

T:M:A treatment showed enhanced tensile strength results where the increase in both tensile strength and stress increased with the increase in surface modification duration. The highest increase in strength was observed after soaking time of 24 hours which enhanced the tensile stress and tensile strain by 60% and 109% respectively.

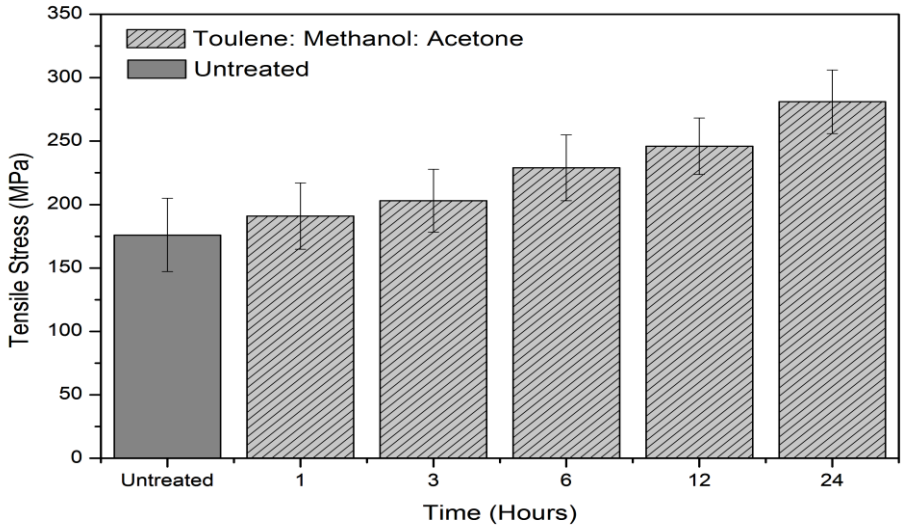

Figure 29 Tensile stress of Toluene: Methanol: Acetone DPF treatment

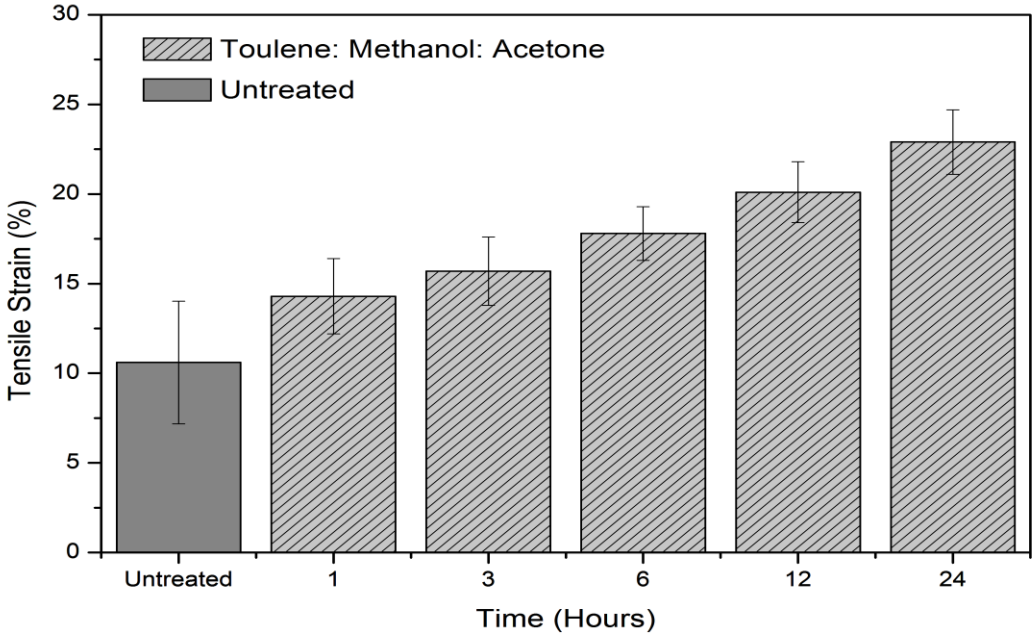

Figure 30 Tensile strain of Toluene: Methanol: Acetone DPF treatment

Starch Treatment

Moreover, the effect of starch showed a positive impact on the mechanical properties of DPF. Starting with the results of the SL of the fibre with respect to various starch concentrations and soaking times which are presented in Table 32.

Table 32 SL% of DPF under different concentration & soaking conditions

Soaking Time (min)	**Starch Loading (%)**		
	3	**6**	**9**
3	*6.8*	*9.8*	*8.4*
6	*7.4*	*11.6*	*9.8*
9	*7.1*	*7.6*	*7.4*

Results showed that the SL% increased with the soaking time until it reached its maximum value then deceased again with respect to the soaking time. At low concentration and soaking time SL% values are low because soaking increases the cross-sectional area of the fiber at the same time the fiber surface become lustrous. As a result, starch can easily diffuse in the fiber and react with cellulose in low soaking time. At higher starch concentration, SL value decreases with increase in starch concentration. The decrease in starch loading value at

higher concentration and soaking time could be associated with the fact that the swelling of the cellulose backbone with water is insufficient because of low water concentration. As a result, starch molecules are incapable of penetrating the cellulose molecules in the presence of low solvent concentration. This may cause a smaller number of reacting sites at the cellulose backbone and thus continue to reduce the active sites as water concentration decrease with higher starch concentration. In higher soaking time, the fiber become twisted, shrinks, and changes its outer fibrillar layers. DPF showed a maximum value of 11.6 % when immersed in 6% starch solution for 6 min soaking time. The mechanical properties of DPF showed to have a correlation with the SL%, where all starch treated fibres showed higher tensile strength. Tensile strength of DPF subjected to starch solution treatment showed positive results were at maximum SL% the tensile strength was improved by 53% compared to the untreated DPF having a value of 267 MPa.

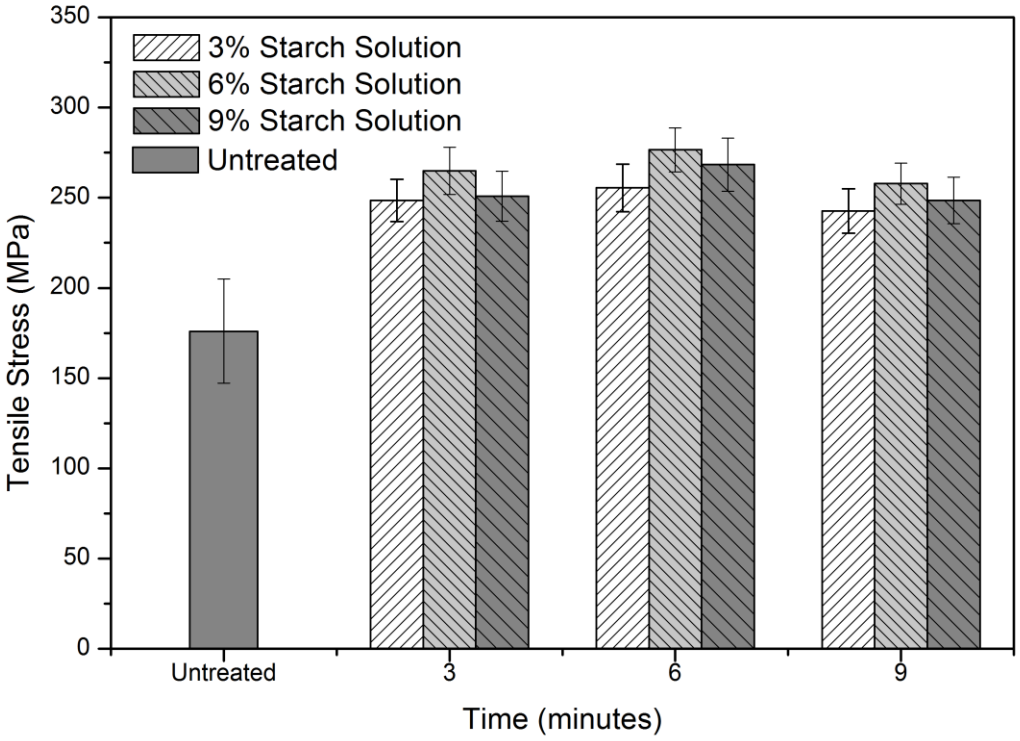

Figure 31 Tensile stress of treated DPF in starch solution

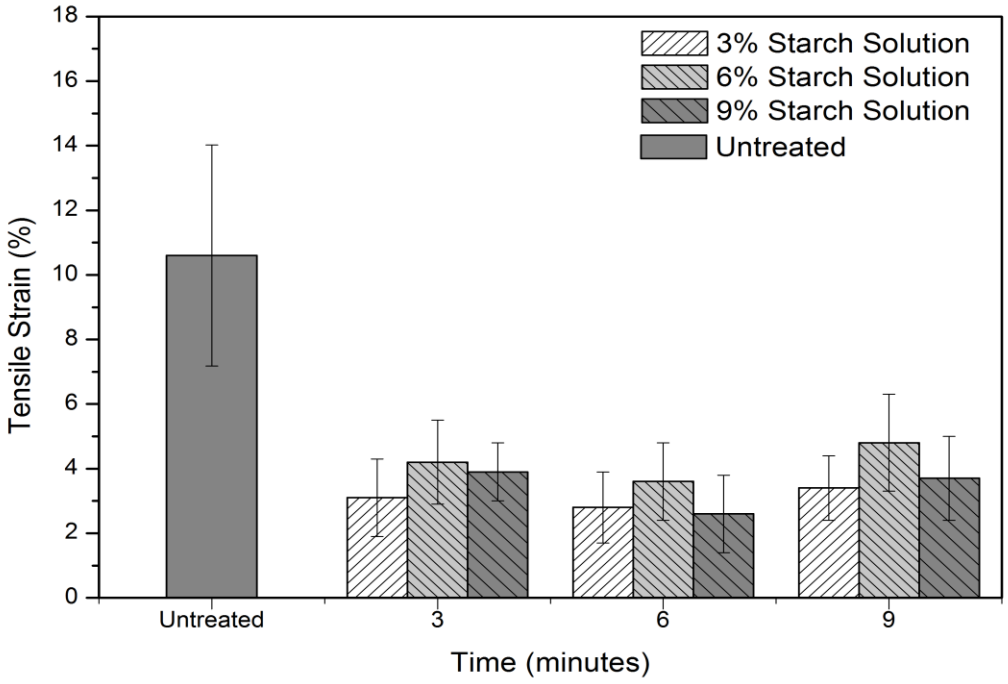

Figure 32 Tensile Strain of treated DPF in starch solution

4.2.2. Chemical composition

Table 33 shows the various chemical components present in DPF. Untreated DPF has the highest lignin value and the lowest cellulose content compared to the surface modified fibres. The increase in cellulose content and the decrease in the lignin content enhances the theories of effective surface modification that removes impurities and lignin and brings together the cellulose within the internal structure making it more compacted and aligned, thus enhances the overall strength of the fibre, and provides better surface morphology for enhanced interfacial bonding when used as a reinforcement.

Table 33 Chemical composition (%) of surface modified DPF

Treatment	Cellulose	Hemicellulose	Lignin	Ash	Other
Untreated	37.30	11.70	33.53	3.77	13.70
Water retting (room temp.) @120 hrs	40.21	12.11	27.87	4.22	15.59
Water retting (hot temp.) @120 hrs	43.27	14.23	23.14	4.95	14.41
3% NaOH – 1 Hr	35.43	13.50	30.51	6.18	14.38
3% NaOH – 24 Hr	43.11	14.61	22.33	5.23	14.72

Treatment	Cellulose	Hemicellulose	Lignin	Ash	Other
6% NaOH – 24 Hr	51.22	14.55	22.91	3.21	8.11
9% NaOH – 1 Hr	35.39	8.69	24.40	10.74	20.78
9% NaOH – 24 Hr	37.28	13.26	26.68	9.65	13.13
T:M:A – 1 Hr	40.40	12.00	33.16	2.66	11.78
T:M:A – 24 Hr	50.55	14.89	20.58	1.65	12.33
6 % SS – 6 min	41.70	14.85	27.44	2.21	13.71

4.2.3. Chemical structure in relation to the surface modification

The chemical structure of untreated and various treatments effect on DPF were analysed using FTIR. The functional groups present in DPF such as lignin, cellulose, pectin and hemicellulose and their respective Infrared bands are demonstrated in Table 34 and Table 35. FTIR spectrum investigates the shifted or transformed functional groups within DPF after subjected to different types of treatments. Figure 33 to Figure 36 show the FTIR spectra, demonstrating the wavenumber against the transmittance, for the untreated and treated DPFs. The broad peaks ranging from 3,272 cm^{-1} – 3,284 cm^{-1} are attributed to the, – OH, hydroxyl groups of hemicellulose and cellulose. These broad peaks were found to decrease after subjected to surface modification treatment. Untreated DPF, the band at 2918 cm^{-1} corresponds to the C – H stretching of lignin which is shifted to 2,850 cm^{-1} after treating the fibre clearly indicates the removal of lignin [18]. Moreover, untreated DPF should show an intensity absorbance at 1,631 cm^{-1} which corresponds to C=O groups of pectin and hemicellulose which have disappeared when treated with NaOH, water, T:M:A and remained when treated with starch solution. The characteristic peak 1,035 cm^{-1} corresponding to C-O stretching of lignin in the untreated DPF showed a transition to lower wave lengths due to the removal of lignin from the surface.

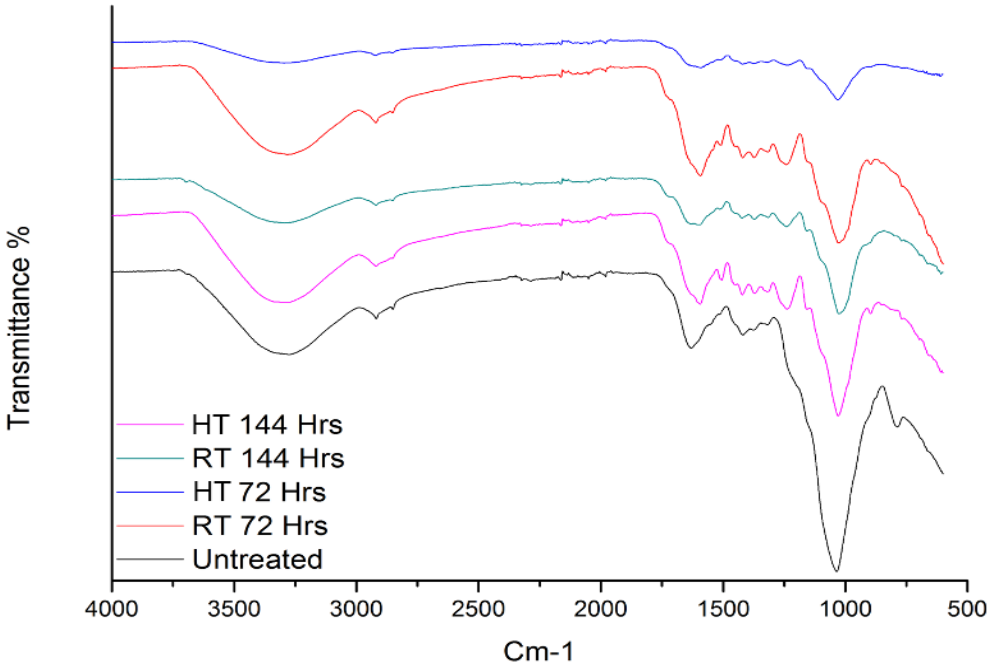

Figure 33 FTIR spectra of untreated DPF and water retting DPF

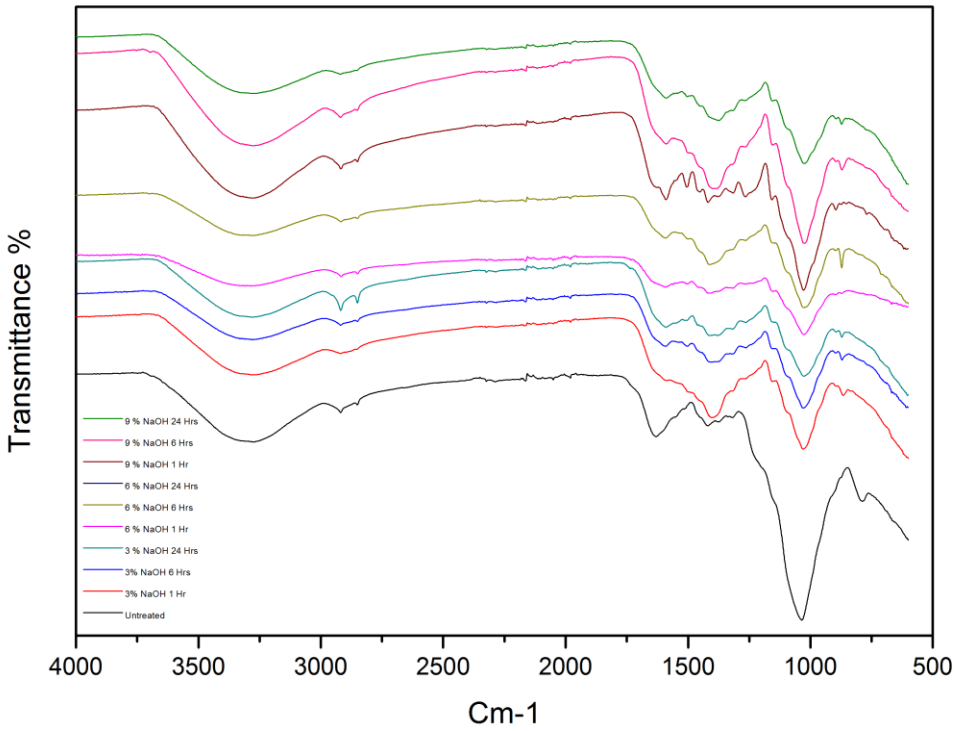

Figure 34 FTIR spectra of untreated DPF and NaOH treated DPF

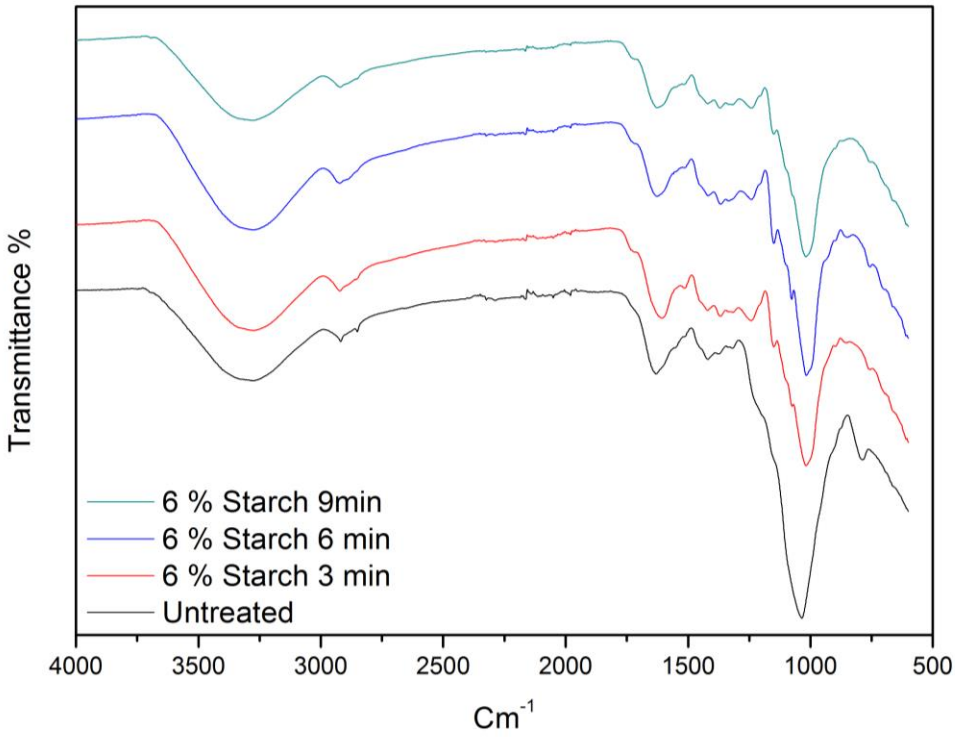

Figure 35 FTIR spectra of untreated DPF and starch treated DPF

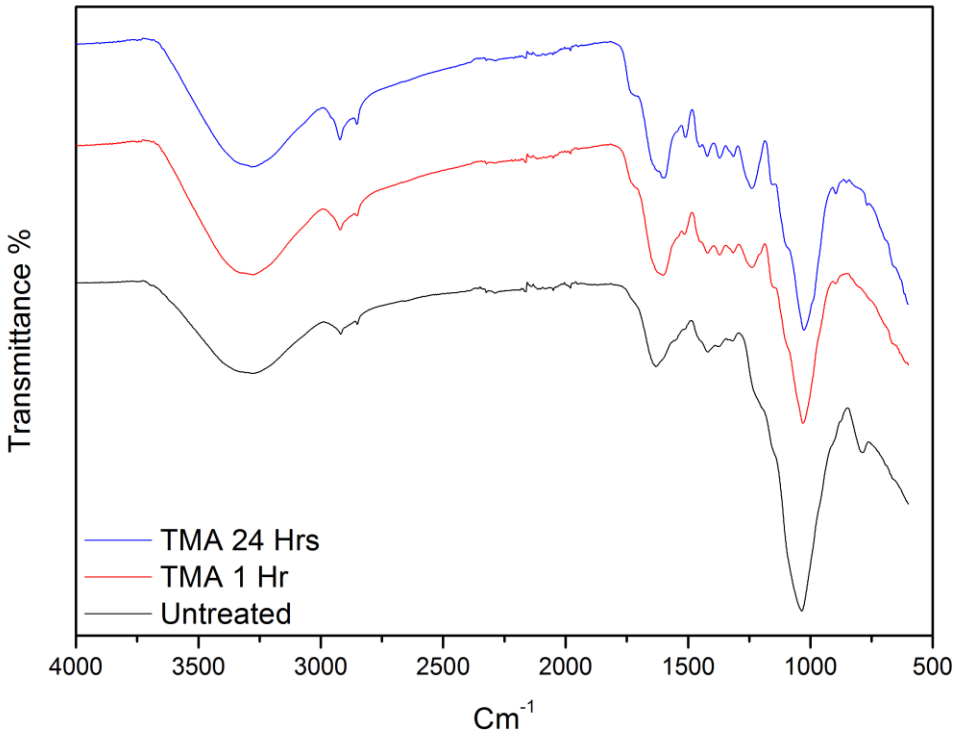

Figure 36 FTIR spectra of untreated DPF and T:M:A treated DPF

Table 34 FTIR analysis of alkali treated DPF

Intensity absorbance (cm^{-1})										Possible Assignments
Untreated	**3% NaOH 1 h**	**3% NaOH 6 h**	**3% NaOH 24 h**	**6% NaOH 1 h**	**6% NaOH 6 h**	**6% NaOH 24 h**	**9% NaOH 1 h**	**9% NaOH 6 h**	**9% NaOH 24 h**	
3278	3272	3278	3277	3284	3284	3278	3276	3277	3278	O–H stretching
2918	2919	2198	2918	2917	2918	2919	2918	2918	2919	C–H stretching vibration in cellulose and hemicellulose
2286	-	-	2850	-	-	-	-	-	-	
2163	-	2115	2112	2051	2114	2163	2113	2162		
2051	-	-	-	-	-	-	-	-	-	
1981	-	1980	1981	1980	-	-	-	-	-	
1631	-	-	-	-	-	-	-	-	-	C=O stretching of carboxylic acid orester
-	-	1592	1591	1592	1592	1589	1590	1588	1588	Aromatic C=C stretching
-	-	1502	-	-	-	1503	1503	-	-	
-	-	-	-	-	-	-	1451	-	-	CH_2 symmetric bending in lignin
1418	1400	1407	1408	1412	1409	1384	1418	1396	1373	
-	-	-	-	-	-	-	1315	-	-	O–H bending
-	-	-	-	-	-	-	1157	-	-	Antisymmetric bridge C–O–C stretching
1035	1028	1030	1027	1025	1027	1027	1027	1024	1027	C–O/C–C/C–H stretching vibration

Intensity absorbance (cm^{-1})										Possible Assignments
Untreated	**3% NaOH 1 h**	**3% NaOH 6 h**	**3% NaOH 24 h**	**6% NaOH 1 h**	**6% NaOH 6 h**	**6% NaOH 24 h**	**9% NaOH 1 h**	**9% NaOH 6 h**	**9% NaOH 24 h**	
-	-	-	-	-	-	896	896	-	--	COC, CCO and CCH deformation and stretching (b- Glucosidic linkage)
787	865	871	871	-	872	872	-	871	872	

Table 35 FTIR of water, T:M:A, and SS treated DPF

Intensity absorbance (cm^{-1})										Possible Assignments
Untreated	**RT Water 72 h**	**BT Water 72 h**	**RT Water 144 h**	**BT Water 144 h**	**T:M:A 1 h**	**T:M:A 24 h**	**6% SS 3 min**	**6% SS 6 min**	**6% SS 9 min**	
3278	3293	3297	3282	3297	3277	3279	3273	3281	3276	O–H stretching
2918	2919	2918	2920	2918	2920	2921	2921	2920	2922	C–H stretching vibration in cellulose and hemicellulose
2286	-	-	-	2285	-	-	-	-	-	
2163	-	-	-	-	2163	-	-	-	-	
-	-	-	-	-	2112	2113	2113	-	2116	
2051	2050	2051	2051	2051	-	-	-	-	-	
1981	-	1980	1980	-	-	1981	-	-	-	
1631	-	-	-	-	-	-	-	1627	1627	C=O stretching of carboxylic acid orester

Intensity absorbance (cm^{-1})										Possible Assignments
Untreated	**RT Water 72 h**	**BT Water 72 h**	**RT Water 144 h**	**BT Water 144 h**	**T:M:A 1 h**	**T:M:A 24 h**	**6% SS 3 min**	**6% SS 6 min**	**6% SS 9 min**	
-	1595	1594	1593	1594	1603	1603	1606	-	-	Aromatic C=C stretching
-	-	-	1507	1506	1514	1509	-	-	-	
1418	1421	1421	1420	1421	1420	1420	1420	1419	1419	CH_2 symmetric bending in lignin
-	1372	-	1373	1371	1371	1371	1368	1371	1364	C–H bending in hemicellulose and lignin
-	-	-	1317	1316	1315	1315	-	-	-	O–H bending
-	1241	1236	1242	1238	1240	1240	1243	1240	1241	C–O stretching of acetyl (lignin)
-	-	-	-	-	-	-	1149	1150	1149	Antisymmetric bridge C–O–C stretching
-	-	-	-	-	-	-	-	-	1076	
1035	1024	1032	1028	1029	1031	1027	1018	1019	1016	C–O/C–C stretching vibration
-	-	-	896	896	-	896	-	-	-	b-Glucosidic linkage
-	-	-	-	-	-	852	-	-	847	
787	-	-	-	-	-	-	-	-	-	

4.2.4. Effect of surface modification on crystalline structure

The X-ray diffractograms conducted on the untreated DPF and the optimum treatment concentrations of each treatment was completed and the results unfortunate have not been analysed due to the facilities closure through the pandemic and the critical submission date of my thesis. It is observed while analysing the samples that the major crystalline peak for each sample was detected at approximately 2θ angle = 22.5°, which represent the cellulose crystallographic plane (002) and the average intensity peak at 15.90°. The XRD shows that the intensity of the (002) crystallographic plane was changed depending on the different treatment type.

The crystallinity index (CrI) of the untreated and treated DPF samples were calculated using Equation 54 which described in the testing methods section 3.3.12.2. Results demonstrated that the CrI of DPF increased with alkali treatment. This is thought to be due to better packing and stress relaxation of cellulose chains as a result of the removal of pectin and other amorphous constituents from the fibre [17]. The increase in crystallinity obtained by alkali treating the DPMF is thought to be the main contributing factor for the increase in fibre strength. Other well-defined peaks present by XRD are at $2\theta = 14.8°$ and $2\theta = 16.4°$, and these reflections correspond with the (1$\underline{1}$0) and (1 1 0) crystallographic planes, respectively. When the crystalline cellulose content is high, these two peaks are more pronounced, and when the fibre contains large amounts of amorphous material (such as lignin, hemicelluloses, pectin and amorphous cellulose), these two peaks are smeared and appear as one broad peak [53]. The peaks at 14.8° and 16.4° are more defined for the alkali treated DPF, therefore suggesting that the alkali treatment removed some of the amorphous materials from the fibre.

The reaction between different chemical reagents with cellulose takes place mainly in the amorphous cellulose regions or at the edges of crystalline cellulose regions; the reagents first react with the chain ends on the surface of crystallites, as they cannot diffuse into crystalline region, resulting in the opening of some of the hydrogen-bonded cellulose chains. This results in some conversion of crystalline to amorphous cellulose. The reagent then diffuses into this newly produced amorphous section, reacting with the crystalline cellulose and simultaneously generating more amorphous cellulose.

4.2.5. Morphology and microstructure of DPF

Understanding the surface morphology using SEM analysis of untreated DPF and the effect of different treatments is very vital in utilizing DPF in developing bio-composites. Surface morphology has a significant role in identifying the strength of interfacial bonding when mixed with any matrix system. DPF have a cylindrical shape containing large amount of impurities, fatty substances, wax and uncompleted grown weak fibres as shown in Figure 37. The

chemical composition and the impurities available at the surface of untreated DPF are identified through chemical composition analysis explained in Section 4.2.2. A definitive change in amount of DPF surface impurities and morphological structure was noticed after the treatments applied.

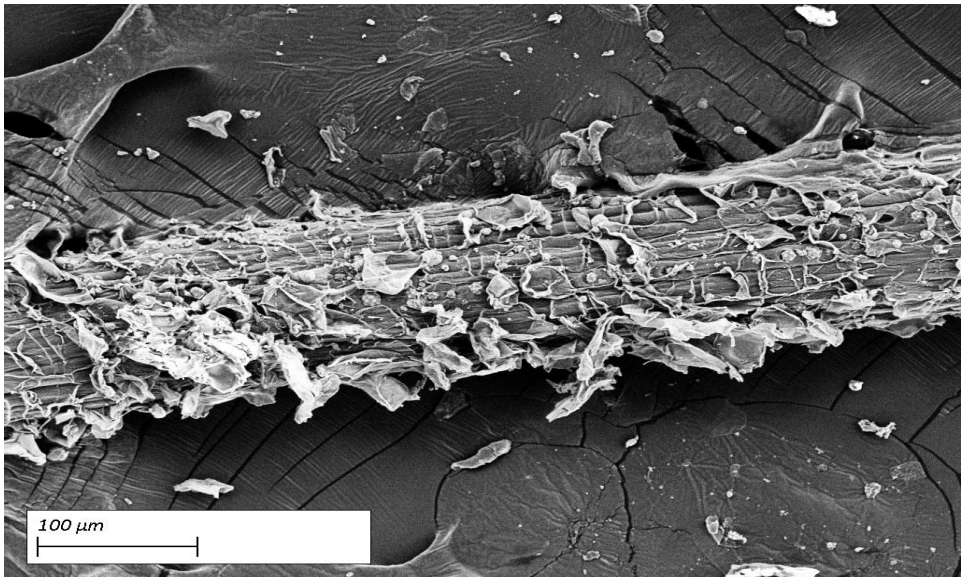

Figure 37 Untreated DPF 500X

Water retting treatment

Soaking DPF in room temperature water had no major effect in comparison to soaking it in hot water. This is because not much of the wax and lignin was dissolved at a low water temperature when compared to warm water. Also, longer water retting duration had better effect on the surface morphology where it is recommended to subject DPF for a longer period approximately 15 days to ensure optimal result output. However, it is considered an economical process in which no chemicals are used. Figure 38 demonstrates the effect of water retting process on the surface morphology of DPF. More porous and better surface morphology/topography is achieved which will provide better interfacial bonding when utilized as a reinforcement.

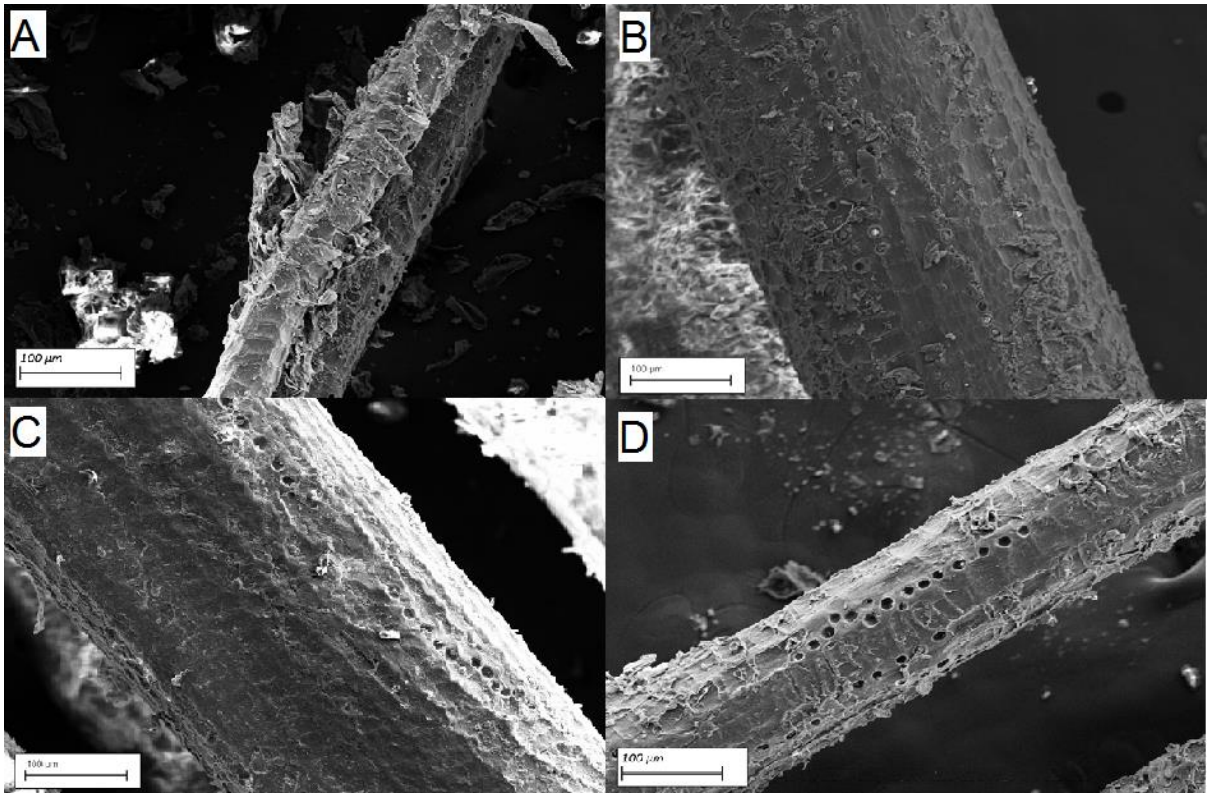

Figure 38 A) 72 hours room temperature 500 X, B) 120 hours room temperature 500X, C) 72-hour hot water 500 X, D) 120 hours hot water 500X

NaOH treatment

Identifying the optimum concentration and soaking duration of NaOH solution is very critical when applied for cleaning natural fibre surfaces from impurities. Three different concentrations were investigated to understand how the surface morphology changes after distinguished time intervals. Figure 39 demonstrates a comparison between the optimum and the worst treatment conditions in terms of tensile strength. Soaking DPF in a low concentration, 3 %, of NaOH solution for a short time interval removes partially surface impurities as shown in Figure 39 (A) thus a longer period is required to ensure full removal of surface impurities to achieve a porous topography as shown in Figure 39 (B). On the other hand, using a higher, 9 %, NaOH solution allows to remove surface impurities at a very short period and for a long-time interval damages the DPF by fracturing its surface making it very brittle as shown in Figure 39 (D). This was observed by the tensile stress testing for DPF treated by 9 % aqueous NaOH solution where the tensile stress increased from 178 MPa to 228 MPa in the first hour then decreased to 98 MPa after 24 hours. Furthermore, achieving a better topography, porous surface provides a larger surface area available for interfacial bonding when blended with matrix systems for developing composites. Another aspect of NaOH treatment is the decrease in DPF diameter after treatment. This is caused by fibrillation, which involves breaking down of the fibre into

smaller fibres as the binding materials, lignin and hemicellulose, were partially removed as reported in [102,116]. The chemical composition shows that after NaOH treatment the lignin and hemicellulose content decreased by 27% and 26% respectively when subjected to 9% aqueous NaOH treatment for 1-hour duration. Thus, reducing the diameter of DPF and the reaction of the DPF with the NaOH solution leads to an increase in the packing and rearrangement of the cellulose chains structure within the DPF, making it more compact, leading to a stiffer and stronger fibre increasing its mechanical properties. This was observed by achieving 143 % increase in tensile stress after treating DPF with 6% NaOH for 3 hours. Also, a decrease in DPF apparent diameter leads to an increase in aspect ratio of DPF which is advantageous for fibre-matrix adhesion by facilitating a good mechanical interlock between the DPF surface and the matrix system.

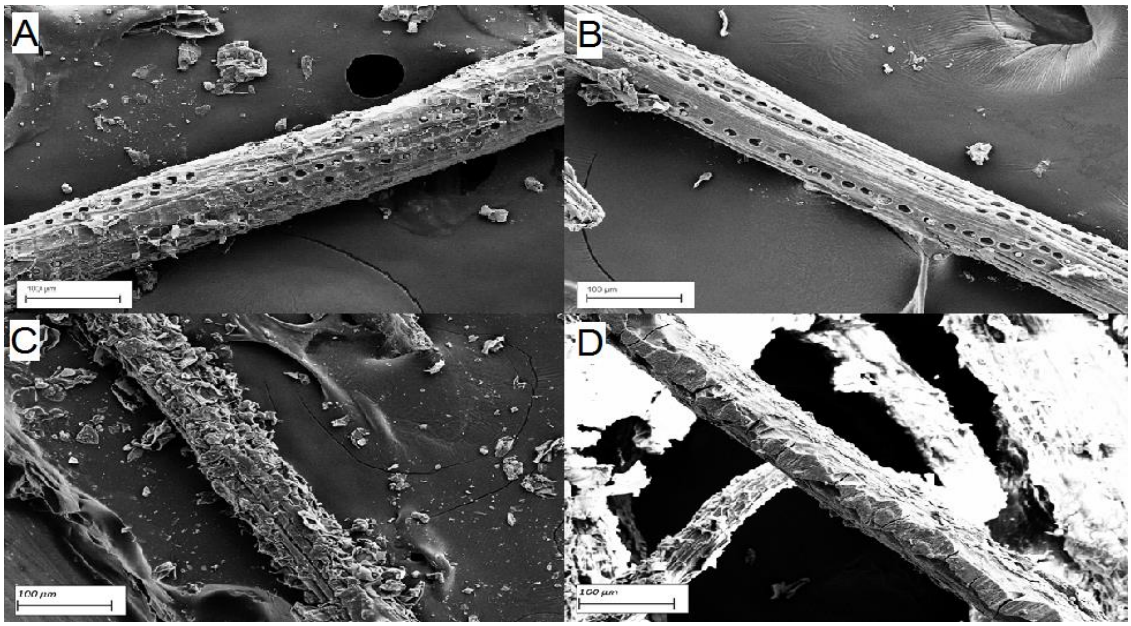

Figure 39 A) 3% NaOH for 24 hours 500X, B) 9% NaOH for 1 hour 500X, C) 3% NaOH for 1 hour 500X, D) 9% NaOH for 24 hours 500X

T:MA treatment

T:M:A solution was obtained from the media of Soxhlet extraction methodology. However, in this experimental work, DPF were immersed in this solution for various treatment durations. The surface topography shows the removal of some impurities from the surface of the fibre. The noticeable fact is that this treatment provided DPF with lowest tensile characteristics.

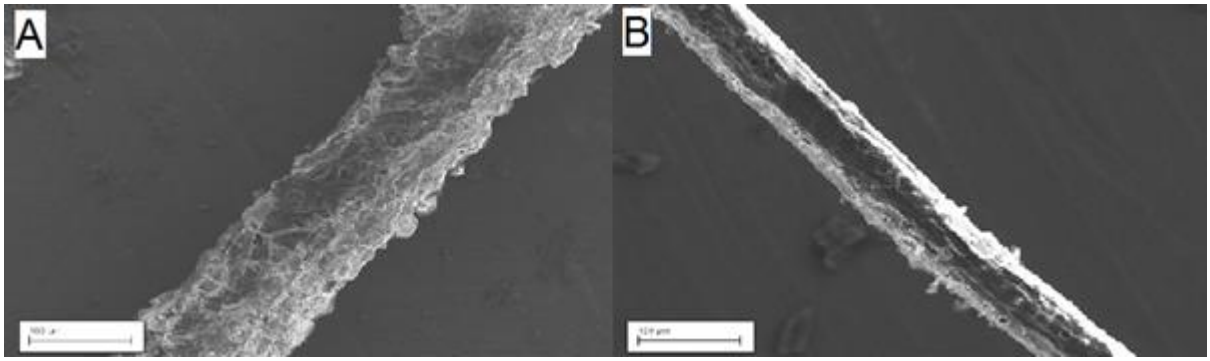

Figure 40 T:M:A for 1 hour, B) T:M:A for 24 hours 500X

Starch treatment

Starch deposits or coatings are observed on the surface of DPF, where the DPF have not fully cleaned by removing their surface impurities. This behaviour was also observed by Macedo et al. (2017) in a previous study evaluating the coating over cotton fibres [191]. It was observed that the initial mass of starch in the solution rules the deposition of the coating in the fibre surface. The process of coating formation is related to the retrogradation of the starch granule in the presence of water. As reported by Ratnayake and Jackson [192], the starch granule in solution will swell by absorbing water and heat increasing the mobility of the molecules leading to the disruption of the granule. The molecules of amylose and Amylopectin tend to segregate. Due to the cross-linked structures, the amylopectin will tend to agglomerate while amylose, with more mobility, will involve this amylopectin core and interact with amylose structures from other disrupted grains, forming a network in the fibre surface. Since the sample of 6%wt. has more available granules, the network will be more cohesive during the gelatinization process. The amylose molecules will interact with fibre surface, being absorbed in the fibre surface, filling the fractures and pores, forming mechanical anchoring for the coupling effect [193].

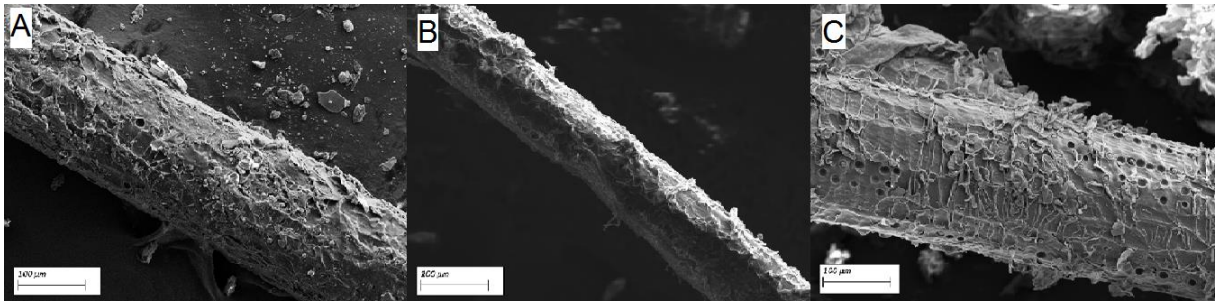

Figure 41 A) 6% starch 3 min 500X, B) 6% starch solution for 6 min 500X, C) 9% starch solution 9 min 500X

4.3. Interim summary

Various surface treatments applied to DPF showed different strength and characteristics depending on the soaking parameters. Tensile strength showed how it is affected depending on the concentration and time. Surface morphology, crystallinity, chemical structure and composition showed improvement with all surface treatment types. The optimal surface treatment obtained was alkali treatment with 6% concentration for 24 hours. Results showed an enhancement of 147% and 59% in tensile stress and tensile strain respectively and a better surface morphology. The highest tensile strain results were obtained by soaking DPF in T:M:A solution for 24 hours, where the strain increased by 109% compared to the untreated DPF

.

Chapter 5: Date Palm Fibre Geometry and its Effect on the Physical and Mechanical Properties of Recycled and Biodegradable thermoplastic composites

5.1. Abstract

This study investigates, evaluates and predicts the effect of DPF diameter size and loading content on both the mechanical and physical properties of DPF reinforced RPVC and PLA composite. The composites are developed using melt-mixing technique which is followed by compression moulding. The influence of the mechanical properties is investigated by evaluating the impact strength, tensile strength and flexural strength. Meanwhile the sieve analysis, thickness swelling (TS), moisture content (MC) and water absorption (WA) characteristics are evaluated. Composite microstructures are examined using optical microscopy to investigate the interfacial bonding between DPF and polymer matrix. Results showed that at 40 wt.% DPF, the TS, MC and WA were the highest demonstrating an increase of 1.57%, 1.76%, and 10.80%, respectively in reinforced RPVC. The flexural strength, tensile strength and impact strength decreased as the loading content increased showing maximum reduction at 40 wt.% loading, varying depending on DPF geometry when reinforced with both RPVC and PLA. Although the results demonstrated a decrease in mechanical properties and an increase in physical properties as DPF loading increased depending on DPF geometry, the results indicate that the developed technologies could be industrialised under the waste management scheme for non-structural applications. Moreover, to determine the effectiveness of DPF orientations in the PLA, the rule of mixtures (ROM), modified ROM, inverse rule of mixture (IROM), modified IROM and Halpin-Tasai were applied with three possible fibre orientations in the composites. The modified ROM and modified IROM closely matches the experimental results with the DPF oriented between 0° to 45° in the direction of compression force of the DPF/PLA composites. Also, the fungal decay and biodegradation of the composites developed are evaluated and investigated. Results showed that composites developed using PLA had higher weight loss (%) when compared to the same samples but mixed with RPVC. Composites with higher DPF content showed high rates of decay when used with different polymer matrix. Also, DPF length had a significant effect on the disintegration of the composites. DPF/PLA reinforced with 40 wt.% DPF showed the highest weight loss (WL%) reaching 5.61% and 5.46% when exposed to Tyromyces palustris and Irpex lacteus respectively. On the other hand, the biodegradation had a higher impact on the disintegration of the composites developed where the biodegradation, WL%, of PLA composites developed with 40 wt.% DPF showed 61.40%.

5.2. Processing of DPF/Polymer Composite

The DPF and polymer matrix were processed in a Barbender Plastograph twin-screw mixer (with Cam blades for mixer type N50EHT) at 190 ^{o}C for RPVC and 170 ^{o}C for PLA at 50 rpm for 6 minutes. Samples with four different mass proportions and six different fibre diameter size was produced with each polymer matrix. The composite fabrication was achieved by initially feeding into the melt-mixing mixer with the required amount of RPVC or PLA powder or pellet respectively for each batch, allowing it to completely melt for 2 minutes, and subsequently feeding in the DPF for 4 minutes to obtain a uniform mixture. Thus, the resulted mixture was grinded to pellets using a 2 mm sieve. The grinded pellets were compression moulded into a 100 mm (L) x 100 mm (W) x 4 mm (T) mould using an electrically heated hydraulic press. Compression moulding procedure involved pre-heating at 190 ^{o}C or 170 ^{o}C for 10 minutes without applied load, followed by 5 minutes compressing at the same temperature under 10 MPa pressure, and subsequently cooling under load until the mould reached 35^{o}C. The compression molded composite was cut using a band saw machine SEALEY SM1304 to achieve 100 mm (L) x 10mm (W) x 4 mm (T) samples for physical and mechanical properties tests.

5.3. Results and Discussion

5.3.1. Effect of DPF geometries and loading content on the physical properties of DPF composites

5.3.1.1 Sieve Analysis

Understanding the sieve analysis of DPF that can be utilized in developing sustainable composites is vital in assessing the particle size distribution and density. The percentage of DPF passing through each sieve size was calculated as shown in Figure 42. The amount of fibre passing through each mesh size could estimate the amount of each sieve size available in the unsieved DPF and can help in interpretation of the results which will be discussed in Sections 5.3.1 and 5.3.2. Figure 42 shows that 97% of the grinded DPF passes through the 1,000 µm sieve, which then 12% gets retained on the 500 µm sieve and 85% passes through. Afterwards, 60% of the DPF gets retained on the 250 µm sieve in which only 28% passes through having 19% retaining on the 125 µm sieve and the remaining 9% passing through. It must be noted that there may be a huge variance in calculating the exact length and diameter passing through a sieve size due to the thread like non-uniform shape of DPF, and this may not be the true representation of the fibre in composites, due to the possibility of fibre being retained on a certain mesh size due to its length but passing through a certain mesh size based on its length, or its diameter, or based on both diameter and length [194]. Also, DPF

has the tendency on clogging the mesh of the sieve while trying to pass through due to its non-uniform diameter, thus decrease the amount of fibre passing through, which leads to a misrepresentation of accurate results. Therefore, it is very difficult to estimate that real particle size distribution.

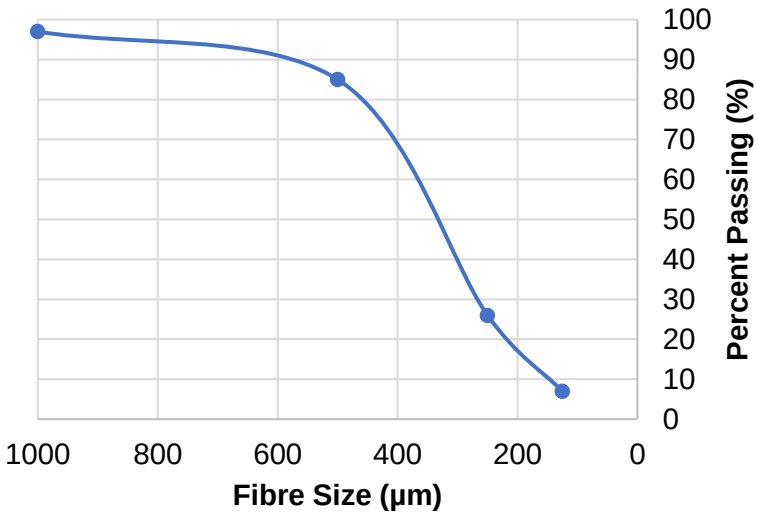

Figure 42 Sieved analysis of DPF

The bulk density of various DPF sieve size was analysed to evaluate the difference in volume of each sieve size having the same wt.% loading (Figure 43). The bulk density is higher for DPF size of ≤125 µm than 125 – 500 µm and then density decreased with the size increased. This is also reflected in the density of their corresponding composites (Table 36). The decrease in the density means that there may be not enough RPVC matrix to blend with the DPF of low density, ≤125 µm and ≥1,000 µm, due to the high volume of DPF available. This may lead to a direct influence on the structure of the composite that hence affects the physical and mechanical characteristics of the composite.

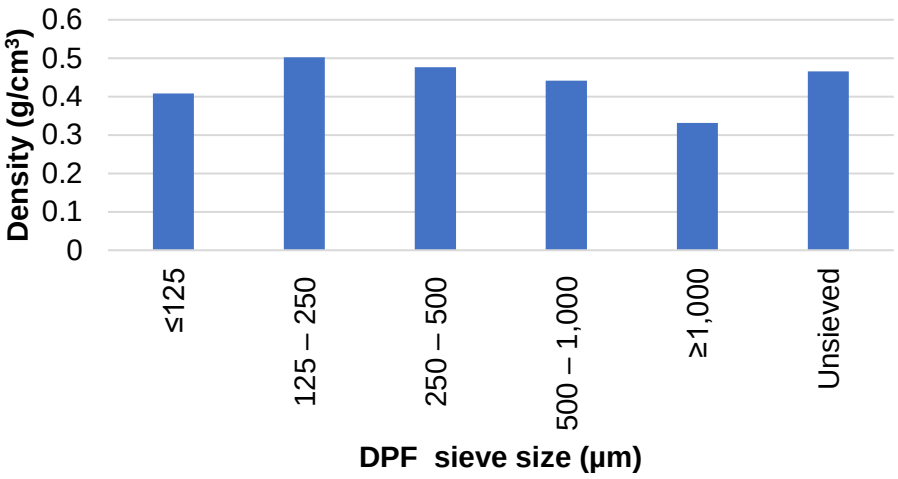

Figure 43 Density of DPF with different diameters

Table 36 RPVC, PLA and DPF sieve size densities

Material	Density (g/cm³)
RPVC	1.2450
PLA	1.1780
≤125 µm DPF	0.4079
125 – 250 µm DPF	0.5024
250 – 500 µm DPF	0.4762
500 – 1,000 µm DPF	0.4413
≥1,000 µm DPF	0.3317
Unsieved DPF	0.4658

Table 37 DPF/PLA bio-composite density (theoretical)

DPF size (µm)	Density (g/cm³) of composites developed at different DPF loading contents (Wt.%)			
	10% DPF	**20% DPF**	**30% DPF**	**40% DPF**
≤125	0.99	0.86	0.75	0.67
125 – 250	1.04	0.93	0.84	0.77
250 – 500	1.03	0.91	0.82	0.74
500 – 1,000	1.01	0.88	0.78	0.71

≥1,000	0.94	0.78	0.68	0.58
Unsieved	1.02	0.90	0.81	0.73

Table 38 DPF/PLA bio-composite (experimental evaluation)

DPF size (µm)	**Density (g/cm^3) of composites developed at different DPF loading contents (Wt.%)**			
	10% DPF	**20% DPF**	**30% DPF**	**40% DPF**
≤125	0.98	0.84	0.72	0.52
125 – 250	1.03	0.89	0.80	0.63
250 – 500	1.01	0.87	0.77	0.64
500 – 1,000	0.99	0.83	0.73	0.61
≥1,000	0.92	0.75	0.62	0.50
Unsieved	0.96	0.80	0.70	0.61

The difference between the experimental and theoretical densities of the bio-composites developed can provide an indication on the volume fraction percentage of voids (Vv %) in the composites. As the Vv % increases within the bio-composites a weaker interface strength due to inadequate adhesion between DPF and PLA which results in crack initiation and growth leading to a reduction in the strength of the composite. Also, the Vv% gives an indication on the physical properties which the WA can be directly proportional related to the Vv%. It is observed from Table 39 that ≤125 µm at 40 wt.% loading content had the highest Vv of 21.72% which can be correlated to the findings of the physical and mechanical tests of the composites where the same DPF size and loading had the highest W_A% content. Also, it can be deduced that as the DPF loading increased the Vv% increase in the composite which directly influences both the physical and mechanical properties negatively.

Table 39 Volume fraction percentage of voids (Vv) in DPF/PLA bio-composite

DPF size (µm)	**V_v (%) at different DPF loading contents (Wt.%)**			
	10% DPF	**20% DPF**	**30% DPF**	**40% DPF**
≤125	0.97	2.32	3.73	21.72
125 – 250	1.26	3.83	5.24	17.72
250 – 500	2.00	3.91	5.96	13.15

500 – 1,000	2.22	5.19	6.92	13.93
≥1,000	2.05	4.28	8.13	13.56
Unsieved	5.61	11.27	13.76	16.98

Table 40 DPF/RPVC composite density (theoretical)

DPF size (µm)	Density (g/cm^3) of composites developed at different DPF loading contents (Wt.%)			
	10% DPF	**20% DPF**	**30% DPF**	**40% DPF**
≤125	1.03	0.88	0.77	0.68
125 – 250	1.08	0.96	0.86	0.78
250 – 500	1.07	0.94	0.84	0.76
500 – 1,000	1.05	0.91	0.81	0.72
≥1,000	0.98	0.80	0.68	0.59
Unsieved	1.07	0.93	0.83	0.75

Table 41 DPF/RPVC composite density (experimental evaluation)

DPF size (µm)	Density (g/cm^3) of composites developed at different DPF loading contents (Wt.%)			
	10% DPF	**20% DPF**	**30% DPF**	**40% DPF**
≤125	1.00	0.82	0.71	0.62
125 – 250	1.05	0.86	0.82	0.70
250 – 500	1.04	0.85	0.75	0.70
500 – 1,000	1.02	0.84	0.73	0.63
≥1,000	0.95	0.74	0.60	0.52
Unsieved	1.03	0.86	0.75	0.63

5.3.1.2 Thickness swelling of DPF composites

Thickness swelling (TS) of the composites were examined for 24 hours to determine the dimensional stability of DPF composite which will aid in identifying its end use. It is directly related to the density, presence of voids, and the interfacial bonding between the fibre and matrix [195]. The results revealed that all samples reached the max TS after 24 hours and no

further increase in thickness was recorded afterwards, presuming that the DPFs have reached maximum saturation and the voids within the composite may fully be filled with water. Figure 44 and Table 42 present the percentage increase in TS for various DPF sieve size at different loading content. Pure RPVC composite has the lowest TS, which is due to its hydrophobic, water-resistant characteristics. The increase in DPF loading in the composite causes an increase in the TS and DPF/RPVC composites reinforced with 40 wt.% DPF loading demonstrated the highest TS, which also corresponds to the highest water absorption (WA). This may attribute to the increase of free hydroxyl groups (OH), such the swelling of the fibres may also push the polymer matrix to expand and generate internal stresses, which may result in delamination between DPF and RPVC within the composite [196]. Also, at high fibre volume fraction, the dispersion of the DPF may be reduced, which leads to an increase in the porosity of the composite, thus increase in water uptake and hence in thickness swelling of the composite [29].

The increase in TS with the increase in loading, fibre volume fraction, of DPF varies among different formulations in relation to the DPF size as shown in Figure 50. Results showed an increasing trend where the TS increases with the increase of DPF size from ≤125 µm to 500 – 1,000 µm as the DPF loading increases from 10 – 40 wt.%, indicating that finer DPF provides a better compacted homogenously mixed composite and better dispersion of DPF, which could enhance the interface between the polymer and fibre, thus reducing the porosity of the composite, therefore, the composite with finer particles demonstrates lower TS compared to that with larger particle size 500 – 1,000 µm. Additionally, the increase of DPF size from ≤125 µm to 500 – 1,000 µm means an increase in the fibre volume fractions under the same loading content (Table 42), which may affect both the dispersion and WA of the fibre as mentioned.

However, the unsieved and ≥1,000 µm DPF showed lower thickness swelling than 125 – 250 µm, 250 – 500 µm, 500 – 1,000 µm, but higher than ≤125 µm DPF as the DPF loading increased from 10 – 30 wt.%. This may reflect a lower volume required at a specific loading content compared to other sieve sizes and this means DPF may be better wrapped with polymer to form a water-resistant layer to prevent water entering the structure of the fibre. This can also be seen from the composites at high DPF volume fraction, 40 wt.%, where a huge increase in TS was observed for unsieved and ≤125 µm. This can be attributed to the fine size and low density of ≤125 µm, as well as the blend of different fibre sizes in unsieved. Thus, there may not be enough RPVC matrix to cover ≤125 µm and unsieved DPF. Therefore, the highest TS% for DPF/RPVC composite was achieved when the composite was reinforced with unsieved DPF at 40 wt.% loading, reaching 1.57%.

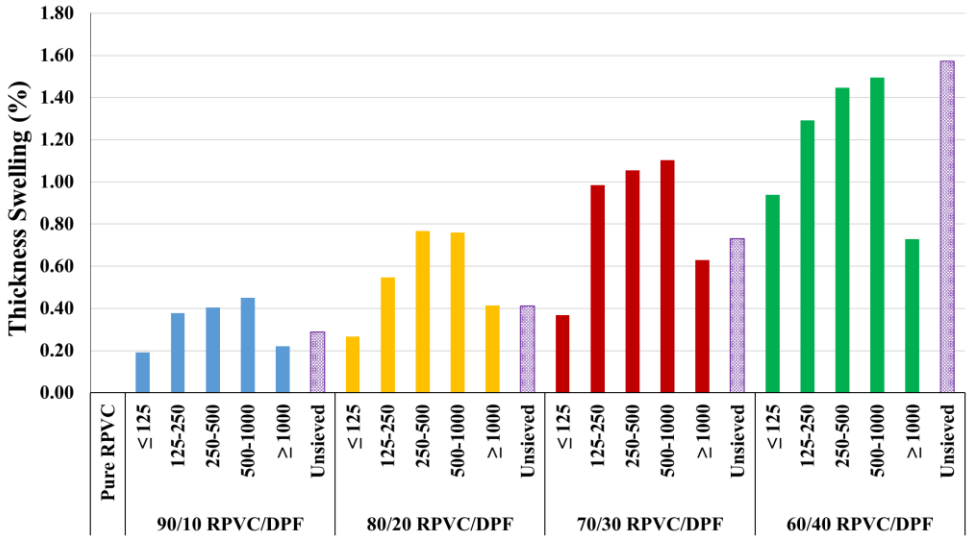

Figure 44 Effect of DPF geometry and loading on TS (%) of DPF/RPVC composite

Table 42 Increase in TS for various DPF sizes at different loadings (%)

Sieve Size (µm)	% increase in TS by the increase of DPF loading (wt.%)		
	20% DPF	30% DPF	40% DPF
≤125	40.10	93.56	392.62
125 – 250	44.51	160.10	240.95
250 – 500	89.14	160.67	257.07
500 – 1,000	68.90	144.90	231.65
≥1,000	88.53	186.55	231.90
Unsieved	42.86	152.94	444.31

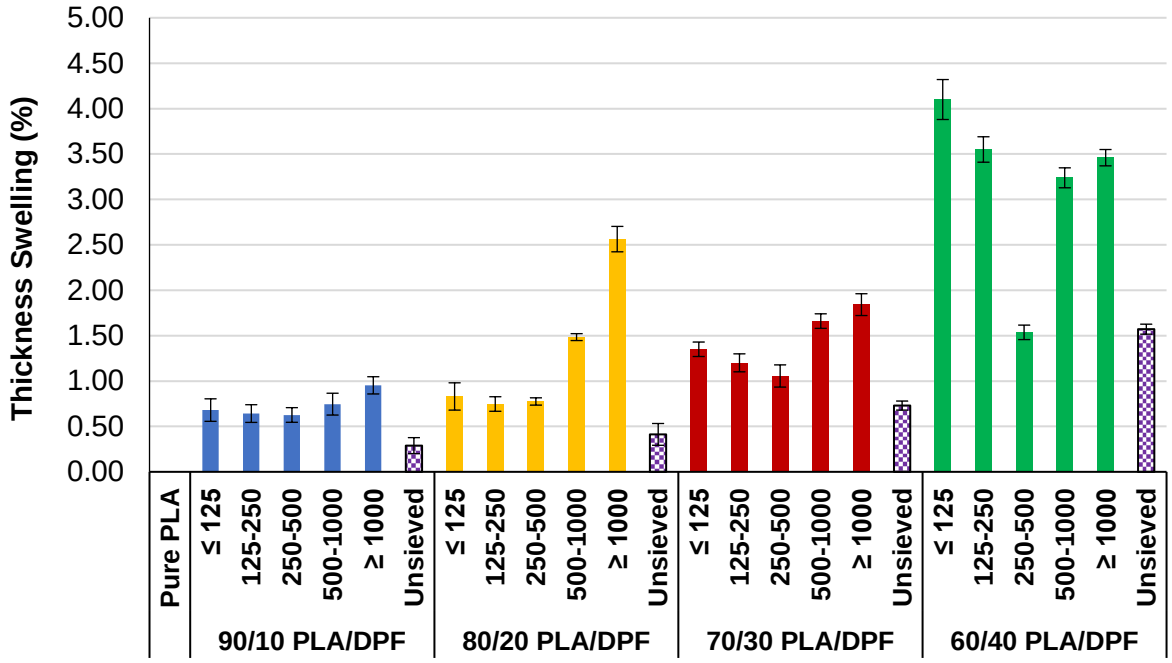

Figure 45 Effect of DPF geometry and loading on TS% of DPF/PLA bio-composite

Table 43 Increase in TS for various DPF sizes at different loadings% of DPF/PLA bio-composite

Sieve Size (μm)	% Increase in TS by the increase of DPF loading (wt.%)		
	20% DPF	30% DPF	40% DPF
≤125	83.12	135.88	410.43
125 – 250	74.74	120.92	355.301
250 – 500	77.50	106.35	154.76
500 – 1,000	148.38	166.21	324.49
≥1,000	256.27	184.71	346.22
Unsieved	41.24	73.15	157.08

5.3.1.3 Moisture content and water absorption of DPF composite

The moisture content (MC) for DPF/RPVC composites after 48 hours are shown in Figure 46. Overall, the composites with high DPF loading, high fibre volume fraction, exhibit higher MC, which is a common phenomenon to WA and TS due to the hydrophilic nature of DPF. However, the effect of DPF geometry on MC of the composite varies depending on the loading content. At a low loading content, an increasing trend in MC is observed as the DPF size increase from ≤125 μm to ≥1,000 μm reaching 0.61%, but at 20 and 30 wt.% loading content,

an increasing trend of MC is observed from ≤125 µm to 500 – 1,000 µm reaching 0.92% and 1.22% respectively, which is followed by a decrease in MC for ≥1,000 µm and unsieved DPF composites. As the DPF sieving size increased the morphology of the DPF changes from powder to a needle-like shape which may develop voids that can be filled with water. Also, during the sample cutting, some of the DPF may get pulled out leaving a cavity that can provide a way for water to be absorbed. Moreover, DPF ≤125 µm provides a larger surface area which may cause a high adherence force between the DPF and RPVC matrix which may prevent water from being absorbed. Consequently, at larger DPF diameter, water may be absorbed more due to the capillary system where bigger DPF diameter is composed of bundle of fibrils with longitudinal space between them causing water to be absorbed. At a high loading content, a decrease in MC of 250 – 500 µm DPF size was observed.

Table 44 illustrates the % increase in MC for various DPF sieve size at different loading content. The results show that the sieve size has significant effect on the % increase in MC at the different loading contents. The most significant increase in MC% was when the loading content of ≤125 µm DPF increased from 30 – 40 wt.% which might have occurred due to the high volume of DPF required at high loading for low sieve size, ≤125 µm, and low density thus not sufficient RPVC matrix to produce a homogenous perfectly compounded mix. Thus, a weak interface will be present between the polymer and the fibre, forming more voids within the composite which will lead to an increase in MC.

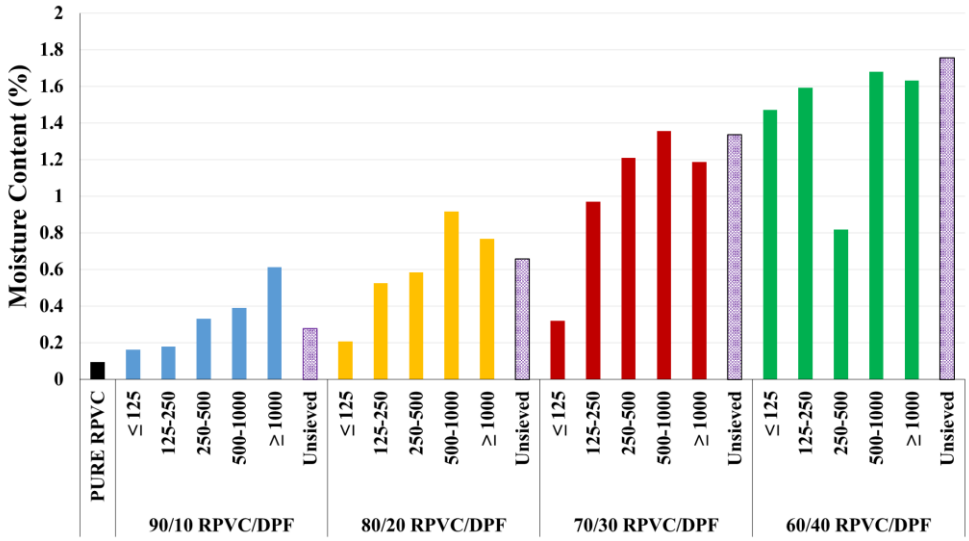

Figure 46 Effect of DPF geometry and loading on MC% of DPF/RPVC composite

Table 44 Increase in MC for various DPF sizes at different loadings% of DPF/RPVC composite

Sieve Size (μm)	% increase in MC by the increase of DPF loading (wt.%)		
	20% DPF	30% DPF	40% DPF
≤125	21.26	98.08	807.86
125 – 250	191.12	437.89	782.79
250 – 500	75.78	263.40	146.33
500 – 1,000	134.18	246.60	329.62
≥1,000	25.23	93.33	165.83
Unsieved	137.07	382.07	533.32

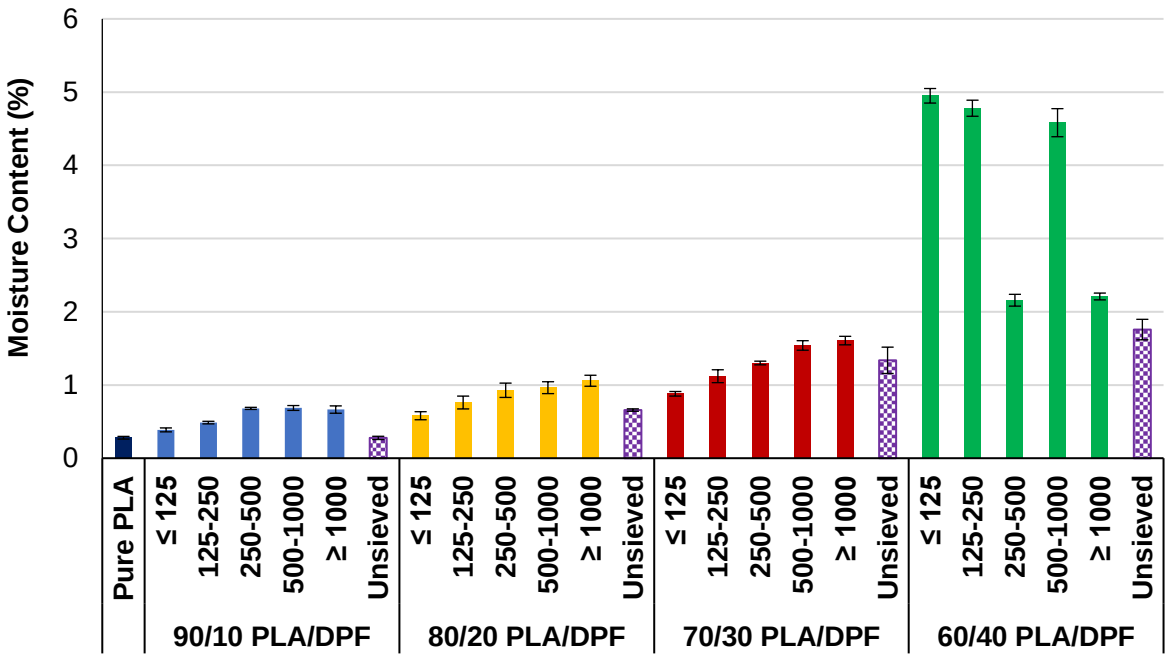

Figure 47 Effect of DPF geometry and loading on MC% of DPF/PLA bio-composite

Table 45 Increase in MC for various DPF sizes at different loadings% of DPF/PLA bio-composite

Sieve Size (µm)	% Increase in MC by the increase of DPF loading (wt.%)		
	20% DPF	30% DPF	40% DPF
≤125	107.14	214.29	1667.90
125 – 250	171.59	300.02	1607.10
250 – 500	231.47	364.35	670.68
500 – 1,000	244.03	450.03	1536.50
≥1,000	277.85	473.73	688.86
Unsieved	134.84	377.53	527.37

Moreover, the WA of the DPF reinforced RPVC composites was conducted to determine the amount of water absorbed under specified conditions for 24 hours. The importance of understanding the WA of the composites developed is to determine their end uses.

Figure 48 and Table 46 demonstrate the increase in WA for various DPF sieve sizes at different loading content and WA% for the composites developed respectively. Results demonstrated that the WA% of pure RPVC was very low which reached 0.13% after 24 hours. It has been reported that although RPVC is hydrophobic, the WA mainly occurred due to some voids formed within the composite while processing the composite or the hydrophilic anionic surface-active agents that are used to wash recycled plastic waste in the recycling process, which reduces the surface tension of water, affecting the WA behavior [197]. The DPF/RPVC composites showed an increase in WA% as the DPF loading increased which follows the same trend as the TS% and MC% of the composites developed. Thus, WA was maximum for composites with 40 wt.% DPF (Figure 48). This increase in WA with the increase of DPF loading may be directly correlated to the hydrophilic nature of DPF which causes a water-DPF interaction responsible for the WA in the composites since the RPVC absorb very low amount of water. The number of free hydroxyl group (OH) of DPF cellulose to form a hydrogen bonding and the diffusion of water into the fibre/matrix interface increase with the increase of DPF loading [198]. Also, DPF have high porosity therefore, higher DPF content leads to a higher amount of water absorbed, resulting in an increase in the composites weight.

Moreover, the composites with 500-1,000 µm DPF showed the highest WA at all loading contents, where WA increased from 2.97 to 10.80% as the DPF loading content increased from 10 to 40 wt.%, means an increase rate of 263% for the DPF loading increased from 10

to 40 wt.% (Table 46). This can be attributed to the higher diameter with high tendency to absorb water within the capillary system. Also, the high range of DPF size available reduces the interfacial bonding with the polymer matrix which creates more voids within the composite, thus increasing the tendency in absorbing water.

All composites with ≤125 µm DPF recorded the lowest WA%, MC% and TS% at loadings 10 – 30 wt.%, which may be attributed to better interfacial bonding between DPF and RPVC matrix system due to a better homogenous compounding, thus more DPF surface area being covered with the RPVC matrix during compounding and lower voids present in the composite developed. This can also be justified by looking at the tensile strength of the composites developed where ≤125 µm DPF sieve size reinforcement at loading 10 – 30 wt.% showed the optimum tensile strength. However, at a loading content of 40 wt.%, ≤125 µm DPF sieve size shows a significant increase in WA, 663.77%. This can be attributed that at 40 wt.%, DPF with low sieve size and low density requires large volume of sample, and the RPVC matrix is not sufficient to produce a homogenous perfectly compounded mix. Thus, a weak interface will be present between the polymer and the fibre, forming more voids within the composite which will lead to an increase in WA to fill the voids until saturation is achieved. This is also confirmed by the mechanical strength of the composites developed where utilizing ≤125 µm DPF sieve size at 40 wt.% shows a significant decrease in strength which is contributed to the weak interfacial bonding between DPF and RPVC.

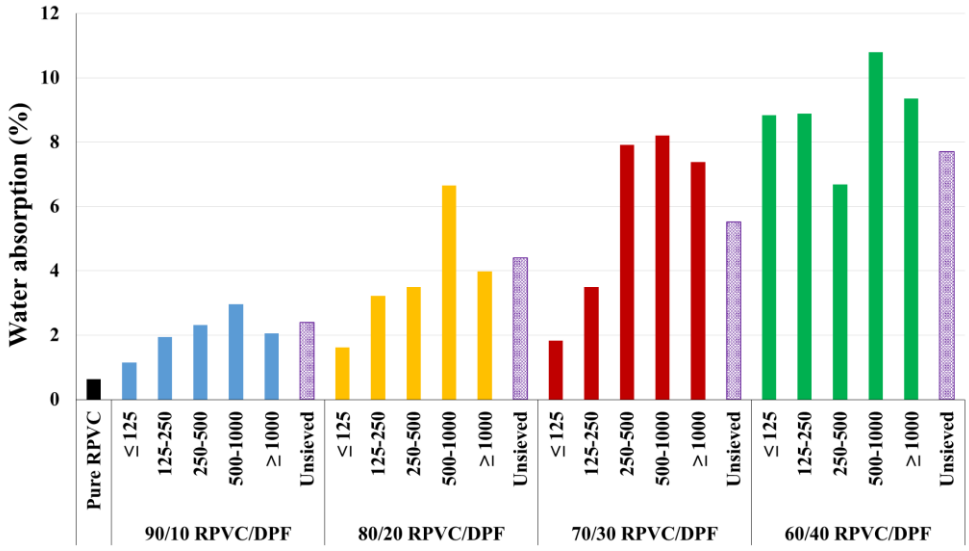

Figure 48 Effect of DPF geometry and loading on WA% of DPF/RPVC composite

Table 46 Increase in WA for various DPF sizes at different loadings of DPF/RPVC composite

Sieve Size (μm)	% increase in WA by the increase of DPF loading (wt.%)		
	20% DPF	30% DPF	40% DPF
≤125	28.42	58.81	663.77
125 – 250	66.18	80.16	357.35
250 – 500	51.21	242.09	189.07
500 – 1,000	123.96	176.03	263.50
≥1,000	93.25	257.98	354.40
Unsieved	83.70	130.33	221.84

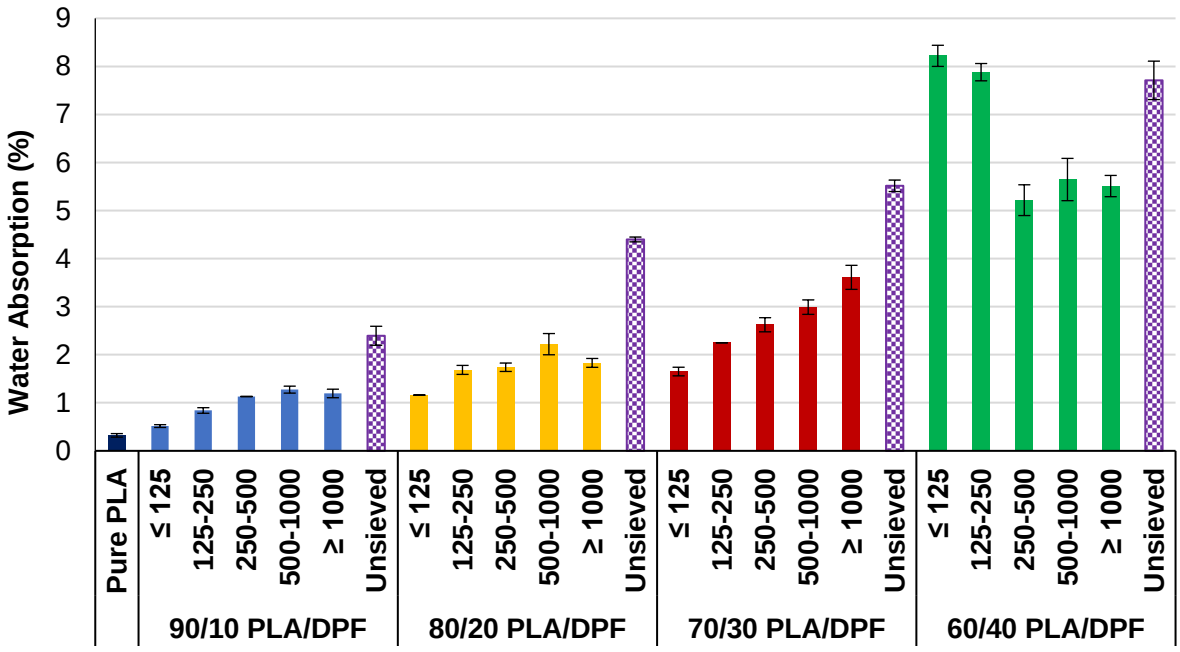

Figure 49 Effect of DPF geometry and loading on WA% of DPF/PLA bio-composite

Table 47 Increase in WA% for various DPF sizes at different loadings of DPF/PLA bio-composite

Sieve Size (μm)	% Increase in WA by the increase of DPF loading (wt.%)		
	20% DPF	30% DPF	40% DPF
≤125	260.02	412.10	2451.22
125 – 250	422.83	598.31	2345.63

Sieve Size (μm)	% Increase in WA by the increase of DPF loading (wt.%)		
	20% DPF	30% DPF	40% DPF
250 – 500	440.03	714.16	1519.01
500 – 1,000	589.01	827.98	1652.34
≥1,000	467.96	1020.40	1610.50
Unsieved	1265.30	1611.91	2292.99

5.3.2. Effect of DPF geometries and loading content on the mechanical properties of DPF composites

When referring to the mechanical properties of the composites, it can be related to the fibre geometry as it may affect the stress transfer of the load applied to the composites which occurs by shear at both interface along the fibre length and at the ends of the fibres. The extent of load transmitted to the fibre is a function of critical fibre length, aspect ratio, which is defined as the fibre length-to-thickness ratio, orientation of fibres and the compatibility between fibre-matrix interfaces [199]. It is apparent that the grinded DPF utilized in the experimental study do not provide fibres with significant length, nevertheless, the results show a clear correlation between the sieve size and the mechanical properties of the composites developed. The addition of grinded DPF results in a decrease in the overall strength of the composite, with the extent increases with the increasing amount of loading content of DPF. The hydrophilic nature or surface characteristic of DPF may be a key contributor, which is incompatible with hydrophobic polymer matrices, resulting in a weakened interface and hence the composite. DPF may also contain waxes and other non-cellulosic substances, such as hemi-cellulose, lignin and pectin, which may create poor adhesion between the RPVC matrix and DPF. Therefore, to improve and develop DPF reinforced polymer composites with better mechanical properties, it is necessary to increase fibres hydrophobicity by introducing DPF to surface modification (surface treatment). Fibre orientation and fibre volume fraction are also considered important parameters to take into consideration in assessing the mechanical properties. In this study, the orientation of the DPF were randomly distributed. A typical phenomena for the fibre volume fraction, is that it significantly affects the mechanical properties where the flexural and tensile strength increases and then decreases after reaching a peak value that corresponds to an optimum fibre fraction which varies from fibre to fibre [200]. However, this phenomenon was not witnessed in the study where all results showed a decrease in the mechanical properties which might be due to the poor interfacial bonding between the DPF and the RPVC matrix.

5.3.2.1 Flexural strength of DPF composite

The effect of volume fraction of DPF and DPF geometry on the flexural strength for DPF reinforced RPVC composite is presented in Figure 50. It is observed that the flexural strength of all DPF reinforced composites developed decrease with the increase in volume fraction of DPF. As mentioned, this may be directly related with the weak interfacial bonding between the DPF and RPVC matrix due to the hydroxyl group present at the surface of DPF which will lead to a weak stress transfer interface for the load applied. Moreover, the decrease in flexural strength as the loading content increased may also be related to the increase in agglomeration occurring in the composite at different concentrations insinuating poor fibre dispersion that inherent path for crack propagation to occur when load is applied. This failure mechanism can be referred to as fibre breakage and interfacial debonding, a particular type of failure that encompasses the debonding occurred between the matrix and fibre [201]. This is especially seen in the fibre followed by cracks in the matrix due to increased stress concentrations at the location containing the weakest matrix-fibre bonding.

DPF size has an influence on the flexural strength of the DPF composites (Figure 50 and Figure 51). Results demonstrate that the unsieved DPF composites have the highest flexural strength among the other sieved DPF composites for both reinforced PLA and RPVC polymers. DPF/RPVC composites showed that the flexural strength increased from ≤125 µm to 125 – 500 µm and then decreased. The ≤125 µm DPF available in the unsieved DPF composite may be able to fill the voids around the larger fibre size, making the composites more compact. The decrease in flexural strength with the DPF size may be due to less compact interface structure, and the increase in the strength of composites with DPF from ≤125 µm to 125 – 500 µm may be attributed to the higher self-strength of the longer DPF than shorter DPF.

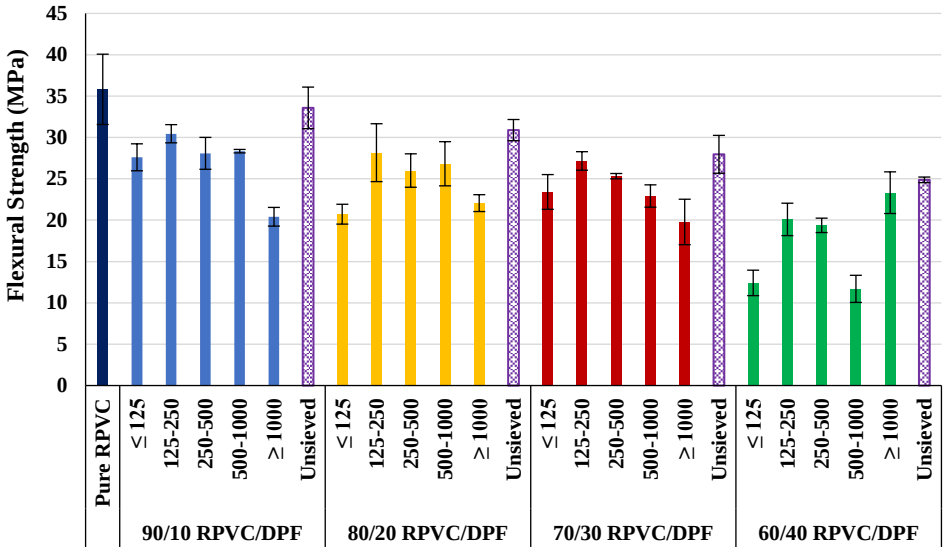

Figure 50 Effect of DPF geometry and loading on flexural strength (DPF/RPVC)

DPF/PLA composites developed showed that the flexural strength was the lowest at ≤125 µm at all DPF loading content. The unsieved DPF showed the highest reinforced strength at all loading content. This may be an attribute that the ≤125 µm DPF available in the unsieved DPF composite may be able to fill the voids around the larger fibre size, making the composites more compact. The decrease in flexural strength with the DPF size may be due to less compact interface structure, and the increase in the strength of composites with DPF from 500 – 1,000 µm and ≥1,000 µm may be attributed to the higher self-strength of the longer DPF than shorter DPF.

It must be noted that the processing process, melt-mixing stage and compression moulding stage may also contribute to the aforementioned results, e.g. the viscosity of the RPVC and PLA should be low enough to impregnate DPF and high enough to avoid spurting out [34]. As DPF is made up of small filaments formed in a bundle, it will take time for wetting them. Thus, the optimal parameters of compression moulding processing and melt-mixing processing are critical to produce quality samples. Several defects such as voids, fibre breakage, residual stress would occur if the processing parameters were not optimal which decreases the flexural strength of DPF/RPVC composite. Moreover, it can be noticed from the flexural results that it does not follow the trend of the tensile strength results discussed in Section 5.3.2.2. The flexural strength is considered when three stress states are induced (tensile, compressive and shear stress) when a flexural loading is applied to a composite.

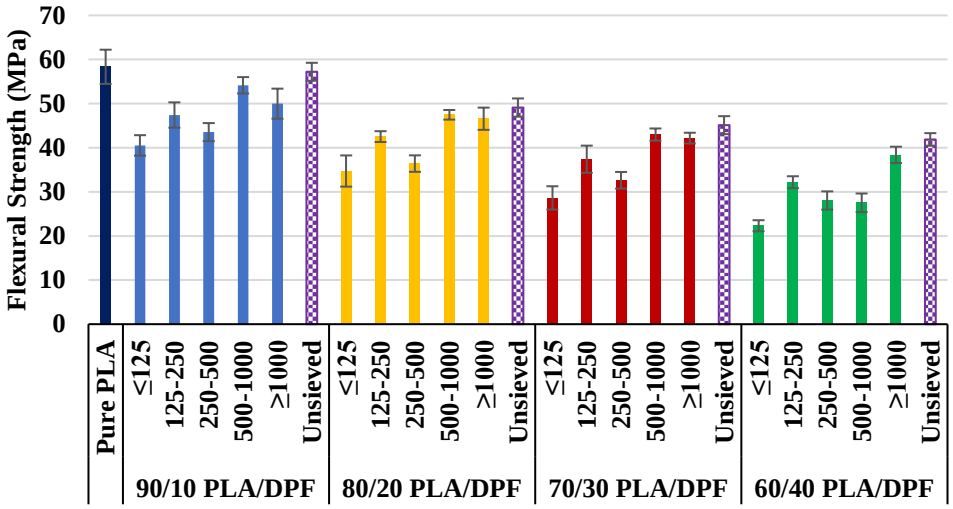

Figure 51 Effect of DPF geometry and loading on flexural strength (DPF/PLA)

It is most interesting that the flexural modulus increased with the addition of DPF for almost all combination, 10 – 30 wt.%, except for the composites ≥1000 µm at 10% DPF loading and 500 – 1,000 µm at 40% DPF loading (Figure 52). This clearly demonstrates the contribution of DPF for enhancing the composites.

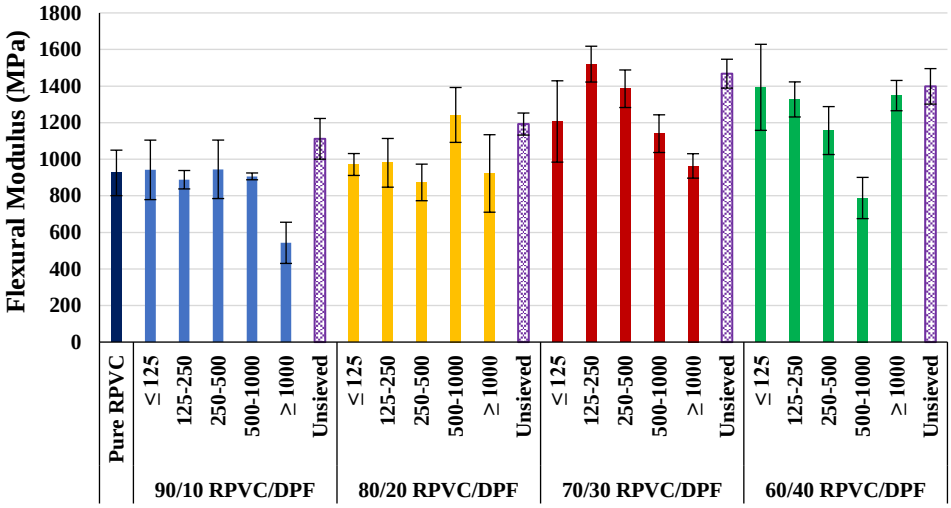

Figure 52 Effect of DPF geometry and loading on flexural modulus (DPF/RPVC)

The addition of unsieved DPF, 125 – 250 µm DPF, 500 – 1,000 µm DPF, and ≥1,000 µm DPF as a reinforcement showed enhancement in the flexural modulus as the content increased from 10 – 30 wt.% then decreased at 40 wt.% content. The decrease observed at 40 wt.% may be an attribute that the volume fraction of the fibre is very high where there is not enough PLA matrix to develop a homogenous mix which resulted in high void fraction formation as demonstrated in Figure 111. Moreover, the addition of ≤125 µm DPF showed no enhancement in the flexural modulus and decreased as the content of DPF increased.

DPF with small geometrical size has a very low aspect ratio where the DPF are in powder for and there is no fibre length that can resist any stress or load applied to the composite.

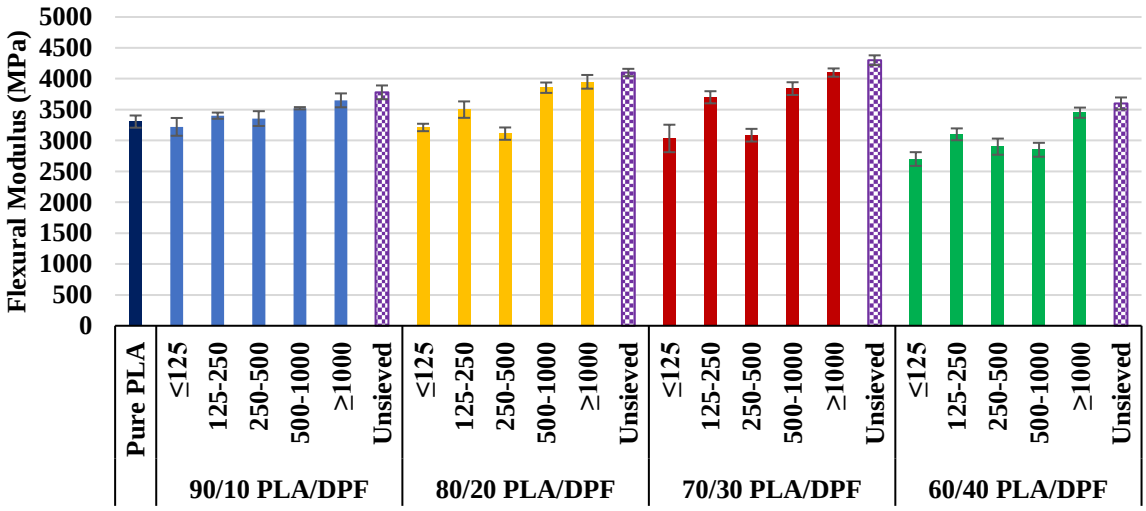

Figure 53 Effect of DPF geometry and loading content on the flexural modulus of DPF/PLA bio-composite

5.3.2.2 Tensile strength

The tensile strength and Young's Modulus in relation to the effect of different DPF geometry and loading content are presented in Figure 54 and Figure 55 respectively. The tensile strength and Young's modulus decrease with the addition of DPF and varies with the different DPF geometry. The decrease in tensile strength with the increase in DPF loading has also been reported by other researchers [123,202–204]. As aforementioned, the weak interfacial bonding between the DPF surface and the polymer matrix (RPVC and PLA) may promote the formation of micro-cracks at the fibre/polymer interface, thus the tensile strength decreases. Also, higher fibre volume fraction can develop porosities during processing, which many forms micro-cracks during testing and thus decreases the tensile strength.

DPF/RPVC composite strength depends on the degree of the applied load that are transmitted to the DPF. Thus, various DPF sieve sizes provide various DPF length with different aspect ratios which will have various effect on the tensile properties of the composite. As shown in Figure 54, at a low loading content, 10 – 20 wt.%, ≤125 µm sieve size accounted to have the highest tensile strength which may be attributed to better interfacial bonding between DPF and RPVC matrix system due to a better homogenous compounding, thus more DPF surface area being covered with the RPVC matrix during compounding forming a more compacted composite. Meanwhile, at a higher loading content, 30 – 40 wt.%, 250 – 500 µm sieve size accounted to have the highest tensile strength and 500 – 1,000 µm sieve size results showed

to have the lowest tensile strength at all loading contents which may considered as the critical DPF diameter for high DPF loading.

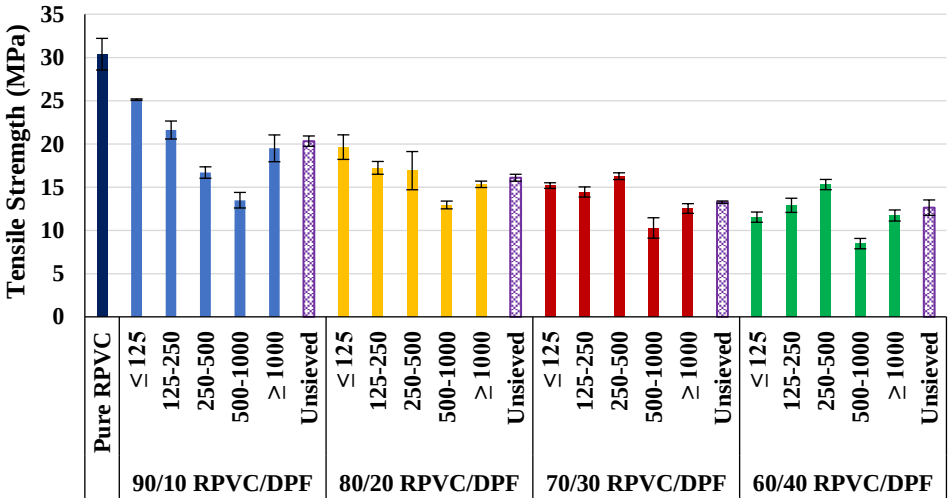

Figure 54 Effect of DPF geometry and loading on tensile strength (DPF/RPVC)

Figure 55 shows that at a low loading content, 10 – 20 wt.%, 500 – 1,000 sieve size accounted to have the highest tensile strength which may be attributed to better interfacial bonding between DPF and PLA matrix system due to a better homogenous compounding and more polymer impregnating through the fibre, thus more DPF surface area being covered with the PLA matrix during compounding forming a more compacted composite. Meanwhile, at a higher loading content, 30 – 40 wt.%, 250 – 500 µm sieve size accounted to have the highest tensile strength and ≤125 µm sieve size results showed to have the lowest tensile strength at all loading contents which may considered as the critical DPF diameter for high DPF loading. The decrease in strength at ≤125 µm sieve size might be an attribute to the low density of DPF which has a high-volume fraction at a high loading weight content where there will not enough polymer to form a homogenously mixed composite.

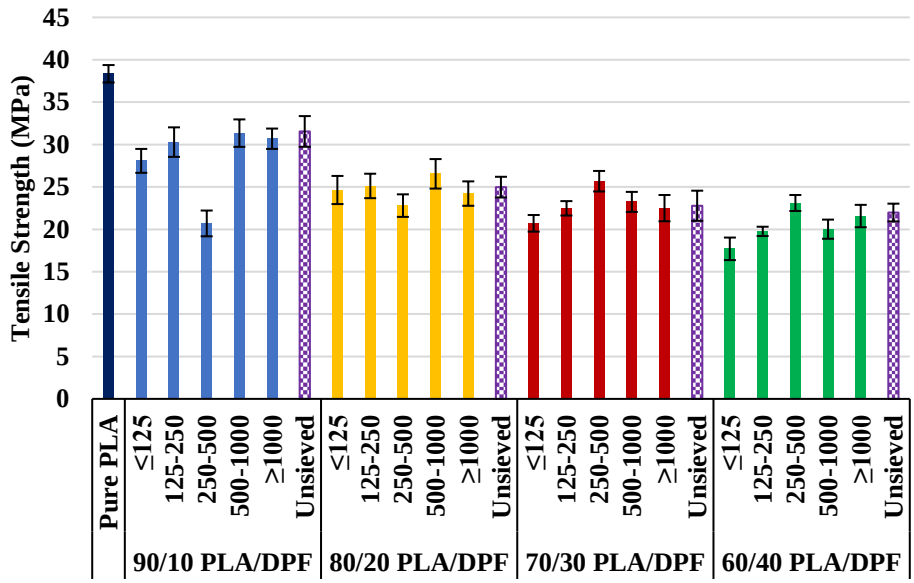

Figure 55 Effect of DPF geometry and loading on tensile strength (DPF/PLA)

The stiffness of the composites developed, which are characterized by the Young's modulus, decreased with increasing the loading content of DPF. The stiffness of the composites developed, which are characterized by the Young's modulus, decreased with increasing the loading content of DPF. DPF (mesh) used in this work are very ductile and characterized by very low modulus of elasticity and high elongation at break as reported in [12]. Such behaviour has been observed in previous research work of [92,93,129]. This behaviour is also very similar to the behaviour of the coconut coir fibre, with tensile modulus ranging from 2.0 to 8.0 GPa and elongation 15 to 51% [205]. This high extensibility in the fibre under tensile loading is attributed to the cellular structure of the fibre shown in Figure 56 which results in much lower resistance to lateral contraction and hence lower stiffness in axial direction during loading. Such low fibre stiffness results in a composite with low elastic modulus.

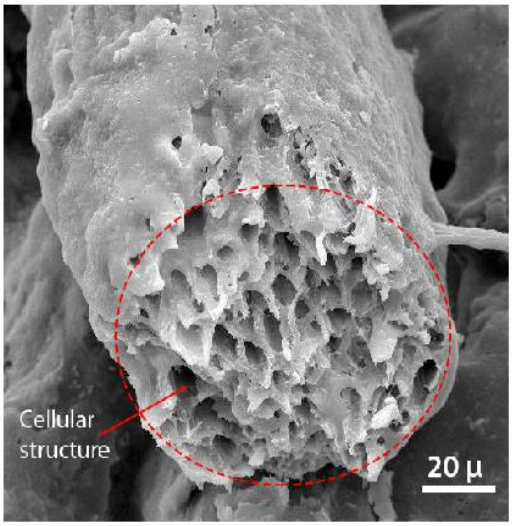

Figure 56 SEM image of the cellular structure of DPF

Comparing the effect of various sieve sizes on the Young's modulus, at a low loading content, 10 – 20 wt.%, ≤125 µm sieve size accounted to have the highest Young's Modulus. This can be due to the fine particle size of low sieve size provides a larger surface area for interfacial bonding and a more compacted composite. Meanwhile, at a higher loading content, 30 – 40 wt.%, 250 – 500 µm sieve size accounted to have the highest Young's Modulus value. Comparing to the tensile strength, 500 – 1,000 µm sieve size results in the lowest stiffness. This can be in common with the same phenomenon for explaining the tensile strength results.

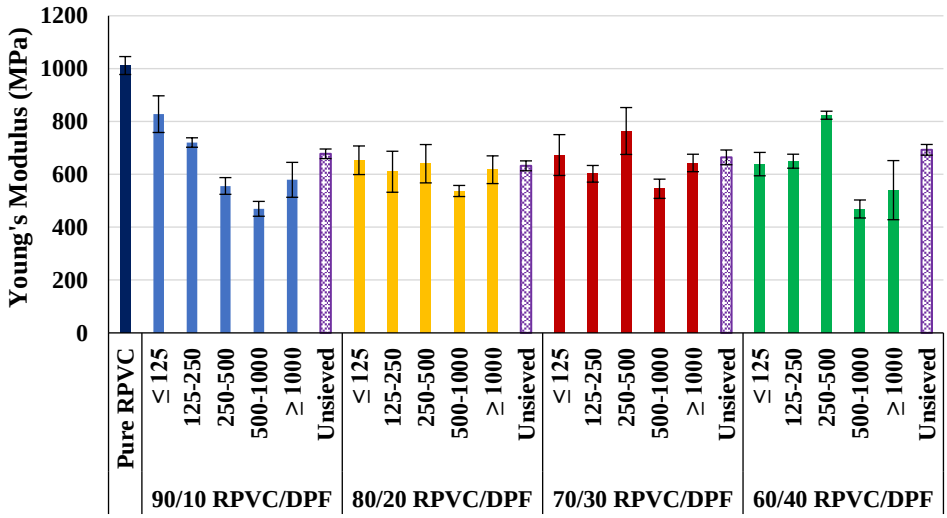

Figure 57 Effect of DPF geometry and loading on Young's Modulus of DPF/RPVC composite

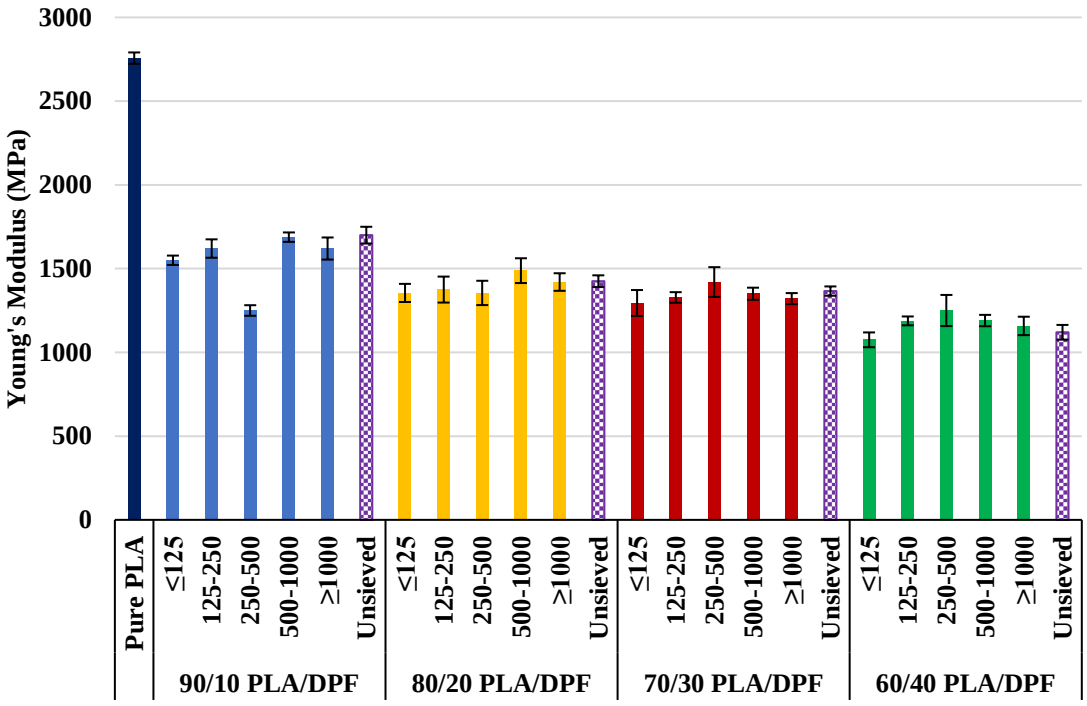

Figure 58 Effect of DPF geometry and loading content on Young's Modulus of DPF/PLA bio-composite

5.3.2.3 Impact strength

The toughness of the composites developed was measured with a Charpy notched impact test, as shown in Figure 59 and Figure 60. Overall, the impact strength of the composites developed decreased with the increase in DPF loading content. The results clearly demonstrate poor-energy absorbing capabilities of the DPF reinforced composites, which can be discussed by addressing two mechanisms where DPF can decrease the impact strength of the composite. The first mechanism is the prevention of deformation and ductile mobility of polymer molecules as DPF, resulting in a decrease in the ability of the developed reinforced composites to absorb energy during crack propagation. The second mechanism involves DPF induced stress concentrations, formed by the agglomerations of DPF, that required less energy to initiate a crack. Such regions might occur at area of weak interfacial bonding, DPF ends, and regions where DPF contact each other, which aids in creating voids within the developed composite that requires low energy for crack initiation [206,207].

Moreover, the results shown in Figure 59, DPF/RPVC show a similar phenomenon to flexural strength results, shown in Figure 50, where 125 – 250 µm sieve size gave rise to the optimal results at all loading contents, having an impact strength of 8.02 KJ/m^2. However, none of the reinforced composites developed reached the impact strength of the pure RPVC composite, 13.77 KJ/m^2. On the other hand, the results shown in Figure 60, DPF reinforced PLA composites showed that the optimal impact strength was achieved for the unsieved DPF at all

DPF loading content, having a maximum impact strength of 10.52 KJ/m^2 at 10 wt.% DPF loading content.

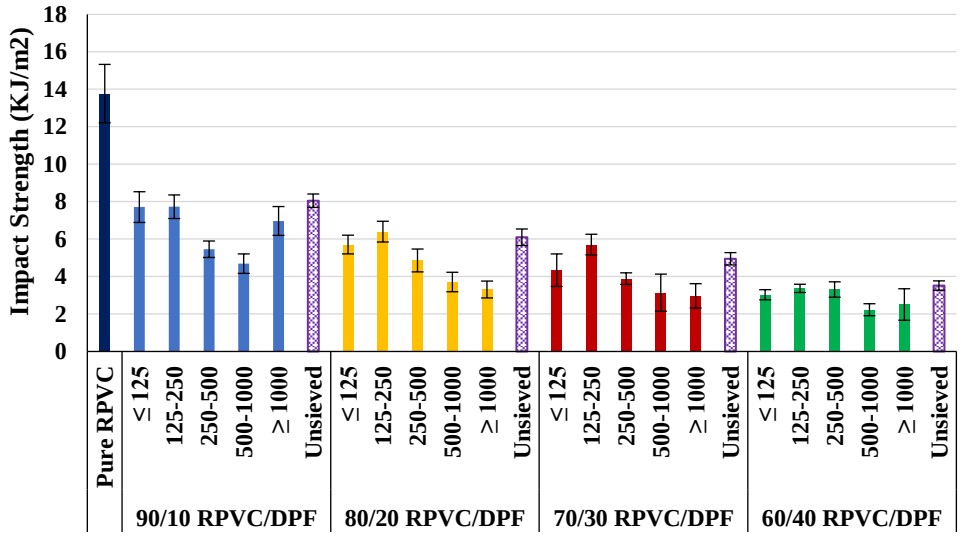

Figure 59 Effect of DPF geometry and loading on impact strength (DPF/RPVC)

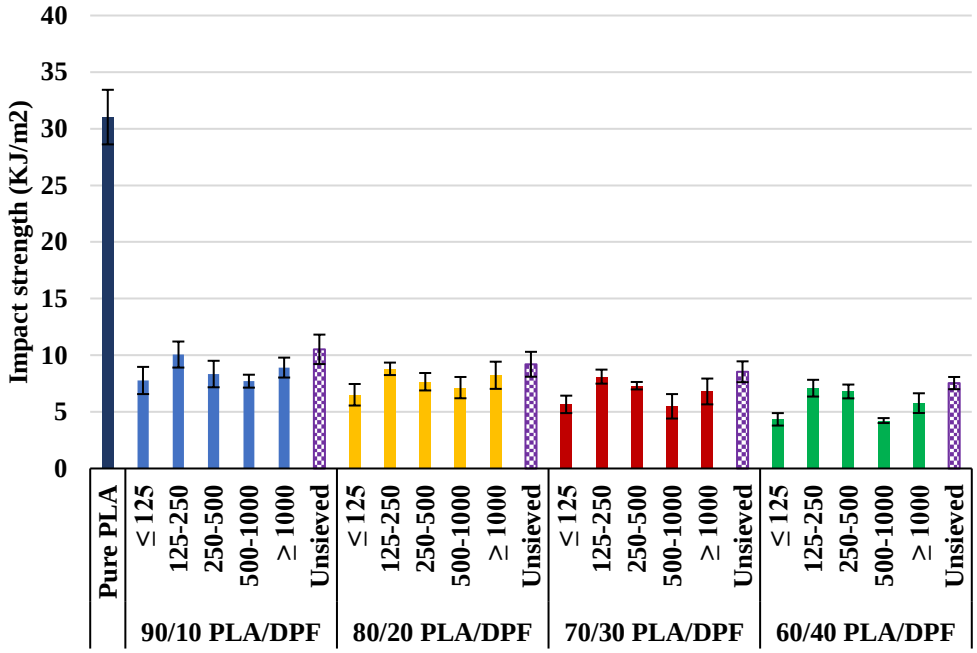

Figure 60 Effect of DPF geometry and loading on impact strength (DPF/PLA)

5.3.3. Micromechanical model

In general, purpose of addition of short fibre into the polymer matrix is to improve the mechanical performance of the composite. However, as shown in section 5.3.2 that the addition of fibre results in the decrease in overall performance of the composite developed which is quite interesting and should be explored due to various possible reasons. To identify the reason, micromechanics modelling of composite is performed using rule of mixing,

modified rule of mixing, inverse rule of mixing, modified Inverse rule of mixing and Halpin-Tasai Equations.

Volume fraction (V_f) of the fibre and matrix were calculated using Equation 15. Void fraction (Vv) of the composites was calculated using density of the composite as listed in Table 36. Diameter of fibre is measured from Scanning Electron Microscope image of single cross sectional DPF. Youngs Modulus and Flexural modulus of the composites were calculated from the compressed moulded samples using Tensile strength test and Flexural strength. Young's modulus of the DPF is considered as 5 GPa as reported in chapter 4 in this thesis.

Table 48 Volume fraction percentage of DPF (V_f) in DPF/PLA bio-composite

DPF size (µm)	**V_f (%) at different DPF loading contents (Wt.%)**			
	10% DPF	**20% DPF**	**30% DPF**	**40% DPF**
≤125	0.24	0.42	0.55	0.66
125 – 250	0.21	0.37	0.50	0.61
250 – 500	0.22	0.38	0.51	0.62
500 – 1,000	0.23	0.40	0.53	0.64
≥1,000	0.28	0.47	0.60	0.70
Unsieved	0.22	0.39	0.52	0.63

Table 49 Volume fraction percentage of DPF (V_f) in DPF/RPVC bio-composite

DPF size (µm)	**V_f (%) at different DPF loading contents (Wt.%)**			
	10% DPF	**20% DPF**	**30% DPF**	**40% DPF**
≤125	0.25	0.43	0.57	0.67
125 – 250	0.22	0.38	0.52	0.62
250 – 500	0.23	0.40	0.53	0.64
500 – 1,000	0.24	0.41	0.55	0.65
≥1,000	0.29	0.48	0.62	0.71
Unsieved	0.23	0.40	0.53	0.64

Table 50 Volume fraction percentage of matrix (V_M) in DPF/PLA bio-composite

DPF size (µm)	V_M (%) at different DPF loading contents (Wt.%)			
	10% DPF	20% DPF	30% DPF	40% DPF
≤125	0.76	0.58	0.45	0.34
125 – 250	0.79	0.63	0.50	0.39
250 – 500	0.78	0.62	0.49	0.38
500 – 1,000	0.77	0.60	0.47	0.36
≥1,000	0.72	0.53	0.40	0.30
Unsieved	0.78	0.61	0.48	0.37

Table 51 Volume fraction percentage of matrix (V_M) in DPF/RPVC bio-composite

DPF size (µm)	V_M (%) at different DPF loading contents (Wt.%)			
	10% DPF	20% DPF	30% DPF	40% DPF
≤125	0.75	0.57	0.43	0.33
125 – 250	0.78	0.62	0.48	0.38
250 – 500	0.77	0.60	0.47	0.36
500 – 1,000	0.76	0.59	0.45	0.35
≥1,000	0.71	0.52	0.38	0.29
Unsieved	0.77	0.60	0.47	0.36

5.3.3.1 Numerical Model 1 – DPF aligned in direction of tensile force:

Figure 61 showed schematic representation of Model 1 scenario where all short fibres are aligned opposite to the direction of the compression force. Test samples were prepared from 4mm compression moulded sheet and assuming fibres are aligned in the direction of the tensile testing i.e., iso-strain condition for Young's modulus. The fibre-oriented composite is loaded in the longitudinal direction of fibre alignment, strain in the fibre, matrix, and composite are considered equal.

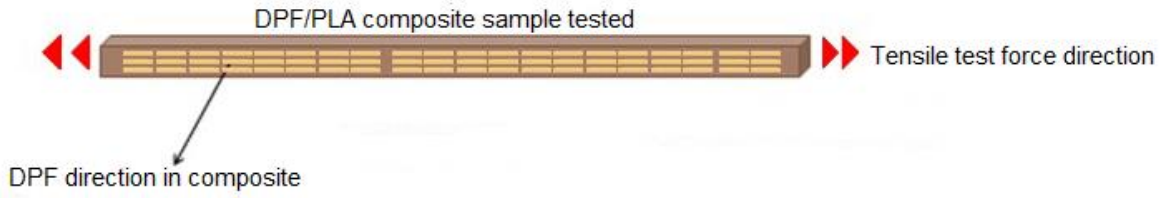

Figure 61 Schematic representation of numerical model 1

Numerical calculations were performed using ROM Equation 14, Modified ROM Equation 16 & Halpin Tsai Equation 19 for four different fibre sizes ≤125 µm, 125 – 250 µm, 250 – 500 µm and 500 – 1,000 µm. Young's modulus value of the tensile test results was considered as the experimental data.

Figure 62 to Figure 69 exhibit elastic modulus of the composite at various volume fraction of DPF and four different fibre sizes. The numerical values were higher than all experimental results which clearly indicate that fibres are not oriented in the direction of tensile loading. Unaligned Fibres impacted on the decrease in elastic modulus of the overall composite as shown in Table 52 and Table 53. In this numerical model, the weak interfacial bonding and the effect of short DPF not having achieved the critical aspect ratio have not been taken into consideration.

Table 52 Comparison of ROM, Modified ROM and Halpin Tsai model with experimental results of DPF/PLA composite

Composition content Wt. %	DPF Size (µm)	Youngs Modulus (MPa)	ROM (K=1)	ROM (K=0.2)	ROM (K=0.375)	ROM (K=0.5)	Halpin-Tsai Ɛ= 2(L/D)
Pure PLA	**-**	2757	2757	2757	2757	2757	2757
90/10 PLA/DPF	**≤125**	1550	3302	2330	2543	2695	3220
	125-250	1620	3221	2394	2575	2704	3165
	250-500	1250	3241	2378	2567	2702	3207
	500-1000	1688	3270	2355	2555	2698	3251
	≥1,000	1620	3392	2260	2507	2684	3374
	unsieved	1700	3249	2372	2563	2701	3239
80/20 PLA/DPF	**≤125**	1355	3697	2020	2387	2649	3586
	125-250	1375	3586	2108	2431	2662	3505
	250-500	1355	3614	2086	2420	2659	3566
	500-1000	1488	3655	2054	2404	2654	3628
	≥1,000	1420	3812	1931	2342	2636	3791
	unsieved	1425	3626	2077	2415	2657	3612
70/30 PLA/DPF	**≤125**	1295	3998	1785	2269	2615	3881
	125-250	1328	3881	1876	2315	2628	3793
	250-500	1420	3911	1853	2303	2625	3860

	500-1000	1350	3954	1819	2286	2620	3926
	≥1,000	1321	4111	1697	2225	2602	4090
	unsieved	1366	3924	1843	2298	2623	3909
60/40 PLA/DPF	**≤125**	1075	4233	1601	2176	2588	4125
	125-250	1188	4125	1685	2219	2600	4039
	250-500	1250	4153	1663	2208	2597	4105
	500-1000	1190	4193	1632	2192	2592	4167
	≥1,000	1158	4334	1522	2137	2576	4316
	unsieved	1120	4165	1654	2203	2596	4151

Table 53 Comparison of ROM, Modified ROM and Halpin Tsai model with experimental results of DPF/RPVC composite

Composition Wt. %	**DPF Size (μm)**	**Youngs Modulus (MPa)**	**ROM (K=1)**	**ROM (K=0.2)**	**ROM (K=0.375)**	**ROM (K=0.5)**	**Halpin-Tsai Ɛ= 2(L/D)**
Pure RPVC	**-**	1012	1011.8	1011.75	1011.75	1011.75	1011.8
90/10 RPVC/DPF	**≤125**	828	2022	1009	1230	1389	1560
	125-250	720	1873	1009	1198	1333	1533
	250-500	621	1910	1009	1206	1347	1672
	500-1000	470	1964	1009	1218	1367	1813
	≥1,000	579	2186	1008	1266	1450	2048
	unsieved	678	1925	1009	1209	1353	1843
80/20 RPVC/DPF	**≤125**	610	2738	1007	1385	1656	2065
	125-250	653	2537	1007	1342	1581	2020
	250-500	640	2588	1007	1353	1600	2243
	500-1000	537	2661	1007	1369	1627	2453
	≥1,000	617	2942	1006	1430	1732	2772
	unsieved	632	2609	1007	1358	1608	2496
70/30 RPVC/DPF	**≤125**	602	3272	1005	1501	1855	2531
	125-250	673	3066	1006	1456	1778	2476
	250-500	764	3119	1006	1468	1798	2741
	500-1000	545	3195	1005	1484	1826	2976
	≥1,000	643	3471	1005	1544	1929	3306
	unsieved	664	3141	1005	1473	1806	3022
60/40 RPVC/DPF	**≤125**	639	3686	1004	1591	2010	2962
	125-250	650	3496	1004	1549	1939	2904
	250-500	824	3546	1004	1560	1957	3180
	500-1000	469	3616	1004	1575	1983	3410
	≥1,000	540	3861	1003	1629	2075	3716
	unsieved	393	3566	1004	1565	1965	3455

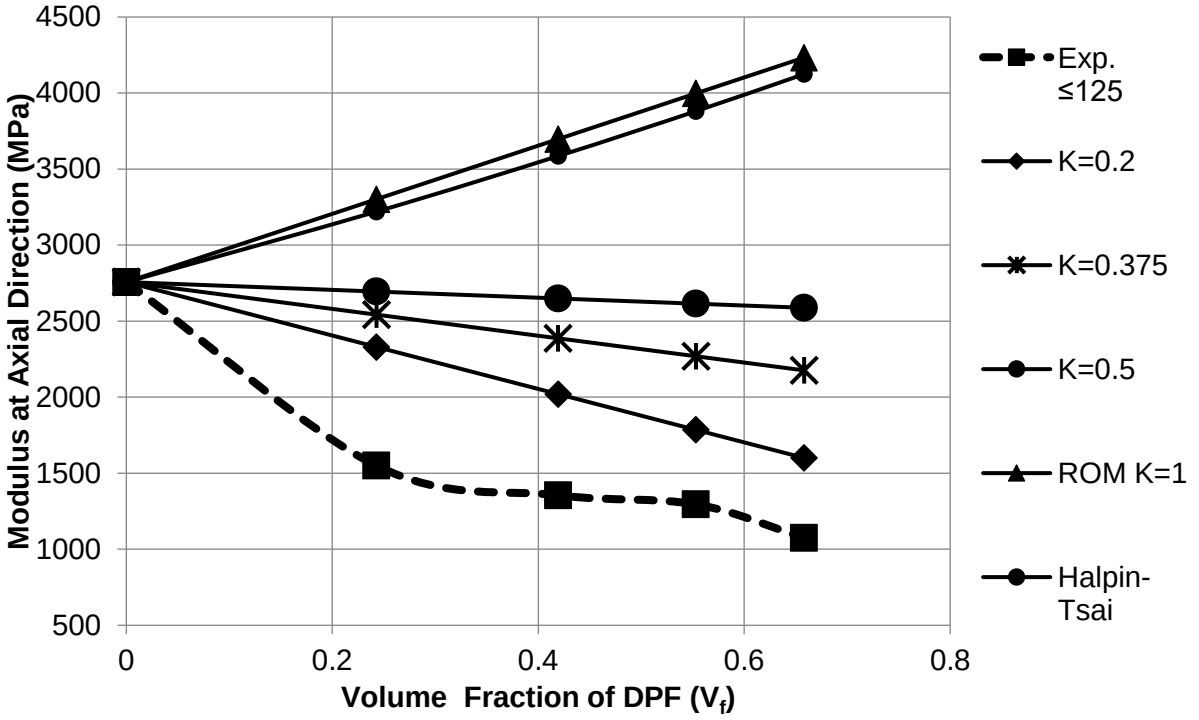

Figure 62 Comparison of ROM, Modified ROM and Halpin Tsai model with experimental results of DPF/PLA composites reinforced with ≤125 μm DPF size (model 1)

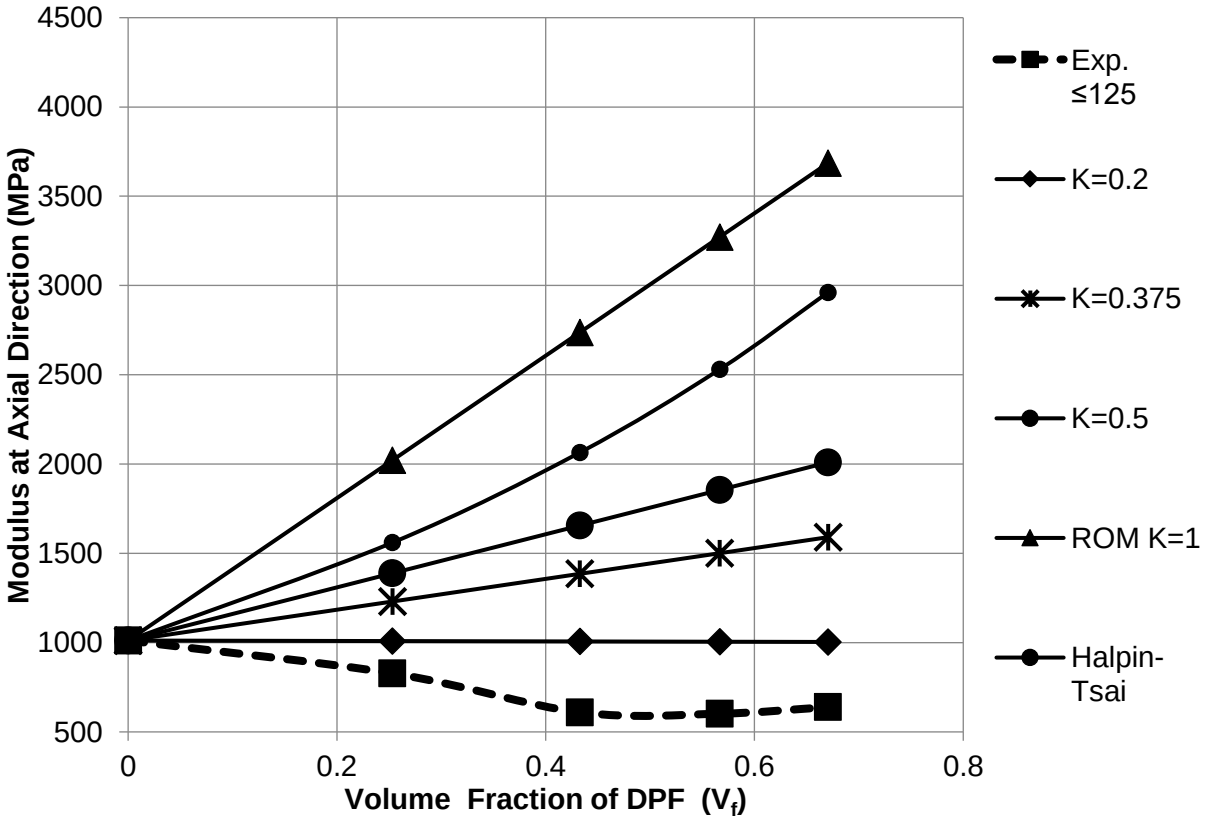

Figure 63 Comparison of ROM, Modified ROM and Halpin Tsai model with experimental results of DPF/RPVC composites reinforced with ≤125 μm DPF size (model 1)

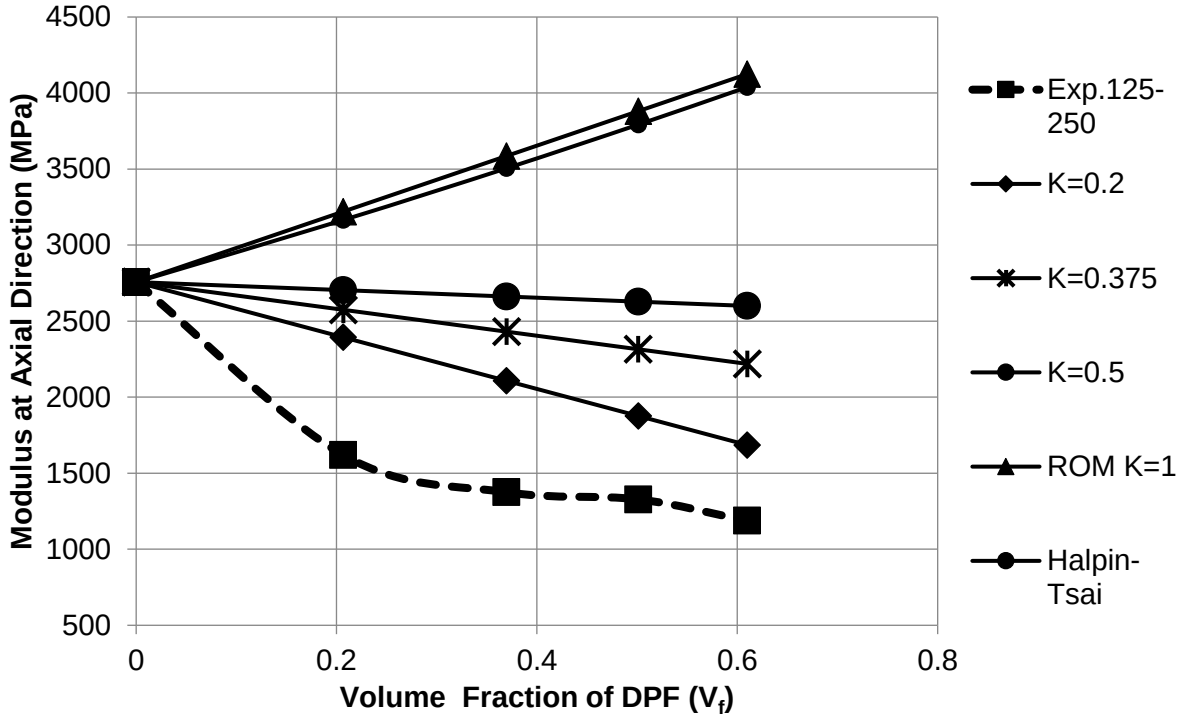

Figure 64 Comparison of ROM, Modified ROM and Halpin Tsai model with experimental results of DPF/PLA composites reinforced with 125 – 250 µm DPF size (model 1)

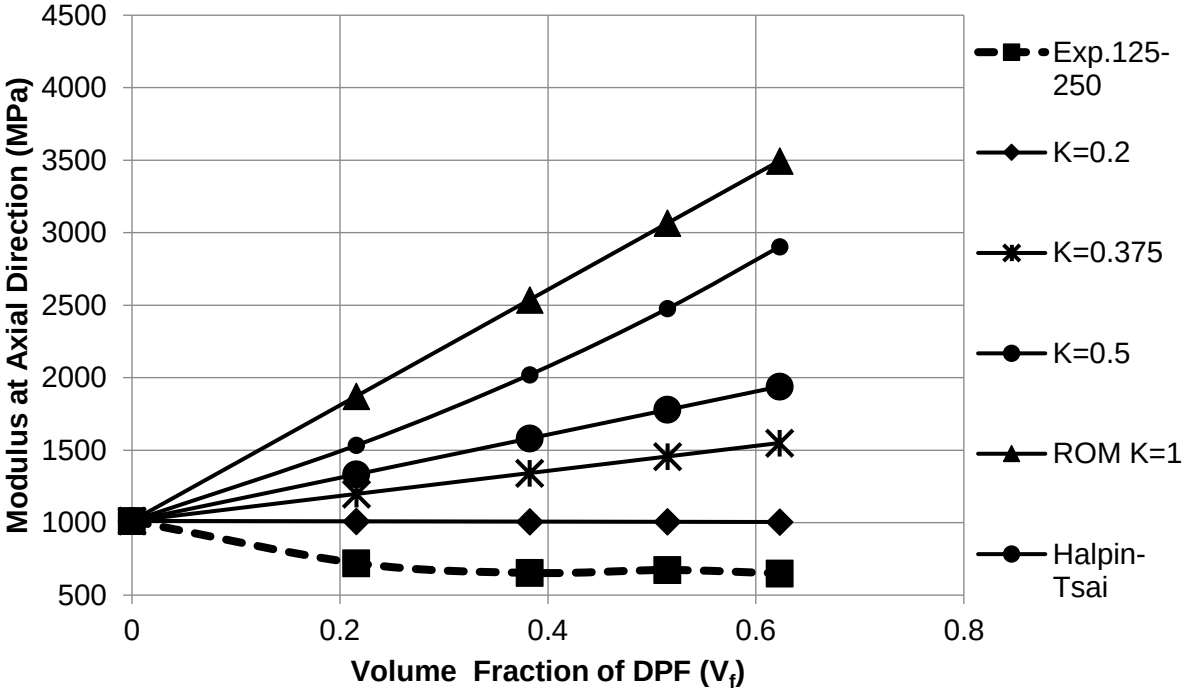

Figure 65 Comparison of ROM, Modified ROM and Halpin Tsai model with experimental results of DPF/RPVC composites reinforced with 125 – 250 µm DPF size (model 1)

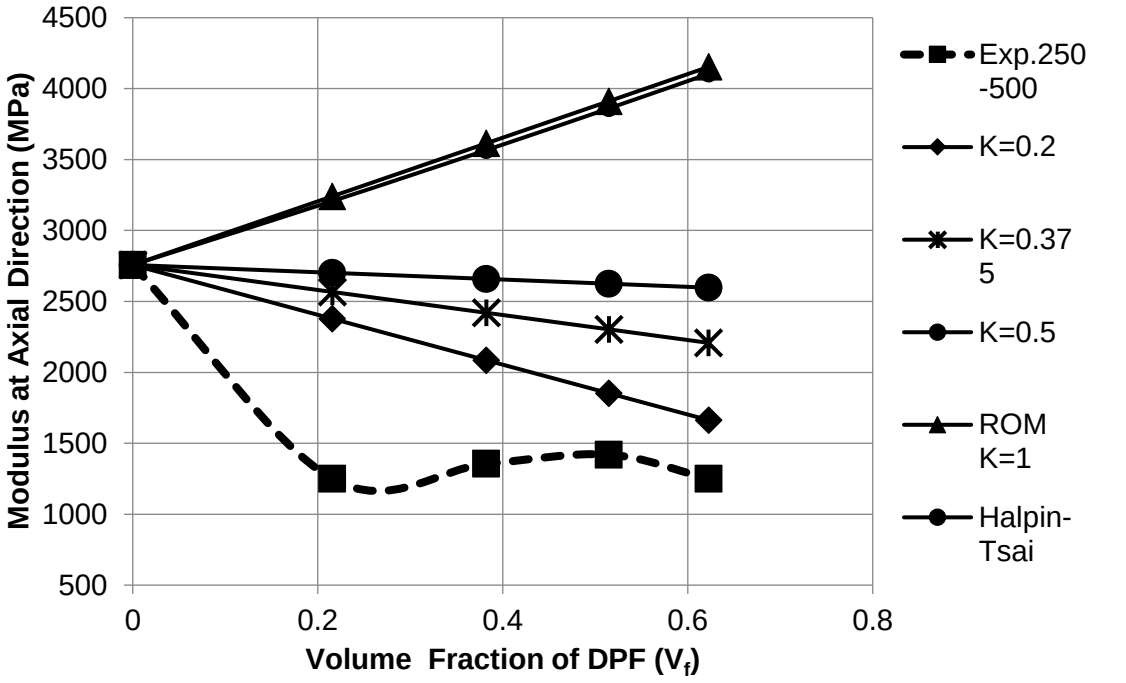

Figure 66 Comparison of ROM, Modified ROM and Halpin Tsai model with experimental results of DPF/PLA composites reinforced with 250 – 500 µm DPF size (model 1)

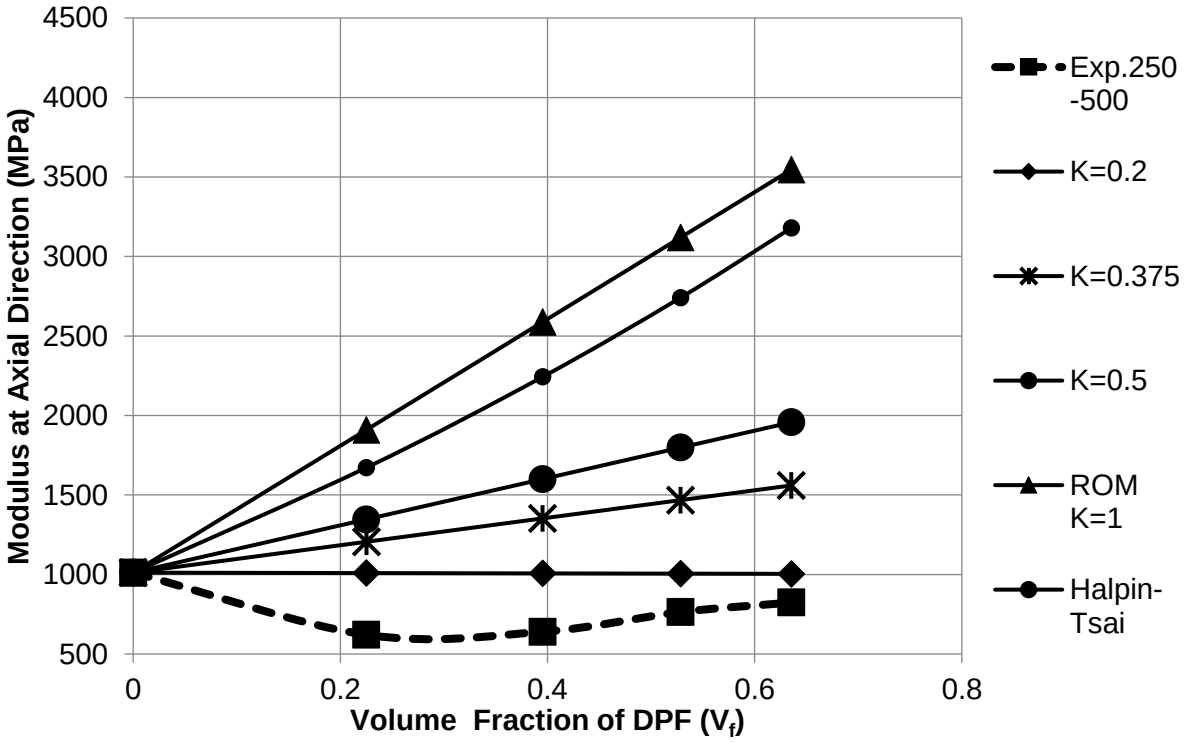

Figure 67 Comparison of ROM, Modified ROM and Halpin Tsai model with experimental results of DPF/RPVC composites reinforced with 250 – 500 µm DPF size (model 1)

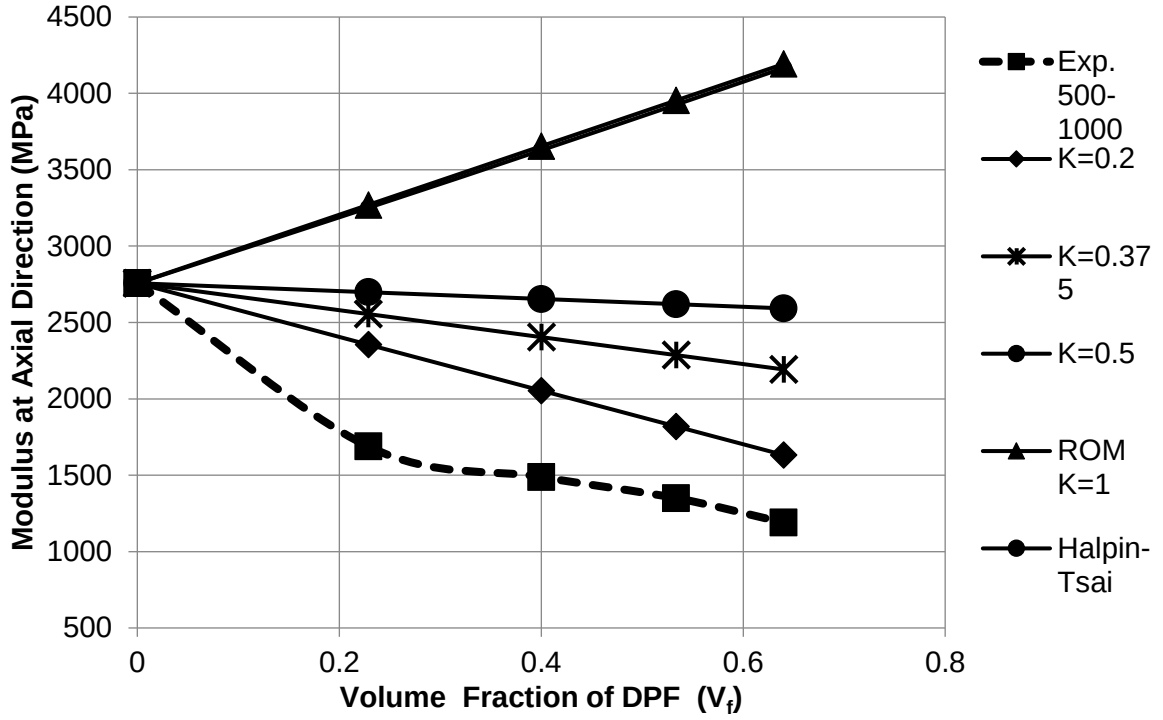

Figure 68 Comparison of ROM, Modified ROM and Halpin Tsai model with experimental results of DPF/PLA composites reinforced with 500 – 1,000 µm DPF size (model 1)

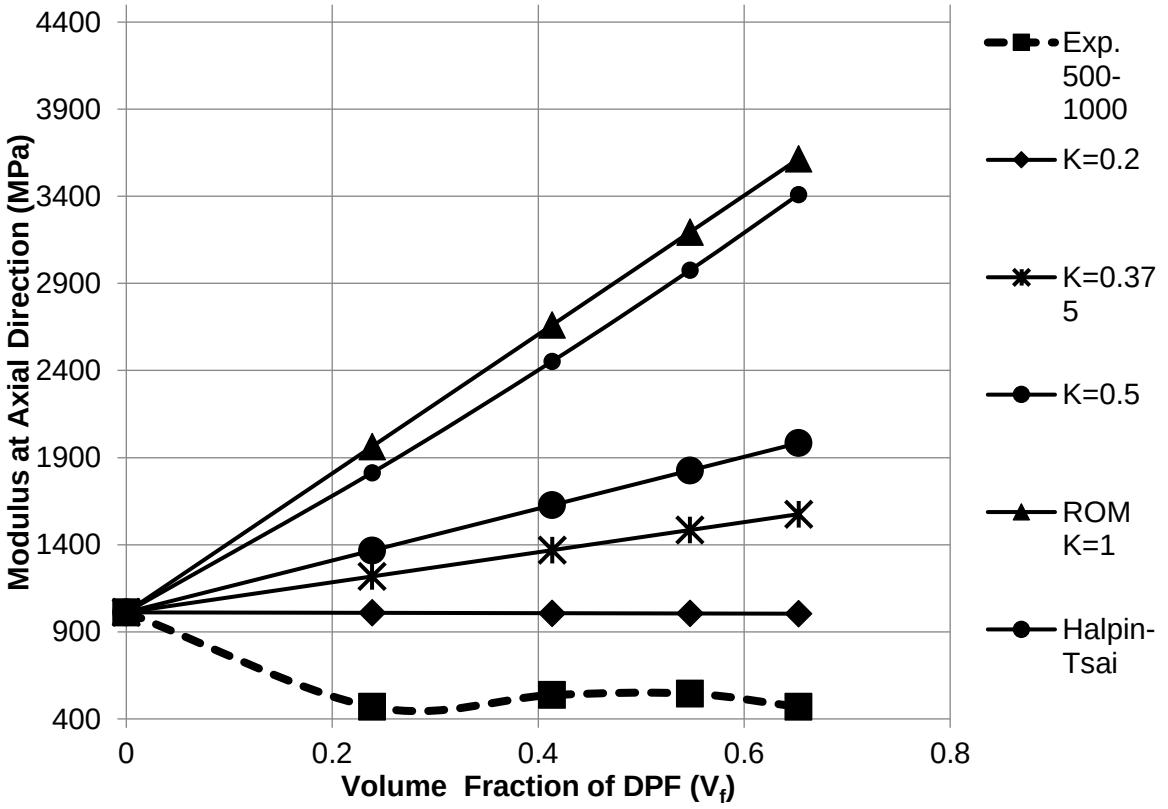

Figure 69 Comparison of ROM, Modified ROM and Halpin Tsai model with experimental results of DPF/RPVC composites reinforced with 500 – 1,000 µm DPF size (model 1)

ROM provide the upper bound of the elastic modulus of composites based on the volume fractions and elastic modulus of constituents Table 1. As long as the reinforcement is continuous and aligned, ROM provides the highest modulus that can be achieved. Due to ROM's disregard for the inhomogeneity caused by the size, shape, and orientation of short fibres, the results demonstrated that the modulus predicted by ROM is higher than experimental values. When considering short fibre reinforced composites, ROM is always regarded as the upper limit of elastic modulus. Also, ROM disregards the random distribution orientation of the fibre which has a direct effect on the modulus of the composites. Furthermore, PLA/DPF composites developed showed the increase in modulus as the content of DPF increased can be attributed to the higher packaging of DPF within the same volume. The experimental results where close to modified ROM with K = 0.2, which can be due ot the DPF being oriented randomly with uniform distribution within three dimensions in the composite and it can be assumed that the DPF were inclined closely perpendicular to the direction of the tensile force.

5.3.3.2 Numerical Model 2 – DPF aligned perpendicular to tensile force:

Figure 70 showed schematic representation of Model 2 scenario where all short fibres are aligned in the direction of the compression force. Test samples were prepared from 4mm compression moulded sheet and assuming fibres are opposite to the direction of the tensile testing i.e iso-stress condition for Young's modulus. The fibre-oriented composite is loaded in the transverse direction of fibre alignment, stress in the fibre, matrix, and composite are considered equal.

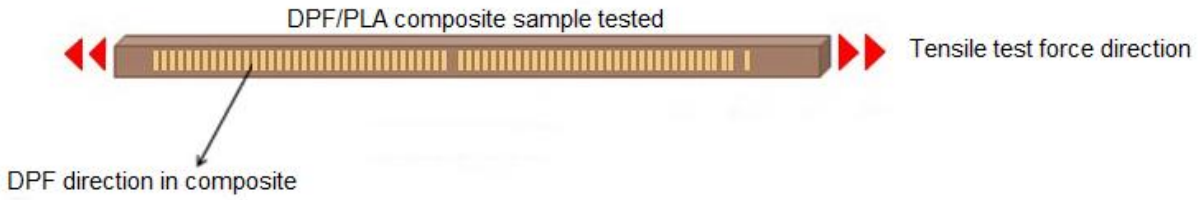

Figure 70 Schematic representation of numerical model 2

Numerical calculations were performed using IROM Equation 17, Modified IROM Equation 18 & Halpin Tsai Equation 19 for four different fibre sizes ≤125 µm, 125-250µm, 250-500µm and 500 – 1,000 µm. Young's modulus value of the tensile test results was considered as the experimental data. For Equation 19, Young's modulus of fibre at transverse direction is considered as 1 GPa to fit the numerical curve.

Figure 71 to Figure 78 exhibit elastic modulus of the composite at various volume fraction of DPF and four different fibre sizes. The numerical values were higher than experimental results

for IROM and Halpin Tsai model as shown in Table 54. As for modified IROM model Equation 18, when elastic modulus of fibre E_{F_2} at 1 GPa, numerical curve synchronized with the experimental curve indicates that DPF fibre contributes around 20% to the overall performance of the composite. The overall results showed that fibres are oriented more towards the transverse direction than the axial direction.

Table 54 Comparison of IROM, Modified IROM and Halpin Tsai model for DPF/PLA composite (model 2)

Composition Wt. %	DPF Size (μm)	Youngs Modulus (MPa)	IROM	IROM (n=0.4)	IROM (n=0.5)	IROM (n=0.6)	Halpin-Tsai Ɛ= 2(L/D)
Pure PLA	**-**	2757	2757	2757	2757	2757	2757
90/10 PLA/DPF	**≤125**	1550	3094	1547	1635	1710	3209
	125-250	1620	3039	1628	1721	1800	3139
	250-500	1250	3052	1607	1698	1776	3156
	500-1000	1688	3072	1577	1667	1743	3181
	≥1,000	1620	3158	1472	1553	1625	3288
	unsieved	1700	3058	1598	1689	1767	3163
80/20 PLA/DPF	**≤125**	1355	3396	1294	1353	1407	3570
	125-250	1375	3305	1349	1415	1476	3465
	250-500	1355	3327	1334	1398	1457	3491
	500-1000	1488	3360	1314	1376	1432	3529
	≥1,000	1420	3494	1247	1298	1346	3679
	unsieved	1425	3337	1328	1392	1450	3502
70/30 PLA/DPF	**≤125**	1295	3667	1184	1225	1263	3864
	125-250	1328	3557	1222	1269	1313	3747
	250-500	1420	3584	1212	1257	1299	3777
	500-1000	1350	3625	1198	1240	1281	3819
	≥1,000	1321	3780	1153	1187	1220	3979
	unsieved	1366	3596	1207	1252	1294	3789
60/40 PLA/DPF	**≤125**	1075	3912	1123	1151	1178	4108
	125-250	1188	3795	1149	1183	1215	3994
	250-500	1250	3825	1142	1174	1205	4024
	500-1000	1190	3868	1132	1163	1191	4065
	≥1,000	1158	4027	1101	1125	1148	4217
	unsieved	1120	3838	1139	1171	1201	4036

Table 55 Comparison of IROM, Modified IROM and Halpin Tsai model for DPF/RPVC composite (model 2)

Composition Wt %	Fibre Size In μm	Youngs Modulus In MPa	IROM	IROM (n=0.4)	IROM (n=0.5)	IROM (n=0.6)	Halpin-Tsai

							Ε= 2(L/D)
Pure RPVC	**-**	1012	1012	1012	1012	1012	1012
90/10 RPVC/DPF	**≤125**	828	1268	688	716	739	1522
	125-250	720	1222	714	742	765	1436
	250-500	621	1233	707	735	758	1457
	500-1000	470	1250	698	726	749	1488
	≥1,000	579	1322	665	690	713	1621
	unsieved	678	1238	705	732	756	1465
80/20 RPVC/DPF	**≤125**	610	1545	605	625	643	2001
	125-250	653	1456	624	646	666	1854
	250-500	640	1478	619	640	660	1890
	500-1000	537	1510	612	633	651	1943
	≥1,000	617	1648	589	607	623	2162
	unsieved	632	1487	617	638	657	1905
70/30 RPVC/DPF	**≤125**	602	1846	567	581	595	2452
	125-250	673	1717	580	597	612	2266
	250-500	764	1749	577	592	607	2313
	500-1000	545	1796	572	587	601	2380
	≥1,000	643	1991	556	568	580	2647
	unsieved	664	1762	575	591	605	2332
60/40 RPVC/DPF	**≤125**	639	2175	545	555	565	2878
	125-250	650	2011	555	567	578	2673
	250-500	824	2052	552	564	574	2725
	500-1000	469	2111	549	559	570	2800
	≥1,000	540	2352	537	546	554	3084
	unsieved	393	2069	551	562	573	2747

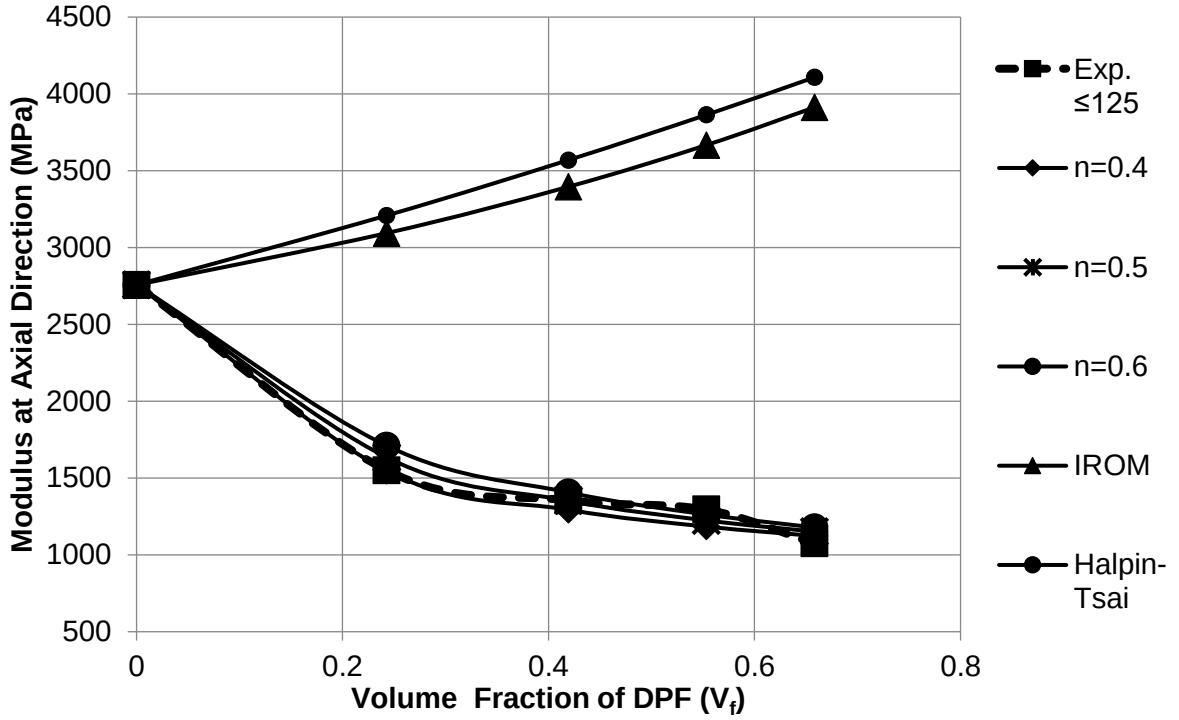

Figure 71 Comparison of IROM, Modified IROM and Halpin Tsai model with experimental results of DPF/PLA composites reinforced with ≤125 μm DPF size (model 2)

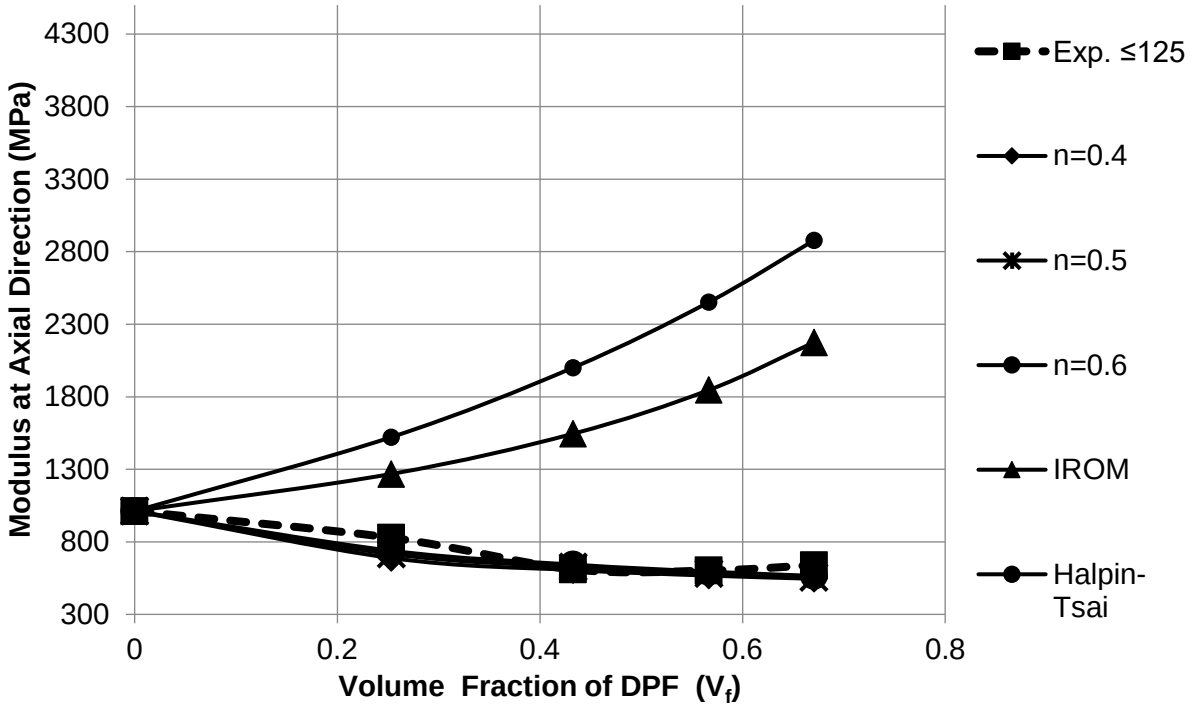

Figure 72 Comparison of IROM, Modified IROM and Halpin Tsai model with experimental results of DPF/RPVC composites reinforced with ≤125 µm DPF size (model 2)

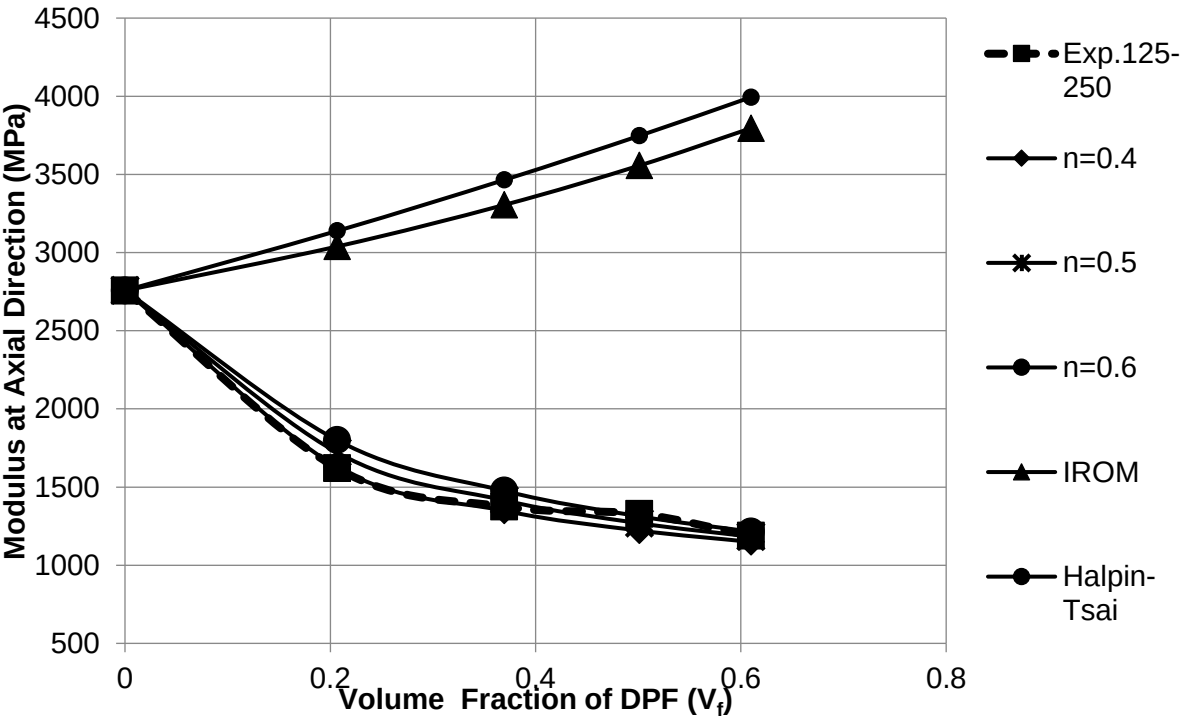

Figure 73 Comparison of IROM, Modified IROM and Halpin Tsai model with experimental results of DPF/PLA composites reinforced with 125 – 250 µm DPF size (model 2)

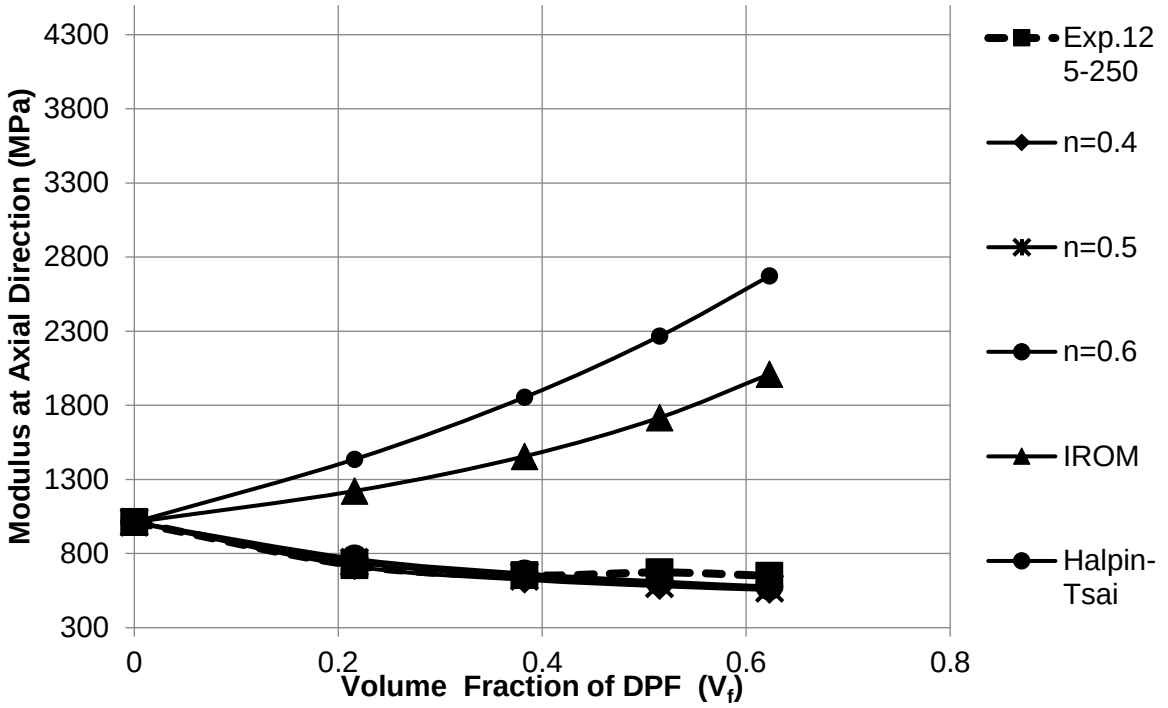

Figure 74 Comparison of IROM, Modified IROM and Halpin Tsai model with experimental results of DPF/RPVC composites reinforced with 125 – 250 µm DPF size (model 2)

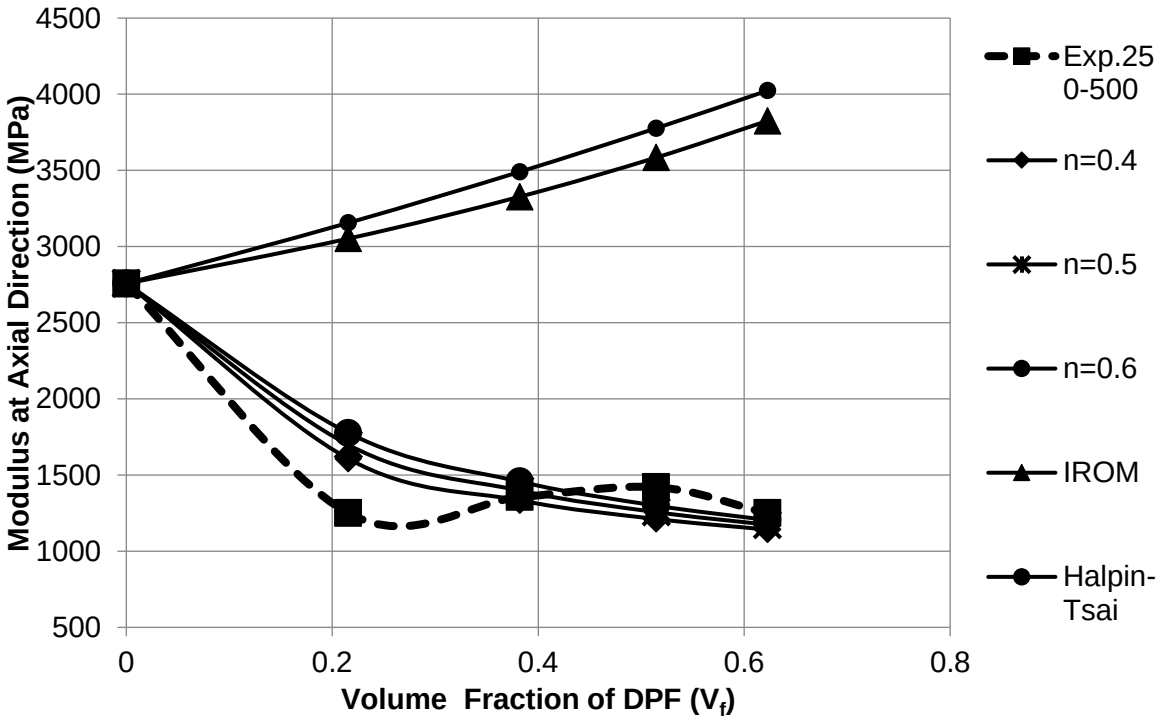

Figure 75 Comparison of IROM, Modified IROM and Halpin Tsai model with experimental results of DPF/PLA composites reinforced with 250 – 500 µm DPF size (model 2)

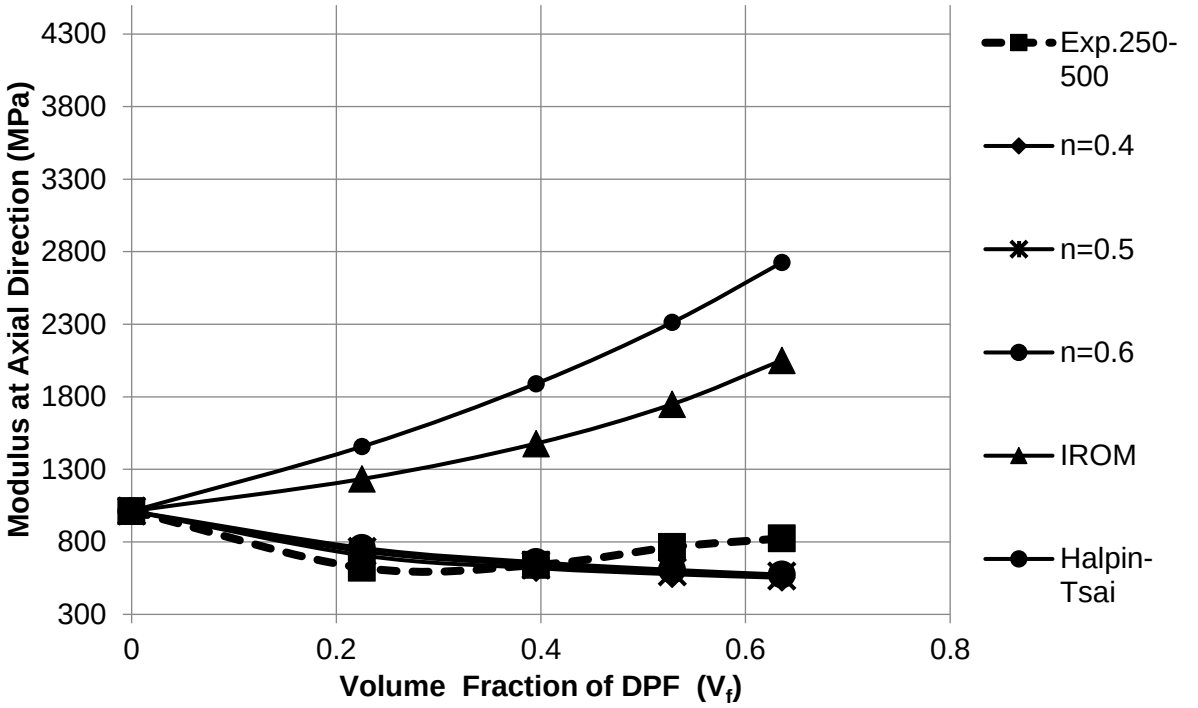

Figure 76 Comparison of IROM, Modified IROM and Halpin Tsai model with experimental results of DPF/RPVC composites reinforced with 250 – 500 µm DPF size (model 2)

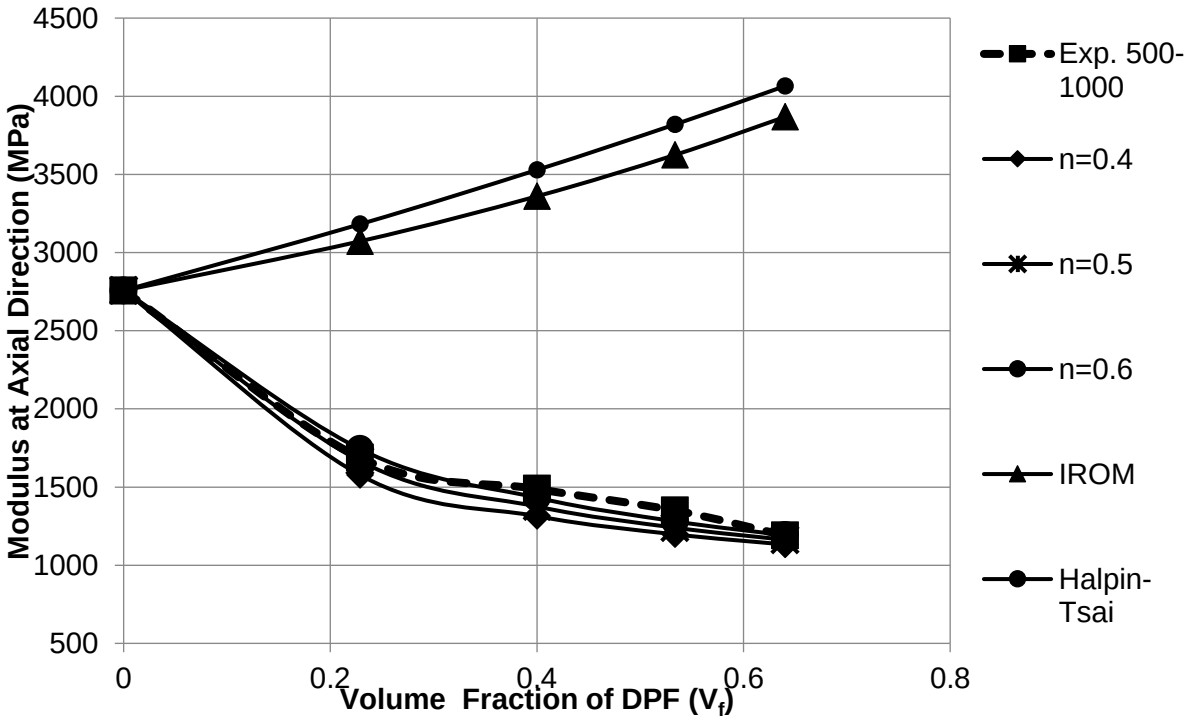

Figure 77 Comparison of IROM, Modified IROM and Halpin Tsai model with experimental results of DPF/PLA composites reinforced with 500 – 1,000 µm DPF size (model 2)

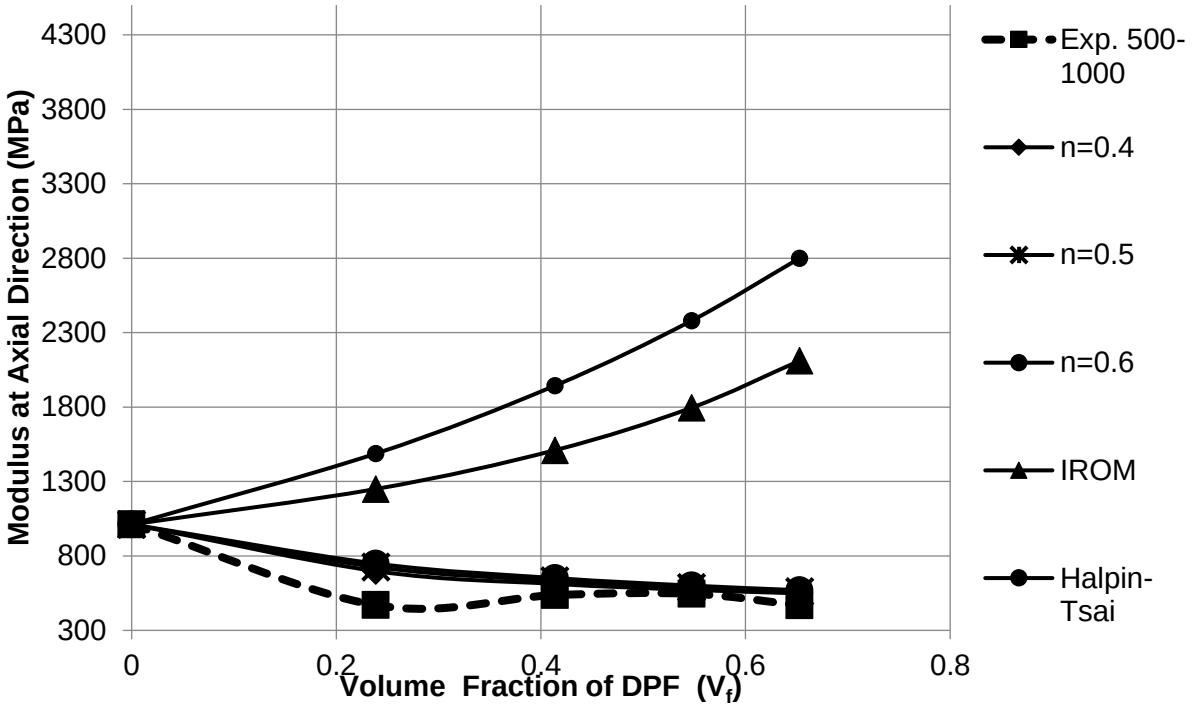

Figure 78 Comparison of IROM, Modified IROM and Halpin Tsai model with experimental results of DPF/RPVC composites reinforced with 500 – 1,000 µm DPF size (model 2)

The equal stress is assumed at fibre and at the matrix for transverse loading. When fibres were inclined, each component experience a different stress and assumption of equal stress is no longer valid for the composite. At n=1, standard inverse rule of mixture Equation 5 is obtained. For elastic regions, usually n ranging from 0.4 to 0.6 is considered and it correlate well with experimental result as shown in Table 54 and Table 55 and Figure 71 to Figure 78. The result proves that fibres were aligned transverse to the direction of tensile force. In addition, results confirm the numerical model 2 and validate that fibres are oriented perpendicular to the direction of tensile force.

5.3.3.3 Numerical Model 3 – DPF aligned in direction of flexural force:

In principle, if fibers are oriented at an angle, their strength along the fiber direction will be more than the other directions. To validate Numerical Model 2, Figure 79 showed schematic representation of numerical Model 3 scenario where all short fibres are aligned in the direction of the compression force. Test samples were prepared from 4mm compression moulded sheet and assuming fibres are aligned in the direction of the Flexural strength test i.e. iso-strain condition for Flexural modulus. The fibre-oriented composite is loaded in the longitudinal direction of fibre alignment, strain in the fibre, matrix, and composite are considered equal.

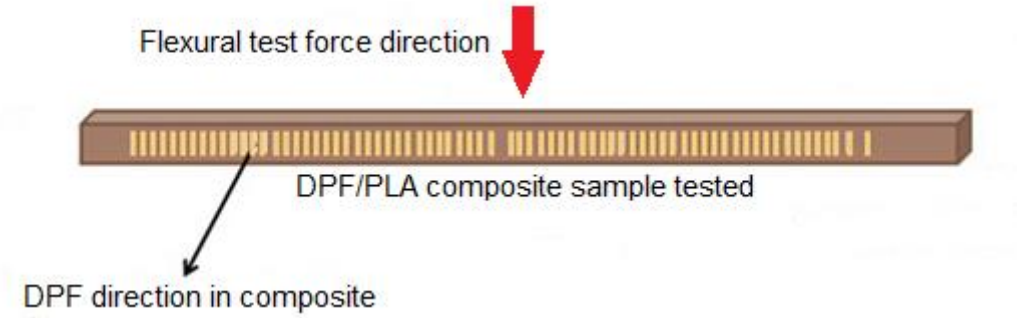

Figure 79 Schematic representation on numerical model 3

Numerical calculations were performed using ROM Equation 14, Modified ROM Equation 16 and Halpin Tsai Equation 19 for four different fibre sizes ≤125 µm, 125-250µm, 250-500µm and 500-1000µm. Flexural modulus value of the Flexural strength results was considered as the experimental data. Please note that isotropic materials like polymers, flexural modulus of elasticity is equivalent to the tensile modulus (Young's modulus) of elasticity.

Figure 80 to Figure 87 exhibit elastic modulus of the composite at various volume fractions of DPF and four different fibre sizes. All experimental results fall in between ROM (k=1) and ROM (k=0.5) which clearly indicate that fibres are oriented between 0° to 45° in the direction of flexural loading. It also proves that short fibres in the compression moulded samples aligned more likely towards the direction of the compression force. The result shows that improvement in the performance of mechanical properties can be expected in the compression moulded direction.

Table 56 Comparison of ROM, Modified ROM and Halpin Tsai for DPF/PLA composite (model 3)

Composition Wt. %	DPF size (µm)	Flexural modulus (MPa)	ROM (K=1)	ROM (K=0.2)	ROM (K=0.375)	ROM (K=0.5)	Halpin-Tsai Ɛ= 2(L/D)
Pure PLA	**-**	3306	3306	3306	3306	3306	3306
90/10 PLA/DPF	**≤125**	3220.82	3717	2746	2958	3110	3676
	125-250	3402.35	3656	2829	3010	3139	3629
	250-500	3355	3671	2809	2997	3132	3655
	500-1000	3522	3694	2778	2979	3122	3684
	≥1,000	3650	3785	2654	2901	3078	3777
	unsieved	3780	3678	2800	2992	3129	3673
80/20 PLA/DPF	**≤125**	3211	4016	2339	2706	2968	3961
	125-250	3500	3932	2454	2777	3008	3892
	250-500	3111	3953	2425	2759	2998	3930
	500-1000	3855	3984	2383	2733	2983	3971
	≥1,000	3950	4103	2221	2633	2927	4093

	unsieved	4100	3962	2413	2752	2994	3956
70/30 PLA/DPF	**≤125**	3033	4243	2031	2515	2860	4185
	125-250	3700	4155	2150	2589	2902	4112
	250-500	3085.79	4178	2119	2570	2891	4153
	500-1000	3840	4210	2076	2542	2876	4197
	≥1,000	4100	4328	1914	2442	2820	4319
	unsieved	4300	4187	2107	2562	2887	4180
60/40 PLA/DPF	**≤125**	2700	4421	1788	2364	2775	4368
	125-250	3100	4339	1900	2433	2814	4297
	250-500	2900	4361	1871	2415	2804	4337
	500-1000	2850	4390	1830	2390	2790	4378
	≥1,000	3450	4497	1685	2300	2739	4488
	unsieved	3520	4369	1859	2408	2800	4363

Table 57 Comparison of ROM, Modified ROM and Halpin Tsai for DPF/RPVC composite (model 3)

Composition Wt. %	**DPF size (μm)**	**Flexural modulus (MPa)**	**ROM (K=1)**	**ROM (K=0.2)**	**ROM (K=0.375)**	**ROM (K=0.5)**	**Halpin-Tsai Ɛ= 2(L/D)**
Pure RPVC	**-**	925	925	925	925	925	925
90/10 RPVC/DPF	**≤125**	942	1957	944	1166	1324	1457
	125-250	888	1805	941	1130	1265	1435
	250-500	945	1842	942	1139	1280	1580
	500-1000	906	1898	943	1152	1301	1729
	≥1,000	543	2124	947	1205	1389	1970
	unsieved	1112	1858	942	1143	1286	1766
80/20 RPVC/DPF	**≤125**	971	2689	958	1336	1607	1954
	125-250	980	2484	954	1289	1528	1916
	250-500	873	2536	955	1301	1548	2152
	500-1000	1242	2610	956	1318	1577	2376
	≥1,000	922	2898	961	1385	1688	2705
	unsieved	1192	2557	955	1306	1556	2429
70/30 RPVC/DPF	**≤125**	1206	3235	968	1463	1818	2420
	125-250	1520	3024	964	1414	1736	2373
	250-500	1385	3078	965	1427	1757	2656
	500-1000	1140	3155	966	1445	1787	2908
	≥1,000	963	3438	971	1511	1896	3251
	unsieved	1468	3101	965	1432	1766	2966
60/40 RPVC/DPF	**≤125**	1393	3657	975	1562	1981	2856
	125-250	1327	3464	972	1517	1906	2806
	250-500	1157	3514	973	1529	1926	3103
	500-1000	788	3586	974	1545	1953	3353
	≥1,000	1348	3837	979	1604	2050	3672
	unsieved	1398	3535	973	1534	1934	3408

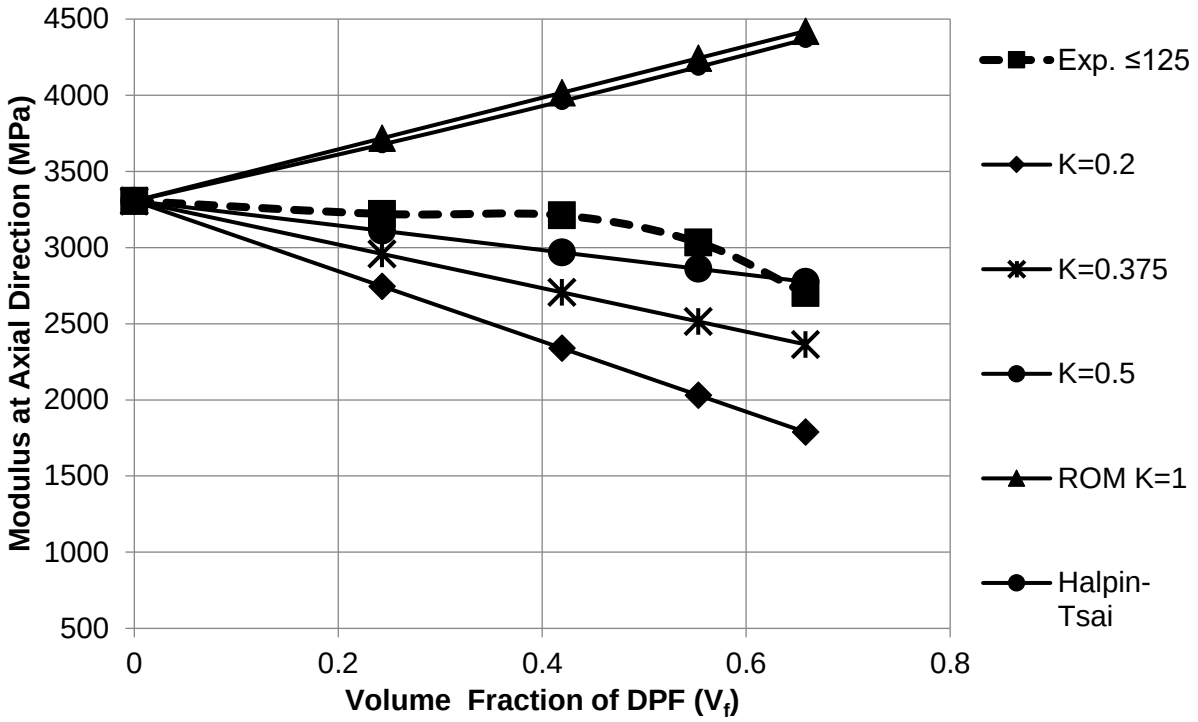

Figure 80 Comparison of ROM, Modified ROM ad Halpin Tsai model with experimental results of DPF/PLA composites reinforced with ≤125 μm DPF size (model 3)

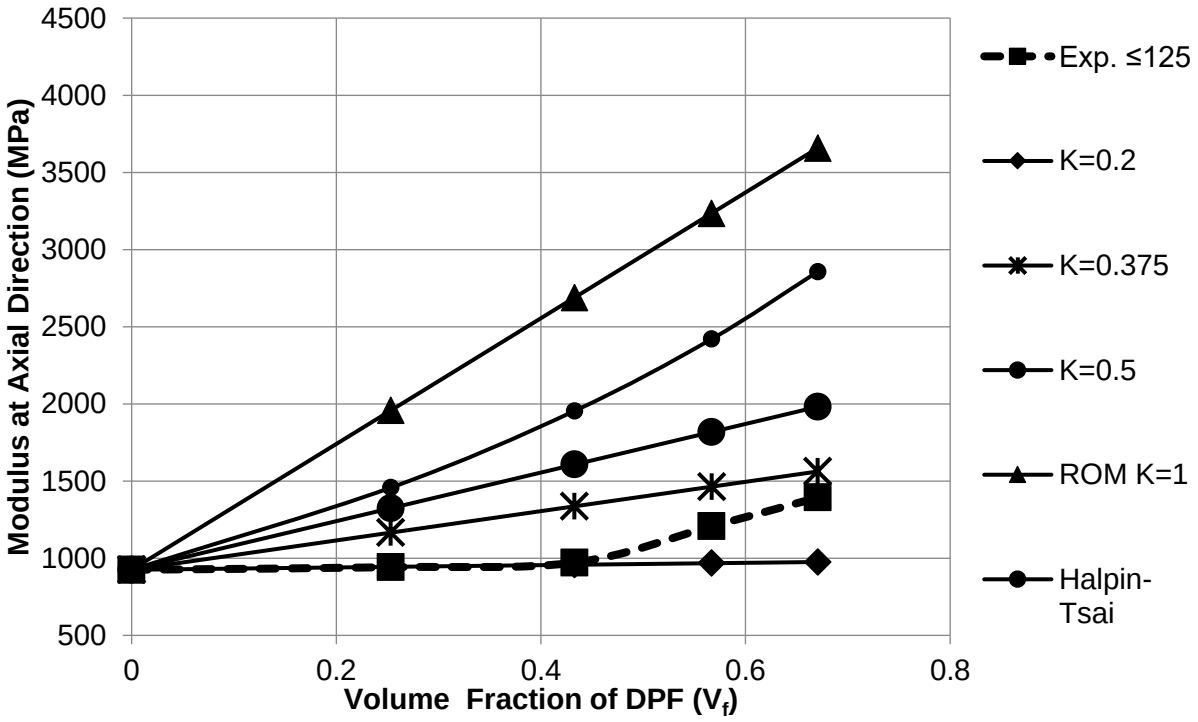

Figure 81 Comparison of ROM, Modified ROM ad Halpin Tsai model with experimental results of DPF/PLA composites reinforced with ≤125 μm DPF size (model 3)

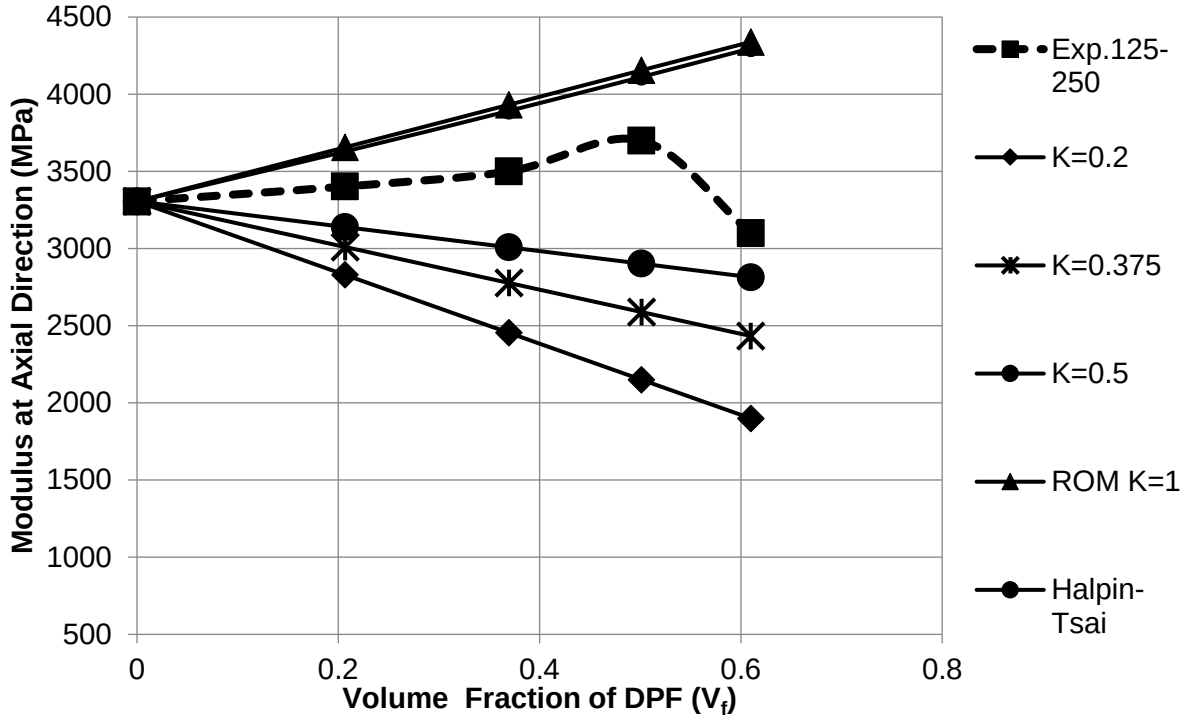

Figure 82 Comparison of ROM, Modified ROM ad Halpin Tsai model with experimental results of DPF/PLA composites reinforced with 125 – 250 µm DPF size (model 3)

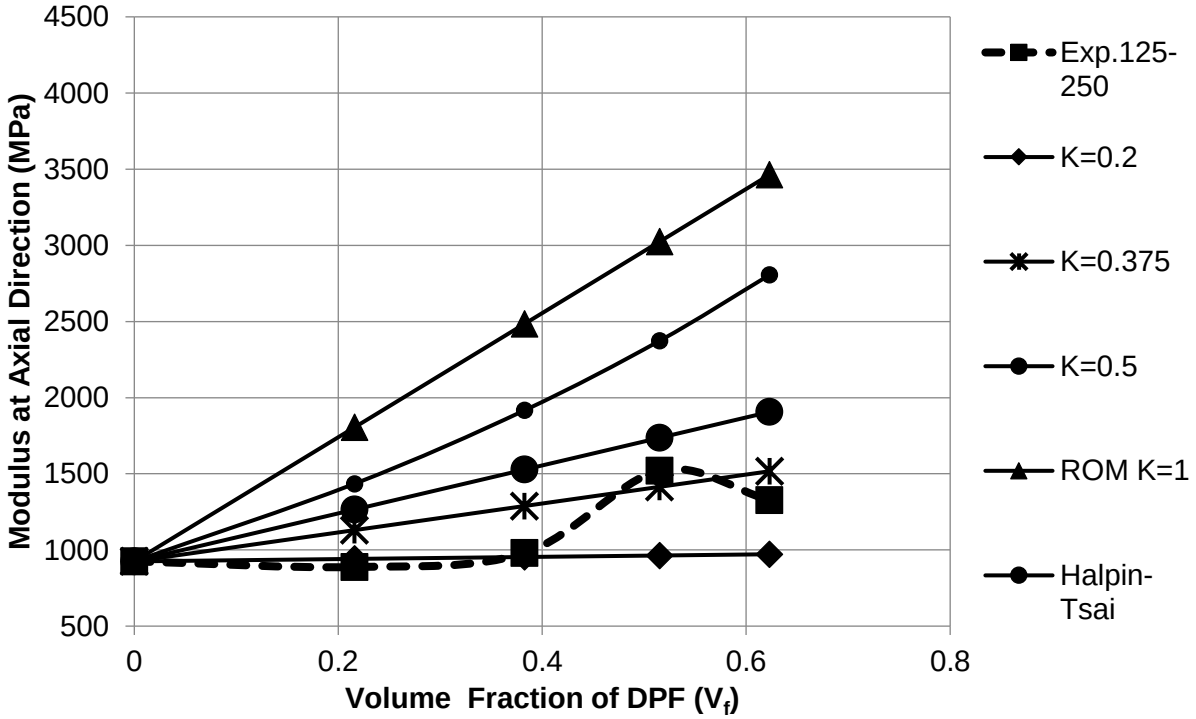

Figure 83 Comparison of ROM, Modified ROM ad Halpin Tsai model with experimental results of DPF/RPVC composites reinforced with 125 – 250 µm DPF size (model 3)

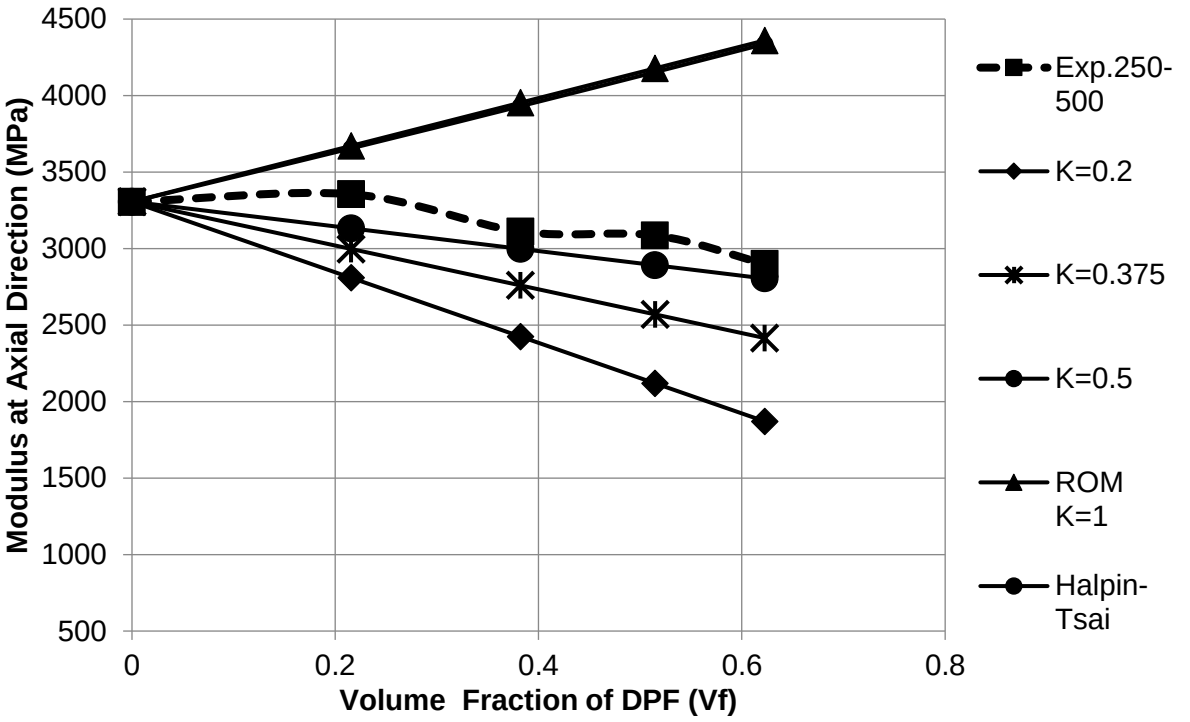

Figure 84 Comparison of ROM, Modified ROM ad Halpin Tsai model with experimental results of DPF/PLA composites reinforced with 250 – 500 µm DPF size (model 3)

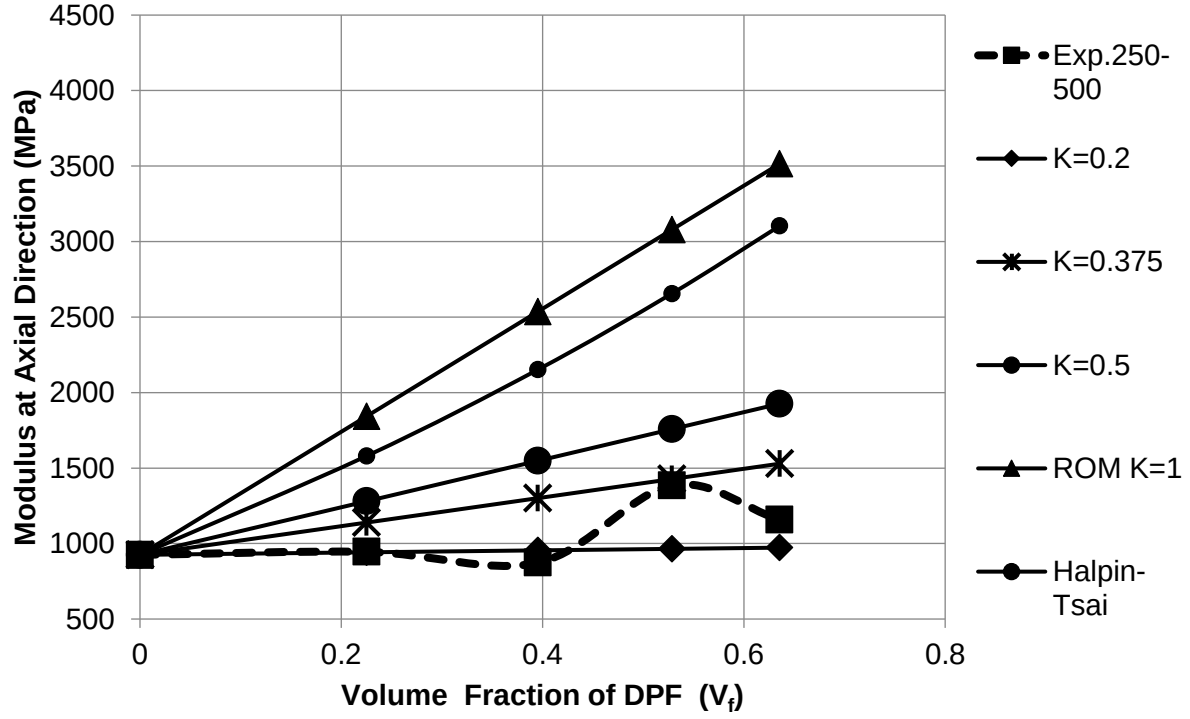

Figure 85 Comparison of ROM, Modified ROM ad Halpin Tsai model with experimental results of DPF/RPVC composites reinforced with 250 – 500 µm DPF size (model 3)

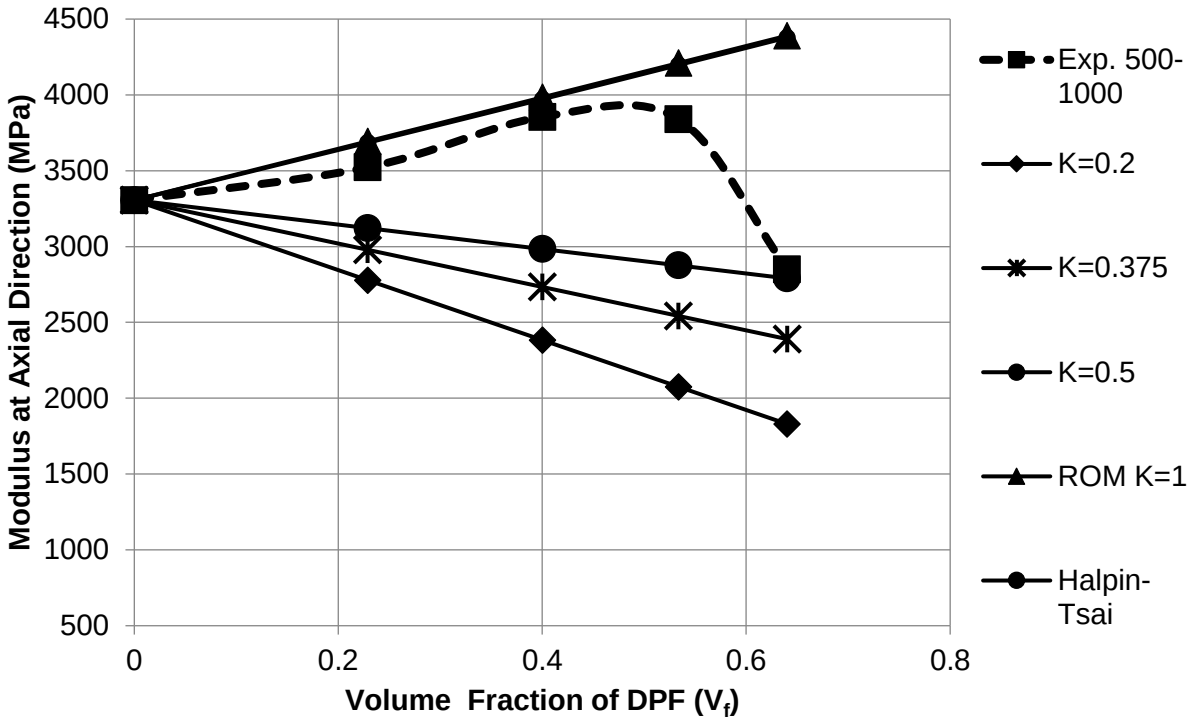

Figure 86 Comparison of ROM, Modified ROM ad Halpin Tsai model with experimental results of DPF/PLA composites reinforced with 500 – 1,000 µm DPF size (model 3)

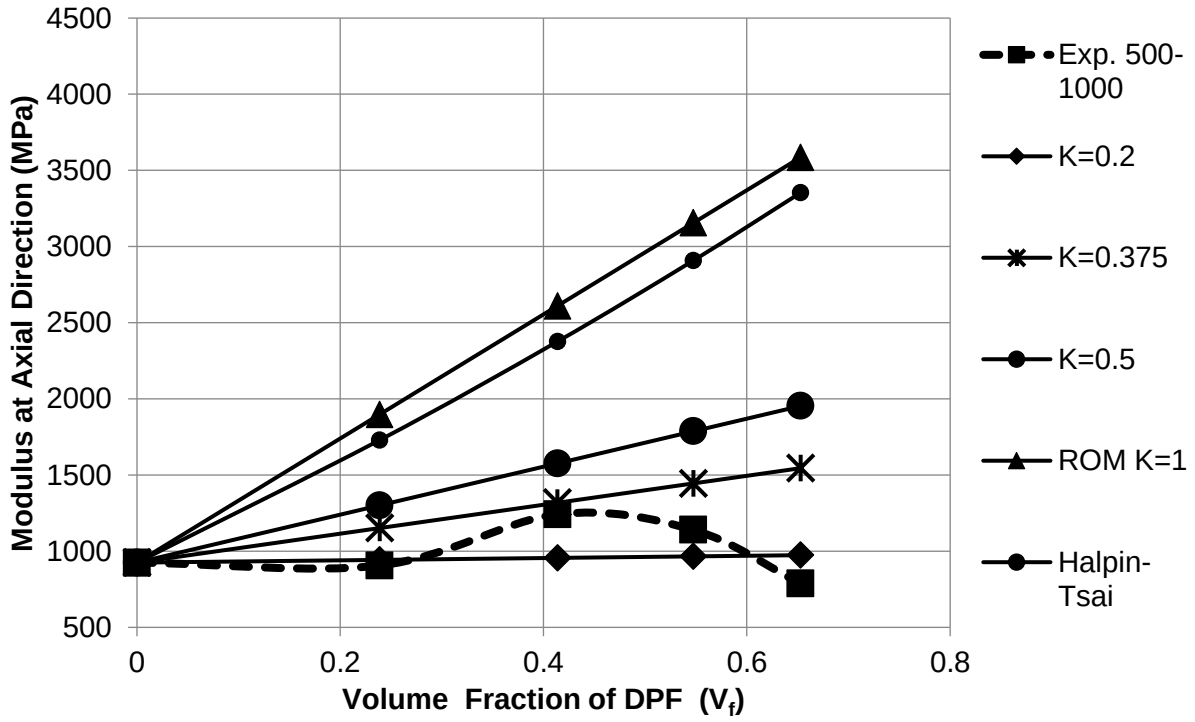

Figure 87 Comparison of ROM, Modified ROM ad Halpin Tsai model with experimental results of DPF/RPVC composites reinforced with 500 – 1,000 µm DPF size (model 3)

5.3.4. Mathematical model

5.3.4.1 FEM simulation results

During compression, materials tend to displace from the gap at Bottom mould wall. FEM simulation confirmed the flow pattern and showed that there is a flow alignment from 0° to 30° from center of the mould to the wall of the mould. Therefore, fibre has the probability to align between 0° to 30° in the flow as shown in Figure 88. Researchers used to consider the fibre alignment from 0° to 90° in the flow domain [186–189]. But for laboratory compression moulding, during compression stage, materials tend to displace from the mould wall which affects the orientation of the fibre between 0° to 30°. Therefore, limits set by the previous researchers will not be applicable for this research and equation derived by [186,187] is modified to suits the current flow phenomena of laboratory compression moulding.

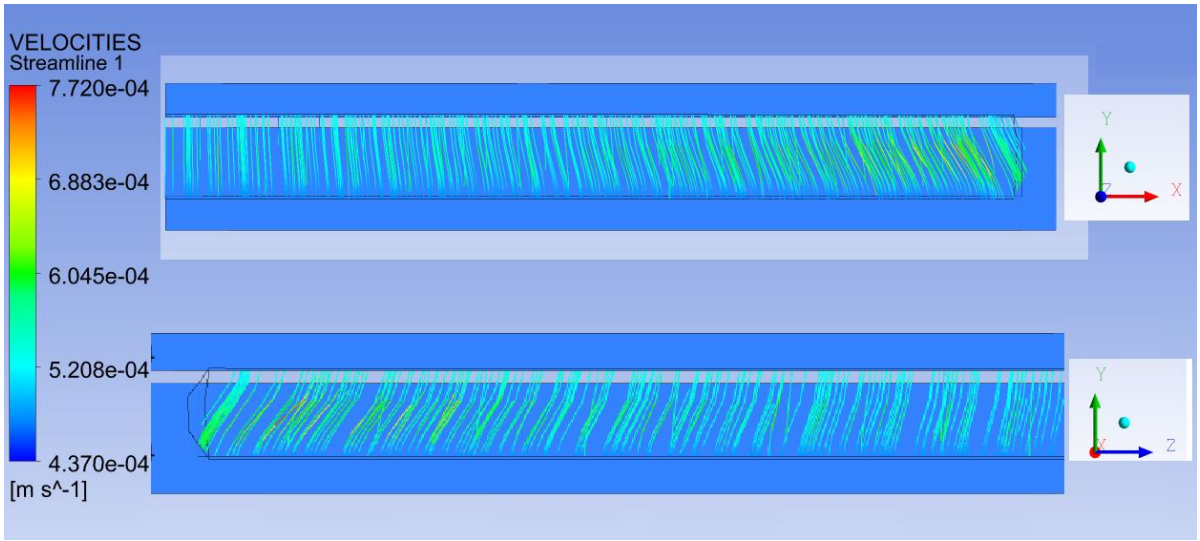

Figure 88 FEM

5.3.4.2 Elastic modulus at axial (compression)direction

Compression moulded samples were tested for Flexural strength test and found that short fibres aligned in the direction of the compression force improved the mechanical performance of the composite. As the expected, Elastic modulus of composite were improved and fibres were aligned between 0° to 30° in the direction of the applied force.

Derived mathematical model using Equation 47 and Equation 51 showed close match with experimental results for various lengths of the fibres. The experimental result validates both FEM model and mathematical model. Figures showed notable deviations at some points due to the assumption of perfect adhesion between the fibre and matrix. As shown in Figure 111 presence of debonding between fibres and PLA matrix increases the error percentage in the mathematical model.

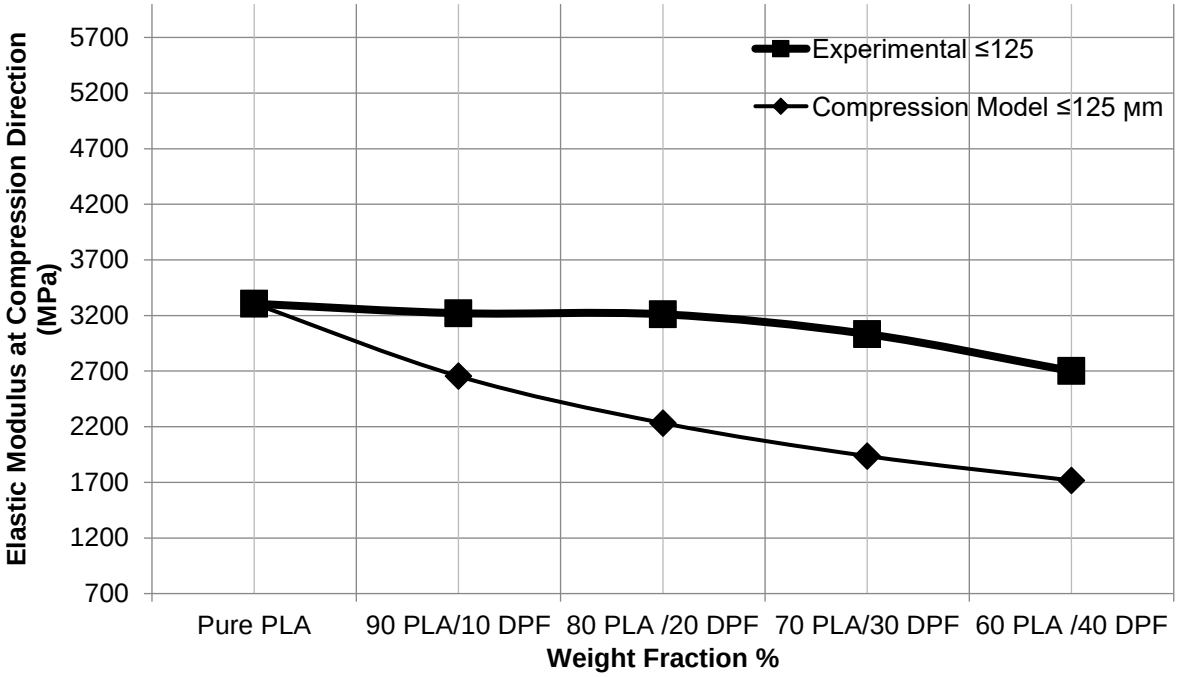

Figure 89 Comparison of experimental results to predicted elastic modulus of DPF/PLA composites reinforced with ≤125 μm DPF size (compression direction)

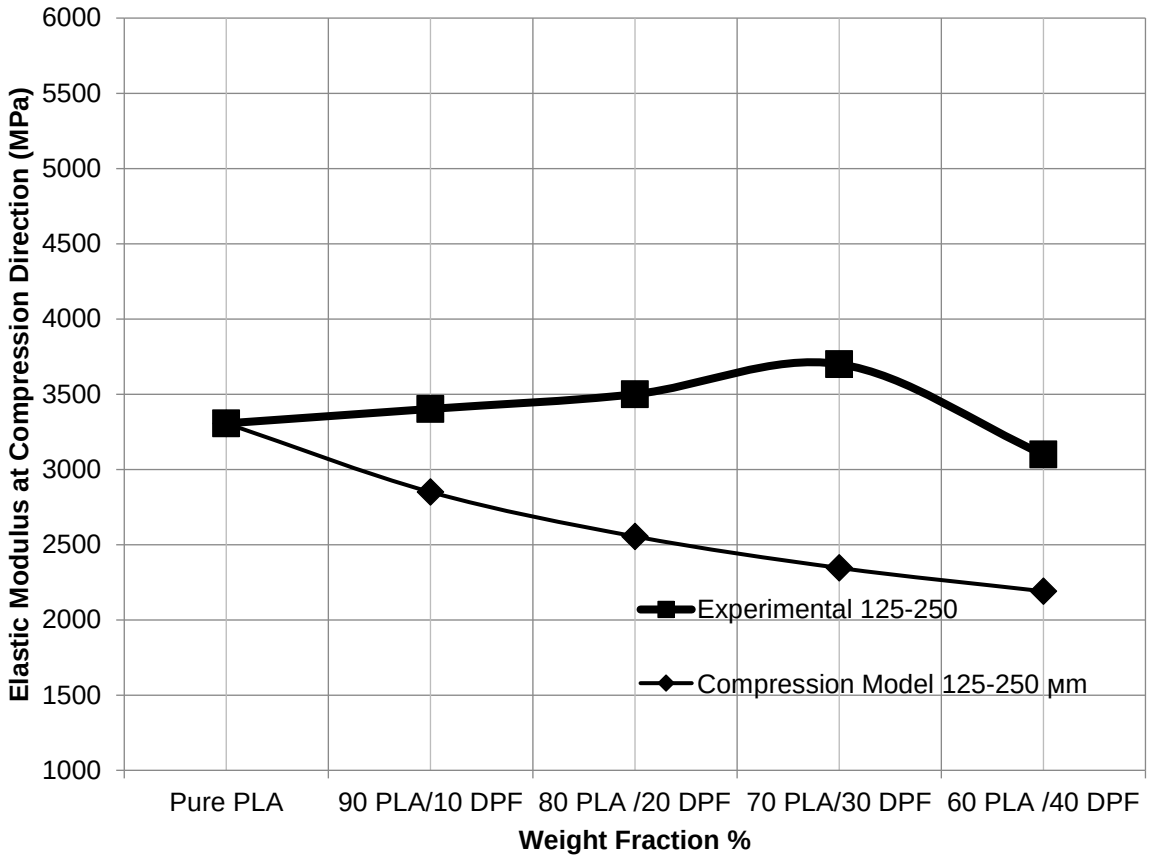

Figure 90 Comparison of experimental results to predicted elastic modulus of DPF/PLA composites reinforced with 125 – 250 μm DPF size (compression direction)

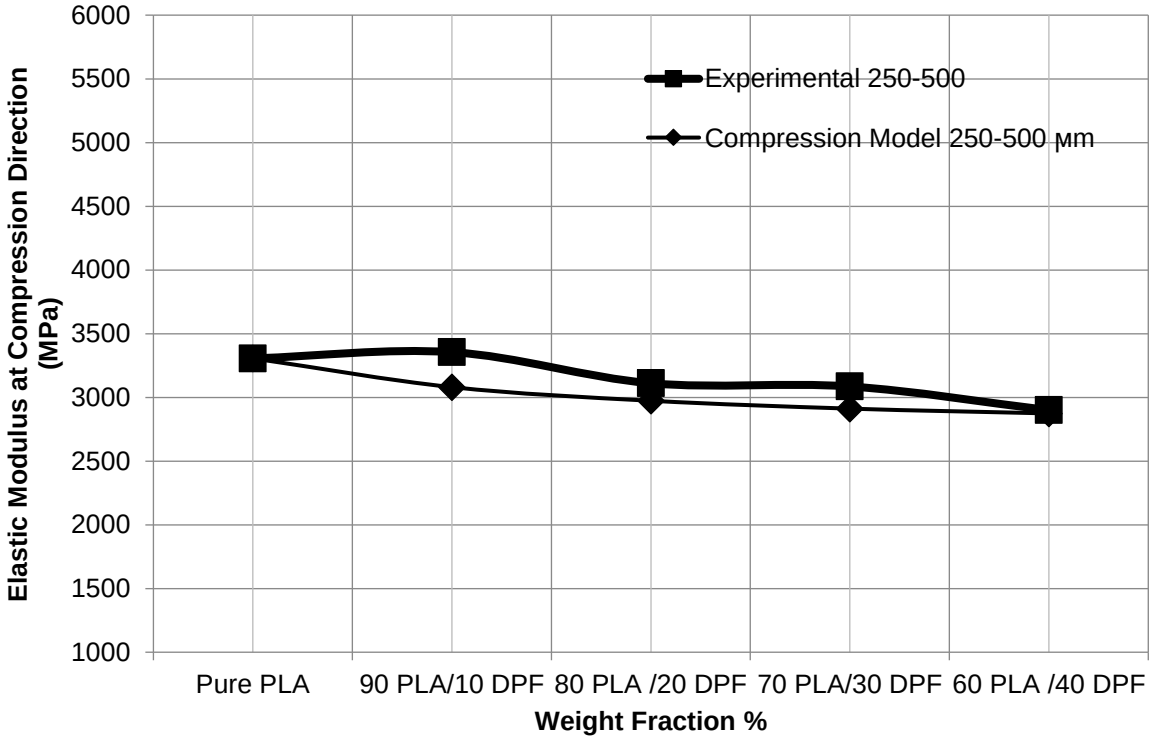

Figure 91 Comparison of experimental results to predicted elastic modulus of DPF/PLA composites reinforced with 250 – 500 µm DPF size (compression direction)

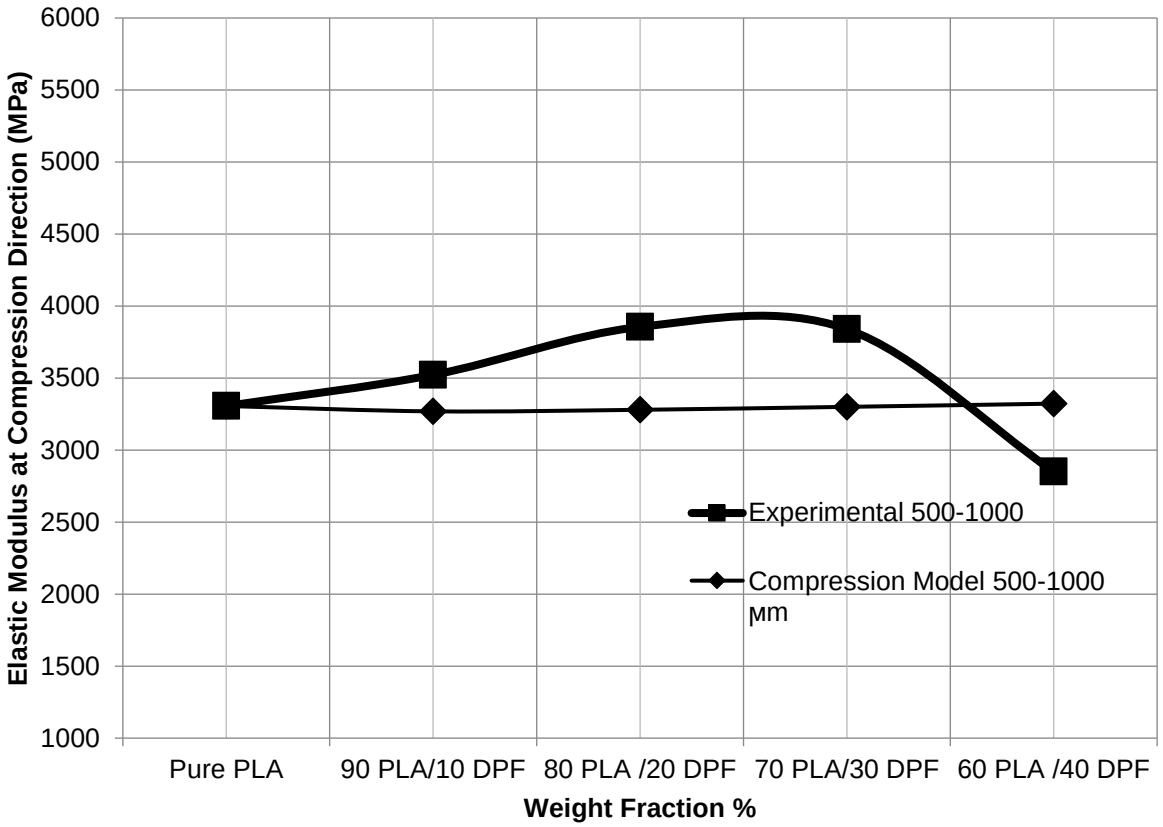

Figure 92 Comparison of experimental results to predicted elastic modulus of DPF/PLA composites reinforced with 500 – 1,000 µm DPF size (compression direction)

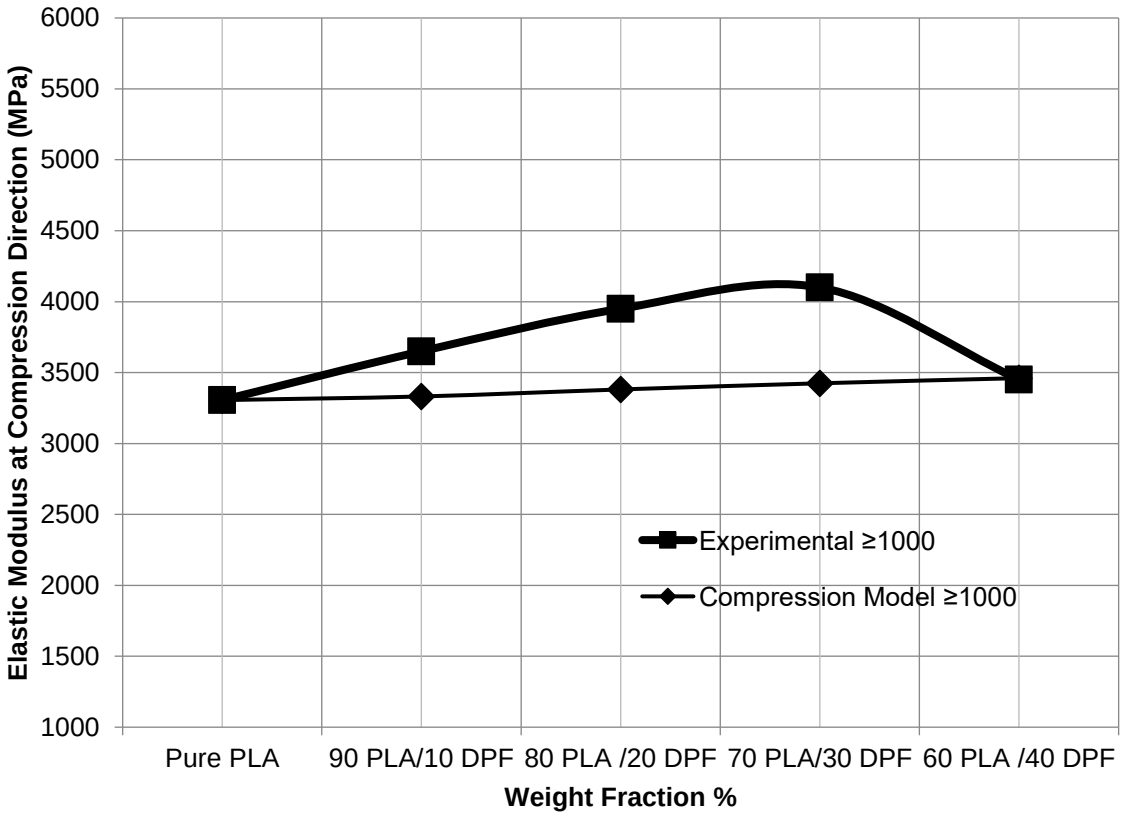

Figure 93 Comparison of experimental results to predicted elastic modulus of DPF/PLA composites reinforced with ≥1,000 µm DPF size (compression direction)

5.3.4.3 Elastic modulus at tensile direction

Compression moulded samples were tested for tensile strength test and found that short fibres were aligned perpendicular to the direction of the applied force and decreased the overall mechanical performance of the composite. As expected from FEM results, Elastic modulus of composite were decreased, and fibres were aligned between 60° to 90° to the direction of the applied force.

Derived mathematical model using Equation 51 and Equation 53 showed close match with experimental results for various lengths of the fibres. The experimental result validates both FEM model and mathematical model.

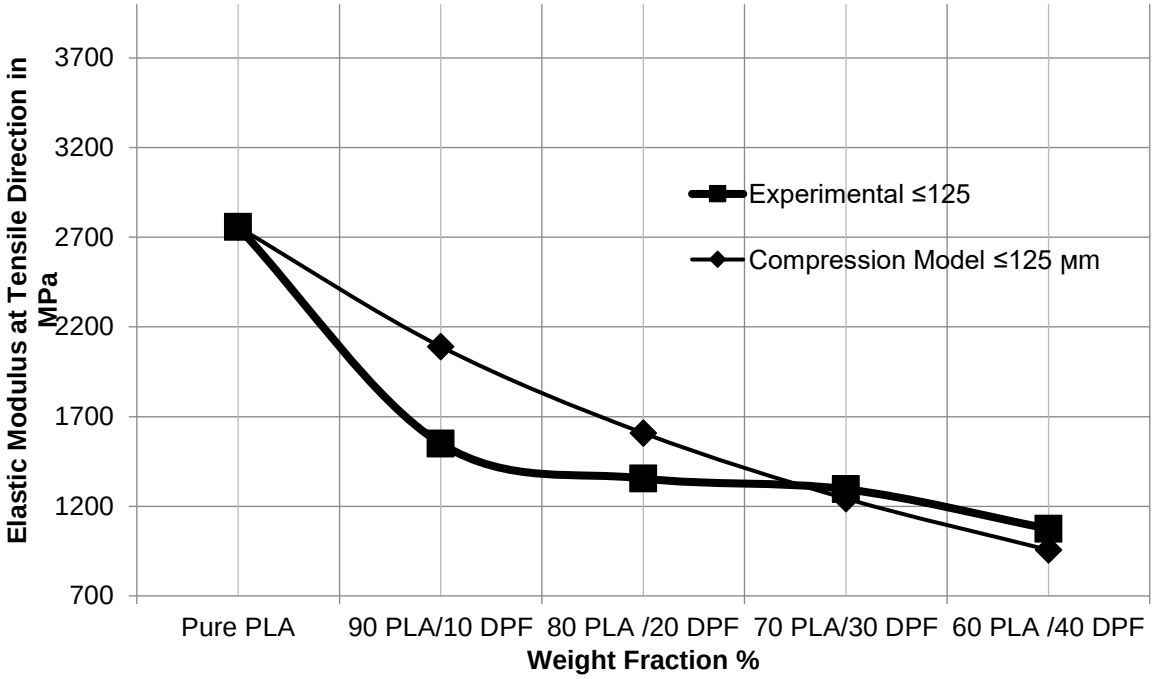

Figure 94 Comparison of experimental results to predicted elastic modulus of DPF/PLA composites reinforced with ≤125 μm DPF size (tensile direction)

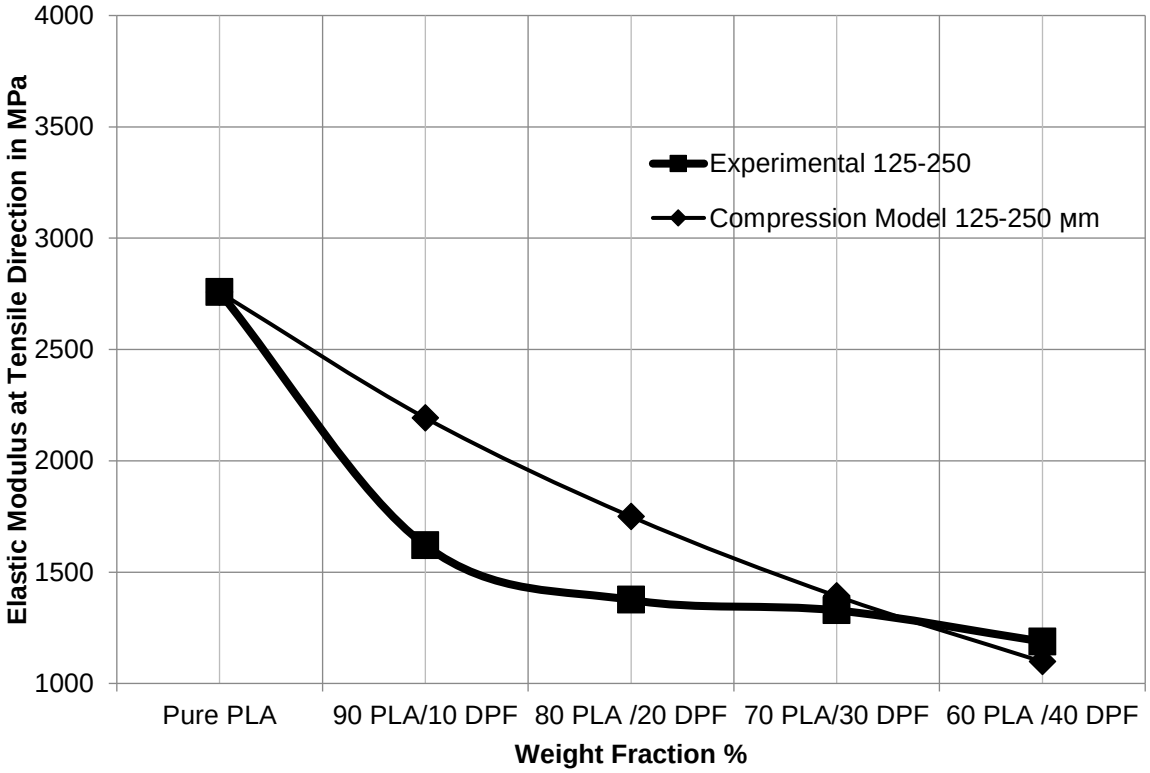

Figure 95 Comparison of experimental results to predicted elastic modulus of DPF/PLA composites reinforced with 125 – 250 μm DPF size (tensile direction)

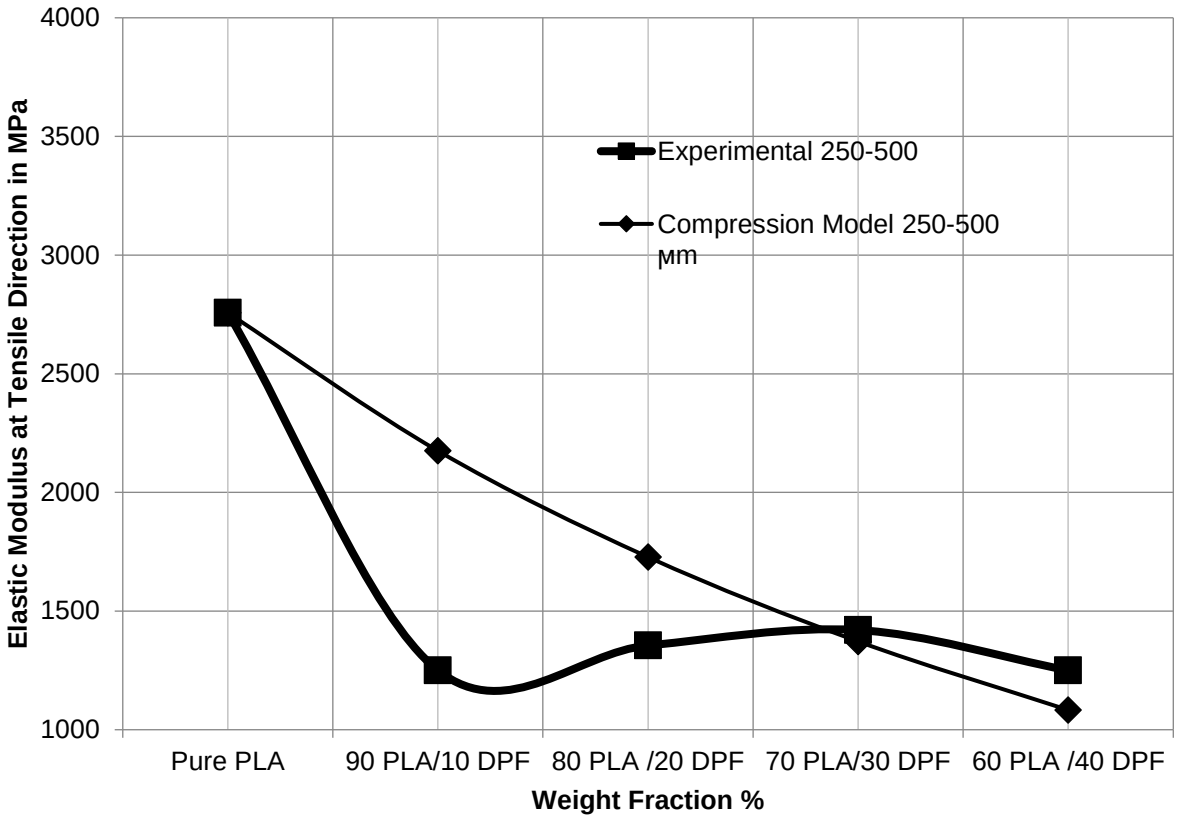

Figure 96 Comparison of experimental results to predicted elastic modulus of DPF/PLA composites reinforced with 250 – 500 μm DPF size (tensile direction)

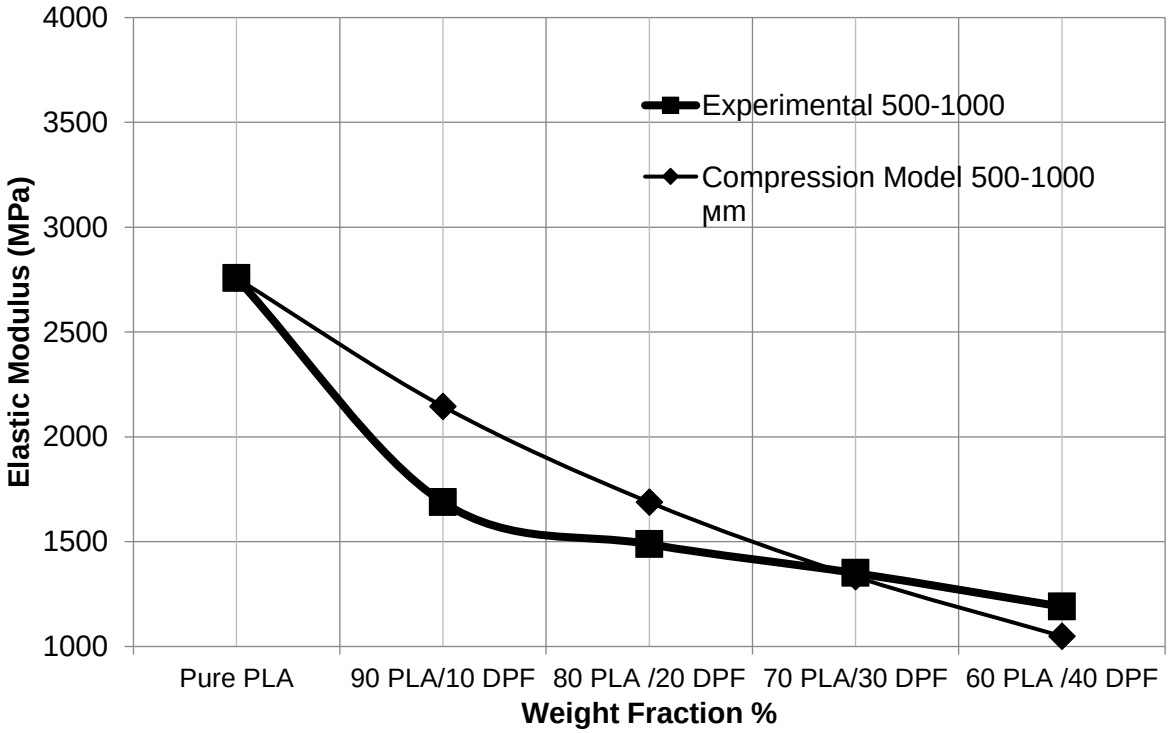

Figure 97 Comparison of experimental results to predicted elastic modulus of DPF/PLA composites reinforced with 500 – 1,000 μm DPF size (tensile direction)

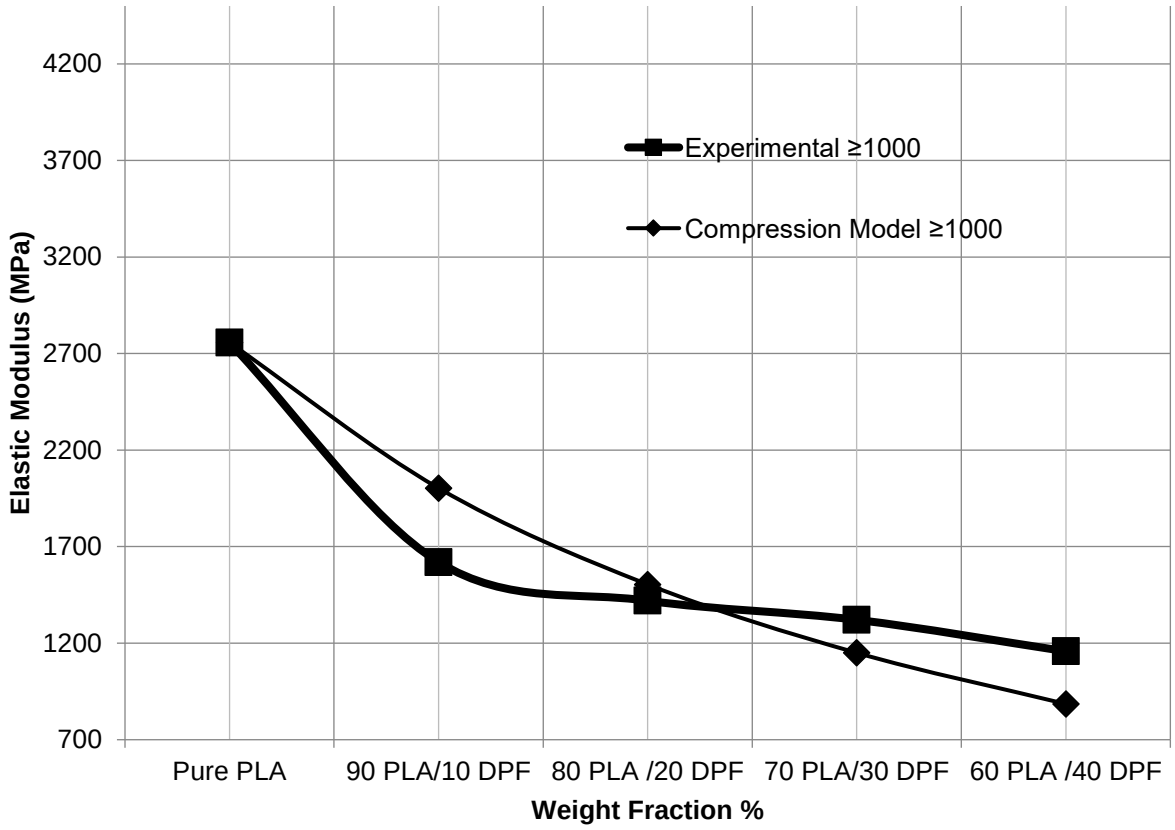

Figure 98 Comparison of experimental results to predicted elastic modulus of DPF/PLA composites reinforced with ≥1,000 µm DPF size (tensile direction)

5.3.5. Effect of DPF geometry and loading content on the biodegradation and disintegration of the composites

5.3.5.1 Fungal biodegradation

Decay resistance of mini blocks samples obtained from the modified composites panels and *Pinus sylvestris* wood control samples against *Tyromyces palustris* and *Irpex lacteus* is reported in Figure 99 and Figure 100. After 8 weeks of fungal exposure, the results clearly demonstrate that the fungal activity of the test decay fungi was high enough under the test conditions, and this allowed us to compare the decay resistance (mean percent mass loss) for the composites panels. The mass losses caused by both tested fungi species were drastically decreased when compared with the control specimens. Slight mass loss of < 5 % was recorded with the modified composites against the brown rot fungus *Tyromyces palustris* while the percentage of mass loss in the control samples recorded approximate 30%. Meanwhile, the modified composites performed well against *Irpex lacteus* and sustained a mass loss of ≤ 5% while the control specimens suffered a mass loss of 28%. The present results strongly indicate that the modified composites exhibited a significant improvement in the decay-resistance when compared with the solid wood control samples. This can be attributed to the

water-repellent effect of the used resin (thermoplastic polymer matrix, PLA and RPVC) which play an important role in preventing the wood based modified composites from absorbing moisture during fungal exposure leading to un-appropriate conditions for fungal decay. As expected, the pure thermoplastic specimens (PLA and RPVC) exhibited no fungal decay. Meanwhile, by adding the DPF with the rest of treatments, distinct mass losses were recorded.

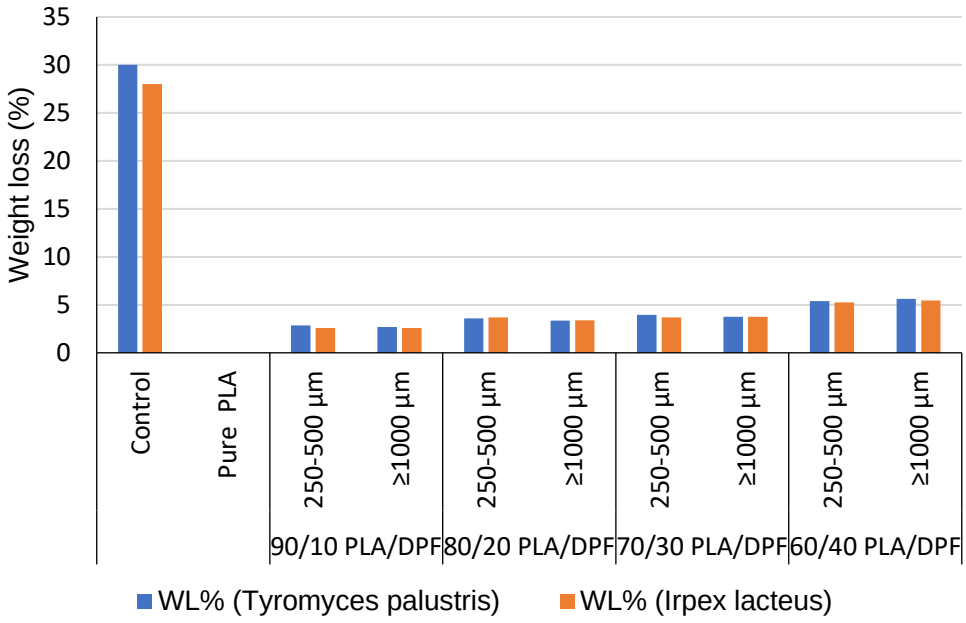

Figure 99 Decay resistance of DPF/PLA composite and control solid wood samples (Pinus sylvestris) against Tyromyces palustris and Irpex lacteus.

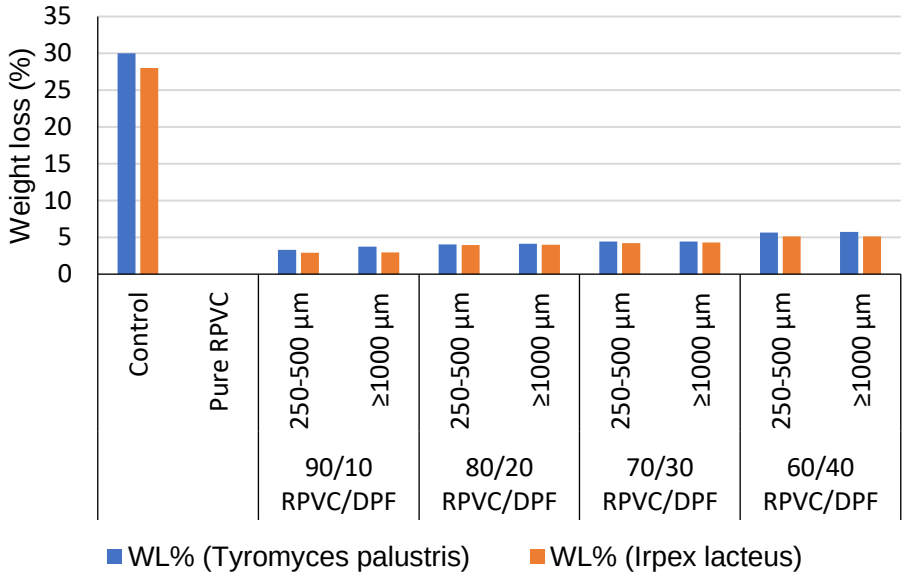

Figure 100 Decay resistance of DPF/RPVC composite and control solid wood samples (Pinus sylvestris) against Tyromyces palustris and Irpex lacteus

These data indicated that all DPF modified composite samples showed significant resistant against both brown and white rot fungi used in this trial when compared to the control solid wood samples (*Pinus sylvestris*) Figure 99 and Figure 100. In this context, it seems that the DPF modified composites could be used as wood alternative in the above ground applications such as frames, outdoor decking, windows, and furniture. The obtained data revealed an increasing in the mass loss percentages by the addition of natural fibers (DPF). It seemed that the fungal durability of the produced biopolymer composites is governed by many factors like moisture absorption and biodegradability of natural fiber. Christian (2019) has stated that moisture absorption increases with increase in fiber volume fraction. Meanwhile, the biopolymer composites manufactured with hydrophobic biopolymers (like PLA and RPVC) show significant resistant against fungal degradation when compared to the control natural wood blocks. These results were supported with those obtained by Bari et al. (2018) who stated that the natural fibers can be protected from fungal degradation by making them less hygroscopic and less susceptible to fungal enzymes. The gained fungal resistant was attributed to the surface modification of natural fibers by thermoplastic addition treatments and thereby reduces the moisture content below fungal requirement for growth [208]. The same behavior was noted by Mohareb et al. (2015) who found a considerable fungal resistant for the reinforced biopolymer composites using thermoplastic polyester resin with flax and jute fabrics [209]. Consequently, the noticeable fungal durability reported in this study with the produced biopolymer composites made them suitable for use in the above ground hazard 3 applications.

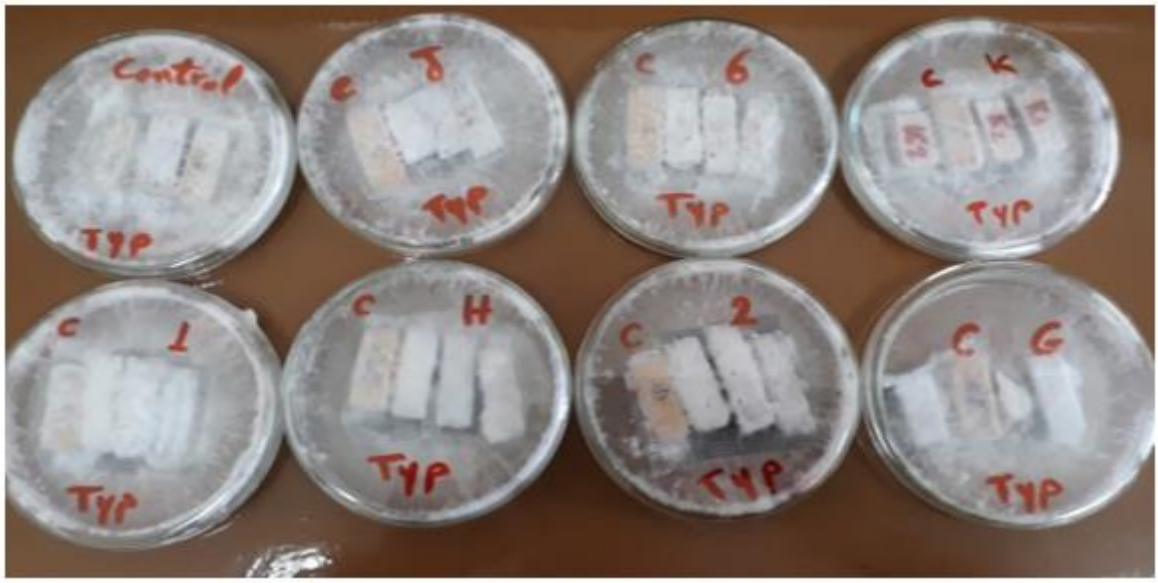

Figure 101 Decay resistance of the modified DPF composite and control solid wood samples (Pinus sylvestris) against brown rot fungus Tyromyces palustris (TYP)

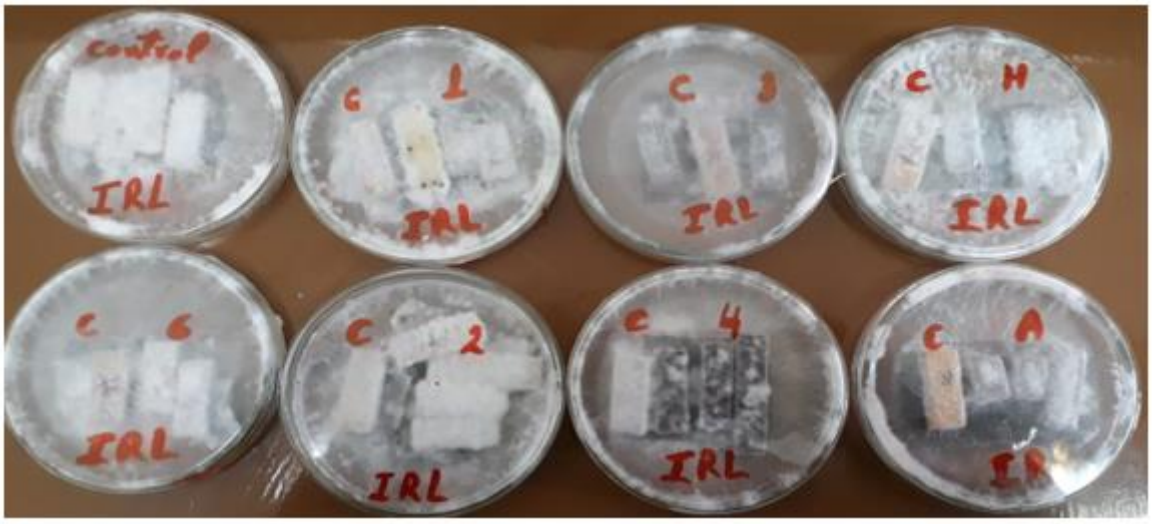

Figure 102 Decay resistance of the modified DPF composite and control solid wood samples (Pinus sylvestris) against white rot fungus Irpex lacteus (IRL)

5.3.5.2 Disintegration

Figure 103 shows the results of the disintegration test which caried on pure PLA and PLA/DPF with different blend ratio and fiber length. Results were calculated after duration of 90 days of exposing the samples to composting at laboratory conditions. Results show a weight loss and indication of disintegration for all samples. The level of weight loss and disintegration are varied according to the blending ratio and fiber length. In general, results indicate that as the DPF length increased the disintegration of the composite material increased. As, the microorganisms attached the DF fiber causing damage to the reinforcement (DPF) by causing

hole and cracking over the samples. Which result in a disintegration to samples. This is clearly seen in the images of the samples, whereas samples turn to be very brittle and breaks easily. Results also indicated that as the blend ratio of the DPF increased the disintegration of the composite samples increased. This may attribute to the higher DPF length the close the fiber to the edges or to the surface of the samples to be attacked by the microorganisms.

Therefore, the soil burial tests conducted with these produced composites showed that the microorganisms load in soil biodegrades and disintegrate the DPF and the PLA composites by creating holes, cracking over it and promote microorganisms' growth and thereby accelerated their degradation [59,210]. On the other hand, samples made of DPF/RPVC showed no sign of disintegration as there were no weight loss occurred to any of the samples.

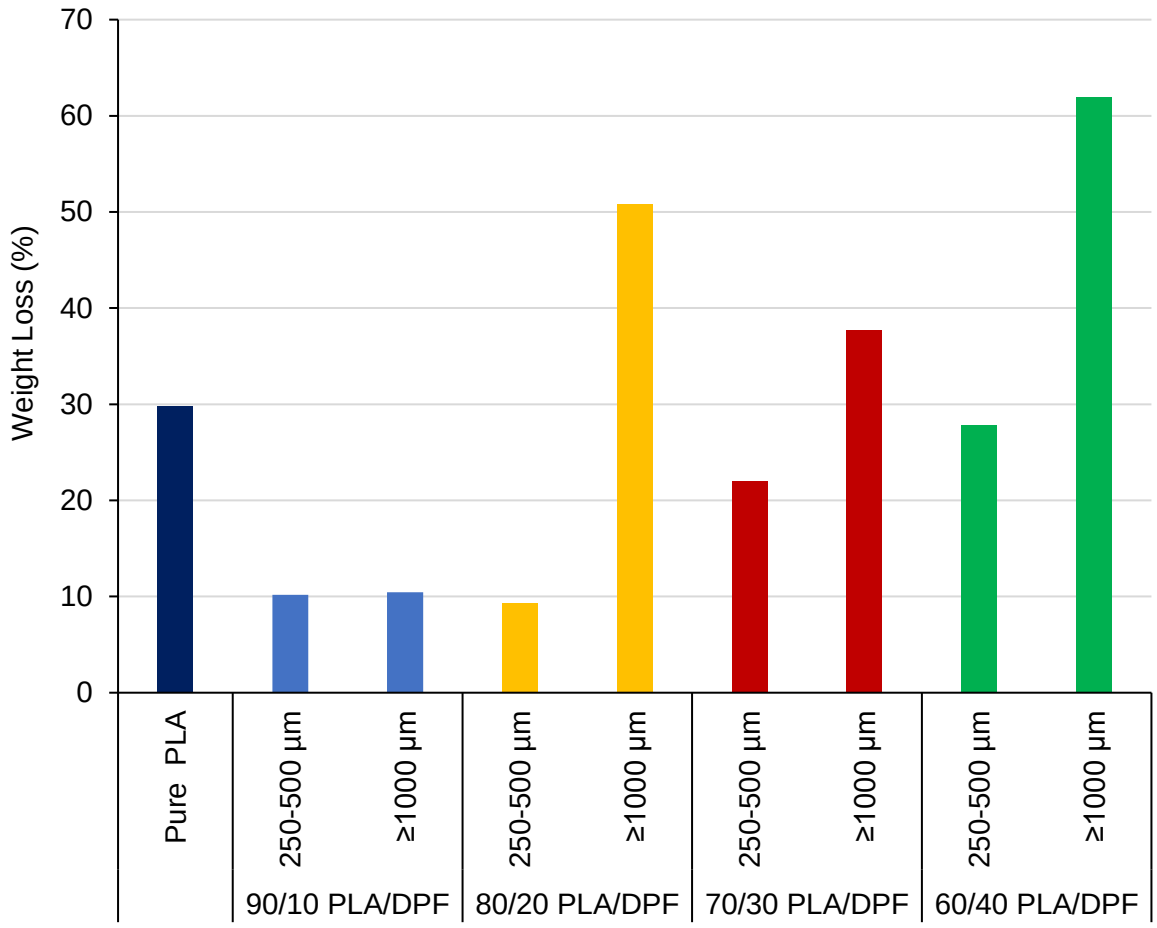

Figure 103 Biodegradation of DPF/PLA composite with different DPF loading content and size

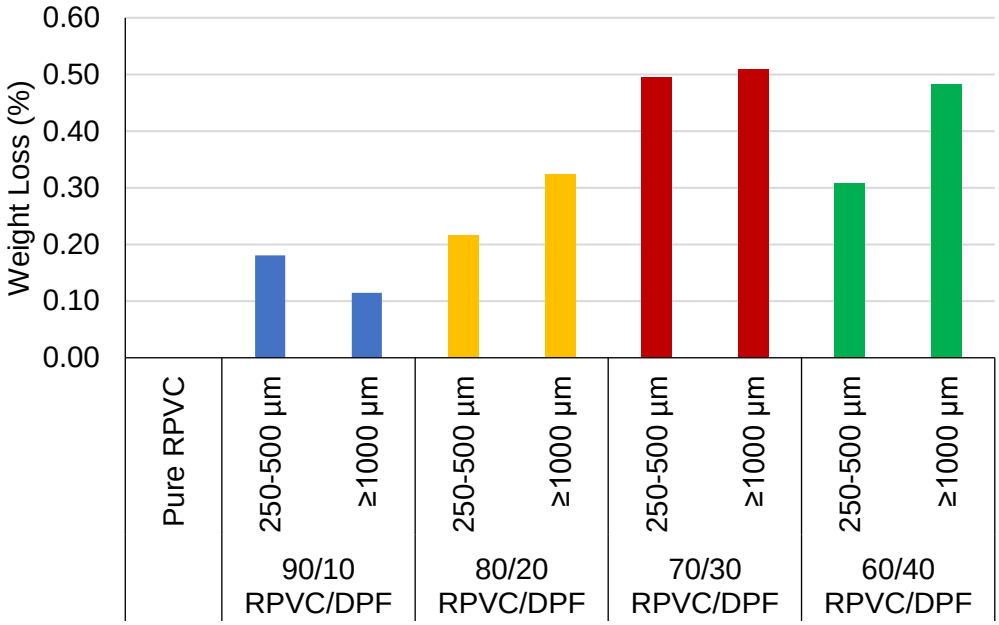

Figure 104 Biodegradation of DPF/RPVC composite with different DPF loading content and size

Figure 105 DFP/PLA (90/10) composite with ≥ 1,000 µm before the test (top) and after the test (bottom)

5.3.6. Influence of various DPF geometries on the microstructure of the composite

Figure 106 to Figure 109 show the cross-section morphologies of DPF/RPVC composites under different magnification ratios. Figure 106 shows the cross Section of reinforced RPVC with DPF with the sieved size of ≥ 1,000 µm (Figure 106 A) and 500 – 1,000 µm (Figure 106 B). It is clearly demonstrated that the addition of large size DPF in the matrix system creates

micro-cracks around the fibres and provides a low surface area, resulting in a weaker composite which is explained by the poor mechanical and physical properties. Therefore, the failure mode is mostly related to the propagation of the voids and cracks in the matrix system but is also related to the fibre pull-out because of using untreated DPF, which provides a poor interfacial bonding due to their hydrophilic nature.

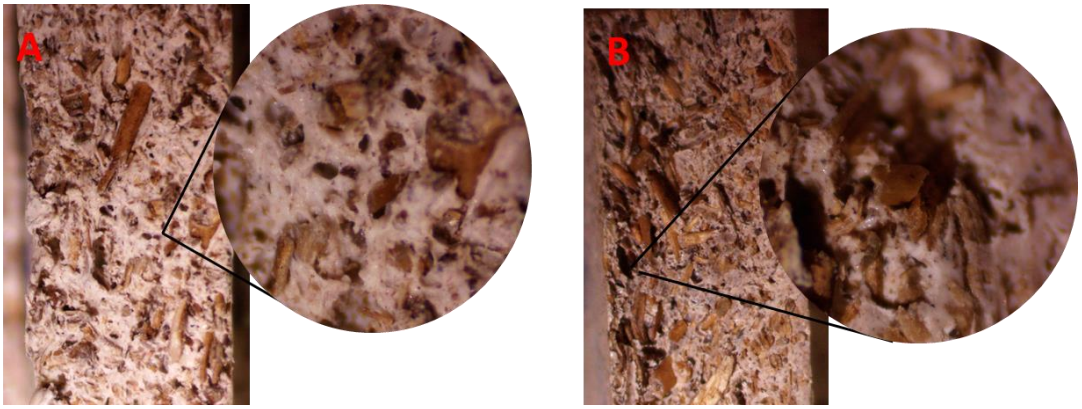

Figure 106 Microstructure of ≥ 1,000 µm (A) and 500 - 1,000 µm (B) sieved DPF/RPVC composite

On the other hand, unsieved DPF offers a mixture of various sizes of DPF, which includes both long fibres with high aspect ratio that can be used as a stress-transfer and DPF powder particles that can fill the cracks and voids occurred by the large fibres. This will create a compacted composite with enhanced strength. Since the amount of DPF powder particles are low as demonstrated by the sieve analysis, it may not be sufficient to fill all voids in the composite thus large voids are present around large fibres as shown in Figure 107.

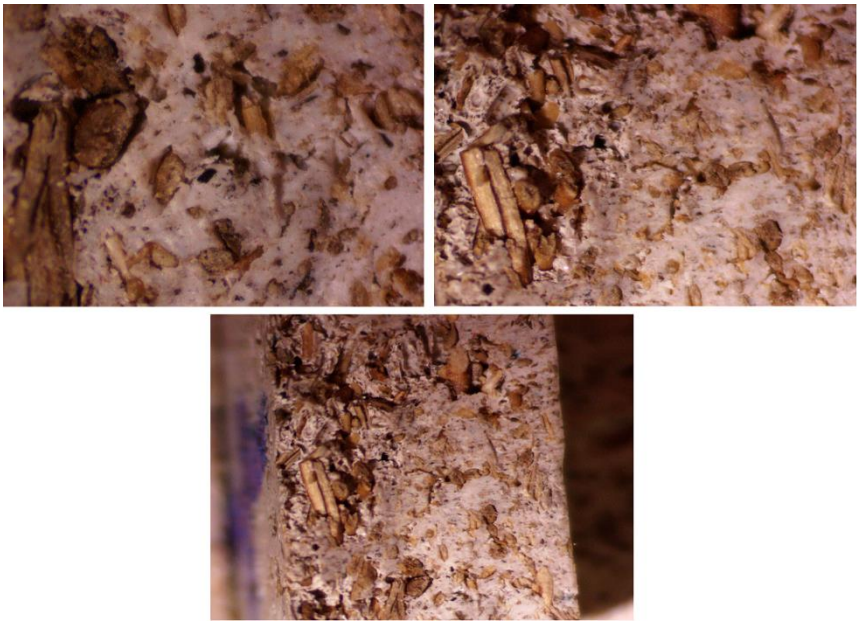

Figure 107 Microstructure of unsieved DPF/RPVC composite

Figure 108 shows the cross-Section of the DPF/RPVC composite reinforced with DPF with sieving size of 125 – 250 µm (Figure 108 A), and 250 – 500 µm (Figure 108 B). The composites show low voids compared to DPF/RPVC composites with sieving size 500 and 1,000 µm DPFs. Image also shows that high volume of DPF due to the small size of the used DPF at sieving size 125 – 250 µm and 250 – 500 µm. This high volume of the DPF causes a higher coherent and adhesion between the matrix and DPF. This may lead to the higher mechanical properties of these composite than those reinforced with 500 and 1,000 µm.

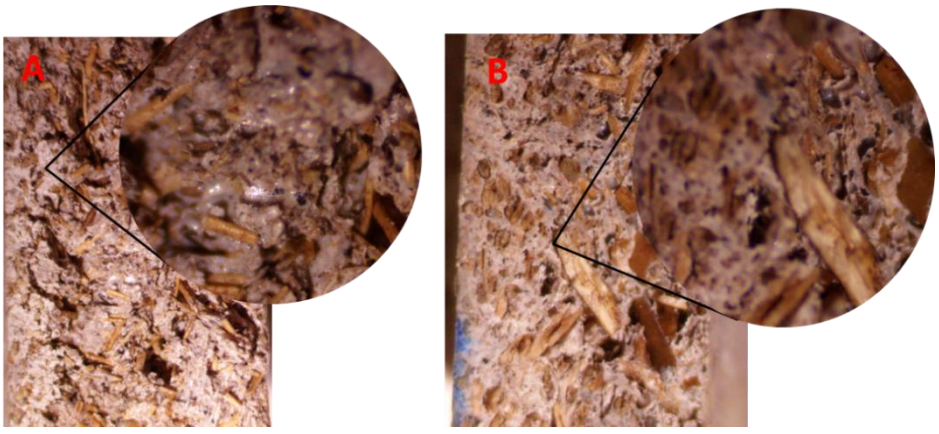

Figure 108 Microstructure of 125 - 250 µm (A) and 250 - 500 µm (B) sieved DPF/RPVC composite

DPF particles or powder collected at the pan of the sieving machine, ≤125 µm, provided a highly homogenous and compacted structure, where all the particles are enclosed with the RPVC matrix with minimum voids visible. This reflects the homogenous mixing achieved using

finer DPF, which covers a large surface for interfacial bonding. However, the large surface area covered by the particle does not provide an ideal stress-transfer when a load is applied. It must be noted that the voids present in Figure 109 may be due to the processing process, where the DPF powder was not perfectly mixed with RPVC matrix due to the low density of DPF and high volume of DPF compared to the volume of RPVC; the volume of DPF is much higher than that of the RPVC which will make it difficult to achieve a fully homogenous mixed composite.

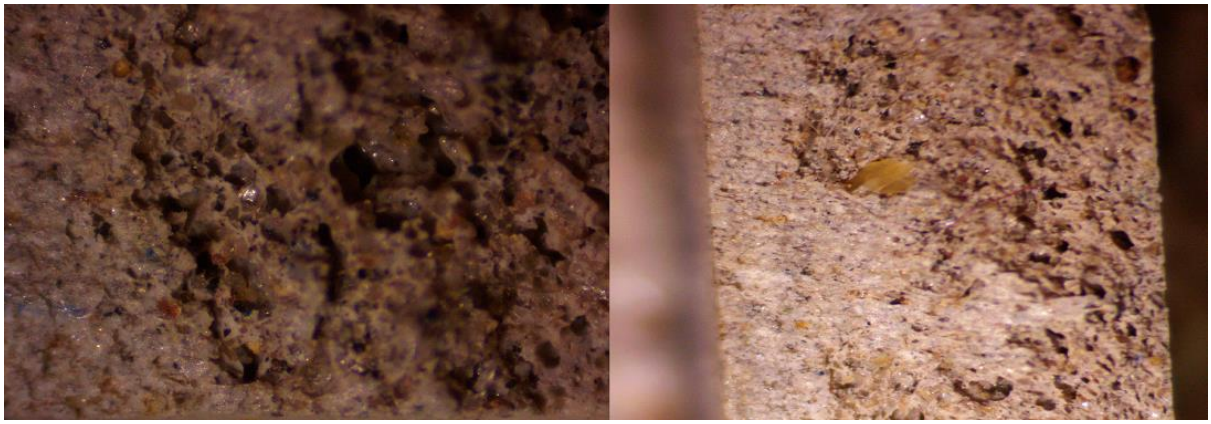

Figure 109 Microstructure of 125 µm sieved DPF/RPVC composite

Furthermore, Figure 110 demonstrates the interfacial bonding between DPF and RPVC matrix with various DPF loading content. According to the SEM images, large voids are located between the DPF fibres and the RPVC matrix due to the low fibre-matrix adhesion which led to fibre pull-out which affected the mechanical and physical properties negatively. It can be observed that as the fibre loading increases, DPF debonding increased resulting in more voids occurring between the DPF and the RPVC matrix which leads to an increase in porosity of the composite that affected the mechanical properties negatively and increases high water absorption of the composite increasing its thickness swelling.

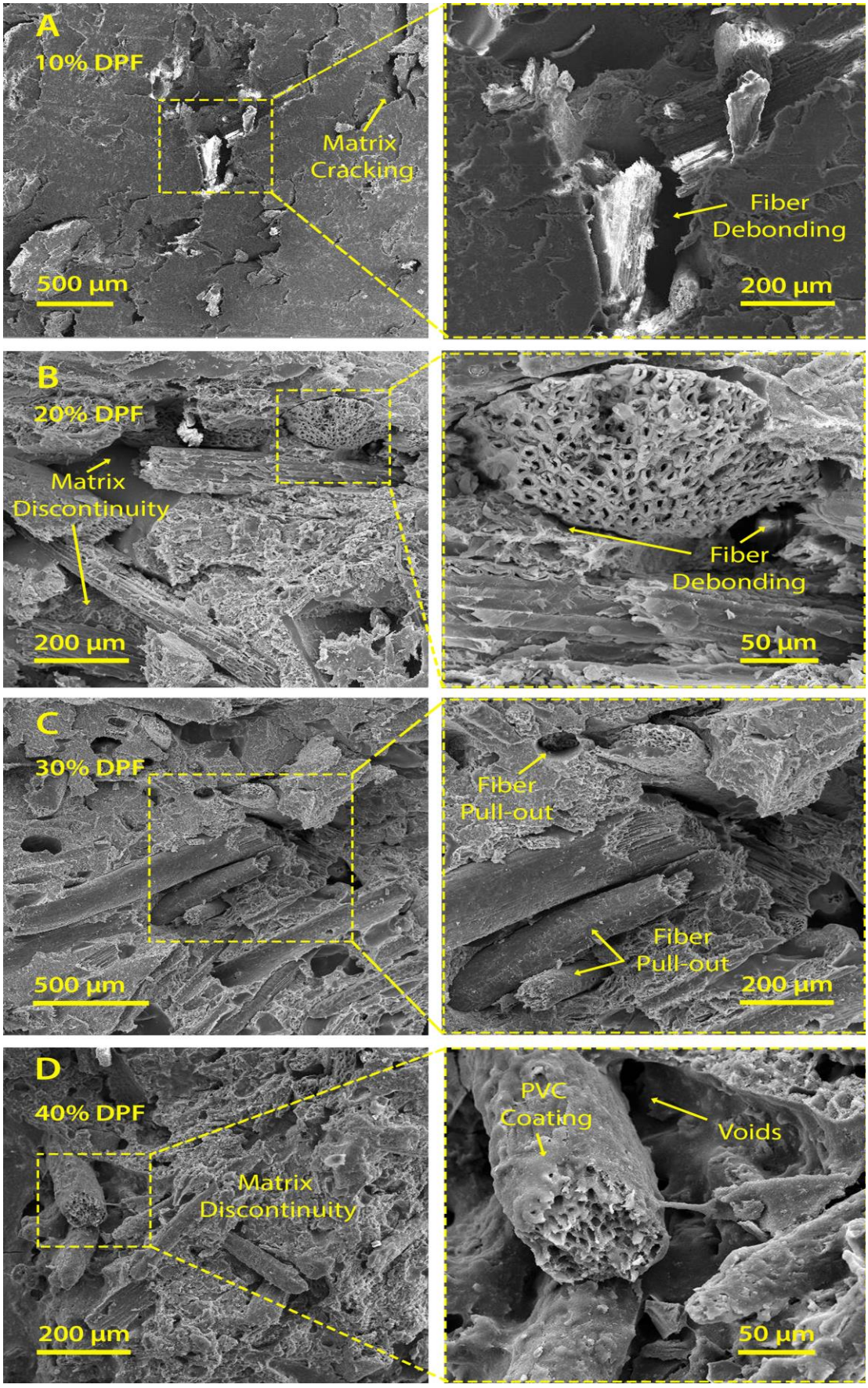

Figure 110 DPF/RPVC bio-composite with various DPF loading content

Figure 111shows the SEM microstructure of PLA bio-composite samples with varying DPF size and weight fractions. DPF is a plant fibre that has a hierarchical structure starting from the nano-cellulose crystals up to the technical fibre bundles shown in Figure 111B. The technical fibre is made up of bundle of elemental cellulose fibrils which are held together by lignin and hemicellulose. DPF fibrils are characterized by large lumens and small wall thickness creating a cellular structure within the bundle as shown in Figure 13c. The technical fibre has rough surface in the form of hexagonal scales as shown in Figure 13d. While there is poor compatibility between DPF functional groups and PLA, yet the loads can still be transferred from the PLA matrix to the fibre by the interlocking mechanism resulting from the rough fibre surface. The smaller the DPF sieve size the larger the surface area in contact with the PLA matrix, hence better load transfer efficiency and less fibre pull-out are observed. On the other hand, increasing the fibre weight fraction results in voids formation as shown in Figure 111C, due to the high melt viscosity of PLA and difficulty to completely wet the fibres. Under loading the fibre undergoes elastic deformation until debonding from the matrix due to the poor inter-facial strength as shown in Figure 111A, further loading results in propagation of the debonding front until the fibre is completely pulled out.

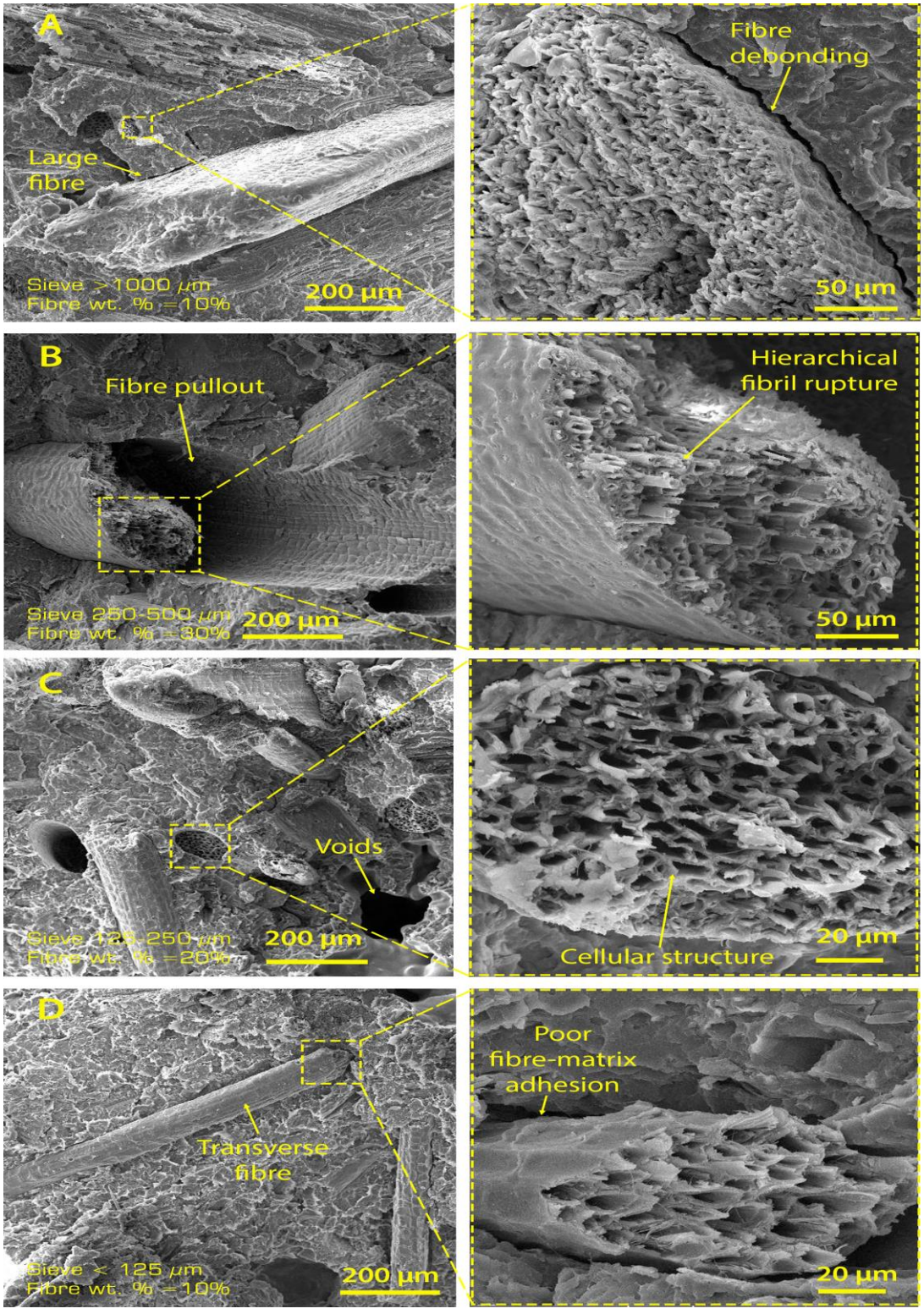

Figure 111 DPF/PLA bio-composite with various DPF loading content

The microstructure of thermoplastic composites, DPF/PLA, developed with ≥ 1,000 μm DPF size and varying weight fractions contents (10, 20, and 30) wt.% is shown in Figure 112. It was observed that samples reinforced with 40 wt.% DPF content went under complete disintegration where it was very difficult to conduct the microstructure analysis. The presence

of the voids within the microstructure of the composite was due to the weak interfacial bonding between the polymer matrix and the DPF which enhanced the biological attack leading to the degradation of DPF, thus disintegration of the matrix. As the size of the fibre increased the more voids was present which accelerated the biodegradation rate of the samples. It was noticed the fibre structure undergoes smudging. The fungal attack was randomly done where it was noticed that in Figure 112 (#C) the decay occurred longitudinally and split the DPF in the longitudinal direction, but in Figure 112 (#G) the decay occurred at the end or tip of the DPF.

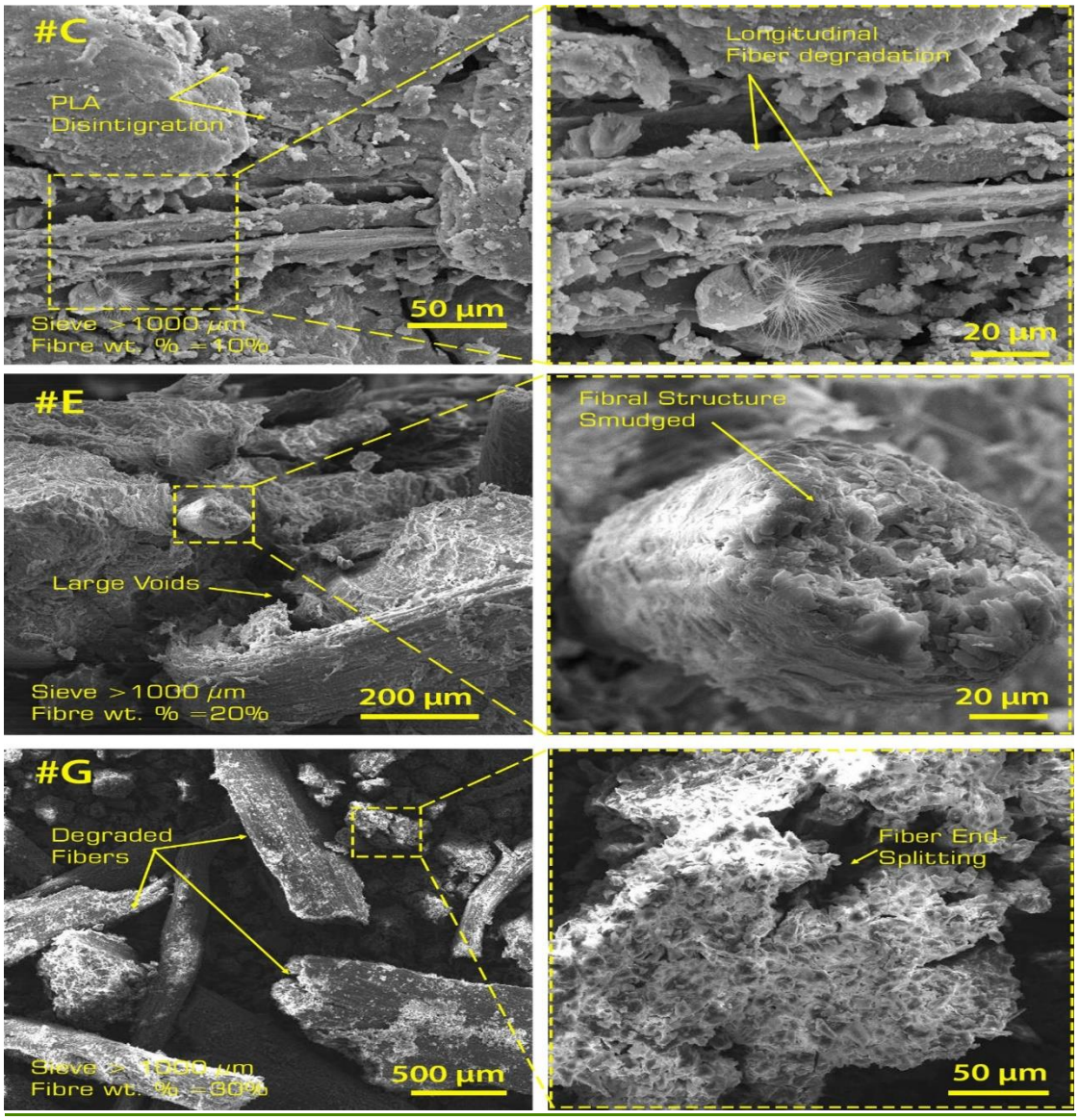

Figure 112 SEM of DPF/PLA for sieve size ≥1,000 µm with different DPF contents

5.4. Interim Summary

Sustainable composites of DPF reinforced RPVC and PLA were successfully developed using melt-mix blending and compression moulding processing technologies that could be

industrialised for various applications (i.e. construction and automotive industries). The sieve size analysis identified the particle distribution of DPF and showed the size range available in the grinded fibres. The bulk density varied in correspondence to each sieve size which was crucial in specifying the volume of DPF required as a reinforcement. Low density meant a high volume at a given loading content, leading to insufficient polymer matrix to form a perfectly blended composite.

The utilization of DPF affected the mechanical and physical properties of both DPF/RPVC and DPF/PLA composites negatively where various DPF sieve sizes had different effects and the loading content reduced the mechanical strength of the composite despite its fibre sieve size. As the DPF loading increased within the composite, 10 – 40 wt.%, the TS, WA and MC % increased due to their hydrophilic nature, which magnified poor matrix-fibre interaction, creating more voids within the composite. Moreover, the DPF geometry also had an influence on the physical properties of both DPF/PLA and DPF/RPVC composites. At DPF loading, 10 – 40 wt.%, TS, MC and WA increased having highest values of 1.57%, 1.63%, and 10.80% respectively. The tensile strength, flexural strength and impact strength of the DPF/RPVC composites decreased as the loading content of DPF increased. Unsieved DPF accounted to the highest flexural and impact strengths between the various DPF geometries. The tensile strength varied according to the DPF geometry size, where at low DPF loading, 10 – 20 wt.%, ≤125 µm had the best tensile strength and at high loading content, 30 – 40 wt.%, 250 – 500 µm had showed optimal tensile strength.

Furthermore, this study proposed a methodology which predicts the orientation of fibres in a thermoplastic matrix developed using compression moulding of DPF/PLA composite through numerical simulation and compared it to experimental results which is a prime interest of any research developing composites. Similarly, to injection moulded, orientation of fibres can be expected in the flow direction of the compression moulding for short natural fibres. Also, this result helps the researchers to choose the sample preparation method for short natural fibres based on their type of application, in larger extend, results can be applicable to all short fibres. Model 1 showed that numerical results were deviated from the experimental results due to DPF is not oriented in the direction of tensile force. Model 2 predicted that DPF contributed with only 20% of its modulus to the PLA/DPF composite and the fibre are aligned perpendicular to the direction of the tensile force. Model 3 showed the validation of numerical simulation with the experimental results and identified that DPF is oriented 0° to 45° in the direction of compression melt flow. Future work can be done for developing short DPF composite using injection moulding and duplicate this methodology of analysis to further identify the numerical correlation for fibre orientation in short fibre DPF composite.

Furthermore, the FEM simulation of Lab Scale compression moulding machines exhibits the probability of fibre orientation limits from 0° to 30° on the compression load direction. Based on FEM results, the theories for elastic modulus of short fibre reinforced composite materials for Lab Scale compression moulding process were developed using the calculation of force sustained by fibres crossing the scan line. The model exhibits similar trajectory with the experimental results with minor deviations due to the assumption of strong bond between the fibre and matrix. The mathematical model clearly explains the concept behind the elastic modulus of short fibre composite prepared using lab scale compression moulding. Fibres tends to align in the direction of the compression force, so Elastic modulus at compression direction is always higher than other direction of the testing samples. Predicted Elastic modulus of reinforced short fibre composite can be applicable to all short fibres whose length is equal or lesser than the thickness of the compression moulded samples and consider density of the fibre is lesser than the density of the matrix.

The evaluation of biodegradation of the composites developed is to benchmark it with WPC where its production face continuous harsh legislation and market limitations due to it biodegradability although great advances have been considered to enhance its mechanical and physical characteristics. The biodegradability, colour, and texture of thermoplastic composites reinforced with DPF are affected by fungal attack. The rate of biodegradation and disintegration depends on several environmental factors such as temperature, micro-organisms, radiation and moisture. Therefore, this study paves the way for introducing 100% biodegradable WPC composite or utilizing recycled thermoplastic to produce WPC using DPF as a reinforcement. In previous investigations done by the same authors the mechanical and physical strength of the developed composites DPF/PLA and DPF/RPVC achieved the standard requirements to be produced as WPC. For WPC indoor and outdoor applications, understanding the disposal and biodegradability resistance to microbial exposition is crucial. DPF/PLA showed more significant disintegration results when compared to DPF/RPVC composites. This is due to the biodegradable characteristics of PLA which is not applicable to RPVC. Results showed the higher content of DPF showed an increase in the weight loss of the samples exposed to fungal decay and disintegration. DPF/PLA composites did not demonstrate significant weight loss under fungal decay in 8 weeks where the composites with 40 wt.% DPF showed the highest WL% reaching 5.61% and 5.46% when exposed to Tyromyces palustris and Irpex lacteus respectively. On the other hand, the biodegradation had a higher impact on the disintegration of the composites developed where the biodegradation, weight loss, of PLA composites developed with 40 wt.% DPF showed 61.40%.

Chapter 6: Effect of Date Palm Fibre Reinforcement and its Processing Parameters on the Physical and Mechanical Properties of Polyester Composites

6.1. Abstract

An increase in demand for utilizing date palm tree (DPT) agricultural biomass waste, the most abundant NF in the MENA region, as a reinforcement for polymer matrix to develop sustainable composites. To develop and achieve DPF reinforced composite with ultimate properties and cost-effective, it is very important to understand the forming principles by studying the influence of the processing processes. Thus, this research investigates the effect of processing parameters, one of the factors that significantly influence the properties and characteristics of NF reinforced polymer composite. Processing time, temperature and pressure effect on the physical and mechanical properties of date palm fibre (DPF) reinforced unsaturated polyester resin (UPR) composite are evaluated. The composites are developed using hand-layup technique which is followed by compression moulding. Two different temperatures (90 and 110 ^{o}C), three different loading weight (10, 15, and 20 ton) are examined for three different durations, (3, 6, and 9 min). The influence on the mechanical properties is investigated by evaluating the impact strength, tensile strength and flexural strength. Meanwhile thickness swelling (TS) and water absorption (WA) characteristics are investigated to understand the dimensional behaviour of the developed composites. Composite microstructures are examined using optical microscopy to investigate the interfacial bonding between DPF and UPR matrix.

6.2. Processing of DPF/ UPR composite

The DPF and UPR resin were mixed using a hand lay-up technique at room temperature (23 ± 2) ^{o}C. Samples of constant DPF loading content of 30 wt.% and UPR of 70 wt.% was used. The samples were compression moulded into 300 mm (L) x 300 mm (W) x 4 mm (T) panels using an electrically heated hydraulic press. Compression procedure involved various heating temperature, time and pressure which are the investigated parameters in this research study. Three different temperatures (90 and 110 ^{o}C), subjected for three different weight loads (10 ton, 15 ton, 20 ton) for three time durations (3 min, 6 min, and 9 min). Subsequently, the samples are subjected to cooling under the load applied until the mould reached 35 ^{o}C. Afterwards, the compression molded composite was cut using a band saw machine SEALEY SM1304 to achieve 100 mm (L) x 10 mm (W) x 4 mm (T) samples for physical and mechanical properties tests.

6.3. Results and discussion

6.3.1. Effect of processing parameters on the physical properties

6.3.1.1 Thickness swelling of DPF composite

TS of the composites were examined for 24 hours to determine the effect of processing conditions on the dimensional stability of DPF composite. It is directly related to the density, presence of voids, and the interfacial bonding between the fibre and matrix [195]. The results revealed that all samples reached maximum TS after 24 hours and no further increase in thickness was recorded afterwards, presuming that the DPFs have reached maximum saturation and the voids within the composite may fully be filled with water. Figure 113 presents the percentage increase in TS with various processing parameters. UPR has the lowest TS, 0.69%, due to its hydrophobic characteristics. It has been observed that although pure UPR is hydrophobic, the TS mainly occurred due the water uptake that occurred by the composite due to some voids formed within the composite while processing.

DPF reinforced UPR composites showed an increase in TS when compared to pure UPR at all processing conditions which can be directly correlated to the hydrophilic nature of DPF where DPF will absorb water which may swell the fibre and push the polymer matrix to expand and generate internal stresses, which may result in delamination between DPF and UPR within the composite [196].

The increase in processing duration led to a decrease in TS for composites processed with the same temperature and pressure. T110:P10 composites showed the highest decrease in TS as the processing time increased where the TS decreased by 37.87% and 42.01% after 6 and 9 minutes when compared to its corresponding TS at 3 minutes respectively. T110:P15 and T110:P20 composites did not show significant decrease when the processing duration increased where the TS decreased by 5.34% and 9.92% for T110:P15 composites and 5.22% and 8.70% for T110:P20 after 6 and 9 minutes when compared to its corresponding TS at 3 minutes respectively. However, a noticeable result for samples processed at 90 ^{o}C, for 9 minutes under 15 tons, T90:P15, showed the highest TS and did not follow the trend mentioned where the TS decreased by 12.57% when the processing duration increased from 3 to 6 minutes and then significantly increased by 73.75% when the processing duration increased from 6 to 9 minutes.

The effect of processing temperature when considering that the processing duration and pressure are constant, comparing 90 and 110 ^{o}C, results showed that the higher processing temperature 110 ^{o}C developed composites with lower TS%. The effect of processing pressure when considering that the processing temperature and duration are constant, comparing

between 10, 15 and 20 ton of pressure applied while compression moulding, results showed that for 90 ^{o}C processed samples at 3 and 6 minutes the 15 tons composites showed the lowest TS%. Meanwhile, for 110 ^{o}C processed samples, 10 ton demonstrated lowest TS% when the processing duration was for 6 and 9 minutes and 20 tons at low processing duration, 3 minutes.

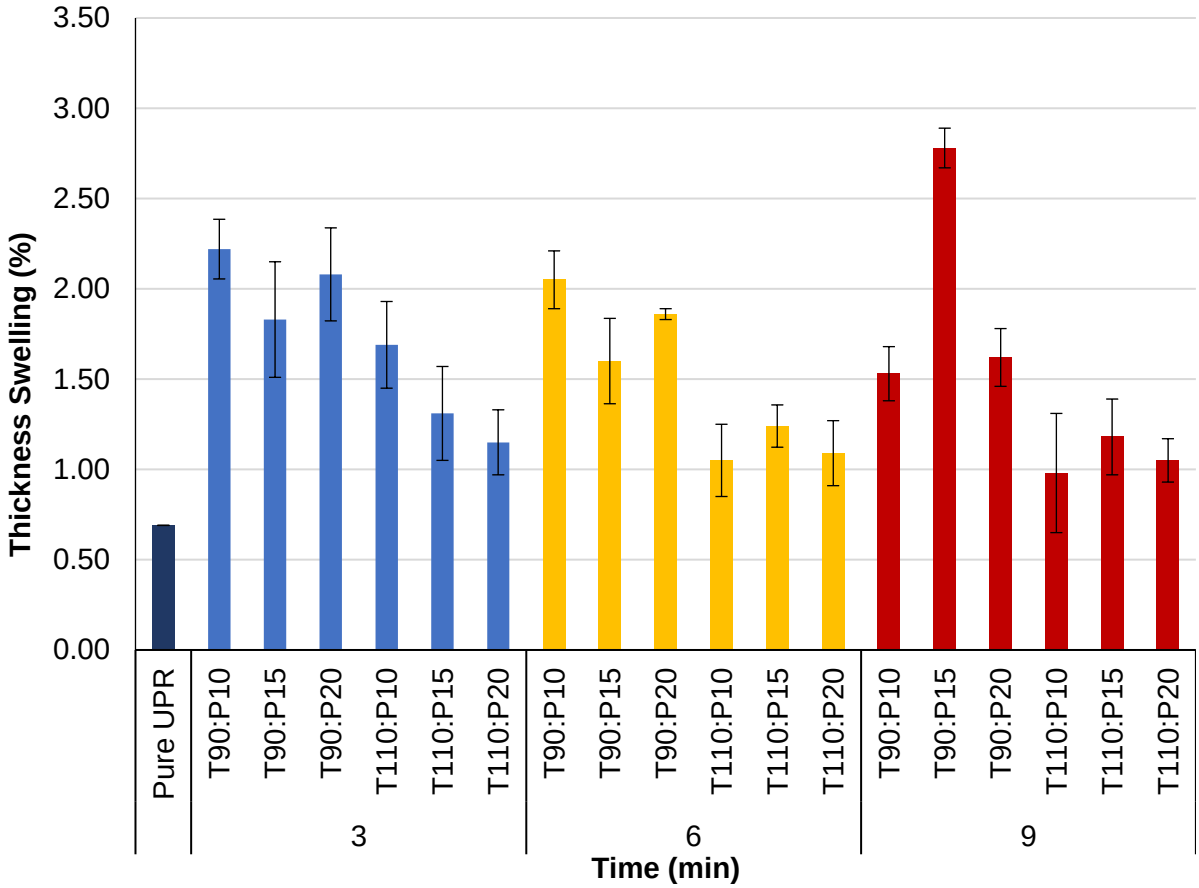

Figure 113 Effect of processing parameters on TS (%)

6.3.1.2 Water absorption of DPF composite

The water absorption (WA) of DPF reinforced UPR composites was conducted to determine the amount of water absorbed under specified conditions for 24 hours. The importance of understanding the WA of the composites developed is to determine their end uses. Figure 114 demonstrates the increase in WA for various processing parameters. Results demonstrated that the WA% of pure UPR composites was very low which reached 0.32% after 24 hours. It has been observed that although pure UPR is hydrophobic, the WA mainly occurred due to some voids formed within the composite while processing the composite. DPF reinforced UPR composites showed an increase in WA when compared to pure UPR at all processing conditions which can be directly correlated to the hydrophilic nature, free hydroxyl group, of

DPF which causes a water-DPF interaction responsible for the WA in the composites since UPR absorb very low amount of water.

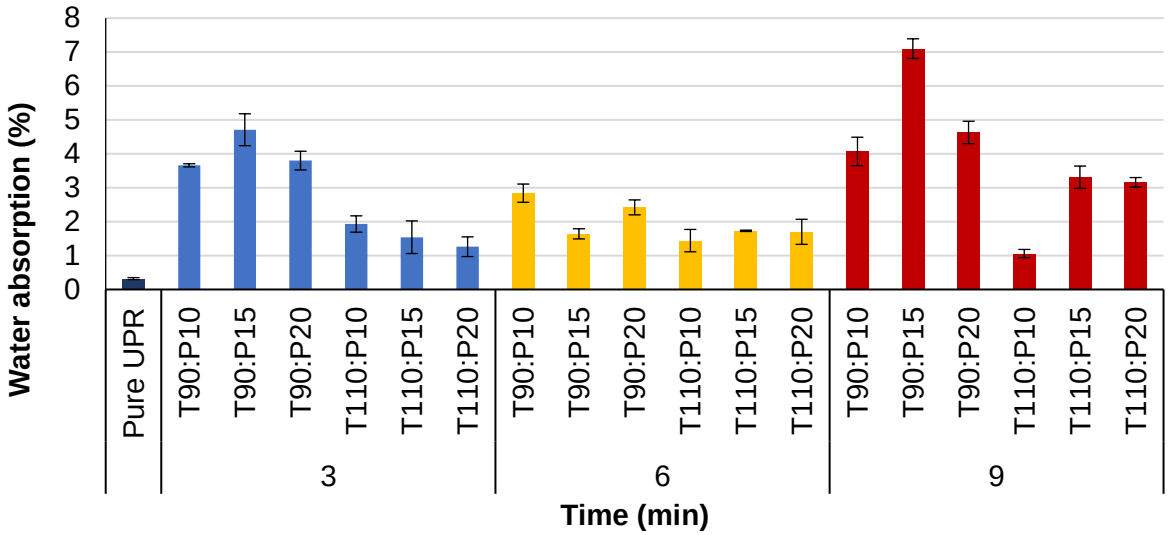

Figure 114 Effect of processing parameters on WA (%)

6.3.2. Effect of DPF processing parameters on the mechanical properties

When referring to the mechanical properties of the composites, it can be related to the fibre interfacial bonding with UPR which may affect the stress transfer of the load applied to the composite.

The hydrophilic nature or surface characteristic of DPF may be a key contributor, which is incompatible with hydrophobic polymer matrices, resulting in a weakened interface and hence the composite. DPF may also contain waxes and other non-cellulosic substances, such as hemi-cellulose, lignin and pectin, which may create poor adhesion between the UPR matrix and DPF. Therefore, to improve and develop DPF reinforced polymer composites with better mechanical properties, it is necessary to increase fibres hydrophobicity by introducing DPF to surface modification (surface treatment).

6.3.2.1 Flexural strength of DPF composite

The effect of processing parameters on the flexural strength of DPF reinforced UPR composite is presented in Figure 115. It is observed that the flexural strength of all DPF reinforced UPR composites developed decrease with various processing parameters. As mentioned, this may be directly related with the weak interfacial bonding between the DPF and UPR matrix due to the hydroxyl group present at the surface of DPF which will lead to a weak stress transfer interface for the load applied. Also, utilizing a high DPF loading content 30 wt.% may attribute

to an increase in agglomeration occurring in the composite insinuating poor fibre dispersion that inherent path for crack propagation to occur when load is applied. This failure mechanism can be referred to as fibre breakage and interfacial debonding, a particular type of failure that encompasses the debonding occurred between the matrix and fibre [201]. This is especially seen in the fibre followed by cracks in the matrix due to increased stress concentrations at the location containing the weakest matrix-fibre bonding.

However, each processing parameters have a different influence on the flexural strength of the composite (Figure 115).

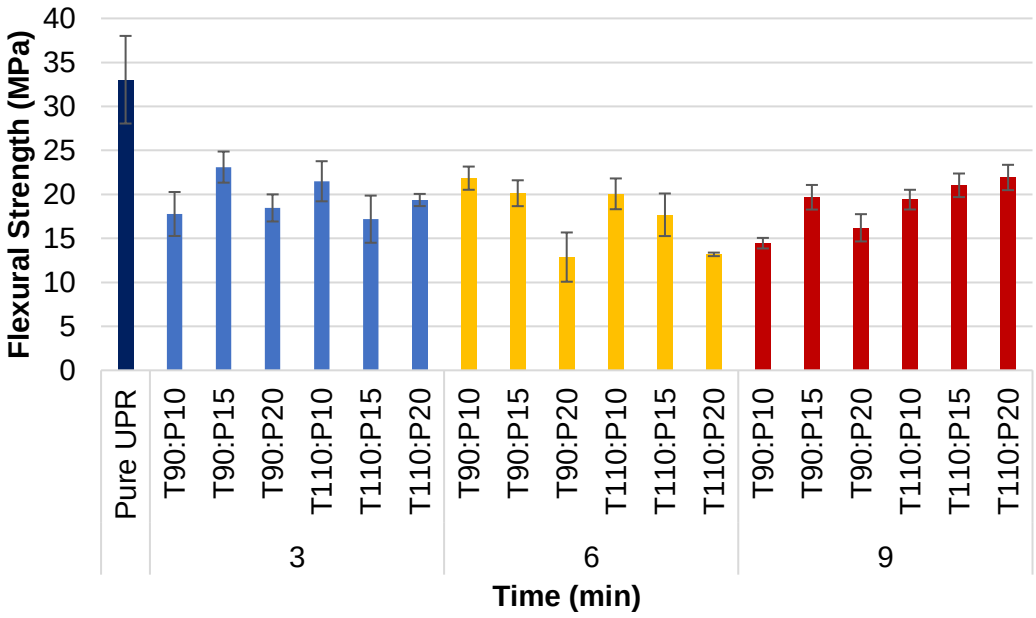

Figure 115 Effect of processing parameters on flexural strength

It is most interesting that the flexural modulus of T110:P10 composites increased by 25.47% at 3 min which was also witnessed for T110:P15 and T110:P20 composites where the flexural modulus increased by 7.52% and 13.35% at 9 minutes of processing duration compared to UPR. The rest of the composites developed showed a significant decrease in flexural modulus where the highest decrease was shown by T110:P20 composites at 6 minutes.

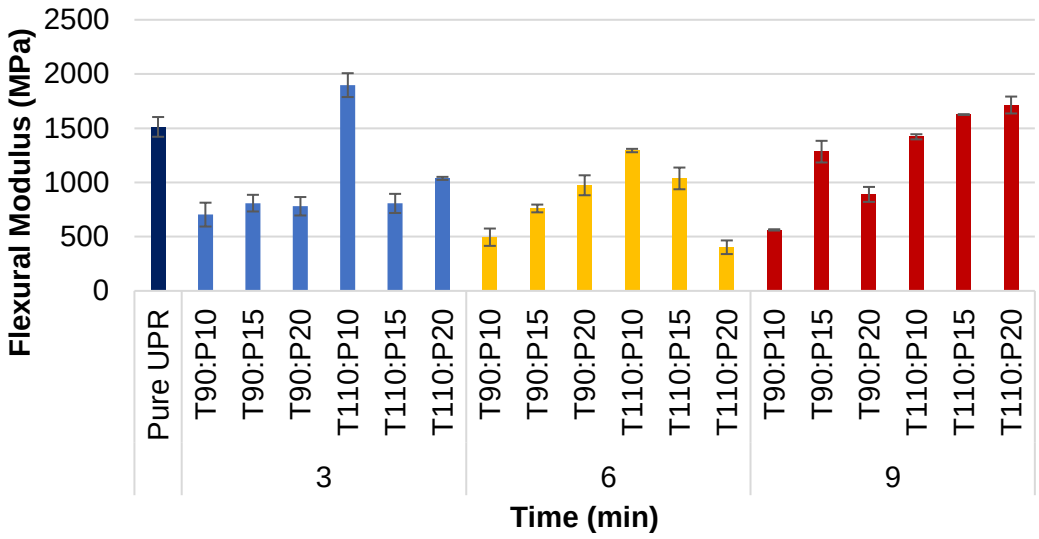

Figure 116 Effect of processing parameters on flexural modulus

6.3.2.2 Tensile strength of DPF composite

The effect of processing parameters (temperature, time and pressure) on the tensile properties, tensile strength and Young's modulus of DPF reinforced UPR composite is shown in Figure 117 and Figure 118 respectively. The tensile strength increases when the processing pressure is low, 10 ton, for all composites processed at 110 ^{o}C at various processing durations. Composites processed at 90 ^{o}C showed an increase in strength at 3 min and 6 min and then showed a decrease when the processing duration reached 9 min. Composites processed at 15 and 20 tons showed a decrease in tensile strength. Composites processed at higher temperature, consider the processing pressure and duration are constant, demonstrated better results. This phenomenon may be an attribute of the better viscosity of matrix at higher temperatures which will aid in matrix impregnation into DPF, thus enhanced contact surface area between the matrix and the fibre which improves tensile strength.

Composites processed at 110 ^{o}C with processing pressure of 10 tons for 9 minutes showed the optimal tensile strength with an enhancement of 25.59%. On the other hand, composites processed at 90 ^{o}C subjected to 15 tons for 9 minutes demonstrated 54.13% reduction in tensile strength.

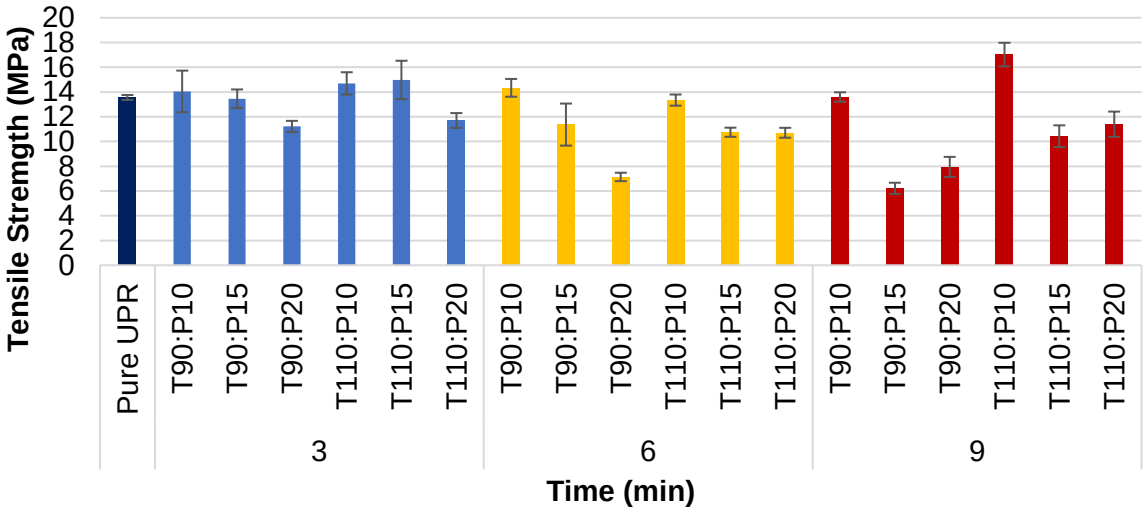

Figure 117 Effect of processing parameters on tensile strength

The effect of processing conditions on the stiffness of the composites developed, which are characterized by the Young's modulus, is demonstrated in Figure 118. Comparing the effect of various processing parameters on the Young's modulus, composites processed at higher temperatures showed enhanced modulus. This phenomenon may be an attribute of the better viscosity of matrix at higher temperatures which will aid in matrix impregnation into DPF, thus enhanced contact surface area between the matrix and the fibre which improves modulus. Comparing the same temperature and pressure processed composites, Young's modulus decreased as the processing duration increased when the composites where subjected to 90 ^{o}C. Composites processed at 110 ^{o}C with processing weight of 10 tons for 9 minutes showed the optimal Young's modulus with an enhancement of 16.87%.

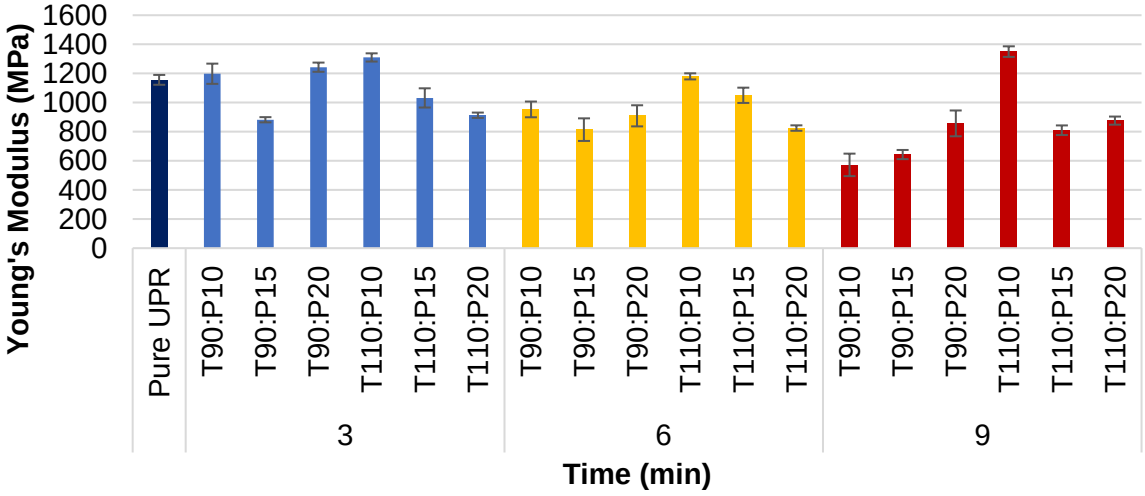

Figure 118 Effect of processing parameters on Young's modulus

6.3.2.3 Impact strength of DPF composite

The effect of processing conditions on the toughness of DPF reinforced UPR composite is presented in Figure 119. Overall, the impact strength of the composites developed increased at different processing parameters investigated demonstrating an enhanced energy absorbing capability. The main reason is that DPF provides stiffness to UPR, thus increasing the overall impact strength of the composite. The increase in temperature demonstrated composites with better impact strength which may be resulting from better enhancement of wetting between DPF and UPR. Composites processed at 110 ^{o}C with processing pressure of 10 tons for 9 minutes showed the optimal tensile strength with an enhancement of 113.90%. When composites were processed at 90 ^{o}C, 15 tons of processing pressure was considered the optimal at various processing durations. However, composites processed at 110 ^{o}C, 10 tons of processing pressure was considered the optimal at various processing durations. Evaluating the effect of processing time on the impact strength of the composites developed, it can be observed that impact strength increased as the processing time increased when comparing composites processed at the same temperature and pressure. Thus, correlating the processing parameters together, it can be deduced that at high temperature, 110 ^{o}C, the increase in pressure allowed more matrix to overflow from the mould which increased the fibre pull-out between the matrix and the DPF which decreased its toughness.

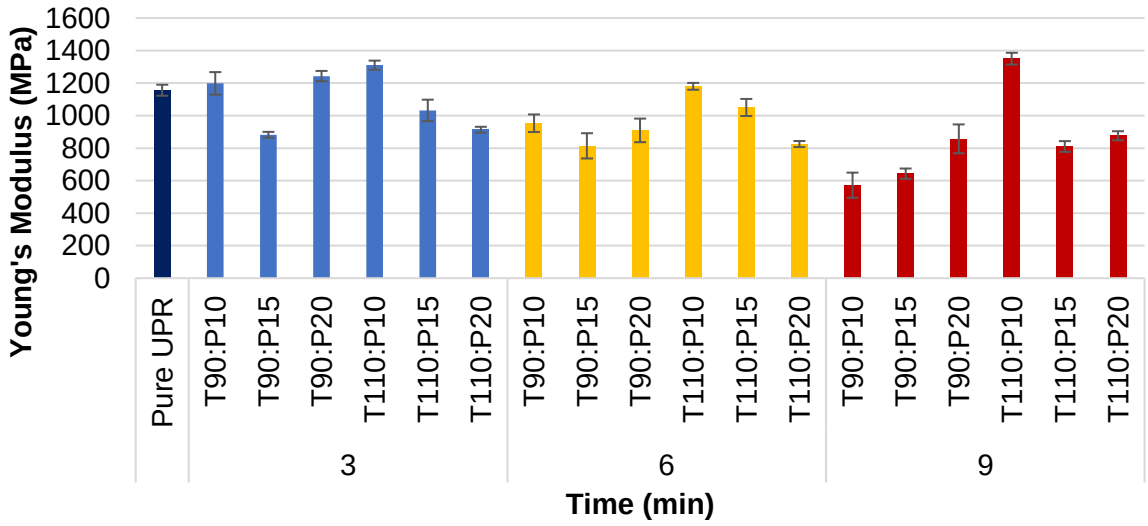

Figure 119 Effect of processing parameters on impact strength

6.3.3. Effect of DPF on the microstructure of the composite

Figure 120 demonstrates the interfacial bonding between DPF and PET matrix. According to the SEM images, large voids are located between the DPF fibres and the UPR matrix due to the low fibre-matrix adhesion which led to fibre pull-out which affected the mechanical and

physical properties negatively. It can be observed that DPF debonding resulted in more voids occurring between the DPF and the UPR matrix which leads to an increase in porosity of the composite that affected the mechanical properties negatively and increases high water absorption of the composite increasing its thickness swelling.

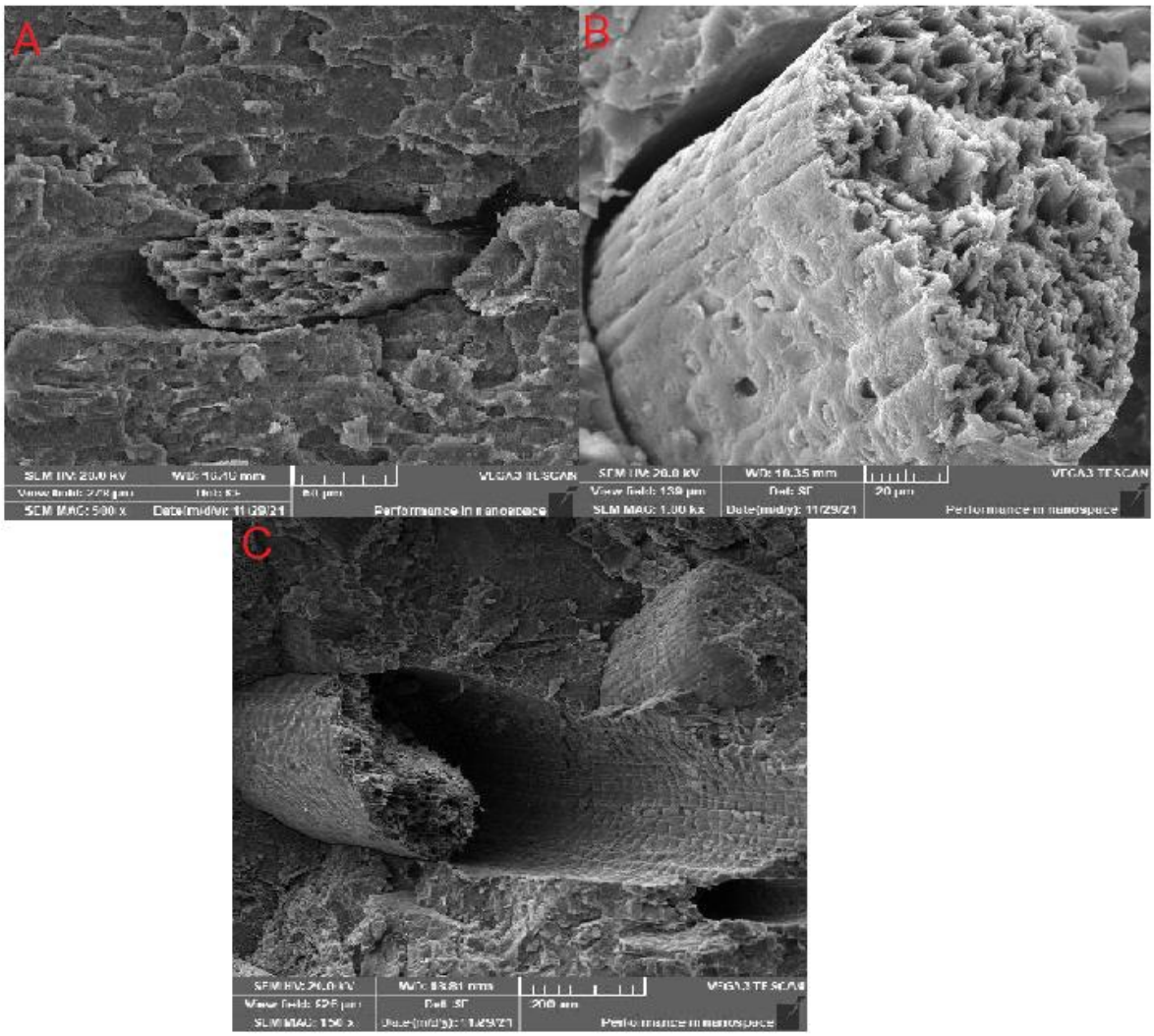

Figure 120 Microstructure of polyester reinforced DPF

6.4. Interim summary

The performance of DPF reinforced polymer composites is influenced by the composite manufacturing process. In the compression moulding process for the fabrication of short natural fibre composites, the preparation before compression moulding and parameters involved during the process collectively have a significant effect on the mechanical properties of the composites. However, since the mixture was initially mixed using a hand lay-up methodology this factor will be neglected. The pressure, temperature and holding duration of the compression moulding are the vital parameters which showed different effects on the mechanical and physical properties of the developed composites. The moulding temperature is not in the range that the DPF degrades however its effect on the polymer matrix should be evaluated and investigated. For the compressive pressure, a good choice of compression pressure ensures an enhanced interfacial bonding between the DPF and polymer matrix and avoids any damaged fibre structure, which will affect the performance of bio-composites. Also, excessive pressure will lead to the flow of the polymer matrix outside the mould providing a smaller amount of matrix available for bonding with DPF. The last important consideration is the press duration, which is associated with adequate temperature and pressure in developing the composite. Composites developed with higher processing temperature showed better physical properties, a decrease in water absorption and thickness swelling. Sample T110:P10 showed a significant enhancement on both tensile strength and impact strength with values of 25.59% and 113.9% respectively. Thus, to understand the processing parameters principle in processing composite huge amount of data should be collected through experimental investigation where statistical approaches can be adapted for optimization.

Chapter 7: Effect of Date Palm Fibre Characteristics on the Mechanical and Physical Properties of Cementitious Reinforced Composites

7.1. Abstract

This chapter discusses the evaluation and the performance of different cementitious binders reinforced with varying percentages and length of untreated and alkali treated DPF to develop low-cost NF reinforced mortars for construction applications. The research first involved the evaluation the ideal water to cement ratio required for the experimental work. Afterwards, the investigation of the effect of length of DPF (10 mm, 20 mm, 30 mm 40 mm) at varying DPF loading content (1, 2, 3 wt.%). Subsequently, the effect of alkaline treatment was applied to enhance the interfacial bonding between the DPF and the binder. The mechanical properties involved testing the flexural and compressive strength of the mortars at 7 and 28 days after subjecting the sample to two different curing conditions, water bath and ambient room temperature conditions, investigating the effect of curing conditions on the sample's characteristics. Also, the physical property of the samples, water absorption, is evaluated to evaluate the relationship with the investigated parameters. The same experimental work was implemented on 100% OPC bind and replacing 50 wt.% of OPC with a waste material, GGBS, to decrease the negative environmental impact of utilizing OPC and reduce the amounts of GGBS deposited into landfills and to investigate the effect of binder on the characteristics of the composite developed. Results showed a great approach in developing DPF reinforced cementitious composite with enhanced strength for non-structural applications. The inclusion of 20 mm treated DPF at a loading content of 1 wt.% showed an enhancement in strength by 37.49% and 19.36% of flexural and compressive strength respectively at 28 days of ageing in a water bath when the binder was 100% OPC. Consequently, with 50% OPC substitution with GGBS, the inclusion of 20 mm treated DPF at a loading content of 1 wt.% showed an enhancement in strength by 57.13% and 30.97% of flexural and compressive strength respectively at 28 days of ageing in a water bath. Curing conditions highlighted the importance of water to enhance the hydration of OPC and OPC/GGBS, which is responsible on the strength enhancement which directly affects the mechanical properties of the composite. Alkali treatment of DPF demonstrated higher mechanical properties enhancing the optimal mix designs' flexural strength and compressive strength by 20.42% and 24.90% respectively at 28 days of water curing when compared to the untreated optimal mix in respective to GGBS/OPC mortars.

7.2. Experimental procedures

The mix proportion ratio used for the cementitious mortars was Binder: Sand = 1:1.5 by weight with water-to-binder ratio equal to 0.45 based on several optimisation cycles of mix workability. The binders used for making the mortars consisted of 100% OPC, and OPC and GGBS which were mixed at 50%:50% based by weight. The DPF reinforced cementitious mortars had varying loading content and length of DPF. DPF was added by 1, 2, and 3 (wt.%) of binder. The length varied from 10 mm, 20 mm, 30 mm, and 40 mm for each varying DPF loading content as shown in Table 58 and Table 59.

Table 58 Experimental design for DPF reinforced OPC composites

DPF (Wt.%)	DPF Length (mm)	DPF (g)	Sand (g)	OPC (g)	Water (g)
0	0	0	1,050	700	315
1	10	7	1,050	700	315
1	20	14	1,050	700	315
1	30	21	1,050	700	315
1	40	7	1,050	700	315
2	10	14	1,050	700	315
2	20	21	1,050	700	315
2	30	7	1,050	700	315
2	40	14	1,050	700	315
3	10	21	1,050	700	315
3	20	7	1,050	700	315
3	30	14	1,050	700	315
3	40	21	1,050	700	315

Table 59 Experimental design for DPF reinforced OPC/GGBS composite

DPF (Wt.%)	DPF Length (mm)	DPF (g)	Sand (g)	OPC (g)	GGBS (g)	Water (g)
0	0	0	1,050	350	350	315
1	10	7	1,050	350	350	315

DPF (Wt.%)	DPF Length (mm)	DPF (g)	Sand (g)	OPC (g)	GGBS (g)	Water (g)
1	20	14	1,050	350	350	315
1	30	21	1,050	350	350	315
1	40	7	1,050	350	350	315
2	10	14	1,050	350	350	315
2	20	21	1,050	350	350	315
2	30	7	1,050	350	350	315
2	40	14	1,050	350	350	315
3	10	21	1,050	350	350	315
3	20	7	1,050	350	350	315
3	30	14	1,050	350	350	315
3	40	21	1,050	350	350	315

DPF were treated chemically by immersing the fibres in 6% of aqueous NaOH solution for 3 hours then immersed for 5 min in a solution of aqueous acetic acid to neutralize, based on recommendations from the study done by (Chapter 4). Afterwards, DPF are washed with water and placed in an oven at 60 ^{o}C for 24 hours to ensure no moisture is left in the fibres.

Binder, sand, water and DPF were mixed to prepare the fresh mortar using Kenwood mixer (KVL8300S). Initially, the binder, sand, and DPF were dry mixed for two minutes then water was added and mixed for another two and half minutes ensuring that the mix is homogenously mixed. Afterwards, the fresh mortar is casted into prismatic, 40 x 40 x 160 mm^3, polystyrene moulds and left to cure at room temperature. After 24 hours, the samples were demoulded, labelled and either immersed in a water bath with water temperature 19 ± 1 ^{o}C or left in a controlled humidity and temperature room for curing.

7.3. Results and discussion

7.3.1. Effect of DPF length and loading content on the flexural strength

The utilization of DPF with various length and loading content had various effect on the flexural strength of the composites developed as shown in Figure 121 and Figure 122. This section will not take into consideration composites developed using treated DPF and cured under air curing conditions as they will be discussed later in Section 7.3.3 and 7.3.4 respectively which

discusses the effect of DPF treatment and curing conditions on the mechanical properties of the developed composite. The results showed that OPC composites developed with untreated DPF with 20 mm length at a loading content of 1%, cured in a water bath showed an enhancement in the flexural strength with optimal results of an increase in 59.95% and 27.22% at 7 and 28 days of curing respectively as shown in Figure 121. This was also observed for OPC/GGBS composites cured in water bath where the optimal mix design, B2, showed an enhancement in the flexural strength with optimal results of an increase in 55.61% and 30.47% at 7 and 28 days of curing respectively as shown in Figure 122.

A scrutiny of the results shows that the composites with 1 wt.% DPF loading content with various lengths exhibit the highest flexural strength after 7 and 28 days compared to those loaded with 2 and 3 wt.% DPFs. Although after 28 days, DPFs reinforced mortars exhibit almost the same flexural strength at 2 wt.% DPF loading. It can be stated that the effect of DPFs length is neglected for DPFs loading 2 wt.%. An increase in the fibre length, beyond 20 mm, and increase in loading content, more than 2 wt.%, had corresponding reductions in the flexural strength at 7 days of curing, suggesting that the prevalence of fibre agglomeration is effective on mechanical properties after this loading content. DPF have an inherent tendency to agglomerate within the cementitious matrix courtesy of the formation of hydrogen bonding of hydroxyl groups [20,21]. These hydrogen bonds consequently lead to a reduction in the dispersion of the fibres within the matrix and hence, magnifies poor matrix - fibre interaction [22–24]. The fibre agglomeration is also detrimental as it restricts matrix impregnation and thus, results in more porosity which is negatively proportional to mechanical properties, thus lower flexural strength is displayed by the longer fibres [25].

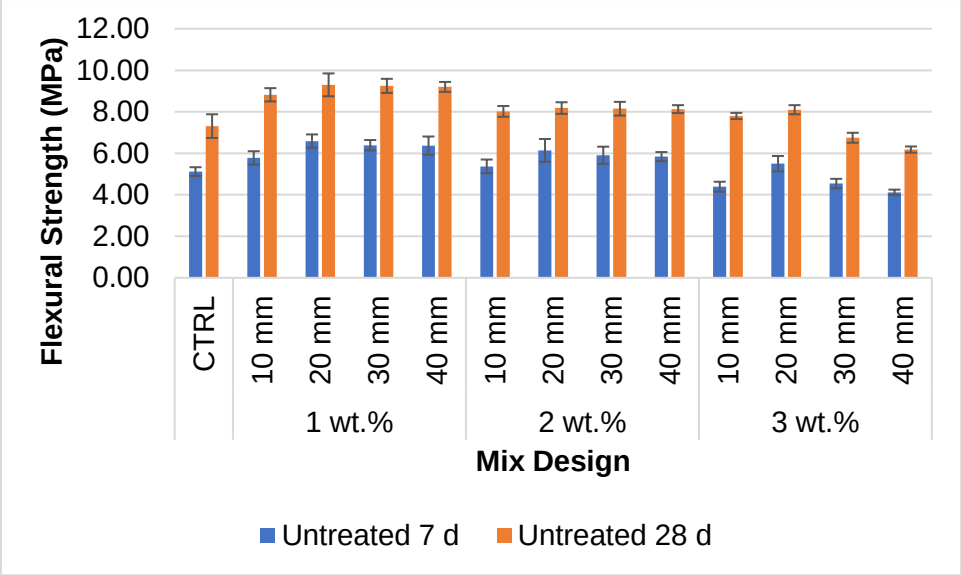

Figure 121 Flexural strength of water cured OPC reinforced with untreated DPF mortars at 7 and 28 days

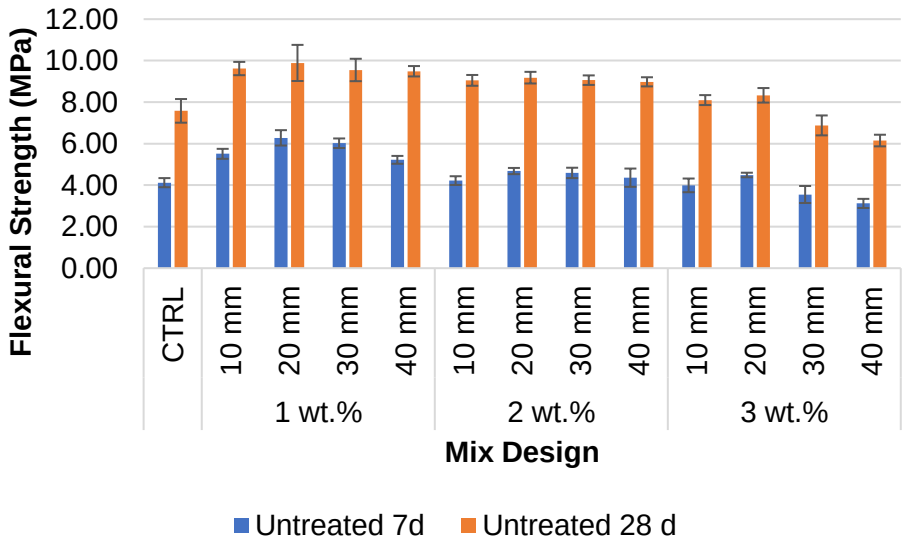

Figure 122 Flexural strength of water cured of OPC/GGBS reinforced with untreated DPF mortars at 7 and 28 days

Short DPF, 10 mm, might not provide enough length for optimal stress transfer within the matrix system. Having discussed the apparent justification to state that 20 mm DPF reinforced samples performed better than their counterpart, it is important to highlight that the optimum results can only be witnessed at the fibre's critical length. If the fibre's length falls on the shorter side of the spectrum, 10 mm, the fibres will be unable to carry significant load and will experience failure prior to the fibre fracture load. However, the difference is not significant when compared to 20 mm DPF which may be an attribute that shorter fibre has better

dispersion within the matrix and produced better interfacial bonding and less voids when compared to longer fibre, 30 and 40 mm but also did not meet the critical length to provide the optimum stress transfer phenomena. Furthermore, if the fibre is of enough length and not too short, the tensile stress is zero at the fibre ends and a maximum tensile stress value can be observed at the midpoint of the fibre upon the application of load [26]. This sufficient length is the critical length and due to the zero-shear stress at the midpoint, there is an apparent variation in shear stresses when comparing the midpoint and the fibre end. This results in a 'shear effect' causing a build-up of tensile stress in the fibre allowing it to confidently tolerate the tensile load that is transferred from the matrix to the fibre through the fibre/matrix interface [27]. Consequently, as the aspect ratio decreases below the critical ratio, assuming a constant diameter of DPF with decreasing lengths, the end effects mentioned above become more significant and hence reduce the stiffness and efficiency of the fibres in reinforcing the composite [28]. Alternatively, fibres that fall on the longer side of the spectrum, 30 mm and 40 mm, can also be deemed to be unsatisfactory in terms of producing enhanced mechanical properties due to the agglomeration of the fibres mentioned previously combined with other occurrences, such as fibre curling and fibre bending leading to inefficient and ineffective stress transfer [29,30]. Furthermore, another crucial influential factor to the flexural strength of the developed composites is that of the extent of DPF loading content, DPF volume fraction, within the mortar samples. The critical fibre loading content that provided the best results was accounted to 1% DPF loading when reinforced with both matrix types, OPC and OPC/GGBS, depicting flexural values with improvements as high as 27.22% and 30.47% in comparison to the unreinforced control samples, CTRL, at 28 days for OPC and OPC/GGBS reinforced composites respectively. The remaining two DPF loading content, i.e., 2% and 3%, for the same fibre length (20 mm), demonstrated best corresponding flexural strengths having 9.10% and 9.06% enhancements respectively at 28 days of curing for OPC reinforced mortars. Also, OPC/GGBS mortars comparing the same fibre length (20 mmm) for 2 and 3 wt.% loading showed flexural strength enhancement of 20.51% and 19.39% respectively at 28 days of curing. The results are found to be in agreement with several researchers who investigated mechanical properties of cementitious matrices based on the fibre content [11,20,22,167,211]. This phenomenon can better be understood by initially considering the effect that the fibre content has on the workability of the mortar mixture. The workability is affected negatively when the loading of the DPF into the mortar mixture increases. The addition of DPF interrupts the mineral skeleton of the cementitious matrix, hence, generating voids within the matrix leading to an increase in the porosity. Thus, porosity and strength have an indirect proportional relationship, a higher level of porosity has lower corresponding strengths; as was experienced also by Alatshan and his colleagues [212]. Additionally, another vital factor is the agglomeration of fibres within the matrix. Its common occurrence with longer fibres is also

reflected to mortars with larger concentration of fibres, if not on a larger scale, i.e. higher fibre contents are more susceptible to agglomeration than longer lengths. Hence, a combination of the two would hypothetically provide a sample with very weak results, a hypothesis which was solidified in this experiment as the samples that were characterised by the longer length in the largest tested concentration, composites reinforced with DPF 3 wt.% and 40 mm length displayed the lowest flexural strength, a decrease of 18.10% and 35.51%, when compared to the optimal mix, for OPC and OPC/GGBS composites reinforced with DPF 2 wt.% and 10 mm length respectively at 28 days of curing.

Therefore, this is undoubtedly detrimental for the mortars due to several reasons that are discussed by interpreting the gel bonds, wall effect, inter-facial transition zone (ITZ), and internal bleeding. Gel Bonds can be described when fibres are inputted into the matrix in large dosages, there is a larger tendency for the fibres to agglomerate into 'fibre clusters' or 'fibre balls' [213]. This consequently means that there are a lesser number of fibre end points that are in contact with the cement, hence reducing the facilitation for fibre – matrix bonding leading to lower strengths overall. This generation of clumped fibre regions within the matrix insinuates a lower surface area that is in contact with the cement paste. This is unideal as it means a lower potential area for the developments of cement gel bonds in the fibre – cement paste interface zone. A reduced rate of cement gel bond development consequently leads to a decrease in the composite strength. Furthermore, the wall effect can be described when the fibres agglomerate, they form a clump which indicates an increase in the surface area. If the maximum particle size is considered to be large in proportion to the mould size, the packing and compaction of the mixture along with the uniformity of distribution of the large particles are affected [214]. This occurrence can be referred to as the wall effect and is experienced when the smaller aggregates and the cement particles experience an inability to be packed closely to the larger particles which in turn shows a lower packing of the mortar. As a result, there is now a greater requirement to fill the voids created by the low packing. This is more significant in the area closer to the walls of the mould and hence the amount of cement paste required to take up the space between the larger particles and the wall of the mould is greater than the actual amount of cement paste that is available in the mixture. Consequently, due to an inadequacy of cement paste, there will be an increased rate of porosity indicating lower strengths in the mortar samples. Moreover, DPFCC composites can be recognized chemically as two phased materials comprising of the DPF phase and the cementitious matrix phase. The transitionary area in between the phases can be referred to as the inter facial transition zone (ITZ). This zone can be considered as a weak area in the DPFCC as it is a plane where there is an abundance of stress concentrations courtesy of the differences in the E value of the two materials: fibre and the cement paste. Therefore, it is important to keep the ITZ as thin

as possible to ascertain higher compressive and flexural strengths. Furthermore, more reasons as to why the ITZ is a zone of weakness are discussed as follows. Firstly, it can be assumed that the weakness is due to the wall effect discussed above but on a more minute scale. The microstructure of the cement paste in the ITZ is different to that of the remainder of the cement paste because during the mixing stage, cement particles experience the inability to be packed close to the larger agglomerated 'fibre clusters/balls.' This means that the amount of cement present for the purposes of filling the voids is lower. Consequently, this leads to a larger porosity in the cement paste in the ITZ as opposed to the cement paste that exists further away from the ITZ. As a higher rate of porosity dictates lower strengths, the ITZ is a zone of weakness which is underscored by the size of the 'fibre balls', i.e. the wall effect is more pronounced the larger the particle size. Secondly, the hydration of the cement in the ITZ is also crucial behind the weakness of it. The ITZ is a thin zone which is approximately 50 µm wide and only contains completely hydrated cement which consequently means larger $Ca(OH)_2$ crystals. The completely hydrated cement suggests that the w/c ratio is of higher magnitude within the ITZ as opposed to other areas and hence implies reduced strengths. Moreover, the large $Ca(OH)_2$ crystals insinuate a higher degree of porosity which again highlights a reduction in strength. As a result, it can be conclusively said that the ITZ is a zone of weakness and its area needs to be minimized to achieve higher compressive strengths in the mortar. To summarise, a larger singular fibre clump due to higher fibre concentrations means more porosity due to wall effect but also means a corresponding larger ITZ which results in lower mechanical strengths [215]. Additionally, the internal bleeding phenomena can be described as follows; the larger particle formed due to agglomeration can lead to a higher propensity for internal bleeding to take place. The reason behind this is that the larger the fibre cluster, the higher the chance for water accumulating underneath the large particle. Furthermore, a higher water presence leads to the existence of weak bonds because once evaporation of the water takes place, there is a resultant void formation in the area where there was water originally. The negative effect of this is augmented because all the voids which are formed through this approach have an orientation in an identical direction. This consequently means an easier path for crack propagation and hence reduced strengths in the mortar [99].

7.3.2. Effect of DPF length and loading content on the compressive strength of DPFCC

As aforementioned, the utilization of the critical fibre length and loading content is crucial in ensuring that the produced composites are of desirable qualities. The execution of this experiment resulted in results that greatly solidify the usage of DPF within cementitious mixtures. As can be observed from Figure 123 and Figure 124, the utilisation of 20 mm DPF

yielded the most optimal results, with compressive strengths depicting as much as 3.53% and 4.90% enhancements when comparing to the unreinforced control samples, CTRL OPC and CTRL OPC/GGBS composites, after 28 days of curing. This is in opposition to the rest of the resulted obtained on the compressive strength of DPF composites investigated by other researchers.

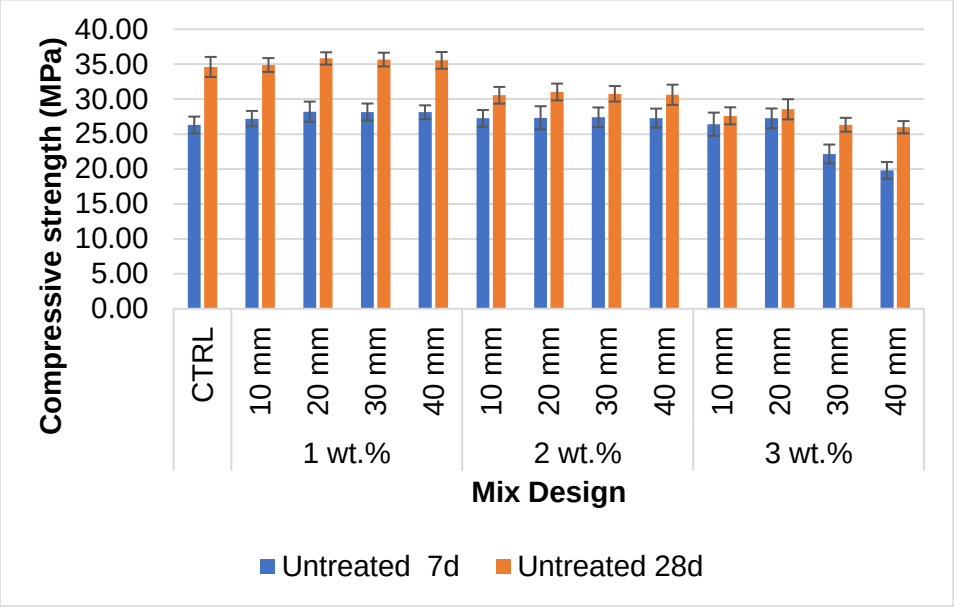

Figure 123 Compressive strength of water cured OPC reinforced with untreated DPF mortars at 7 and 28 days

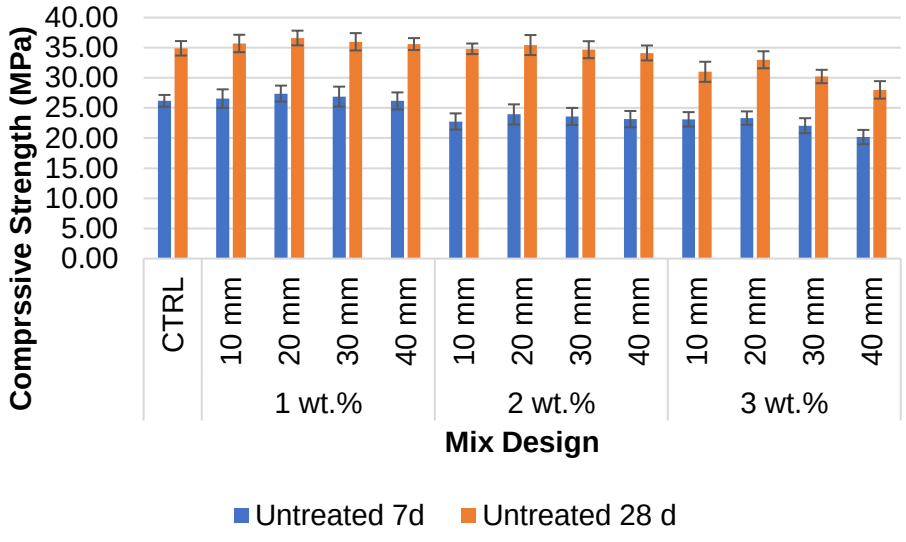

Figure 124 Compressive strength of water cured untreated DPF reinforced OPC/GGBS mortars at 7 and 28 days

Appertaining to the results demonstrated in Figure 123 and Figure 124, out of the samples that possess better compressive strength than the control samples for the 7d and 28d

compressive tests respectively, the 20 mm DPF reinforced samples appear for most of them as opposed to the 10 mm, 20mm, and 40 mm DPF samples. This reinforces a commonly recurring theme in literature which insinuates that a shorter fibre usage has better composite strength implications which is fundamentally due to a reduction in fibre entanglements which would have otherwise occurred with longer fibres. The entanglements would result in decreased fibre – matrix bonding resulting in a reduction in the interfacial bond strength within the overall composite [22,167,216–218]. Furthermore, it can be stated that the optimum granular composition was superior for the 20 mm fibres as opposed to the various other length as the 20 mm can better enclose larger granulates leading to reduced porosities and hence higher compressive values [165].

Another vital characteristic of the cementitious samples that significantly impacts the mechanical properties is the fibre content where the results are found to be in agreement with several researchers who investigated mechanical properties of cementitious matrices based on the fibre content [11,20,22,167,211]. It can be observed that establishing a negative correlation between the fibre content and compressive strength is deemed sensible. This is justified by the fact that the optimum result, OPC and OPC/GGBS composites reinforced with DPF 2 wt.% and 10 mm length, obtained courtesy of this experimental study was characterised by a 1% fibre concentration, depicting a maximum value of 3.53% and 4.90% enhancements in the compressive strength of the mortars when comparing against the unreinforced control samples, CTRL OPC and CTRL OPC/GGBS composites respectively. However, greater than 1% DPF loading exhibited negative impact in the compressive strength of the sample. This can be due to several factors, starting with that there might be preliminary cracks in the sample tested as it’s a residual sample from the flexural tested sample. Also, due to the hydrophilic nature of the DPF, a weak interfacial bonding might have occurred with the cementitious thus reducing the overall strength of the sample.

Moreover, another aspect that should be considered is the effect that the fibre content has on the workability of the mortar mixture. The workability is affected negatively when the loading of the DPF into the mortar mixture increases. The addition of DPF interrupts the mineral skeleton of the cementitious matrix, hence, generating voids within the matrix leading to an increase in the porosity. Thus, porosity and strength have an indirect proportional relationship, a higher level of porosity has lower corresponding strengths; as was experienced also by Alatshan and his colleagues [212]. Additionally, another vital factor is the agglomeration of fibres within the matrix. Its common occurrence with longer fibres is also reflected to mortars with larger concentration of fibres, if not on a larger scale, i.e., higher fibre contents are more susceptible to agglomeration than longer lengths. Hence, a combination of the two would hypothetically provide a sample with very weak results, a hypothesis which was solidified in

this experiment as the samples that were characterised by the longer length in the largest tested concentration, OPC and OPC/GGBS composites reinforced with DPF 3 wt.% and 40 mm length, displayed the lowest compressive strength, a decrease of 27.47% and 7.21%, when compared to the optimal mix, OPC and OPC/GGBS composites reinforced with DPF 2 wt.% and 10 mm length respectively at 28 days. There is a significant difference in decrease in compressive strength between the two matrix systems for when comparing the same DPF characteristics and processing parameters. This will be discussed in Section 7.3.4.1. Additionally, the increase in DPF loading content can have the same phenomena as discussed in 7.3.1 the effect on gel bonds, wall effect, ITZ and heterogeneity. Furthermore, undoubtedly the 1% fibre concentrations within the cementitious matrix deemed to be the most domineering as more than half of the samples that were stronger than the controls were composed of 1% fibre contents. This is in line with a plethora of papers that have discussed the relationship between the fibre content and mechanical properties of the composites [11,20–22,167,211,219,220]. Furthermore, the idea of a lower fibre content having beneficial outcomes due to its usage is solidified by the idea of fibre – matrix interface. Beyond a particular fibre content percentage, there is an apparent non – homogenous mix relating to poor and lower fibre – matrix adhesion qualities resulting in lower mechanical capabilities of the composite [211]. On the other hand, a lower fibre content can be attributed to a better and more organised distribution within the mix which allows for more restriction when it comes to fibre pull – out [218]. Furthermore, the detailed effect of fibre within the mortar can be deduced from the explanation in Section 7.3.1.

7.3.3. Effect of alkali surface modification on the flexural and compressive strength of DPFCC

The application of surface modification techniques for NF generally and DPF specifically, has been reported by many researchers to increase the interfacial bonding between the DPF and the matrix system producing DPFCC with improved mechanical properties [12,29,110,221,222]. This theoretical approach was solidified in this experiment as the alkali treated DPF depicted the highest flexural strengths when utilized as a reinforcement with OPC and OPC/GGBS matrix systems. DPF reinforced OPC matrix demonstrated 28.71% and 27.48% improvements of flexural strength opposed to the control samples utilizing untreated DPF, CTRL A, at 7 and 28 days of ageing in a water bath respectively for 20 mm DPF length at 1% DPF loading content. Alternatively, the best result produced by the treated DPF samples demonstrated 32.42% and 37.48% improvements as opposed to the control samples at 7 and 28 days of ageing in a water bath respectively. This shows an increase of 10% in strength for using the treated DPF compared to the untreated DPF for 20 mm DPF at 1% DPF loading content at 28 days respectively of curing in a water bath. On the other hand, treated DPF

reinforced OPC/GGBS matrix demonstrated highest flexural strengths which had 79.55% and 57.12% improvements opposed to the control samples as discussed earlier at 7 and 28 days of ageing in a water bath respectively for OPC/GGBS composites reinforced with DPF 2 wt.% and 10 mm length. This shows an increase of 26.65% in strength for using the treated DPF compared to the untreated DPF for OPC/GGBS composites reinforced with DPF 2 wt.% and 10 mm length at 28 days respectively of curing in a water bath. Alternatively, the best result produced by the untreated fibre samples demonstrated 56.60% and 30.47% improvements as opposed to the control samples at 7 and 28 days of ageing in a water bath respectively. This shows an increase of 26.07% in strength for using the treated DPF compared to the untreated DPF for OPC/GGBS composites reinforced with DPF 2 wt.% and 10 mm length at 28 days respectively of curing in a water bath. Moreover, it has been also represented that the addition of various DPF had an enhancement on all samples produced.

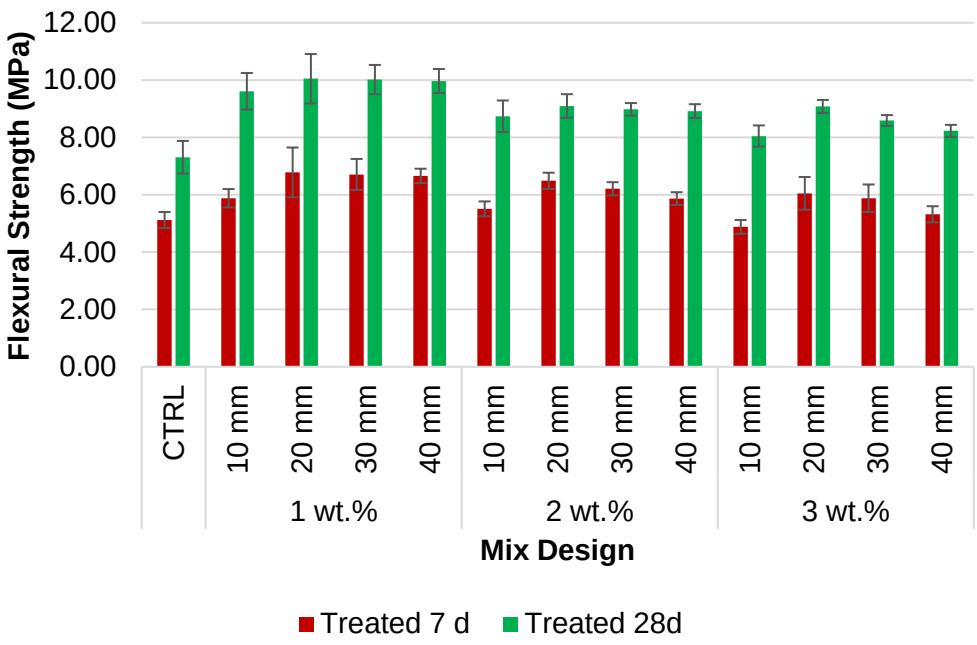

Figure 125 Flexural strength of water cured OPC reinforced with treated DPF mortars

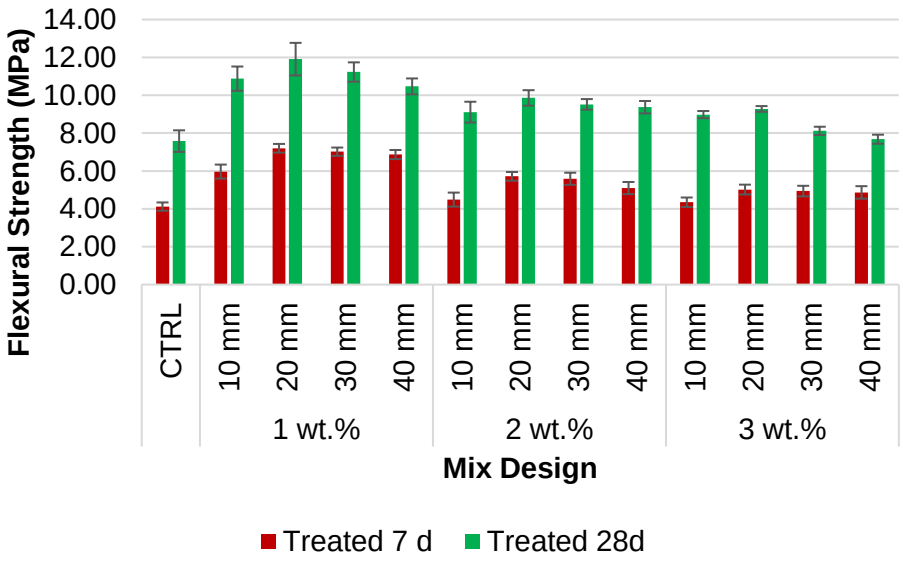

Figure 126 Flexural strength of water cured OPC/GGBS reinforced with treated DPF mortars

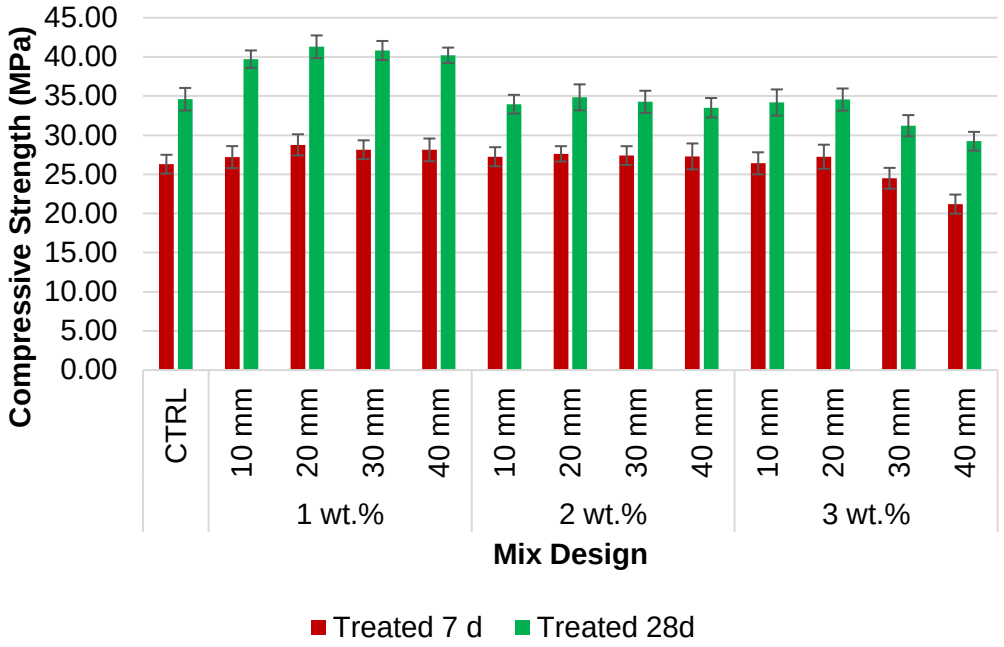

Figure 127 Compressive strength of water cured OPC reinforced with treated DPF mortars

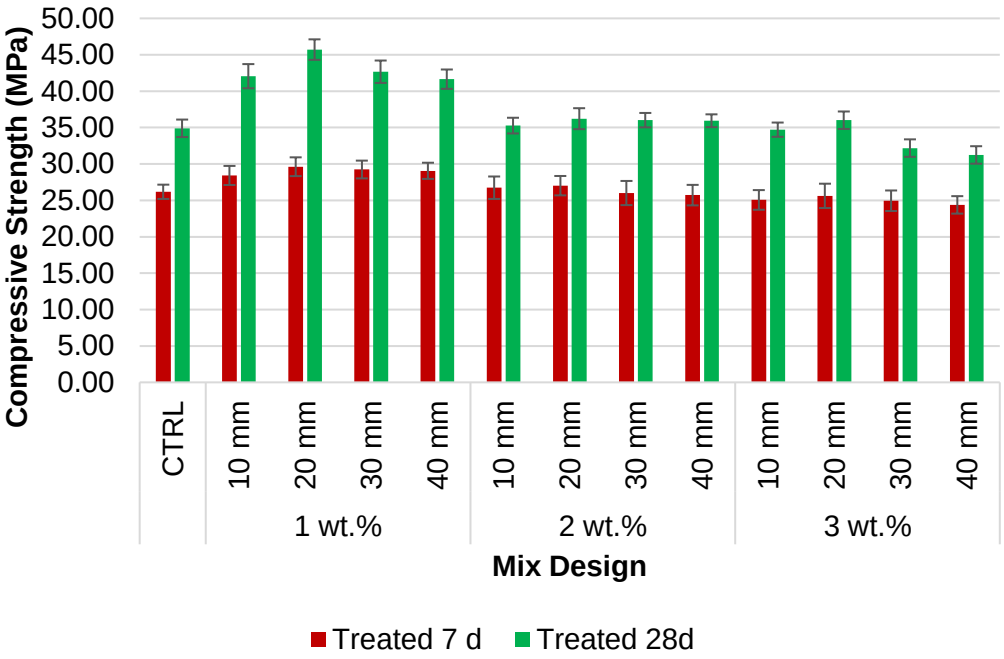

Figure 128 Compressive strength of water cured treated DPF reinforced OPC/GGBS mortars

The enhancement in the mechanical strength upon the usage of treated fibres is ascribable to the fact that, surface modification (especially mercerisation) leads to the removal of extraneous components such as inorganic compounds, gums, sugars etc. that could potentially have a detrimental effect on the formation of cement – cement and fibre – cement

bonds [223,224]. The alkali treatment also facilitates the removal of fibre constituents such as wax, hemicellulose, pectin, lignin, fat, hence, exposing the cellulose underneath [12,120,225,226]. Consequently, there is an increase in the exposed surface area of the DPF which enhances the interfacial bonding with the matrix. Furthermore, the treatment also leads to the modification of an important contributor to the fibre strength and in turn the composite strength, i.e. the cellulose structure. This particular cellulose modification is experienced through improvements in the cellulose crystallinity by the removal of extraneous impurities that would have otherwise affected the cellulose crystallinity negatively [227,228]. Moreover, the alkaline treatment also initiates the removal of volatile products accompanied by bond rupture which in turn promotes fibre fibrillation [89]. Also, alkali treatment enables an optimum level of cell wall swelling, allowing the penetration of chemical molecules into the crystalline regions [229]. Consequently, the lignocellulosic hydroxyl groups are readily available for hydration reactions [89,226,230,231]. Furthermore, considering that the stress is transferred from the matrix system to the fibre at the interface, the existence of enough interface bonding is crucial for achieving the maximum stress transfer, thus attaining an ideal reinforcement. As discussed earlier, NFRC and DPFRC currently have a limited applicability due to the limited interaction between the polar hydrophilic fibres and the nonpolar matrix that is hydrophobic in nature. This results in poor interfacial bonding and low resistance towards moisture, hence, affecting the long – term durability of the composite. These issues are avoided by bringing the fibres and matrix within intimate proximity to each other, a circumstance achieved through the incorporation of wettability which is promoted by surface modification. This is displayed experimentally as the treated DPF depict optimum results on a higher rate as opposed to the untreated ones. The latter of the two, experiences insufficient fibre wetting which correspondingly results in interfacial defects that can act as hubs for stress concentrations [232]. Hence, surface modification is an effective precursor that permits enhanced fibre wettability which forms better interfacial bonding strength and thereby enhancing the mechanical properties of the composites; as was experienced in this research and by previous papers [11,233,234].

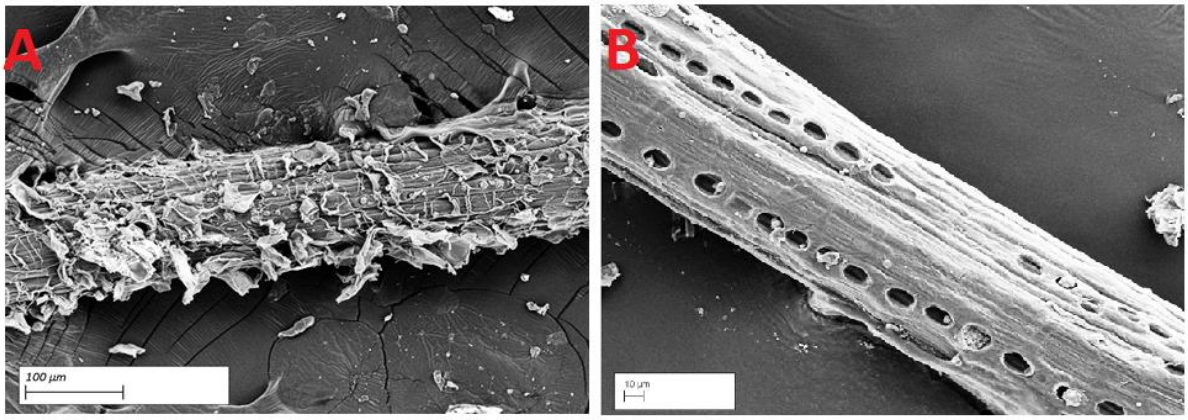

Figure 129 A) Untreated DPF 500X, B) 6% NaOH for 3 hours treated DPF 1,000X

Furthermore, appertaining to previous discussions, the promising samples in this experimental study exhibited enhanced characteristics due to a good rate of dispersion achieved chemically, where the -OH groups are replaced by more hydrophobic organic moieties that promotes an increase in the affinity between the fibre and the matrix, thus, decreasing the amount of hydrogen bonding and in turn an increase in dispersity, while the opposite occurred for the weaker samples. Therefore, as the untreated samples are weaker in comparison to the treated, it can be seen that the former exhibits less ideal rates of dispersions primarily due to the agglomeration resulting from the formation of hydrogen bonding of the hydroxyl groups [47]. To enhance the dispersity of DPF for functionalising, surface modifications are necessary and hence, the NaOH treatment used in this research proved to be effective.

7.3.4. Effect of matrix system, curing conditions and fine aggregates on the mechanical properties of DPFCC

This section will discuss the factors that are not associated with the characteristics of DPF but has a vital influence on the overall mechanical properties of DPFCC. It is mandated to consider the following factors, i.e. matrix system type, curing conditions and aggregate type as equally important factors as DPF characteristics.

7.3.4.1 Effect of matrix system

The choice of matrix system used for developing cementitious composites can be considered as the most dominant non – fibre related factor that has an influence on the composite's mechanical properties. This was reflected in this experimentation as both the binder choices, OPC and GGBS, demonstrated varying mechanical properties when considering the ageing duration of the mortar samples prior to testing, i.e., 7 or 28 days.

It can be deduced that DPFCC developed using OPC/GGBS as the cementitious matrix system possessed better mechanical properties at 7 days compared to DPFCC developed

using 100% OPC matrix system. It is worth noting that this is applicable when the samples cured in an ideal environment, water bath and after 28 days of curing due to the weak early strength gain of GGBS. The phenomena of weak early strength gain demonstrated by pozzolanic materials has been experimentally reported by many other researchers and been justified that the pozzolanic cementitious composites exhibits slower rates of strength gain during early stages of ageing, i.e. 7 days of ageing. This can be explained due to the little presence of calcium hydroxide ($Ca(OH)_2$) in the GGBS atomic structure, as reported in Section 3.3.1, which leads to a slow pozzolanic reaction as opposed to a faster rate when using 100% OPC. This has been justified in this experimental study and which is demonstrated from in the graphs where that after 28 days of ageing, DPFCC composed of a cementitious matrix system of both OPC and GGBS had better mechanical properties than DPFCC with just OPC as a cementitious matrix. Also, a significant increase from the 7 days 28 days strength is noticed.

Moreover, discussing the relationship between the DPF and the choice of selection of the cementitious matrix system, it can be acknowledged for its utmost significance to the overall composite characteristics. The optimal results of DPFCC composed from 100% OPC cementitious matrix system portrayed enhancements of 37.48% and 19.36% for the flexural and compressive strength respectively at 28 days of ageing in a water bath. On the other hand, DPFCC composed from 50% OPC: 50% GGBS cementitious matrix system depicted the optimal results with increase in flexural and compressive strengths by 57.12% and 30.97% respectively after 28 days of ageing in a water bath. These results indicate that utilizing pozzolanic material produced as waste, GGBS, in replacing a major amount of OPC in the cementitious matrix develops more sustainable composites with an average improvement in mechanical strength by 16%. This can be attributed to the “alkali attack” phenomena experienced by DPF in cementitious composites produced with OPC as a cementitious matrix system. The “alkali attack” endorses DPF degradation that is caused by the migration of hydration products into the DPF walls and lumen [223]. Hence, initiating pozzolanic reactions in the presence of GGBS induces reductions of portlandite ($Ca(OH)_2$) and the soluble alkali content of OPC, thus reducing the alkalinity of the overall cementitious matrix system which prevents DPF from deterioration. This justifies the better strengths achieved by DPFCC composed of GGBS and OPC at 28 days of ageing as opposed to early ageing development stages.

Furthermore, the durability experienced by pozzolanic cementitious binders is highlighted theoretically by the concept of the Lime Saturation Factor (LSF) which is essentially a ratio of CaO to the other oxides [235]. In other words, it depicts a ratio of the alite to belite content in the agglomeration of mortar components. A quantified version of the LSF enables a further

understanding of the relationship between this ratio and the durability of mortars. The LSF can be calculated as shown in Equation 55 [235].

$$\mathrm{LSF} = \frac{\mathrm{CaO} - 0.7\mathrm{SO_3}}{2.8\mathrm{SiO_3} + 1.2\mathrm{Al_2O_3} + 0.65\mathrm{Fe_2O_3}} \quad \text{Equation 55}$$

The values of chemical composition of both OPC and GGBS based on Table 26, reported in Section 3.1.3 are substituted in Equation 55 to calculate the LSF as shown in Equation 56 and Equation 57.

$$\mathrm{LSF\ (OPC)} = \frac{70.91 - 0.7(5.36)}{2.8(15.28) + 1.2(3.16) + 0.65(2.07)} = 1.40 \quad \text{Equation 56}$$

$$\mathrm{LSF\ (GGBS)} = \frac{45.44 - 0.7(2.64)}{2.8(33.60) + 1.2(10.43) + 0.65(3.10)} = 0.40 \quad \text{Equation 57}$$

Based on the calculated LSF for both GGBS and OPC, an immense difference is observed. The LSF of OPC and GGBS was calculated to be 1.40 and 0.40 respectively, a 71.4% difference when compared OPC to GGBS. Appertaining to these calculated values, one can conclusively say that the presence of CaO is relatively lower in GGBS as opposed to OPC which was a dominant factor in LSF calculation. The reason as to why this plays a significant role in the durability of the mortar is because upon the production of lime through hydration, the lime travels through the ionic water due to its high solubility. This consequently leads to the crystallisation of the free lime which is in turn engulfed by large capillary pores. The GGBS initiates a reaction with the excess free lime resulting in the production of a gel that blocks the above-mentioned pores indicating a reduced level of porosity [236] . Since, GGBS has a lower LSF value, there is a lower number of pores due to free lime that need to be filled in contrast with OPC. Henceforth, this not only insinuates increased strengths but also a finer pore structure which serves as an interrupter for chemical migration through the mortar which in turn facilitates the process of keeping the said mortar safe from abrasion. Conclusively, there is a higher level of chemical stability and hence durability, demonstrated by GGBS when compared to OPC. Additionally, lesser abrasion indicates a reduced rate of volume loss which enables the mortar to maintain dimensional stability [1].

7.3.4.2 Effect of curing conditions on flexural and compressive strength

During the primary stages of developing the samples after casting the fresh mixture into their labelled moulds, the mixture is subjected to hardening process which corresponds to the

strength gain due to the exothermic chemical reactions between the cementitious binder and water which, courtesy of which the same binder transforms into a bonding agent for the interfacial transition phases in the cementitious matrix, i.e. the cement paste, the fibre and the fine aggregate phase. The hydration process has a crucial correlation with the strength gain of the samples developed, thus hydration process is an essential factor that must be evaluated in any cementitious composite development experiments. Moreover, the investigation of the effect of curing conditions was done by evaluating water curing conditions, water bath immersion of the samples at temperature (20 ± 2) ^{o}C according to BS EN 12390-2, and air curing conditions, samples kept in a controlled room at temperature (20 ± 2) ^{o}C, according to BS EN 12390-2.

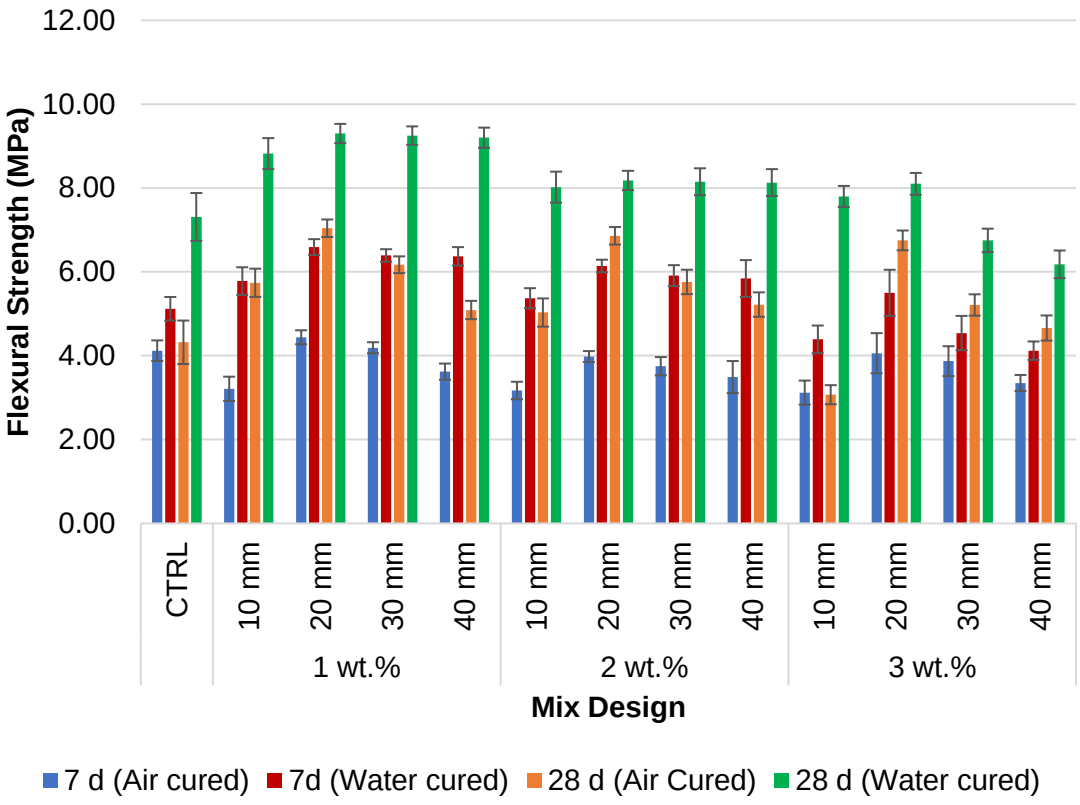

Figure 130 Flexural strength of different curing OPC reinforced untreated DPF mortars

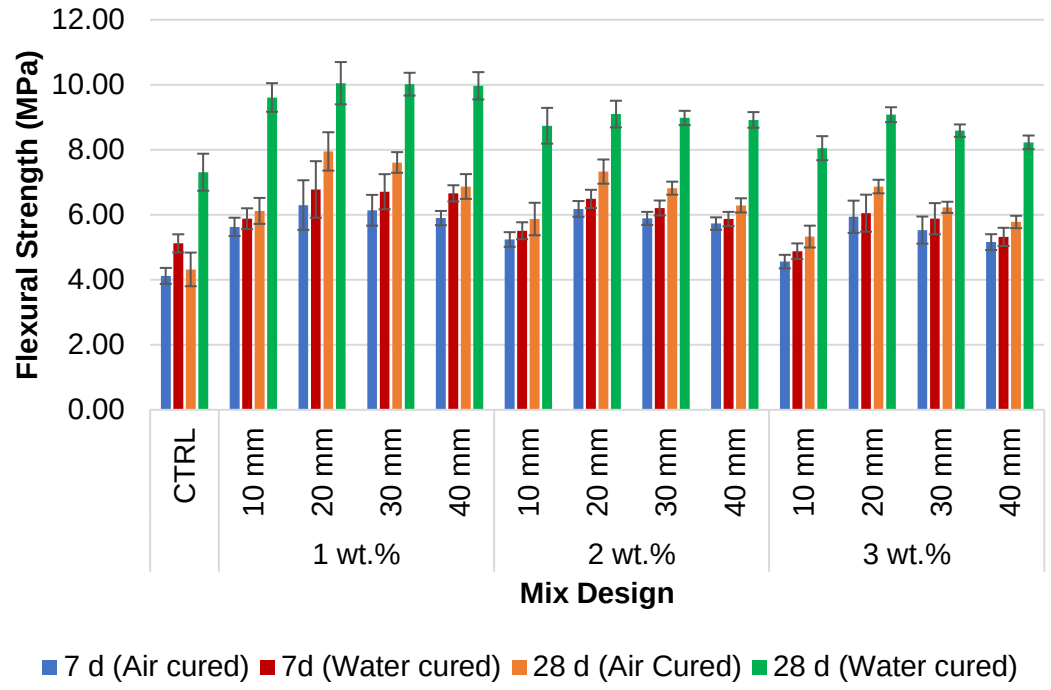

Figure 131 Flexural strength of different curing OPC reinforced treated DPF mortars

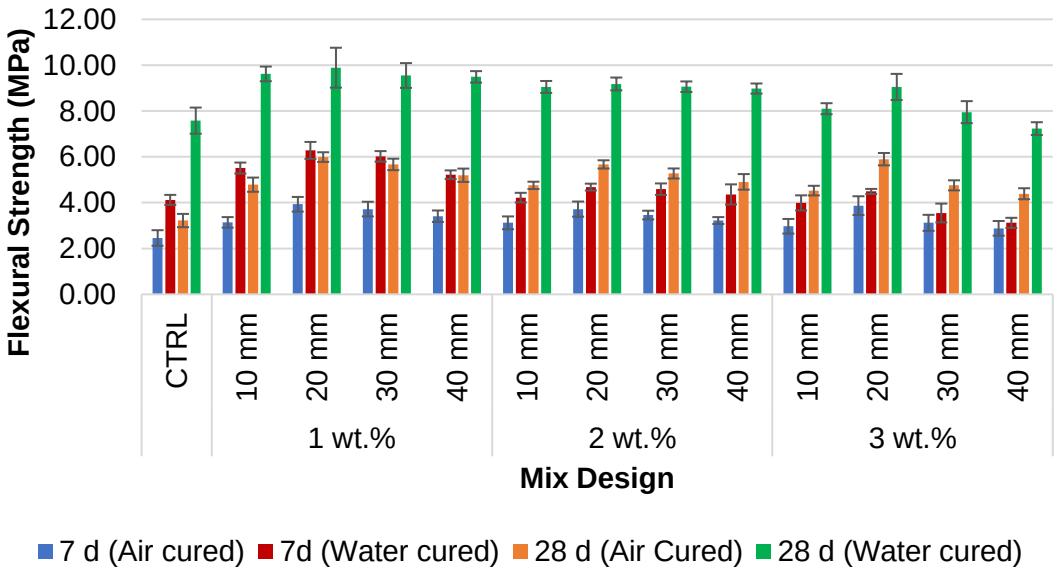

Figure 132 Flexural strength of different curing OPC/GGBS reinforced untreated DPF mortars

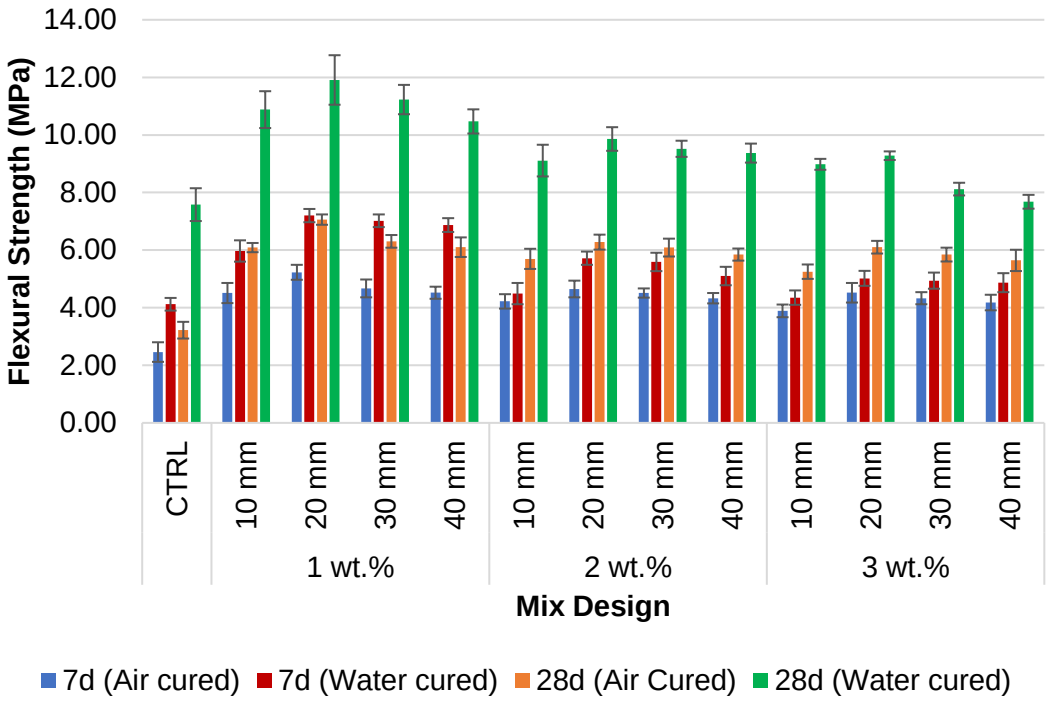

Figure 133 Flexural strength of different curing conditions of OPC/GGBS reinforced treated DPF mortars

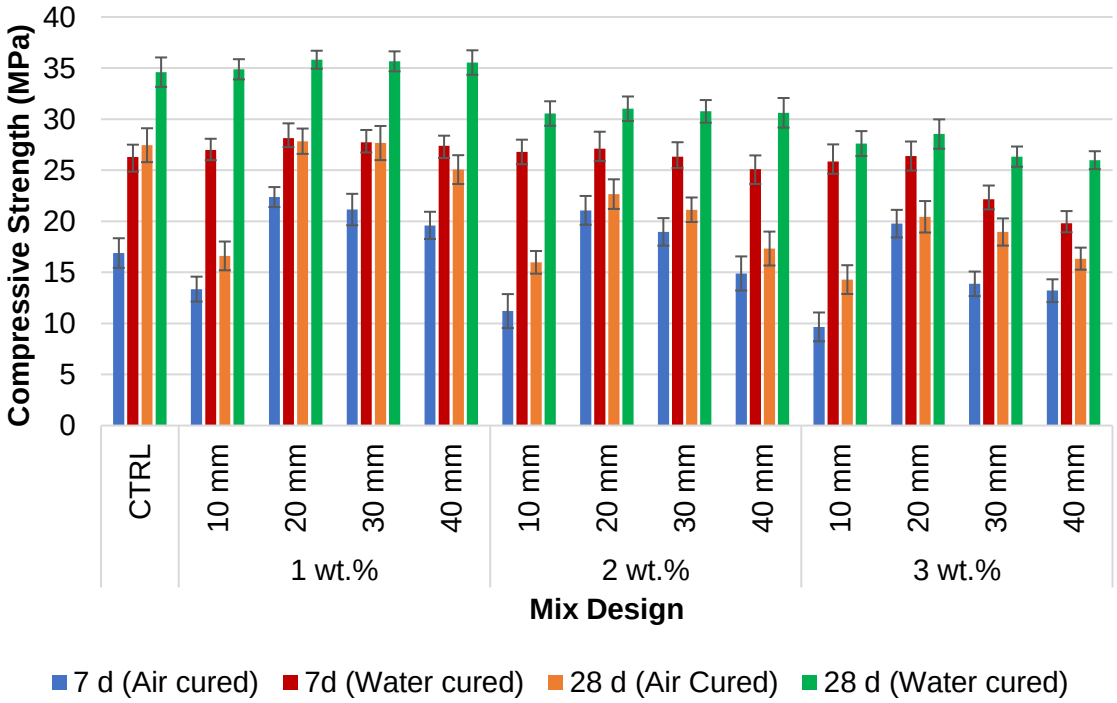

Figure 134 Compressive strength of different curing conditions for OPC reinforced untreated DPF mortars

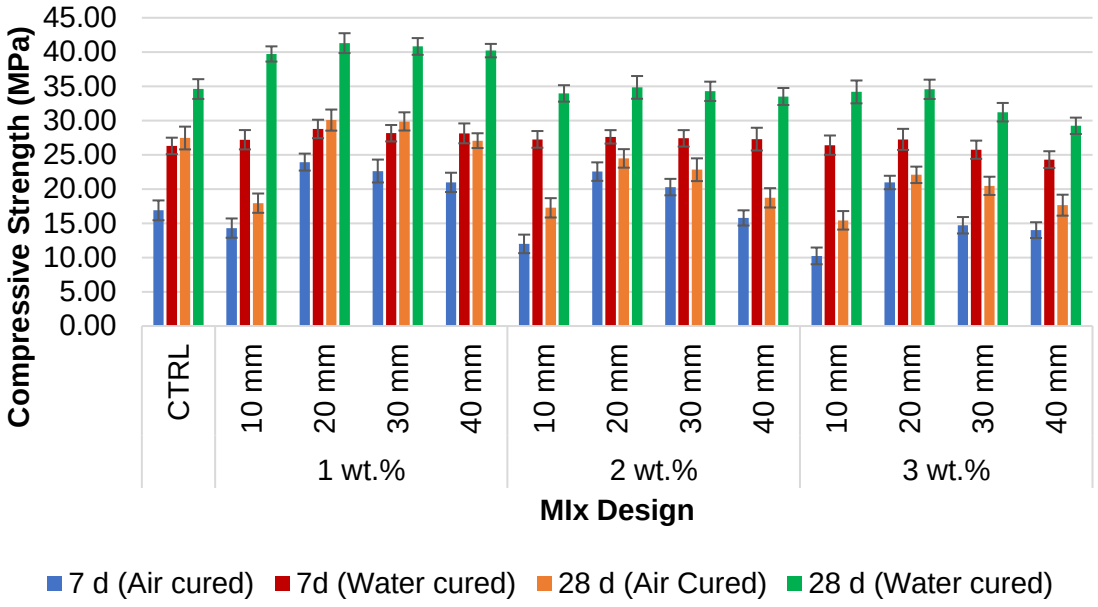

Figure 135 Compressive strength of different curing conditions for OPC reinforced treated DPF mortars

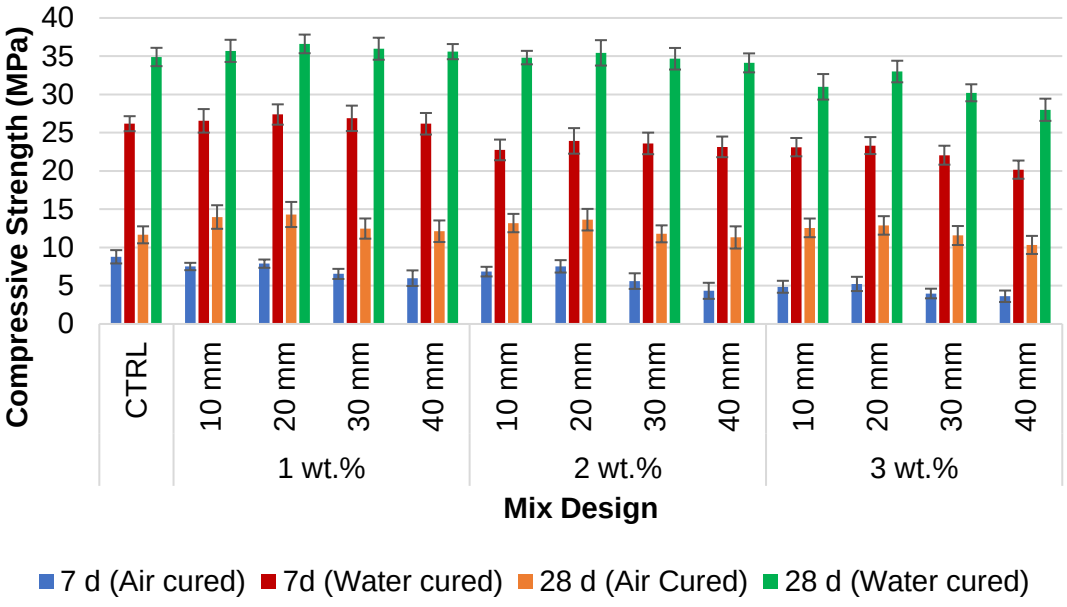

Figure 136 Compressive strength of different curing conditions for OPC/GGBS reinforced untreated DPF mortars

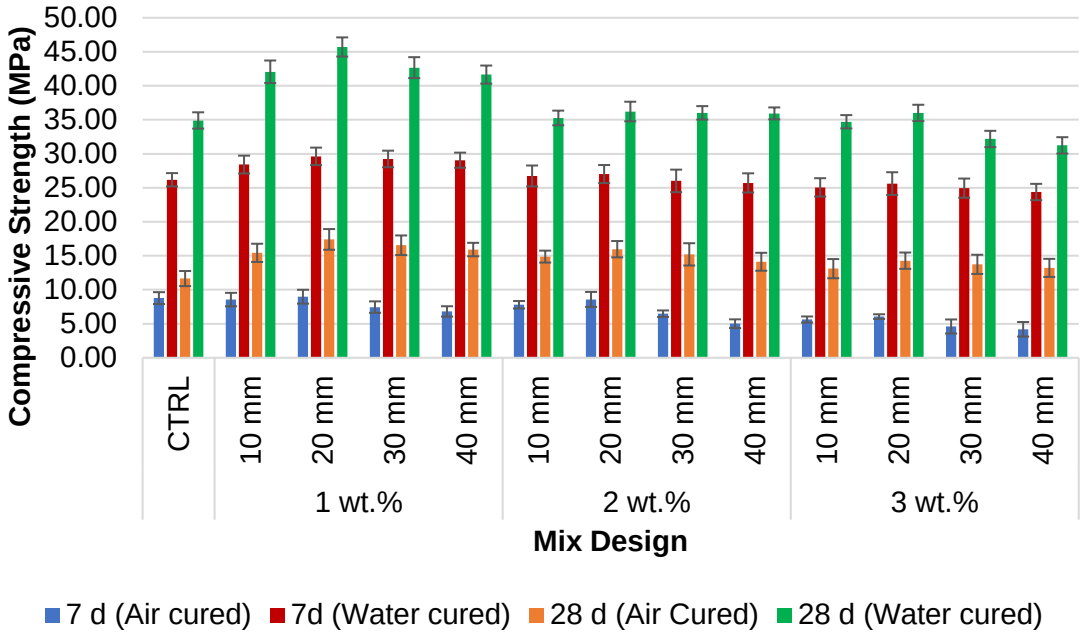

Figure 137 Compressive strength of different curing conditions for OPC/GGBS reinforced treated DPF mortars

As shown in from Figure 130 to Figure 137, there is a great difference between the strengths of the composites developed during the different type of curing conditions using different matrix. This can be evaluated quantitatively where OPC/GGBS mortars showed a flexural strength increase of 68.9% from 7.06 MPa to 11.91 MPa when comparing the treated composites with highest flexural strength cured under air conditions and water bath respectively. Additionally, a remarkable difference was noticed for samples tested to evaluate their compressive strength which showed increase of 162.6% from 17.41 MPa to 45.71 MPa when comparing the treated with highest compressive strength cured under air conditions and water bath respectively. The reasons for the remarkable difference between the different curing conditions can be justified by the theory of hydration and its process. This can be justified on a microscopic level where the capillary porosity of cementitious composites can be defined as the existence of capillary pores varying from 2.5 nm to 50 nm in an adequately hardened cement paste (HCP) [237]. The hydration process begins an exothermic reaction once the capillary pores in the sample are filled with water. Due to the heat produced by the hydration process, the sample temperature increases which consequently lead the water from the capillary pores to evaporate, initiating dryness. The occurrence of dryness in the absence of enough water for further hydration of the cement will develop a dehydrated gel, which forms an interruptive barrier from transforming into calcium silicate minerals such as C_3S which contributes to the early strength gain in the samples [238]. Moreover, another issue caused by the evaporation of water from the capillary pores is the loss of volume which is originally

present in the cement paste which creates voids, thus establishing the direct proportionally between the void generation and the rate of evaporation [239]. This in turn signifies higher levels of porosity which have corresponding strength reductions experienced by the specimens. As evaporation is experienced more by air cured samples as opposed to the water cured, the latter is less porous and hence allows for enhanced mechanical properties. Thus, it can be deduced that it is crucial to limit the rate of water loss from a cementitious mixture. This is accomplished by curing methods where the fundamental purpose is to sustain saturation in the mortar by keeping it either fully saturated, i.e. moist, or saturated and surface-dry (SSD); until the capillary pores in the cement paste are filled by the hydration reaction products [240]. This is essential as the occupation of the spaces results in a lower capillary porosity and a relating strength increase. The water curing method performs the above objectives of preventing the water evaporation whilst maintaining appropriate relative humidity in a more efficient and effective manner as opposed to air curing. The reason behind the domineering stance of water curing over air curing is courtesy of the increased availability of water experienced by the specimens in the water tank which in turn provokes a higher rate water ingress into the cement cores that is required for hydration to occur, a stark contrast to the samples left out in the chamber.

On the contrary, mortars developed with GGBS have weak results in air cured conditions which can be attributed to the rate of heat generation which slows down the hydration process of the mortar, thus creating voids which weakens the mechanical properties [241]. Moreover, the fact that despite the higher rates of water loss in the DPF reinforced mortars, the water cured samples still depicted increases in the mechanical properties when compared to the controls, is an occurrence that can be attributed to a possibility that the water absorbed by the fibres is available and utilised later for further cement hydration [213]. This enhanced depiction of mechanical properties due to water curing of DPF and NF reinforced mortar specimens has been evaluated in previous experimental studies [20,99,232,242].

Furthermore, another reaction that can be taken into consideration to account for having the water cured samples demonstrate better strength is carbonation shows a considerable relationship with the alkalinity of the mortar. It is recapitulated that the alkalinity of ordinary mortars is relatively high with pH exceeding values of 13 which occurs due to the formation of calcium hydroxide, $Ca(OH)_2$, during the hydration phase [243]. However, Toledo and his colleagues reported that $Ca(OH)_2$ is gradually dissipated due to a combination to the atmospheric carbon dioxide, CO_2, leading to the production of calcium carbonate, $CaCO_3$, in a process referred to as carbonation. Thus, forming a less alkaline mortar insinuating a pH value of the pore water to be lower than 9 [223]. Carbonation reaction be expressed as a balanced in Equation 58:

$$Ca(OH)_2 + CO_2 \rightarrow CaCO_3 + 3H_2O$$ Equation 58

Moreover, this procedure in the HCP can be classified as a deteriorative process not in the short term, but the longer run due to the fact that there are apparent compressive and flexural strength increases in the short term as opposed to long, due to carbonation. This is particularly observed in the GGBS/OPC samples and can be accounted for due to certain pozzolanic reactions in the cement paste that reduce the alkalinity within the composite and hence indicate lesser likelihoods of 'alkali attacks'. This particular circumstance has also been recorded in a study focusing on vegetable fibre reinforcements [244]. However, prolonged CO_2 diffusion can result in a negative impact on the strength and especially the durability of mortar due to reasons explained as follows. For carbonation to occur at its optimum rate, the relative humidity at room temperature must be within the 50 – 75% range [235,245–247]. As indoor humidity normally falls within this range (typically 65%), it is safe to assume that the tested samples were subject to carbonation. A factor that has a significant effect on carbonation is that of permeability and porosity. Theoretically, a higher value for either or both the parameters corresponds to a higher rate of CO_2 diffusion which results in a greater degree of carbonation. Since porosity is directly related to the curing type, it can be said that air cured samples are prone to increased rates of carbonation as they are more porous allowing for more CO_2 diffusion and hence, reduced mechanical properties and durability with ageing. Furthermore, the most favourable condition for the carbonation reaction is when there is sufficient moisture for the reaction but not enough to act as a barrier. This has been also reported by Futtuhi (1986) that an increase in water curing duration demonstrates a considerable decrease in the depth of carbonation penetration [248]. Thus, fully immersing the mortars in water baths provides the barrier to slow the carbonation process and will show enhanced mechanical properties and durability with ageing.

7.3.4.3 Effect of fine aggregates

As mentioned in chapter 3, the fine aggregates, sand, utilised in this experimental study were subjected to oven drying to avoid aggregated saturation influence on the DPFCC. The intentional drying of the tested aggregates results in a phenomenon where the aggregates are bone-dry insinuating the presence of solely air-filled pores on the surface of the aggregates, i.e., a characterized unsaturated surface. On the contrary, when an alternate usage of moist (oversaturated) aggregates is opted for prior to the mixing stages, the output mortar displays a strength reduction of approximately 5 – 10% as opposed to the option of unsaturated aggregate, viz. dry aggregate, conferring to the works of Neville (1995) [214]. The underlying reason for the decrease in strength due to oversaturated aggregates is due to the pores of the aggregate being filled with water, hence displaying wet surfaces. Consequently, the moisture

content of the aggregates is larger than the allowable absorption of the respective aggregates which results in excess water to be in the mixture; hence, an increased w/c ratio. Now, according to Abrams' law, the strength of the mortar mixture is inversely proportionate to the quantified amount of water in the w/c ratio [249]. Therefore, the usage of moist aggregates should be avoided for developing higher-grade mortars. However, for other saturation percentages of the aggregates, the mortar strength is not compromised; but rather the workability of the mortar is affected. Before further discussion of this, it is crucial to discuss the effective w/c ratio in the mortar mixture. This parameter can be defined as the fraction of total volume of water that is able to react with the cement over the total volume of cement in the mixture [250]. Water is essential in the mixture for the purposes of initiating cement reactions, hydration process, and workability. The existence of aggregates implies the inevitable absorption of water from the cement mixture by the aggregates; the intensity of which depends on the absorption capacity of the aggregates. Conclusively, there is a potential reduction in the volume of water that could have reacted with the cement. Therefore, this insinuates a reduced effective w/c value as opposed to the actual w/c ratio. A reduced effective w/c ratio has direct relations with a loss in workability despite potential strength and durability proliferations due to a reduction in the water content from the cement paste because of absorption from the pores of the aggregate. Thus, this results in an increased viscosity of the paste leading to reduced cohesion and henceforth, development of voids in the developed composite. Furthermore, if the aggregates are saturated or partially saturated, it is a generalized practice to assume that prior to setting, the aggregates have absorbed enough water to reduce the effective water content which as discussed before, corresponds with lower workability; this is commonly experienced in more arid climates. This reduced workability is contrasted by the usage of dry aggregates, like the fine aggregates dried before utilization in this experimental study. Due to practically none of the voids being filled with water, the dry aggregates are subjected to instantaneous deposition of cement paste on the surface and the pores which acts as a prevention to water percolation. However, as water is less viscous than the cement paste, there is still some absorption of water demonstrated by the dry aggregates. With the case of dry aggregates, the water ingress depth is larger as it has to penetrate a greater distance from the aggregate surface [214,251]. Therefore, there is lower water absorption by the aggregate which indicates more water available for the hydration reaction of the binder. This in turn leads to a higher effective w/c ratio and hence greater workability encountered by operators. However, it is vital to note that the addition of the dry aggregates at a later stage while mixing the mortar, i.e., after the cement and water being mixed, it would have an opposite effect on the workability compared to what is discussed above. When the aggregates are introduced subsequently to the other materials, the aggregates will tend to absorb water from the cement paste for the purposes of filling the pores. This in turn decreases

the amount of water in the mixture suggesting a reduced workability as otherwise, particles would have been able to slip over one another more easily and efficiently [252]. Therefore, the order of adding the material into the mix is a vital affecting factor of the mixture behaviour and mechanical properties. Additionally, it is also important to note that fine aggregates like the sand utilised in this experimental study was observed to have an occurrence that can be referred to as bulking. This only occurs when the moisture content in the mix is higher than desired. It can be defined as the apparent escalation in the volume of the sand in a mixture caused by the sand particles being thrusted apart courtesy of water films. Consequently, there is a reduced mass of sand which otherwise would have filled a larger volume in the mix. As a result, there is an evident deficiency of sand/ fine aggregate which in turn leads to the appearance of the mortar mix to be classified as 'stony', an instance which causes an increased propensity for the hardened composite to honeycomb or segregate. Thus, accordingly, there will be a reduction in the strength as well. Therefore, it is important to monitor the moisture content in the fine aggregates which is achieved by oven drying the fine aggregates beforehand [214].

7.3.5. Water absorption of date palm fibre cementitious composites

The hydrous characteristics of DPFCC is of utmost importance when considering the durability and water resistance properties of the composite. This was experimentally investigated by immersing the various DPFCC into water tanks for 72 hours. The parameters investigated in this chapter, i.e., DPF loading content, DPF length, Contentious matrix types and curing conditions, will be discussed in accordance to their water resistance properties. Hence, several sets of data were acquired which facilitated in evaluating the performance of the samples with respect to water absorption. Based on the results, it is noticed that the addition of DPF as a reinforcement to cementitious matrix system increases the water absorption of the composites significantly, with a maximum increase of 11.98% for composite B12. This finding can be related to the extreme hygroscopic character of DPF which greatly affects the water absorption characteristics of cementitious composites. Several researchers have reported their investigation of the effect DPF on the water absorption of their reinforced composites. However, different approaches and materials were used. Chikhi and his colleagues observed that DPF water absorption capacity directly influences the water absorption rate [173]. This is reinforced by the fact that water absorption levels for individual date palm fibres can reach up to 241% as was observed by Benmansour et al. (2014) They also reported that DPF depicts large capacities of water absorption with sorption levels as high as three times the dry weight [160]. This can be attributed to the porous structure of DPF resulting in a hydrophilic material. These high levels of hygroscopicity can be deemed as a hindrance to the effective development of cementitious composites in industry due to the fact

that it consequently leads to shrinkage and swelling phenomena, making it susceptible to damage. The fibres containing – OH groups are able to combine easily with water, resulting in swelling, plasticising and degradation [253]. As a result, it needs to be contained as much as possible by manipulating several factors that are discussed further in this chapter.

7.3.5.1 DPF length effect and loading content on water absorption of DPFCC

The effect of DPF physical characteristic, length, and the loading content added to the mortar mix are discussed in this section. The water absorption of DPFCC carried significantly in regard to DPF length. The demonstration of the results is done based on the worst and best samples of each length (in terms of their mechanical strengths) are plotted to understand the differences in the water absorption values more holistically.

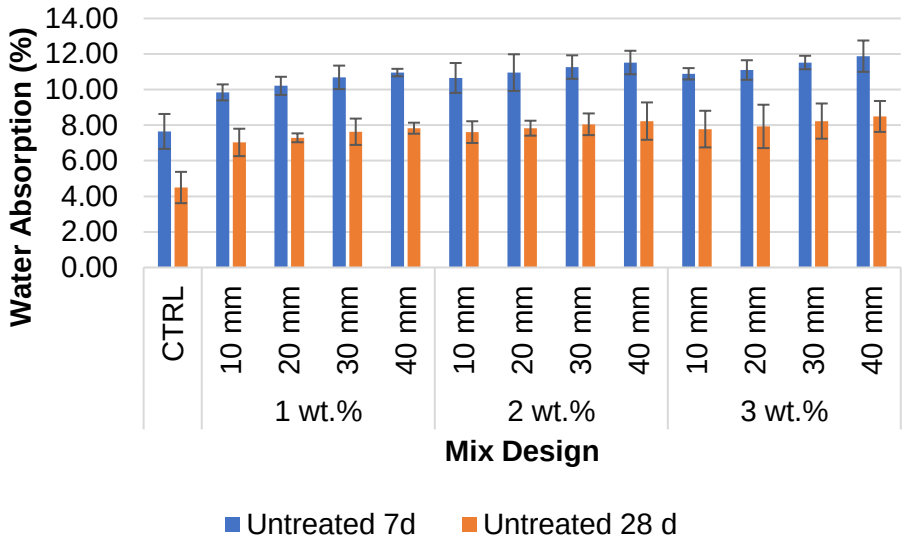

Figure 138 Water absorption of water cured OPC/GGBS reinforced untreated DPF mortars

Deducing from Figure 138, which represents the water absorption of untreated DPF composites cured in a water tank, it can certainly be concluded that at both 7 and 28 days of ageing, the optimal short fibre composite, OPC/GGBS composites reinforced with DPF 1 wt.% and 10 mm length, depicted a lower rate of water absorption 9.84% and 7.03% at 7 and 28 days of curing. This shows a reduction of 3.76% and 3.69% when comparing against the strongest composite, OPC/GGBS composites reinforced with DPF 2 wt.% and 10 mm length, an increase of 28.63% and 56.22% in water absorption when compared to the CTRL OPC/GGBS composites for the same curing durations at 7 and 28 days respectively. In addition to this, the weakest short fibre samples portrayed reductions of 17.17% and 17.20% when comparing against the highest water absorption composites, OPC/GGBS composites reinforced with DPF 3 wt.% and 40 mm length at 7 and 28 days respectively. The underlying reason behind this can be understood by referring to the idea of fibre dispersion and

subsequent void generation. As discussed in Section7.3.1 and 7.3.2, the incorporation of longer fibres led to poor fibre dispersion which resulted in the forming larger number of voids as opposed to the shorter fibres. These voids represent potential sites for water accumulation which consequently leads to more availability of water in the composite and hence, a larger rate of water absorption. As these voids are more omnipresent in the composites with longer fibres, the reason behind the higher absorption rates exhibited by the said composites can be justified, i.e. with the phenomenon of high fibre hydrophilicity. Furthermore, the variation in the fibre/ matrix adhesion in the ITZ; a factor that is worse with longer fibres as discussed previously. The microstructure of the cement paste in the ITZ is different to that of the remainder of the cement paste. The underlying reason behind this is that during the mixing stage, cement particles experience the inability to be packed near the larger agglomerated 'fibre clusters.' This means that the amount of cement present for the purposes of filling the voids is lower. Consequently, this leads to a larger porosity in the cement paste in the ITZ as opposed to the cement paste that exists further away from the ITZ. As a higher rate of porosity dictates higher water contents in the composite, the rate of water absorption is also higher.

7.3.5.2 DPF surface modification effect on water absorption of DPFCC

The primary purpose of surface treatment of DPF is to reduce the hydrophilic character of the fibres and provide a better surface topography by removing surface impurities to enhance the interfacial bonding between the fibre and the cementitious binder. This Section will discuss the water cured samples as they opposed better mechanical properties. Moreover, the hydrophilicity nature of DPF disturbs the rheological behaviour of the mortar in the fresh state which influences the mechanical and physical properties in the hardened state. Several investigations have evaluated that surface modified fibre have exhibited lower water absorption in mortars as opposed by untreated which enables more water absorbed by the cement paste/binder to enhance the hydration process [254–257]. This ideology was also presented and experienced in this experimental study as shown in Figure 139. Comparing the most water absorbed untreated and treated composites, OPC/GGBS composites reinforced with DPF 3 wt.% and 40 mm length, at 7 and 28 days shows 20.73% and 31.63% decrease in water absorption respectively. This can be described as the high hydrophilicity nature of untreated DPF which has a direct positive correlation with water absorption have been reduced with surface modification which decreased its hydrophilicity leading to enhanced water resistance properties. Also, surface modification of DPF produces a protective layer on the interfacial zone which obstruct the penetration of water molecules into the cell walls of DPF preventing thickness swelling of the DPF [230]. Moreover, referring to the main drawback of utilizing DPF and other NF in industrial applications due to their weak interfacial bonding leading to low resistance to moisture, hence affecting the durability of the composite on the

long term. Thus, these drawbacks and concerns are avoided by reducing the moisture absorption of the composite which is promoted by a successful surface modification of the fibre.

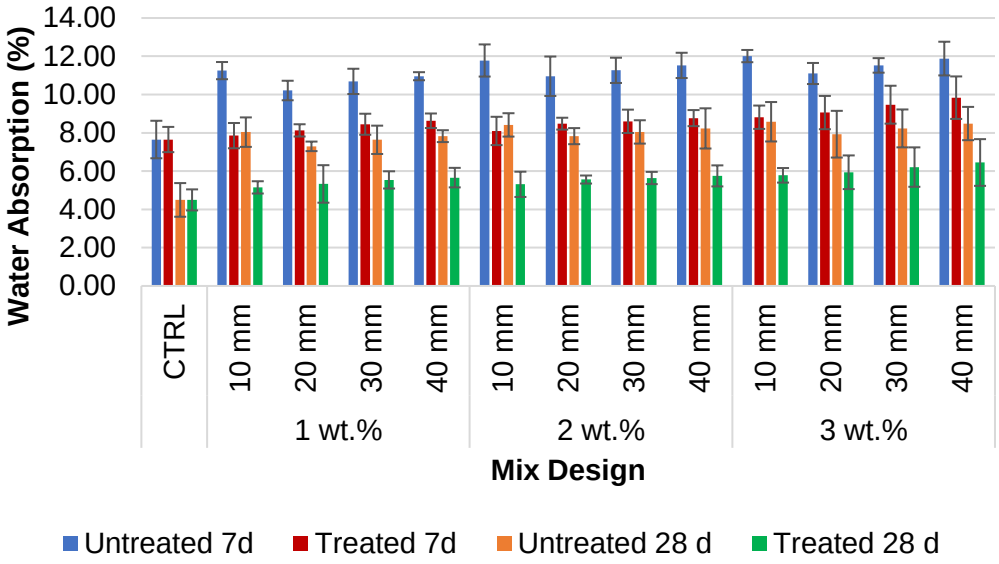

Figure 139 Water absorption of water cured OPC/GGBS reinforced with untreated and treated DPF mortar

7.3.5.3 Cementitious matrix system effect on water absorption of date palm fibre cementitious composites

There is a strong effect on the water absorption behaviour of DPRCC considering the cementitious matrix systems which can be attributed to the fineness which is directly related to the surface area of the cementitious matrix. Based on the binder fineness calculations done in Chapter 3, Section 3.1.1 Table 25, GGBS cementitious matrix exhibited a smoother surface when compared to OPC cementitious matrix system which is related to the increase in fineness of the matrix, where GGBS and OPC had fineness of 521 m^2/kg and 449 m^2/kg respectively.

The high specific surface and fineness of these GGBS particles can induce high reactivity and allow tight packing of a composite's microfabric, with low amounts of micropores and subsequently a greater density and lower permeability. Condren and Pavia (2007) reported that the pozzolanic reaction of GGBS starts at a very early age (producing hydraulic cements that seal pores) and that GGBS significantly decreases the size and content of $Ca(OH)_2$ crystals in the aggregate-paste interface which makes the microstructure of the ITZ aggregate/binder more dense [258].

7.3.6. Interfacial bonding properties

Figure 140 show optical microscopy images of the cross-section view of DPFCC. Samples M-3-2, M-2-4, and M-3-4 were randomly selected for the optical analysis. Figure 140 (a) shows the 3% loading ratio of DPF. This shows the DPF breakage and agglomeration of fibres at high fibre loading. Figure 140 (b) shows how voids are present surrounding the DPF fibre of reinforced samples and the voids present due to fibre pull-out. Figure 140 (c) also shows that as the fibre loading increased the voids created by the pull-out force during the tensile test also increased. This observation cope with the tensile results which shows decrease in the tensile force as the DPF loading increased.

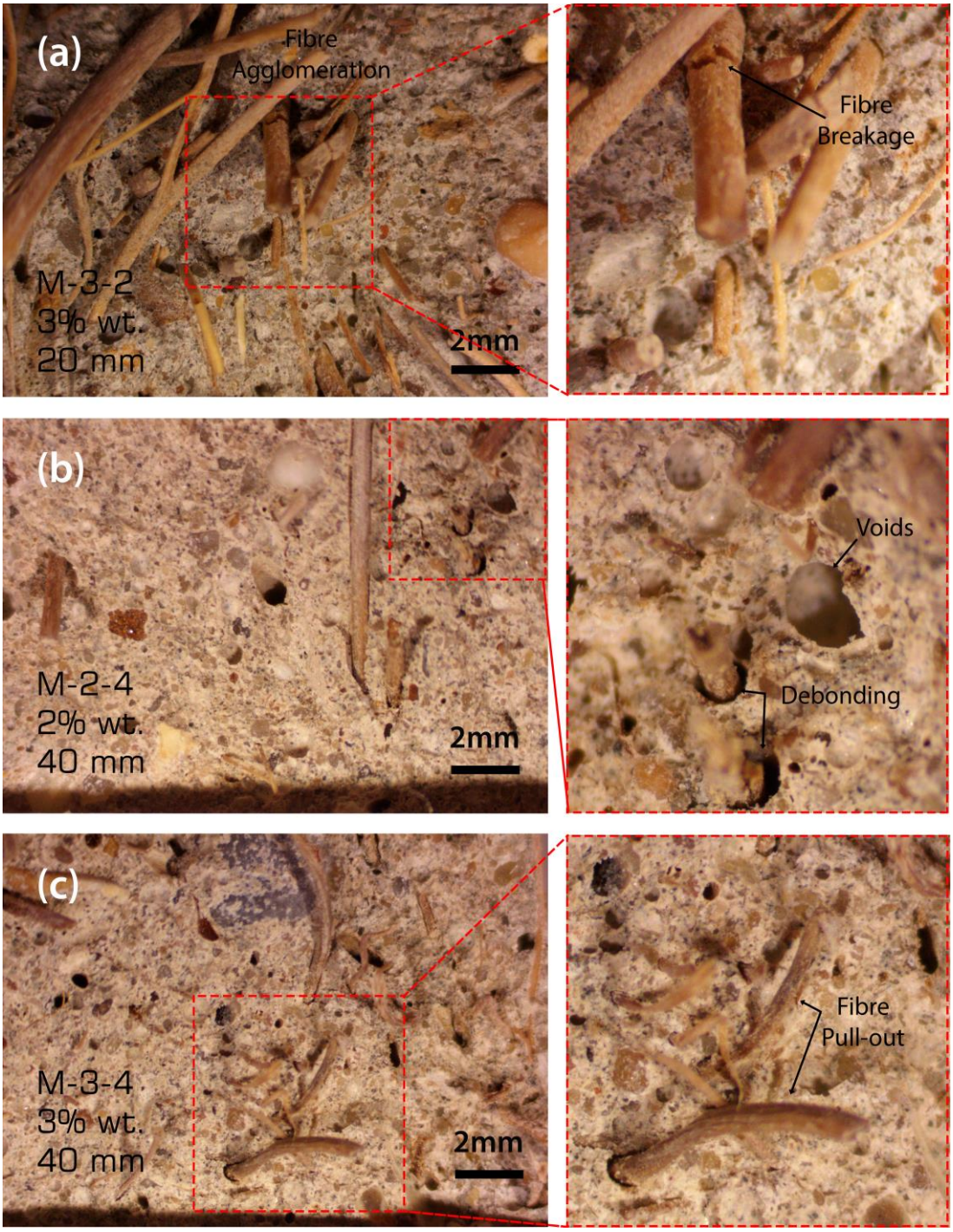

Figure 140 DPF/OPC composite microstructure

7.4. Interim summary

Reinforcing cementitious mortars with DPF which is considered as the most abundant agricultural biomass waste in the MENA region could produce a low-cost sustainable construction and building material. This utilization will aid in decreasing the amount of waste deposited into landfills and burnt annually, thus achieving new trends in composite materials. The investigations done in this study on the mechanical properties, flexural and compressive strength, of DPF reinforced cement mortar showed positive results for being a possible natural material to be utilized in developing sustainable composites. The scientific analysis done in this study can enhance any future research done of DPF or NF reinforced cementitious composites. Several conclusions can be drawn from this experimental research.

- Maximum flexural strength was obtained by utilizing mix design OPC/GGBS composites reinforced with DPF 2 wt.% and 10 mm length with an increase of 79.55% and 57.12% at 7 and 28 days respectively when cured in a water bath. Moreover, maximum compressive strength was obtained by utilizing mix design OPC/GGBS composites reinforced with DPF 2 wt.% and 10 mm length with an increase of 13.14% and 30.97% at 7 and 28 days respectively when cured in a water bath.
- Alkali surface treatment, aqueous NaOH solution, of DPF can conclusively induce enhancement, approximately 10%, of the interfacial bonding between the DPF and the binder matrix system. Hence, this reinforced the idea that for the purposes of generating cementitious composites with promising results, the fibres must undergo treatment prior to the mixing stages.
- Effect of curing conditions has a major impact on the hydration of the binder to produce an HCP with enhanced strength.
- Treated DPFCC had lower water absorption rates in comparison to untreated DPFCC for both water and air curing conditions. The rate of water absorption is directly proportional to the amount of DPF available in the composite and the rate of water absorption of air cured samples is significantly higher than water cured samples. The highest water absorption rate for untreated and treated DPFCC, air cured, was for design mix OPC/GGBS composites reinforced with DPF 3 wt.% and 40 mm length with 17.31 % and 15.68 % respectively at 28 days.
- Microstructural analysis of the samples confirmed the scientific analysis discussed while presenting and analysing the results

Thus, we can conclude that this experimental study has accomplished a successful outcome in utilizing DPF in reinforcing cementitious composites. However, a true success can only be experienced when the aims of this paper are met on an industrial scale. Also, further

researchers are required to broaden the understanding of natural fibre or DPF usage within cementitious mortars. This paper recommends to such researchers to indulge in topics that can be compartmentalized as follows:

- Fibre features: Factors including crack abridgement, water and chloride permeability, durability and more physical property investigation should be done. Also, accelerated ageing tests should be employed for DPF reinforced mortars because although the usage of such composites promotes long lives due to post – crack performance, the fibres are organic products. Therefore, due to possible fungal and bacterial attacks, investigations regarding the deterioration of DPF reinforced composites under different exposure conditions need to be conducted.
- Treatment features: Bio-based treatments should be tested for better environmental impact

Chapter 8: Conclusions and Recommendations

8.1. Summary of the research

NF and its composites have been extensively researched and well established in both industrial and scientific sectors. However, DPF have not yet been extensively investigated thus with the current progress towards sustainability and producing environmentally friendly materials and composites along with the reduction of agricultural biomass waste, a great attention on optimal utilization of DPF in the MENA region became significant as it is considered the most abundant agricultural biomass waste that has good physical, chemical and mechanical properties being abundantly available at a very low cost. This would be superior if DPF become a replacement to synthetic fibres.

Throughout this research study, investigations, and developments of DPF reinforced composites through holistic and systematic approaches where the results obtained are interpreted to generate better understanding mechanisms of formulation and performance of the developed composites. Different approaches were investigated where the evaluation of DPF characteristics were investigated with thermoplastics (RPVC and PLA), thermoset (UPR) and cementitious (OPC and OPC/GGBS) matrix systems to understand the effect of DPF geometry and the effect of matrix system and its processing conditions on the physical and mechanical properties of the composites developed.

8.2. Major conclusions

The scientific contribution attributed from this research investigation can be summarized as the following five conclusive statements:

1) DPF is the most abundant agricultural biomass waste material in the MENA region, more than 3.6 million tons produced annually deposited onto landfills or burnt. DPF physical and mechanical characteristics highlights its importance in utilization for sustainable composite development and reducing its negative environmental impact as a waste material due to their, low cost, high durability, abundancy, physical and mechanical properties. The correlation between its characteristics and abundancy highlights its significance in utilization with various matrix systems. However, extensive research is required to support this utilization and upscaling it to examine its feasibility with various industrial applications. The gaps in literature were identified where the investigation and novel approaches where planned and conducted.
2) Various factors can influence the physical and mechanical properties of DPF while surface modification, removing surface impurities, such as the surface morphology,

microstructure, crystallinity, which can be significantly altered by subjecting the fibre to various surface treatments, (i.e. physical and chemical treatment) where the expose of the fibre to the modification parameters (i.e. duration and concentration) play a vital role in restructuring its internal structure and providing a more porous topography to enhance the interfacial bonding when used as a reinforcement with various hydrophobic matrix systems. Optimal tensile test results were obtained for DPF soaked in 6% NaOH solution for 24 hours. The chemical composition showed a decrease in lignin content of and an increase in cellulose. Thus, various surface treatments and various soaking concentrations and durations had different effect on the characteristics of DPF. Starch solution treatment showed positive results but not as effective as NaOH treatment. However, starch treatment does not have a negative environmental impact as NaOH.

3) The effect of DPF characteristics such as fibre geometry, (i.e. diameter and length), particle distribution, density and loading content were investigated and examined with both polymeric and inorganic matrix systems. Investigating the effect of DPF geometry (≤125 µm, 125 – 250 µm, 250 – 500 µm, 500 – 1,000 µm, ≥1000 µm, and unsieved) and loading content (10, 20, 30, 40 wt.%) with RPVC and PLA matrix systems. The utilization of DPF showed a reduction in the overall strength, flexural, impact and tensile strength, when reinforced with RPVC and PLA. Different DPF particle distributions and sieve sizes had different densities which has an influence on the homogeneity mixing of the composite. Also, different types of thermoplastic polymer showed different bonding with different DPF sieve size depending on its molecular weight. On the other hand, UPR reinforced with DPF showed enhanced mechanical strength. This highlights that the matrix system has a vital role in bonding with DPF depending on its molecular weight which aids in penetrating into the DPF and enhance its interfacial bonding while processing. Although, the mechanical strength of thermoplastic polymers reinforced with DPF decreased, which was mainly due to their hydrophilic nature that can be improved by applying surface modification. However, this utilization can substitute 40 wt.% of RPVC which are PBP and made from crude oil, thus decreasing the cost of the material, and decreasing the plastic consumption by developing products for non-structural applications. The biodegradation and fungal decay of the composites developed showed significant results where their implementation in the construction sector to similar to WPC products is feasible. Moreover, utilizing DPF for with bio-based thermoplastic, PLA, showed that the composite can be successfully degraded by earth worm that can develop vermicompost as manure. This highlights the feasibility of DPF to be utilized within the circular economy scheme by developing fully sustainable and biodegradable

composites. Also, as a first study to predict the strength of DPF composites, various scenarios where evaluated to understand DPF orientation within the composites developed and its effect on the strength of the composite. It was deduced that orientation of fibres can be expected in the flow direction of the compression moulding for short natural fibres. Model 1 showed that numerical results were deviated from the experimental results due to DPF is not oriented in the direction of tensile force. Model 2 predicted that DPF contributed with only 20% of its modulus to the PLA/DPF composite and the fibre are aligned perpendicular to the direction of the tensile force. Model 3 showed the validation of numerical simulation with the experimental results and identified that DPF is oriented 0° to 45° in the direction of compression melt flow. Future work can be done for developing short DPF composite using injection moulding and duplicate this methodology of analysis to further identify the numerical correlation for fibre orientation in short fibre DPF composite. Furthermore, FEM simulation of Lab Scale compression moulding machines exhibits the probability of fibre orientation limits from 0° to 30° on the compression load direction. Based on FEM results, the theories for elastic modulus of short fibre reinforced composite materials for Lab Scale compression moulding process were developed using the calculation of force sustained by fibres crossing the scan line. The model exhibits similar trajectory with the experimental results with minor deviations due to the assumption of strong bond between the fibre and matrix. The mathematical model clearly explains the concept behind the elastic modulus of short fibre composite prepared using lab scale compression moulding. Fibres tends to align in the direction of the compression force, so Elastic modulus at compression direction is always higher than other direction of the testing samples. Predicted Elastic modulus of reinforced short fibre composite can be applicable to all short fibres whose length is equal or lesser than the thickness of the compression moulded samples and consider density of the fibre is lesser than the density of the matrix.

4) Processing parameters were investigated by varying the processing temperature (90 and 110 ^{o}C), processing loading weight applied (10 ton, 15 ton and 20 ton) and the duration of processing (3, 6 and 9 min). The effect on both the physical and mechanical properties has been investigated to understand the mechanisms of changing properties and their correlation to the strength of the composites. The main effect was that each processing parameter had different effect on the composites developed. The increase in temperature from 90 to 100 ^{o}C showed enhancement on the mechanical properties.
5) The mechanism and knowledge on the effect of DPF length (10, 20, 30 and 40 mm), loading content, (1, 2 and 3 wt.% of binder), curing conditions, surface modification

and matrix type on the mechanical and physical properties of DPF reinforced with inorganic matrix system by both using OPC as a pure matrix and substituting half of the OPC with waste pozzolanic material, GGBS, proved to enhance the flexural and compressive strength of the mortars developed by 57.12% and 30.97% respectively. This was achieved by utilizing 20 mm DPF length loaded at 1 wt.% cured in a water bath for 28 days. The effect of curing conditions showed that water cured composites have a significant enhancement in strength which is an attribute to the hydration of cement. Long DPF, 40 mm at high loading content affected the workability of the composite where the fibres showed agglomerations which led to a reduction in both flexural and compressive strength. Results can be compared to substituting synthetic fibres (i.e. glass fibres) as mortar reinforcement which can be successfully utilizing in the construction sector.

8.3. Future work recommendations

This work has established significant contributions to the utilization of DPT agricultural biomass waste. However, continuation and expanding the scope of research in this field to achieve future industrialization products are listed as follow:

- Investigating bio-based surface treatment, that has negative environmental impact on the environment, for DPF to achieve better interfacial bonding to between different matrix systems to develop composites with enhanced mechanical and physical properties.
- The effect of DPF geometry on the biodegradation characteristics when PLA is used as the polymer matrix has been investigated. Different types of biodegradation and in-depth research should be investigated. Also, other bio-based polymers should be investigated, and different biodegradation test conditions should be evaluated to have an enhanced knowledge on the bio-degradation characteristics of DPF reinforced bio-based composites.
- This research investigation has demonstrated that DPF composites are highly affected by the processing parameters. Thus, it is suggested to investigate the effect of other processing parameters (i.e. melt-mixing parameters, injection moulding parameters, 3D printing parameters) and establishing a data base where statistical approach can be applied to produce a model that can aid in upscaling the production of DPF composite with a demo pilot to demonstrate and explore the feasibility in production of DPF composite through various processing technologies.
- Thermo-physical characteristics of DPF composites should be thoroughly investigated where its utilization in developing insulation material could be a new area to be

explored by researchers. Also, DPF with small fibre size, (125 – 250 µm), was observed to a potential substitution in developing vacuum insulation panels (VIP) by substituting fume silica and perlite, where initial experimental trial where carried and positive results were obtained.

- Life Cycle Assessment (LCA) could be performed to analyse the environmental impact of developing composites with DPF along with the life span of the composite from extracting the fibres, processing, and producing the composite. This will present the effect of utilization of DPF on the environment which will aid in exploring its effect on the environment at different stages of its life span.

References

[1] Choudhury R. NATURAL FIBRE REINFRICED CEMENTITIOUS COMPOSITE. Brunel University London, 2020.

[2] Fabris P. Building Desig and Construction 2018. https://www.bdcnetwork.com/global-construction-waste-almost-double-2025 (accessed February 26, 2021).

[3] United Nations n.d. https://sdgs.un.org/goals (accessed January 6, 2022).

[4] Witayakran S, Smitthipong W, Wangpradid R, Chollakup R, Clouston PL. Natural Fiber Composites: Review of Recent Automotive Trends. Elsevier Ltd.; 2017. https://doi.org/10.1016/b978-0-12-803581-8.04180-1.

[5] Rajak DK, Pagar DD, Menezes PL, Linul E. Fiber-reinforced polymer composites: Manufacturing, properties, and applications. Polymers (Basel) 2019;11. https://doi.org/10.3390/polym11101667.

[6] Yin S, Tuladhar R, Shi F, Combe M, Collister T, Sivakugan N. Use of macro plastic fibres in concrete: A review. Constr Build Mater 2015;93:180–8. https://doi.org/10.1016/j.conbuildmat.2015.05.105.

[7] Statista n.d. https://www.statista.com/statistics/741368/world-synthetic-fiber-production/ (accessed June 28, 2021).

[8] Alsaeed T, Yousif BF, Ku H. The potential of using date palm fibres as reinforcement for polymeric composites. Mater Des 2013;43:177–84. https://doi.org/10.1016/j.matdes.2012.06.061.

[9] Herrera-Franco PJ, Valadez-González A. Mechanical properties of continuous natural fibre-reinforced polymer composites. Compos Part A Appl Sci Manuf 2004;35:339–45. https://doi.org/10.1016/j.compositesa.2003.09.012.

[10] Madurwar M V., Ralegaonkar R V., Mandavgane SA. Application of agro-waste for sustainable construction materials: A review. Constr Build Mater 2013;38:872–8. https://doi.org/10.1016/j.conbuildmat.2012.09.011.

[11] Ozerkan NG, Ahsan B, Mansour S, Iyengar SR. Mechanical performance and durability of treated palm fiber reinforced mortars. Int J Sustain Built Environ 2013;2:131–42. https://doi.org/10.1016/j.ijsbe.2014.04.002.

[12] Awad S, Zhou Y, Katsou E, Li Y, Fan M. A Critical Review on Date Palm Tree (Phoenix dactylifera L.) Fibres and Their Uses in Bio-composites. Springer Netherlands; 2020.

https://doi.org/10.1007/s12649-020-01105-2.

[13] Taha I, Steuernagel L, Ziegmann G. Chemical Modifi cation of Date Palm Mesh Fibres for Reinforcement of Polymeric Materials. Part I Examination of Different Cleaning Methods. Polym Polym Compos 2006;14:767–78. https://doi.org/10.1177/096739110601400802.

[14] Lahouioui M, Ben Arfi R, Fois M, Ibos L, Ghorbal A. Investigation of Fiber Surface Treatment Effect on Thermal, Mechanical and Acoustical Properties of Date Palm Fiber-Reinforced Cementitious Composites. Waste and Biomass Valorization 2019. https://doi.org/10.1007/s12649-019-00745-3.

[15] Amirou S, Zerizer A, Haddadou I, Merlin A. Effects of corona discharge treatment on the mechanical properties of biocomposites from polylactic acid and Algerian date palm fibres. Sci Res Essays, 2013;8:946–52. https://doi.org/10.5897/SRE2013.5507.

[16] Matuana LM, Woodhams RT, Balatinecz JJ, Park CB. Influence of interfacial interactions on the properties of PVC/cellulosic fiber composites. Polym Compos 1998;19:446–55. https://doi.org/10.1002/pc.10119.

[17] Pickering KL, Beckermann GW, Alam SN, Foreman NJ. Optimising industrial hemp fibre for composites. Compos Part A Appl Sci Manuf 2007;38:461–8. https://doi.org/10.1016/j.compositesa.2006.02.020.

[18] Zhou F, Cheng G, Jiang B. Effect of silane treatment on microstructure of sisal fibers. Appl Surf Sci 2014;292:806–12. https://doi.org/10.1016/j.apsusc.2013.12.054.

[19] Mittal V, Saini R, Sinha S. Natural fiber-mediated epoxy composites - A review. Compos Part B Eng 2016;99:425–35. https://doi.org/10.1016/j.compositesb.2016.06.051.

[20] Kriker A, Debicki G, Bali A, Khenfer MM, Chabannet M. Mechanical properties of date palm fibres and concrete reinforced with date palm fibres in hot-dry climate. Cem. Concr. Compos., vol. 27, 2005, p. 554–64. https://doi.org/10.1016/j.cemconcomp.2004.09.015.

[21] Raut AN, Gomez CP. Thermal and mechanical performance of oil palm fiber reinforced mortar utilizing palm oil fly ash as a complementary binder. Constr Build Mater 2016;126:476–83. https://doi.org/10.1016/j.conbuildmat.2016.09.034.

[22] Tioua T, Kriker A, Barluenga G, Palomar I. Influence of date palm fiber and shrinkage reducing admixture on self-compacting concrete performance at early age in hot-dry environment. Constr Build Mater 2017;154:721–33.

https://doi.org/10.1016/j.conbuildmat.2017.07.229.

[23] Jambeck JR, Geyar R, Wilcox C, Siegler TR, Perryman M, Andrady A, et al. Plastic waste inputs from land into the ocean. Science (80-) 2015;347:768–71. https://doi.org/DOI: 10.1126/science.1260352.

[24] Awad S, Ghaffar SH, Hamouda T, Midani M, Katsou E, Fan M. Critical evaluation of date palm sheath fibre characteristics as a reinforcement for developing sustainable cementitious composites from waste materials. Biomass Convers Biorefinery 2022. https://doi.org/10.1007/s13399-022-02759-9.

[25] Lahouioui M, Ben Arfi R, Fois M, Ibos L, Ghorbal A. Investigation of Fiber Surface Treatment Effect on Thermal, Mechanical and Acoustical Properties of Date Palm Fiber-Reinforced Cementitious Composites. Waste and Biomass Valorization 2020;11:4441–55. https://doi.org/10.1007/s12649-019-00745-3.

[26] Ekundayo G, Adejuyigbe S. Reviewing the Development of Natural Fiber Polymer Composite: A Case Study of Sisal and Jute. Am J Mech Mater Eng 2019;3:1. https://doi.org/10.11648/j.ajmme.20190301.11.

[27] Peças P, Carvalho H, Salman H, Leite M. Natural Fibre Composites and Their Applications: A Review. J Compos Sci 2018;2:66. https://doi.org/10.3390/jcs2040066.

[28] Dittenber DB, Gangarao HVS. Critical review of recent publications on use of natural composites in infrastructure. Compos Part A Appl Sci Manuf 2012;43:1419–29. https://doi.org/10.1016/j.compositesa.2011.11.019.

[29] Pickering KL, Efendy MGA, Le TM. A review of recent developments in natural fibre composites and their mechanical performance. Compos Part A Appl Sci Manuf 2016;83:98–112. https://doi.org/10.1016/j.compositesa.2015.08.038.

[30] Mahir FI, Keya KN, Sarker B, Nahiun KM, Khan RA. A brief review on natural fiber used as a replacement of synthetic fiber in polymer composites. Mater Eng Res 2019;1:88–99. https://doi.org/10.25082/mer.2019.02.007.

[31] Mohammed L, Ansari MNM, Pua G, Jawaid M, Islam MS. A Review on Natural Fiber Reinforced Polymer Composite and Its Applications. Int J Polym Sci 2015;2015. https://doi.org/10.1155/2015/243947.

[32] Faruk O, Bledzki AK, Fink HP, Sain M. Biocomposites reinforced with natural fibers: 2000-2010. Prog Polym Sci 2012;37:1552–96. https://doi.org/10.1016/j.progpolymsci.2012.04.003.

[33] Koronis G, Silva A, Fontul M. Green composites: A review of adequate materials for automotive applications. Compos Part B Eng 2013;44:120–7. https://doi.org/10.1016/j.compositesb.2012.07.004.

[34] Ho MP, Wang H, Lee JH, Ho CK, Lau KT, Leng J, et al. Critical factors on manufacturing processes of natural fibre composites. Compos Part B Eng 2012;43:3549–62. https://doi.org/10.1016/j.compositesb.2011.10.001.

[35] Rouway M, Nachtane M, Tarfaoui M, Chakhchaoui N, Omari LH, Fraija F, et al. Prediction of Mechanical Performance of Natural Fibers Polypropylene Composites: A Comparison Study. IOP Conf Ser Mater Sci Eng 2020;948. https://doi.org/10.1088/1757-899X/948/1/012031.

[36] Alhijazi M, Safaei B, Zeeshan Q, Asmael M. Modeling and simulation of the elastic properties of natural fiber-reinforced thermosets. Polym Compos 2021;42:3508–17. https://doi.org/10.1002/pc.26075.

[37] Majeed K, Jawaid M, Hassan A, Abu Bakar A, Abdul Khalil HPS, Salema AA, et al. Potential materials for food packaging from nanoclay/natural fibres filled hybrid composites. Mater Des 2013;46:391–410. https://doi.org/10.1016/j.matdes.2012.10.044.

[38] Krishnaiah P. Krishnaiah, Prakash (2017) Development of polylactide and polypropylene composites reinforced with sisal fibres and halloysite nanotubes for automotive and structural engineering applications. The University of Nottingham, 2017.

[39] Dicker MPM, Duckworth PF, Baker AB, Francois G, Hazzard MK, Weaver PM. Green composites: A review of material attributes and complementary applications. Compos Part A Appl Sci Manuf 2014;56:280–9. https://doi.org/10.1016/j.compositesa.2013.10.014.

[40] ANGGRAINI V. Potential of Coir Fibres as Soil Reinforcement. Pertanika J Sch Res Rev 2016.

[41] Zhu C, Richardson RM, Potter KD, Koutsomitopoulou AF, Van Duijneveldt JS, Vincent SR, et al. High modulus regenerated cellulose fibers spun from a low molecular weight microcrystalline cellulose solution. ACS Sustain Chem Eng 2016;4:4545–53. https://doi.org/10.1021/acssuschemeng.6b00555.

[42] Bledzki A., Gassan J. Composites reinforced with cellulose_Bledzki_1999.pdf. Prog Polym Sci 1999;24:221–74.

[43] Li X, Tabil LG, Panigrahi S. Chemical treatments of natural fiber for use in natural fiber-reinforced composites: A review. J Polym Environ 2007;15:25–33. https://doi.org/10.1007/s10924-006-0042-3.

[44] Gurunathan T, Mohanty S, Nayak SK. A review of the recent developments in biocomposites based on natural fibres and their application perspectives. Compos Part A Appl Sci Manuf 2015;77:1–25. https://doi.org/10.1016/j.compositesa.2015.06.007.

[45] Abd Rabou AFN, Radwan ES. The current status of the date palm (Phoenix dactylifera) and its uses in the Gaza Strip, Palestine. Biodiversitas 2017;18:1047–61. https://doi.org/10.13057/biodiv/d180324.

[46] Al-Alawi R, Al-Mashiqri JH, Al-Nadabi JSM, Al-Shihi BI, Baqi Y. Date palm tree (Phoenix dactylifera L.): Natural products and therapeutic options. Front Plant Sci 2017;8. https://doi.org/10.3389/fpls.2017.00845.

[47] Ghori W, Saba N, Jawaid M, Asim M. A review on date palm (phoenix dactylifera) fibers and its polymer composites. IOP Conf. Ser. Mater. Sci. Eng., vol. 368, Institute of Physics Publishing; 2018. https://doi.org/10.1088/1757-899X/368/1/012009.

[48] Jaradat AA, Zaid A. Quality traits of date palm fruits in a center of origin and center of diversity. Food, Agric Environ 2004;2:208–17.

[49] Bouguedoura N, Bennaceur M, Babahani S, Benziouche SE. Date Palm Status and Perspective in Algeria. Date Palm Genet Resour Util 2015:125–68. https://doi.org/DOI https://doi.org/10.1007/978-94-017-9694-1_4.

[50] Chao CCT, Krueger RR. The date palm (Phoenix dactylifera L.): Overview of biology, uses, and cultivation. HortScience 2007;42:1077–82. https://doi.org/10.21273/hortsci.42.5.1077.

[51] Al-Oqla FM, Sapuan SM. Natural fiber reinforced polymer composites in industrial applications: Feasibility of date palm fibers for sustainable automotive industry. J Clean Prod 2014;66:347–54. https://doi.org/10.1016/j.jclepro.2013.10.050.

[52] Nasser RA, Salem MZM, Hiziroglu S, Al-Mefarrej HA, Mohareb AS, Alam M, et al. Chemical analysis of different parts of date palm (Phoenix dactylifera L.) using ultimate, proximate and thermo-gravimetric techniques for energy production. Energies 2016;9. https://doi.org/10.3390/en9050374.

[53] Al-Oqla FM, Alothman OY, Jawaid M, Sapuan SM, Es-Saheb MH. Processing and properties of date palm fibers and its composites. Biomass Bioenergy Process. Prop.,

vol. 9783319076416, Springer International Publishing; 2014, p. 1–25. https://doi.org/10.1007/978-3-319-07641-6_1.

[54] Elseify LA, Midani M, Shihata LA, El-Mously H. Review on cellulosic fibers extracted from date palms (Phoenix Dactylifera L.) and their applications. Cellulose 2019;26:2209–32. https://doi.org/10.1007/s10570-019-02259-6.

[55] Barreveld WH. Date palm products. illustrate. Food and Agriculture Organization of the United Nations; 1993.

[56] Chandrasekaran M, Bahkali AH. Valorization of date palm (Phoenix dactylifera) fruit processing by-products and wastes using bioprocess technology - Review. Saudi J Biol Sci 2013;20:105–20. https://doi.org/10.1016/j.sjbs.2012.12.004.

[57] Asim M, Abdan K, Jawaid M, Nasir M, Dashtizadeh Z, Ishak MR, et al. A review on pineapple leaves fibre and its composites. Int J Polym Sci 2015;2015. https://doi.org/10.1155/2015/950567.

[58] Komuraiah A, Kumar NS, Prasad BD. Chemical Composition of Natural Fibers and its Influence on their Mechanical Properties. Mech Compos Mater 2014;50:359–76. https://doi.org/10.1007/s11029-014-9422-2.

[59] Azwa ZN, Yousif BF, Manalo AC, Karunasena W. A review on the degradability of polymeric composites based on natural fibres. Mater Des 2013;47:424–42. https://doi.org/10.1016/j.matdes.2012.11.025.

[60] John MJ, Anandjiwala RD, Pothan LA, Thomas S. Cellulosic fibre-reinforced green composites. Compos Interfaces 2007;14:733–51. https://doi.org/10.1163/156855407782106546.

[61] John MJ, Thomas S. Biofibres and biocomposites. Carbohydr Polym 2008;71:343–64. https://doi.org/10.1016/j.carbpol.2007.05.040.

[62] El-Morsy M. Studies on the Rachises of the Egyptian Date Palm Leaves for Hardboard Production. Fibre Sci Technol 1980;13:317–23.

[63] Pandey SN, Ghosh SK. The chemical nature of date-palm (phoenix dactylifera- l) leaf fibre. J Text Inst 1995;86:487–9. https://doi.org/10.1080/00405009508658775.

[64] Al-Kaabi K, Al-Khanbashi A, Hammami A. Date palm fibers as polymeric matrix reinforcement: DPF/polyester composite properties. Polym Compos 2005;26:604–13. https://doi.org/10.1002/pc.20130.

[65] Khristova P, Kordsachia O, Khider T. Alkaline pulping with additives of date palm rachis

and leaves from Sudan. Bioresour Technol 2005;96:79–85. https://doi.org/10.1016/j.biortech.2003.05.005.

[66] Kaddami H, Dufresne A, Khelifi B, Bendahou A, Taourirte M, Raihane M, et al. Short palm tree fibers - Thermoset matrices composites. Compos Part A Appl Sci Manuf 2006;37:1413–22. https://doi.org/10.1016/j.compositesa.2005.06.020.

[67] Bendahou A, Dufresne A, Kaddami H, Habibi Y. Isolation and structural characterization of hemicelluloses from palm of Phoenix dactylifera L. Carbohydr Polym 2007;68:601–8. https://doi.org/10.1016/j.carbpol.2006.10.016.

[68] Sbiai A, Kaddami H, Fleury E, Maazouz A, Erchiqui F, Koubaa A, et al. Effect of the fiber size on the physicochemical and mechanical properties of composites of epoxy and date palm tree fibers. Macromol Mater Eng 2008;293:684–91. https://doi.org/10.1002/mame.200800087.

[69] Sbiai A, Kaddami H, Sautereau H, Maazouz A, Fleury E. TEMPO-mediated oxidation of lignocellulosic fibers from date palm leaves. Carbohydr Polym 2011;86:1445–50. https://doi.org/10.1016/j.carbpol.2011.06.005.

[70] Mahdavi S, Kermanian H, Varshoei A. Date palm properties. vol. 5. 2010.

[71] Khiari R, Mhenni MF, Belgacem MN, Mauret E. Chemical composition and pulping of date palm rachis and Posidonia oceanica - A comparison with other wood and non-wood fibre sources. Bioresour Technol 2010;101:775–80. https://doi.org/10.1016/j.biortech.2009.08.079.

[72] Nasser RA, Al-Mefarrej HA. Midribs of Date Palm as a Raw Material for Wood-Cement Composite Industry in Saudi Arabia. World Appl Sci J 2011;15:1651–8.

[73] Saadaoui N, Rouilly A, Fares K, Rigal L. Characterization of date palm lignocellulosic by-products and self-bonded composite materials obtained thereof. Mater Des 2013;50:302–8. https://doi.org/10.1016/j.matdes.2013.03.011.

[74] Mirmehdi SM, Zeinaly F, Dabbagh F. Date palm wood flour as filler of linear low-density polyethylene. Compos Part B Eng 2014;56:137–41. https://doi.org/10.1016/j.compositesb.2013.08.008.

[75] Mohanty JR, Das SN, Das HC, Swain SK. Effect of chemically modified date palm leaf fiber on mechanical, thermal and rheological properties of polyvinylpyrrolidone. Fibers Polym 2014;15:1062–70. https://doi.org/10.1007/s12221-014-1062-6.

[76] Almi K, Benchabane A, Lakel S, Kriker A. Potential utilization of date palm wood as

composite reinforcement. J Reinf Plast Compos 2015;34:1231–40. https://doi.org/10.1177/0731684415588356.

[77] Hegazy S, Ahmed K. Effect of Date Palm Cultivar, Particle Size, Panel Density and Hot Water Extraction on Particleboards Manufactured from Date Palm Fronds. Agriculture 2015;5:267–85. https://doi.org/10.3390/agriculture5020267.

[78] Zhang T, Guo M, Cheng L, Li X. Investigations on the structure and properties of palm leaf sheath fiber. Cellulose 2015;22:1039–51. https://doi.org/10.1007/s10570-015-0570-x.

[79] Mekhermeche A, Kriker A, Dahmani S. Contribution to the study of thermal properties of clay bricks reinforced by date palm fiber. AIP Conf. Proc., vol. 1758, American Institute of Physics Inc.; 2016. https://doi.org/10.1063/1.4959400.

[80] Bourmaud A, Dhakal H, Habrant A, Padovani J, Siniscalco D, Ramage MH, et al. Exploring the potential of waste leaf sheath date palm fibres for composite reinforcement through a structural and mechanical analysis. Compos Part A Appl Sci Manuf 2017;103:292–303. https://doi.org/10.1016/j.compositesa.2017.10.017.

[81] Saleh MA, Al Haron MH, Saleh AA, Farag M. Fatigue behavior and life prediction of biodegradable composites of starch reinforced with date palm fibers. Int J Fatigue 2017;103:216–22. https://doi.org/10.1016/j.ijfatigue.2017.06.005.

[82] Adel A, El-Shafei A, Ibrahim A, Al-Shemy M. Extraction of oxidized nanocellulose from date palm (Phoenix Dactylifera L.) sheath fibers: Influence of CI and CII polymorphs on the properties of chitosan/bionanocomposite films. Ind Crops Prod 2018;124:155–65. https://doi.org/10.1016/j.indcrop.2018.07.073.

[83] Alshammari BA, Saba N, Alotaibi MD, Alotibi MF, Jawaid M, Alothman OY. Evaluation of mechanical, physical, and morphological properties of epoxy composites reinforced with different date palm fillers. Materials (Basel) 2019;12. https://doi.org/10.3390/ma12132145.

[84] Gheith MH, Aziz MA, Ghori W, Saba N, Asim M, Jawaid M, et al. Flexural, thermal and dynamic mechanical properties of date palm fibres reinforced epoxy composites. J Mater Res Technol 2019;8:853–60. https://doi.org/10.1016/j.jmrt.2018.06.013.

[85] Raghavendra S, Lokesh GN. Evaluation of mechanical properties in date palm fronds polymer composites. AIP Conf Proc 2019;2057. https://doi.org/https://doi.org/10.1063/1.5085592.

[86] Belgacem C, Serra-Parareda F, Tarrés Q, Mutjé P, Delgado-Aguilar M, Boufi S. The integral utilization of date palm waste to produce plastic composites. Polymers (Basel) 2021;13. https://doi.org/10.3390/polym13142335.

[87] Raza M, Abu-Jdayil B, Al-Marzouqi AH, Inayat A. Kinetic and thermodynamic analyses of date palm surface fibers pyrolysis using Coats-Redfern method. Renew Energy 2022;183:67–77. https://doi.org/10.1016/j.renene.2021.10.065.

[88] Alves C, Ferrão PMC, Silva AJ, Reis LG, Freitas M, Rodrigues LB, et al. Ecodesign of automotive components making use of natural jute fiber composites. J Clean Prod 2010;18:313–27. https://doi.org/10.1016/j.jclepro.2009.10.022.

[89] Al-Khanbashi A, Al-Kaabi K, Hammami A. Date palm fibers as polymeric matrix reinforcement: Fiber characterization. Polym Compos 2005;26:486–97. https://doi.org/10.1002/pc.20118.

[90] Abu-Sharkh BF, Hamid H. Degradation study of date palm fibre/polypropylene composites in natural and artificial weathering: Mechanical and thermal analysis. Polym. Degrad. Stab., vol. 85, Elsevier Ltd; 2004, p. 967–73. https://doi.org/10.1016/j.polymdegradstab.2003.10.022.

[91] Kriker A, Bali A, Debicki G, Bouziane M, Chabannet M. Durability of date palm fibres and their use as reinforcement in hot dry climates. Cem Concr Compos 2008;30:639–48. https://doi.org/10.1016/j.cemconcomp.2007.11.006.

[92] Rao KMM, Rao KM. Extraction and tensile properties of natural fibers: Vakka, date and bamboo. Compos Struct 2007;77:288–95. https://doi.org/10.1016/j.compstruct.2005.07.023.

[93] Abdal-Hay A, Suardana NPG, Jung DY, Choi KS, Lim JK. Effect of diameters and alkali treatment on the tensile properties of date palm fiber reinforced epoxy composites. Int J Precis Eng Manuf 2012;13:1199–206. https://doi.org/10.1007/s12541-012-0159-3.

[94] Hassan ML, Bras J, Hassan EA, Silard C, Mauret E. Enzyme-assisted isolation of microfibrillated cellulose from date palm fruit stalks. Ind Crops Prod 2014;55:102–8. https://doi.org/10.1016/j.indcrop.2014.01.055.

[95] Alajmi M, Shalwan A. Correlation between mechanical properties with specific wear rate and the coefficient of friction of graphite/epoxy composites. Materials (Basel) 2015;8:4162–75. https://doi.org/10.3390/ma8074162.

[96] Elwaleed AK, Nikabdullah N, Nor MJM, Tahir MFM, Zulkifli R. Sound absorption

properties of a low-density perforated date palm fibres panel. Int J Comput Appl Technol 2015;52:213–9.

[97] Hammood AS. Effect of erosion on water absorption and morphology for treated date palm fiber-reinforced polyester composites. Int J Mech Mechatronics Eng 2015;15:108–14.

[98] Al-Rifaie WN, Al-Niami M. Mechanical performance of date palm fibre-reinforced gypsums. Innov Infrastruct Solut 2016;1:1–7. https://doi.org/10.1007/s41062-016-0022-y.

[99] Boukhattem L, Boumhaout M, Hamdi H, Benhamou B, Ait Nouh F. Moisture content influence on the thermal conductivity of insulating building materials made from date palm fibers mesh. Constr Build Mater 2017;148:811–23. https://doi.org/10.1016/j.conbuildmat.2017.05.020.

[100] Wong KJ, Yousif BF, Low KO. The effects of alkali treatment on the interfacial adhesion of bamboo fibres. Proc Inst Mech Eng Part L J Mater Des Appl 2010;224:139–48. https://doi.org/10.1243/14644207JMDA304.

[101] Methacanon P, Weerawatsophon U, Sumransin N, Prahsarn C, Bergado DT. Properties and potential application of the selected natural fibers as limited life geotextiles. Carbohydr Polym 2010;82:1090–6. https://doi.org/10.1016/j.carbpol.2010.06.036.

[102] Elbadry EA. Agro-Residues: Surface Treatment and Characterization of Date Palm Tree Fiber as Composite Reinforcement. J Compos 2014;2014:1–8. https://doi.org/10.1155/2014/189128.

[103] Sisti L, Totaro G, Vannini M, Celli A. Retting Process as a Pretreatment of Natural Fibers for the Development of Polymer Composites. Lignocellul. Compos. Mater., Springer, Cham; 2017, p. 97–135.

[104] Donaghy J, Levett P, Haylock R. Changes in microbial populations during anaerobic flax retting. J Appl Bacteriol 1980;69:634–41.

[105] Mohanty A, Misra M, Drzal L, Selke S, Harte B, Hinrichsen G. Natural Fibers, Biopolymers, and Biocomposites. 2005.

[106] Ibrahim H, Farag M, Megahed H, Mehanny S. Characteristics of starch-based biodegradable composites reinforced with date palm and flax fibers. Carbohydr Polym 2014;101:11–9. https://doi.org/10.1016/j.carbpol.2013.08.051.

[107] Ibrahim H, Mehanny S, Darwish L, Farag M. A Comparative Study on the Mechanical

and Biodegradation Characteristics of Starch-Based Composites Reinforced with Different Lignocellulosic Fibers. J Polym Environ 2017;26:2434–47. https://doi.org/10.1007/s10924-017-1143-x.

[108] Agrawal R, Saxena N, Sharma K, Thomas S, Sreekala M. Activation energy and crystallization kinetics of untreated and treated oil palm fibre reinforced phenol formaldehyde composites. Mater Sci Eng 2000;277:77–82.

[109] Wazzan AA. The effect of surface treatment on the strength and adhesion characteristics of phoenix dactylifera-L(date palm) fibers. Int J Polym Mater Polym Biomater 2006;55:485–99. https://doi.org/10.1080/009140391001804.

[110] Oushabi A, Sair S, Oudrhiri Hassani F, Abboud Y, Tanane O, El Bouari A. The effect of alkali treatment on mechanical, morphological and thermal properties of date palm fibers (DPFs): Study of the interface of DPF–Polyurethane composite. South African J Chem Eng 2017;23:116–23. https://doi.org/10.1016/j.sajce.2017.04.005.

[111] Keener TJ, Stuart RK, Brown TK. Maleated coupling agents for natural fibre composites. Compos Part A Appl Sci Manuf 2004;35:357–62. https://doi.org/10.1016/j.compositesa.2003.09.014.

[112] Zhou Y, Fan M, Chen L. Interface and bonding mechanisms of plant fibre composites: An overview. Compos Part B Eng 2016;101:31–45. https://doi.org/10.1016/j.compositesb.2016.06.055.

[113] AlMaadeed MA, Nógellová Z, Janigová I, Krupa I. Improved mechanical properties of recycled linear low-density polyethylene composites filled with date palm wood powder. Mater Des 2014;58:209–16. https://doi.org/10.1016/j.matdes.2014.01.051.

[114] AlMaadeed MA, Nógellová Z, Mičušík M, Novák I, Krupa I. Mechanical, sorption and adhesive properties of composites based on low density polyethylene filled with date palm wood powder. Mater Des 2014;53:29–37. https://doi.org/10.1016/j.matdes.2013.05.093.

[115] Taha I, Steuernagel L, Ziegmann G. Optimization of the alkali treatment process of date palm fibres for polymeric composites. Compos Interfaces 2007;14:669–84. https://doi.org/10.1163/156855407782106528.

[116] Alawar A, Hamed AM, Al-Kaabi K. Characterization of treated date palm tree fiber as composite reinforcement. Compos Part B Eng 2009;40:601–6. https://doi.org/10.1016/j.compositesb.2009.04.018.

[117] Shalwan A, Yousif BF. Influence of date palm fibre and graphite filler on mechanical and wear characteristics of epoxy composites. Mater Des 2014;59:264–73. https://doi.org/10.1016/j.matdes.2014.02.066.

[118] Eslami-Farsani R. Effect of fiber treatment on the mechanical properties of date palm fiber reinforced PP/EPDM composites. Adv Compos Mater 2015;24:27–40. https://doi.org/10.1080/09243046.2013.871177.

[119] Aldousiri B, Alajmi M, Shalwan A. Mechanical properties of palm fibre reinforced recycled HDPE. Adv Mater Sci Eng 2013;2013. https://doi.org/10.1155/2013/508179.

[120] AlMaadeed MA, Kahraman R, Noorunnisa Khanam P, Al-Maadeed S. Characterization of untreated and treated male and female date palm leaves. Mater Des 2013;43:526–31. https://doi.org/10.1016/j.matdes.2012.07.028.

[121] Anyakora AN. Investigation of Impact Strength Properties of Oil and Date Palm Frond Fiber Reinforced Polyester Composites. Int J Curr Eng Technol Accept 2013;3.

[122] Dehghani A, Madadi Ardekani S, Al-Maadeed MA, Hassan A, Wahit MU. Mechanical and thermal properties of date palm leaf fiber reinforced recycled poly (ethylene terephthalate) composites. Mater Des 2013;52:841–8. https://doi.org/10.1016/j.matdes.2013.06.022.

[123] Mahmoudi N. Use of date palm fibers as reinforcement for thermoplastic-based composites. Mech Ind 2013;14:71–7. https://doi.org/10.1051/meca/2012043.

[124] Amroune S, Bezazi A, Belaadi A, Zhu C, Scarpa F, Rahatekar S, et al. Tensile mechanical properties and surface chemical sensitivity of technical fibres from date palm fruit branches (Phoenix dactylifera L.). Compos Part A Appl Sci Manuf 2015;71:95–106. https://doi.org/10.1016/j.compositesa.2014.12.011.

[125] Hammood AS. Effect of Erosion on Water Absorption and Morphology for Treated Date Palm Fiber-Reinforced Polyester Composites. Int J Mech Mechatronics Eng 2015;15.

[126] Aly NM, ElNashar DE. Polyester/Flax Biocomposites Reinforced Using Date Palm Leaves and Wood Flour As Fillers. Int J Eng Technol 2016;8.

[127] Sharath GP, Kishor BS, Vinod B, Naveen A. Effect of Fiber Length on the Mechanical Properties of Coir and Wild Date Palm Reinforced Epoxy Composites. IJSTE-International J Sci Technol Eng | 2016;2.

[128] Neher B, Bhuiyan MMR, Kabir H, Gafur MA, Qadir MR, Ahmed F. Thermal properties of palm fiber and palm fiber-reinforced ABS composite. J Therm Anal Calorim

2016;124:1281–9. https://doi.org/10.1007/s10973-016-5341-x.

[129] Tahri I, Devin IZ, Ruelle J, Segovia C, Brosse N. Extraction and Characterization of Fibers from Palm Tree. BioResources 2016;11. https://doi.org/10.15376/biores.11.3.7016-7025.

[130] Alzebdeh KI, Nassar MM, Al-Hadhrami MA, Al-Aamri O, Al-Defaai S, Al-Shuaily S. Characterization of mechanical properties of aligned date palm frond fiber-reinforced low density polyethylene. J Eng Res 2017;14:115–23. https://doi.org/10.24200/tjer.vol.14iss2pp115-123.

[131] Ladhar A, Arous M, Kaddami H, Ayadi Z, Kallel A. Correlation between the dielectric and the mechanical behavior of cellulose nanocomposites extracted from the rachis of the date palm tree. IOP Conf. Ser. Mater. Sci. Eng., vol. 258, Institute of Physics Publishing; 2017. https://doi.org/10.1088/1757-899X/258/1/012001.

[132] Zadeh KM, Inuwa IM, Arjmandi R, Hassan A, Almaadeed M, Mohamad Z, et al. Effects of date palm leaf fiber on the thermal and tensile properties of recycled ternary polyolefin blend composites. Fibers Polym 2017;18:1330–5. https://doi.org/10.1007/s12221-017-1106-9.

[133] Benzidane R, Sereir Z, Bennegadi ML, Doumalin P, Poilâne C. Morphology, static and fatigue behavior of a natural UD composite: The date palm petiole 'wood.' Compos Struct 2018;203:110–23. https://doi.org/10.1016/j.compstruct.2018.06.122.

[134] Boukettaya S, Alawar A, Almaskari F, Ben Daly H, Abdala A, Chatti S. Modeling of water diffusion mechanism in polypropylene/date palm fiber composite materials. J Compos Mater 2018;52:2651–9. https://doi.org/10.1177/0021998317752228.

[135] Swain PTR, Das SN, Jena SP. Manufacturing and Study of Thermo-Mechanical Behaviour of Surface Modified Date Palm Leaf/Glass Fiber Reinforced Hybrid Composite. Mater Today Proc 2018;5:18332–41.

[136] Alshabanat M. Morphological, thermal, and biodegradation properties of LLDPE/treated date palm waste composite buried in a soil environment. J Saudi Chem Soc 2019;23:355–64. https://doi.org/10.1016/j.jscs.2018.08.008.

[137] Geethamma VG, Mathew KT, Lakshminarayanan R, Thomas S. Composite of short coir fibres and natural rubber: Effect of chemical modification, loading and orientation of fibre. Polymer (Guildf) 1998;39:1483–91. https://doi.org/10.1016/S0032-3861(97)00422-9.

[138] Thomason JL, Vlug MA. Influence of fibre length and concentration on the properties of glass fibre-reinforced polypropylene: 4. Impact properties. Compos Part A Appl Sci Manuf 1997;28:277–88. https://doi.org/10.1016/S1359-835X(96)00127-3.

[139] Ashori A, Nourbakhsh A. Reinforced polypropylene composites: Effects of chemical compositions and particle size. Bioresour Technol 2010;101:2515–9. https://doi.org/10.1016/j.biortech.2009.11.022.

[140] AlMaadeed MA, Kahraman R, Noorunnisa Khanam P, Madi N. Date palm wood flour/glass fibre reinforced hybrid composites of recycled polypropylene: Mechanical and thermal properties. Mater Des 2012;42:289–94. https://doi.org/10.1016/j.matdes.2012.05.055.

[141] Asadzadeh M, R Khalili SM, EslamiFarsani R, Rafizadeh S. Bending Properties of Date Palm Fiber and Jute Fiber Reinforced Polymeric Composite. Int J Adv Des Manuf Technol 2012;5:59–63.

[142] Mahdi E, Hernández DR, Eltai EO. Effect of water absorption on the mechanical properties of long date palm leaf fiber reinforced epoxy composites. J Biobased Mater Bioenergy 2015;9:173–81. https://doi.org/10.1166/jbmb.2015.1508.

[143] Jamshidian M, Tehrany EA, Imran M, Jacquot M, Desobry S. Poly-Lactic Acid: Production, applications, nanocomposites, and release studies. Compr Rev Food Sci Food Saf 2010;9:552–71. https://doi.org/10.1111/j.1541-4337.2010.00126.x.

[144] Binhussain MA, El-Tonsy MM. Palm leave and plastic waste wood composite for out-door structures. Constr Build Mater 2013;47:1431–5. https://doi.org/10.1016/j.conbuildmat.2013.06.031.

[145] Dhakal H, Bourmaud A, Berzin F, Almansour F, Zhang Z, Shah DU, et al. Mechanical properties of leaf sheath date palm fibre waste biomass reinforced polycaprolactone (PCL) biocomposites. Ind Crops Prod 2018;126:394–402. https://doi.org/10.1016/j.indcrop.2018.10.044.

[146] Mlhem A, Abu-Jdayil B, Tong-Earn T, Iqbal M. Sustainable heat insulation composites from date palm fibre reinforced poly(β-hydroxybutyrate). J Build Eng 2022;54:104617. https://doi.org/10.1016/j.jobe.2022.104617.

[147] Masri T, Ounis H, Sedira L, Kaci A, Benchabane A. Characterization of new composite material based on date palm leaflets and expanded polystyrene wastes. Constr Build Mater 2018;164:410–8. https://doi.org/10.1016/j.conbuildmat.2017.12.197.

[148] Al-Sulaiman FA. Mechanical properties of date palm fiber reinforced composites. Appl Compos Mater 2002;9:369–77. https://doi.org/10.1023/A:1020216906846.

[149] Dehghani A, Madadi Ardekani S, Al-Maadeed MA, Hassan A, Wahit MU. Mechanical and thermal properties of date palm leaf fiber reinforced recycled poly (ethylene terephthalate) composites. Mater Des 2013;52:841–8. https://doi.org/10.1016/j.matdes.2013.06.022.

[150] Noorunnisa Khanam P, AlMaadeed MA. Improvement of ternary recycled polymer blend reinforced with date palm fibre. Mater Des 2014;60:532–9. https://doi.org/10.1016/j.matdes.2014.04.033.

[151] AL-Oqla FM, Hayajneh MT, Al-Shrida MM. Mechanical performance, thermal stability and morphological analysis of date palm fiber reinforced polypropylene composites toward functional bio-products. Cellulose 2022;29:3293–309. https://doi.org/10.1007/s10570-022-04498-6.

[152] Wazzan AA. Effect of fiber orientation on the mechanical properties and fracture characteristics of date palm fiber reinforced composites. Int J Polym Mater Polym Biomater 2005;54:213–25. https://doi.org/10.1080/00914030390246379.

[153] Sbiai A, Maazouz A, Fleury E, Sautereau H, Kaddami H, Einstein A. Short Date Palm Tree Fibers / Polyepoxy Composites Prepared Using RTM process: Effect Of Tempo Mediated Oxidation Of The Fibers. BioResources 2010;5:672–89.

[154] RA I. Effect of Date Palm Seeds on the Tribological Behaviour of Polyester Composites under Different Testing Conditions. J Mater Sci Eng 2015;04. https://doi.org/10.4172/2169-0022.1000206.

[155] Tripathy S, Dehury J, Mishra D. A Study on the effect of Surface treatment on the Physical and Mechanical properties of date-palm stem liber embedded epoxy composites. IOP Conf. Ser. Mater. Sci. Eng., vol. 115, Institute of Physics Publishing; 2016. https://doi.org/10.1088/1757-899X/115/1/012036.

[156] Salih SI, Jasim AS, Hasan AM. Investigation on Mechanical Properties of Hybrid Polymer Composite Reinforced by Rice Husks and Date Palm Fibers as a Construction Material. J Al-Nahrain Univ 2015;18:89–97. https://doi.org/10.22401/jnus.18.3.13.

[157] Saba N, Alothman OY, Almutairi Z, Jawaid M, Ghori W. Date palm reinforced epoxy composites: Tensile, impact and morphological properties. J Mater Res Technol 2019;8:3959–69. https://doi.org/10.1016/j.jmrt.2019.07.004.

[158] Asim M, Jawaid M, Khan A, Asiri AM, Malik MA. Effects of Date Palm fibres loading on mechanical, and thermal properties of Date Palm reinforced phenolic composites. J Mater Res Technol 2020:1–8. https://doi.org/10.1016/j.jmrt.2020.01.099.

[159] Asim M, Jawaid M, Fouad H, Alothman OY. Effect of surface modified date palm fibre loading on mechanical, thermal properties of date palm reinforced phenolic composites. Compos Struct 2021;267:113913. https://doi.org/10.1016/j.compstruct.2021.113913.

[160] Benmansour N, Agoudjil B, Gherabli A, Kareche A, Boudenne A. Thermal and mechanical performance of natural mortar reinforced with date palm fibers for use as insulating materials in building. Energy Build 2014;81:98–104. https://doi.org/10.1016/j.enbuild.2014.05.032.

[161] Abani S, Hafsi F, Kriker A, Bali A. Valorisation of Date Palm Fibres in Sahara Constructions. Energy Procedia, vol. 74, Elsevier Ltd; 2015, p. 289–93. https://doi.org/10.1016/j.egypro.2015.07.608.

[162] Vantadori S, Carpinteri A, Zanichelli A. Lightweight construction materials: Mortar reinforced with date-palm mesh fibres. Theor Appl Fract Mech 2019;100:39–45. https://doi.org/10.1016/j.tafmec.2018.12.011.

[163] Hamza S, Saad H, Charrier B, Ayed N, Charrier-El Bouhtoury F. Physico-chemical characterization of Tunisian plant fibers and its utilization as reinforcement for plaster based composites. Ind Crops Prod 2013;49:357–65. https://doi.org/10.1016/j.indcrop.2013.04.052.

[164] Mokhtari A, Kriker A, Guemmoula Y, Boukrioua A, Khenfer MM. Formulation and Characterization of Date Palm Fibers Mortar by Addition of Crushed Dune Sand. Energy Procedia, vol. 74, Elsevier Ltd; 2015, p. 344–50. https://doi.org/10.1016/j.egypro.2015.07.624.

[165] Alatshan F, Altlomate AM, Mashiri F, Alamin W. Effect of date palm fibers on the mechanical properties of concrete. Int J Sustain Build Technol Urban Dev 2017;8. https://doi.org/10.12972/susb.20170007.

[166] Boumhaout M, Boukhattem L, Hamdi H, Benhamou B, Ait Nouh F. Thermomechanical characterization of a bio-composite building material: Mortar reinforced with date palm fibers mesh. Constr Build Mater 2017;135:241–50. https://doi.org/10.1016/j.conbuildmat.2016.12.217.

[167] Benaimeche O, Carpinteri A, Mellas M, Ronchei C, Scorza D, Vantadori S. The influence of date palm mesh fibre reinforcement on flexural and fracture behaviour of a

cement-based mortar. Compos Part B Eng 2018;152:292–9. https://doi.org/10.1016/j.compositesb.2018.07.017.

[168] Chennouf N, Agoudjil B, Boudenne A, Benzarti K, Bouras F. Hygrothermal characterization of a new bio-based construction material: Concrete reinforced with date palm fibers. Constr Build Mater 2018;192:348–56. https://doi.org/10.1016/j.conbuildmat.2018.10.089.

[169] Zanichelli A, Carpinteri A, Fortese G, Ronchei C, Scorza D, Vantadori S. Contribution of date-palm fibres reinforcement to mortar fracture toughness. Procedia Struct. Integr., vol. 13, Elsevier B.V.; 2018, p. 542–7. https://doi.org/10.1016/j.prostr.2018.12.089.

[170] Kareche A, Agoudjil B, Haba B, Boudenne A. Study on the Durability of New Construction Materials Based on Mortar Reinforced with Date Palm Fibers Wastes. Waste and Biomass Valorization 2019. https://doi.org/10.1007/s12649-019-00669-y.

[171] Chaib H, Kriker A, Mekhermeche A. Thermal Study of Earth Bricks Reinforced by Date palm Fibers. Energy Procedia, vol. 74, Elsevier Ltd; 2015, p. 919–25. https://doi.org/10.1016/j.egypro.2015.07.827.

[172] Hakkoum S, Kriker A, Mekhermeche A. Thermal characteristics of Model houses Manufactured by date palm fiber reinforced earth bricks in desert regions of Ouargla Algeria. Energy Procedia, vol. 119, Elsevier Ltd; 2017, p. 662–9. https://doi.org/10.1016/j.egypro.2017.07.093.

[173] Chikhi M, Agoudjil B, Boudenne A, Gherabli A. Experimental investigation of new biocomposite with low cost for thermal insulation. Energy Build 2013;66:267–73. https://doi.org/10.1016/j.enbuild.2013.07.019.

[174] Chikhi M. Young's modulus and thermophysical performances of bio-sourced materials based on date palm fibers. Energy Build 2016;129:589–97. https://doi.org/10.1016/j.enbuild.2016.08.034.

[175] Braiek A, Karkri M, Adili A, Ibos L, Ben Nasrallah S. Estimation of the thermophysical properties of date palm fibers/gypsum composite for use as insulating materials in building. Energy Build 2017;140:268–79. https://doi.org/10.1016/j.enbuild.2017.02.001.

[176] Bellatrache Y, Ziyani L, Dony A, Taki M, Haddadi S. Effects of the addition of date palm fibers on the physical, rheological and thermal properties of bitumen. Constr Build Mater 2020;239:117808. https://doi.org/10.1016/j.conbuildmat.2019.117808.

[177] Al-Otaibi HM, Al-Suhaibani AS, Alsoliman HA. Physical and Rheological Properties of

Asphalt Modified with Cellulose Date Palm Fibres. Int J Civ Eniromental Eng 2016;10:583–7.

[178] Muniandy R, Jafariahan H, Yunus R, Hassim S. Determination of Rheological Properties of Bio Mastic Asphalt. Am J Eng Appl Sci 2008;1:204–9. https://doi.org/10.3844/ajeassp.2008.204.209.

[179] IS16714:2018. Ground granulated blast furnace slag for use in cement, mortar and concrete – specifications. Bur Indian Stand 2018;3.

[180] Standard B. BS EN 196-6: 2018 BSI Standards Publication Methods of testing cement: Determination of finess. Br Stand 2018.

[181] Swain PTR, Biswas S. Physical and Mechanical Behavior of Al2O3 Filled Jute Fiber Reinforced Epoxy Composites. Int J Curr Eng Technol 2013;2:67–71. https://doi.org/10.14741/ijcet/spl.2.2014.13.

[182] Chow CPL, Xing XS, Li RKY. Moisture absorption studies of sisal fibre reinforced polypropylene composites. Compos Sci Technol 2007;67:306–13. https://doi.org/10.1016/j.compscitech.2006.08.005.

[183] Mohareb A, Thévenon MF, Wozniak E, Gérardin P. Effects of monoglycerides on leachability and efficacy of boron wood preservatives against decay and termites. Int Biodeterior Biodegrad 2010;64:135–8. https://doi.org/10.1016/j.ibiod.2009.12.004.

[184] Voyiadjis GZ, Kattan PI. Mechanics of composite materials with MATLAB. 2005. https://doi.org/10.1007/3-540-27710-2.

[185] Affdl JH, Kardos JL. The Halpin-Tsai equations:a review. Polym Eng Sci 1976;16:344–52.

[186] Cox. The elasticity and strength of paper and other fibrous materials. Br J Appl Phys 1952;72:72–9.

[187] Jayaraman K, Kortschot MT. Correction to the Fukuda-Kawata Young's modulus theory and the Fukuda-Chou strength theory for short fibre-reinforced composite materials. J Mater Sci 1996;31:2059–64. https://doi.org/10.1007/BF00356627.

[188] Fukuda H, Chou TW. A probabilistic theory of the strength of short-fibre composites with variable fibre length and orientation. J Mater Sci 1982;17:1003–11. https://doi.org/10.1007/BF00543519.

[189] Fukuda H, Kawata K. On Young's modulus of short fibre composites. Fibre Sci Technol 1974;7:207–22. https://doi.org/10.1016/0015-0568(74)90018-9.

[190] Mortazavian S, Fatemi A. Effects of fiber orientation and anisotropy on tensile strength and elastic modulus of short fiber reinforced polymer composites. Compos Part B Eng 2015;72:116–29. https://doi.org/10.1016/j.compositesb.2014.11.041.

[191] Macedo JRN, Rocha DB, Rosa DS. Green recoating of cotton fiber by different starching methods. Proc Inst Mech Eng Part L J Mater Des Appl 2017;231:82–8. https://doi.org/10.1177/1464420716674747.

[192] Jackson DS, Ratnayake WA. Gelatinization and Solubility of Corn Starch during Heating in Excess Water : New Insights. J Agric Food Chem 2006;54:3712–6.

[193] Rocha DB, Rosa D dos S. Coupling effect of starch coated fibers for recycled polymer/wood composites. Compos Part B Eng 2019;172:1–8. https://doi.org/10.1016/j.compositesb.2019.05.052.

[194] Madyan OA, Wang Y, Corker J, Zhou Y, Du G, Fan M. Classification of wood fibre geometry and its behaviour in wood poly(lactic acid) composites. Compos Part A Appl Sci Manuf 2020;133:105871. https://doi.org/10.1016/j.compositesa.2020.105871.

[195] Radzi AM, Sapuan SM, Jawaid M, Mansor MR. Water absorption, thickness swelling and thermal properties of roselle/sugar palm fibre reinforced thermoplastic polyurethane hybrid composites. J Mater Res Technol 2019;8:3988–94. https://doi.org/10.1016/j.jmrt.2019.07.007.

[196] Yang HS, Kim HJ, Park HJ, Lee BJ, Hwang TS. Water absorption behavior and mechanical properties of lignocellulosic filler-polyolefin bio-composites. Compos Struct 2006;72:429–37. https://doi.org/10.1016/j.compstruct.2005.01.013.

[197] Sommerhuber PF, Welling J, Krause A. Substitution potentials of recycled HDPE and wood particles from post-consumer packaging waste in Wood-Plastic Composites. Waste Manag 2015;46:76–85. https://doi.org/10.1016/j.wasman.2015.09.011.

[198] Shakeri A, Ghasemian A. Water absorption and thickness swelling behavior of polypropylene reinforced with hybrid recycled newspaper and glass fiber. Appl Compos Mater 2010;17:183–93. https://doi.org/10.1007/s10443-009-9111-9.

[199] Kabir MM, Wang H, Aravinthan T, Cardona F, Lau K-T. Effects of Natural Fibre Surface on Composite Properties : a Review. Energy, Environ Sustain 2007:94–9.

[200] Khan MZR, Srivastava SK, Gupta MK. Tensile and flexural properties of natural fiber reinforced polymer composites: A review. J Reinf Plast Compos 2018;37:1435–55. https://doi.org/10.1177/0731684418799528.

[201] Savastano H, Agopyan V. Transition zone studies of vegetable fibre-cement paste composites. Cem Concr Compos 1999;21:49–57. https://doi.org/10.1016/S0958-9465(98)00038-9.

[202] Vilaseca F, Mendez JA, Pèlach A, Llop M, Cañigueral N, Gironès J, et al. Composite materials derived from biodegradable starch polymer and jute strands. Process Biochem 2007;42:329–34. https://doi.org/10.1016/j.procbio.2006.09.004.

[203] Thwe MM, Liao K. Effects of environmental aging on the mechanical properties of bamboo-glass fiber reinforced polymer matrix hybrid composites. Compos - Part A Appl Sci Manuf 2002;33:43–52. https://doi.org/10.1016/S1359-835X(01)00071-9.

[204] Rana AK, Mandal A, Bandyopadhyay S. Short jute fiber reinforced polypropylene composites: Effect of compatibiliser, impact modifier and fiber loading. Compos Sci Technol 2003;63:801–6. https://doi.org/10.1016/S0266-3538(02)00267-1.

[205] Adeniyi AG, Onifade DV, Ighalo JO, Adeoye AS. A review of coir fiber reinforced polymer composites. Compos Part B Eng 2019;176:107305. https://doi.org/10.1016/j.compositesb.2019.107305.

[206] Abdul Khalil HPS, Issam AM, Ahmad Shakri MT, Suriani R, Awang AY. Conventional agro-composites from chemically modified fibres. Ind Crops Prod 2007;26:315–23. https://doi.org/10.1016/j.indcrop.2007.03.010.

[207] Trotignon JP, Sanschagrin B, Piperaud M, Verdu J. Mechanical properties of mica-reinforced polypropylene composites. Polym Compos 1982;3:230–8. https://doi.org/10.1002/pc.750030409.

[208] Bari E, Morrell JJ, Sistani A. Durability of natural/synthetic/biomass fiber-based polymeric composites: Laboratory and field tests. Durab Life Predict Biocomposites, Fibre-Reinforced Compos Hybrid Compos 2018:15–26. https://doi.org/10.1016/B978-0-08-102290-0.00002-7.

[209] Mohareb ASO, Hassanin AH, Badr AA, Hassan KTS, Farag R. Novel composite sandwich structure from green materials: Mechanical, physical, and biological evaluation. J Appl Polym Sci 2015;132:4–11. https://doi.org/10.1002/app.42253.

[210] Alvarez VA, Ruseckaite RA, Vázquez A. Degradation of sisal fibre/Mater Bi-Y biocomposites buried in soil. Polym Degrad Stab 2006;91:3156–62. https://doi.org/10.1016/j.polymdegradstab.2006.07.011.

[211] Çomak B, Bideci A, Salli Bideci Ö. Effects of hemp fibers on characteristics of cement

based mortar. Constr Build Mater 2018;169:794–9. https://doi.org/10.1016/j.conbuildmat.2018.03.029.

[212] Alatshan F, Altlomate AM, Mashiri F, Alamin W. Effect of date palm fibers on the mechanical properties of concrete. Int J Sustain Build Technol Urban Dev 2017;8:68–80. https://doi.org/https://doi.org/10.12972/susb.20170007.

[213] Li Z, Wang L, Wang X. Compressive and flexural properties of hemp fiber reinforced concrete. Fibers Polym 2004;5:187–97. https://doi.org/10.1007/BF02902998.

[214] Neville AM. Properties of concrete. 4th ed. London: Longman; 1995.

[215] Santos SF, Teixeira RS, Junior HS. Interfacial transition zone between lignocellulosic fiber and matrix in cement-based composites. Sustain. Nonconv. Constr. Mater. using Inorg. Bond. Fiber Compos., Woodhead Publishing Limited; 2017, p. 27–98. https://doi.org/https://doi.org/10.1016/B978-0-08-102001-2.00003-6.

[216] Mansur MA, Aziz MA. A study of jute fibre reinforced cement composites. Int J Cem Compos Light Concr 1982;4:75–82. https://doi.org/10.1016/0262-5075(82)90011-2.

[217] Paramasivam P, Nathan GK, Gupta NC Das. Coconut fibre reinforced corrugated slabs. Int J Cem Compos Light Concr 1984;6. https://doi.org/10.1111/j.1468-2273.1965.tb01084.x.

[218] Zhu WH, Tobias BC, Coutts RSP, Langfors G. Air-cured banana-fibre-reinforced cement composites. Cem Concr Compos 1994;16:3–8. https://doi.org/10.1016/0958-9465(94)90024-8.

[219] Stephens D. Natural fibre reinforced concrete blocks. Afford Water Supply Sanit Proc 20th WEDC Conf 1994:317–21.

[220] Ali M, Liu A, Sou H, Chouw N. Mechanical and dynamic properties of coconut fibre reinforced concrete. Constr Build Mater 2012;30:814–25. https://doi.org/10.1016/j.conbuildmat.2011.12.068.

[221] Kabir MM, Wang H, Lau KT, Cardona F. Chemical treatments on plant-based natural fibre reinforced polymer composites: An overview. Compos Part B Eng 2012;43:2883–92. https://doi.org/10.1016/j.compositesb.2012.04.053.

[222] Yan L, Chouw N, Huang L, Kasal B. Effect of alkali treatment on microstructure and mechanical properties of coir fibres, coir fibre reinforced-polymer composites and reinforced-cementitious composites. Constr Build Mater 2016;112:168–82. https://doi.org/10.1016/j.conbuildmat.2016.02.182.

[223] Tolêdo Romildo D. FD, Ghavami K, England GL, Scrivener K. Development of vegetable fibre-mortar composites of improved durability. Cem Concr Compos 2003;25:185–96. https://doi.org/10.1016/S0958-9465(02)00018-5.

[224] Asasutjarit C, Hirunlabh J, Khedari J, Charoenvai S, Zeghmati B, Shin UC. Development of coconut coir-based lightweight cement board. Constr Build Mater 2007;21:277–88. https://doi.org/10.1016/j.conbuildmat.2005.08.028.

[225] Kumar Sinha A, Narang HK, Bhattacharya S. Effect of Alkali Treatment on Surface Morphology of Abaca Fibre. Mater Today Proc 2017;4:8993–6. https://doi.org/10.1016/j.matpr.2017.07.251.

[226] Mwaikambo LY, Ansell MP. Chemical modification of hemp, sisal, jute, and kapok fibers by alkalization. J Appl Polym Sci 2002;84:2222–34. https://doi.org/10.1002/app.10460.

[227] Beckermann GW, Pickering KL. Engineering and evaluation of hemp fibre reinforced polypropylene composites: Fibre treatment and matrix modification. Compos Part A Appl Sci Manuf 2008;39:979–88. https://doi.org/10.1016/j.compositesa.2008.03.010.

[228] Kabir MM, Wang H, Lau KT, Cardona F, Aravinthan T. Mechanical properties of chemically-treated hemp fibre reinforced sandwich composites. Compos Part B Eng 2012;43:159–69. https://doi.org/10.1016/j.compositesb.2011.06.003.

[229] Jiao C, Xiong J. Accessibility and morphology of cellulose fibres treated with sodium hydroxide. BioResources 2014;9:6504–13. https://doi.org/10.15376/biores.9.4.6504-6513.

[230] Rozman HD, Saad MJ, Mohd Ishak ZA. Modification of oil palm empty fruit bunches with maleic anhydride: The effect on the tensile and dimensional stability properties of empty fruit bunch/polypropylene composites. J Appl Polym Sci 2002;87:827–35. https://doi.org/10.1002/app.11482.

[231] Machaka M, Abou Chakra H, Elkordi Professor A. Alkali Treatment of Fan Palm Natural Fibers for Use in Fiber Reinforced Concrete. Eur Sci J 2014;10:1857–7881.

[232] Chen P, Lu C, Yu Q, Gao Y, Li J, Li X. Influence of fiber wettability on the interfacial adhesion of continuous fiber-reinforced PPESK composite. J Appl Polym Sci 2006;102:2544–51. https://doi.org/10.1002/app.24681.

[233] Bénard Q, Fois M, Grisel M. Roughness and fibre reinforcement effect onto wettability of composite surfaces. Appl Surf Sci 2007;253:4753–8. https://doi.org/10.1016/j.apsusc.2006.10.049.

[234] Sinha E, Panigrahi S. Effect of plasma treatment on structure, wettability of jute fiber and flexural strength of its composite. J Compos Mater 2009;43:1791–802. https://doi.org/10.1177/0021998309338078.

[235] Hewlett P, Liska M. Lea's chemistry of cement and concrete. 5th ed. Butterworth-Heinemann; 2019.

[236] Suresh D, Nagaraju K. Ground Granulated Blast Slag (GGBS) In Concrete – A Review. IOSR J Mech Civ Eng 2015;12:76–82. https://doi.org/10.9790/1684-12467682.

[237] Domone P, Illston J. Their nature and behaviour. Fourth. 2010. https://doi.org/10.4324/9780203927571.

[238] Siddiqui S, Nyberg W, Smith W, Blackwell B, Riding KA. Effect of curing water availability and composition on cement hydration. ACI Mater J 2013;110:315–22. https://doi.org/10.14359/51685665.

[239] Saengsoy W. Effect of curing conditions on hydration reaction and compressive strength development of Fly Ash-cement pastes. Div Solid Waste, Resour Geoenvironmental Eng Hokkaido Univ Http//13387 2008;123:e3.

[240] Idowu O. The effect of improper curing on properties that may affect concrete durability. 2017. https://doi.org/10.1680/jmacr.17.00148.

[241] Attari A, Mcnally C, Richardson MG. Numerical Model for Quantifying Degree of Hydration in Concrete Mixes with Reduced CO 2 Footprint. Numer Model Strateg Sustain Concr Struct 2012:1–10.

[242] Nasir S, Ayoub M, Zafar S, Bilal A, Hazoor A, Kakar E. Experimental Study on Comparison of Strength Properties of Natural Waste Fiber (Coir and Jute) Reinforced Concrete The was this research ratio concrete mix The experimental investigation was of Concrete carried out for both Plain Reinforced Concrete cas 2017;7:105–10.

[243] Hobbs DW. Magazine of Concrete Research. Carbonation Concr Contain Pfa 1988:69–78. https://doi.org/https://doi.org/10.1680/macr.1988.40.143.69.

[244] Agopyan V, Savastano H, John VM, Cincotto MA. Developments on vegetable fibre-cement based materials in São Paulo, Brazil: An overview. Cem Concr Compos 2005;27:527–36. https://doi.org/10.1016/j.cemconcomp.2004.09.004.

[245] Nakarai K, Yoshida T. Effect of carbonation on strength development of cement-treated Toyoura silica sand. Soils Found 2015;55:857–65. https://doi.org/10.1016/j.sandf.2015.06.016.

[246] Liu P, Chen Y, Yu Z, Zhang R. Effect of Temperature on Concrete Carbonation Performance. Adv Mater Sci Eng 2019;2019:1–7. https://doi.org/10.1155/2019/9204570.

[247] Verbeck G. Carbonation of Hydrated Portland Cement. Cem Concr 1958.

[248] Fattuhi NI. Carbonation of concrete as affected by mix constituents and initial water curing period. Mater Struct 1986;19:131–6. https://doi.org/10.1007/BF02481757.

[249] Punima BC, Jain AK, Jain AK. Basic civil engineering. Firewall Media; 2003.

[250] Chen X, Wu S. Influence of water-to-cement ratio and curing period on pore structure of cement mortar. Constr Build Mater 2013;38:804–12. https://doi.org/10.1016/j.conbuildmat.2012.09.058.

[251] J.Punkki. Effect of water absorption by aggregates on properties of high strength lightweight concrete. Proc Int Symp Struct Light Aggreg Concr 1995;Sandefjord:604–16.

[252] Gardiner A, MacDonald K. Aggregate moisture in concrete 2013. https://www.concreteconstruction.net/producers/aggregate-moisture-in-concrete_o (accessed January 14, 2021).

[253] Zhu J, Zhu H, Abhyankar H, Njuguna J. Effect of fibre treatment on water absorption and tensile properties of flax/tannin composites. Int. Conf. Compos. Mater., 2013.

[254] Ramadevi P, Sampathkumar D, Srinivasa CV, Bennehalli B. Effect of alkali treatment on water absorption of single cellulosic abaca fiber. BioResources 2012;7:3515–24. https://doi.org/10.15376/biores.7.3.3515-3524.

[255] Bismarck A, Aranbefwi-Askargorta I, Springer J, Lampke T, Wielage B, Stamboulis A, et al. Cellulose Fibers ; Surface Properties and the the Water Uptake Behavior. Polym Compos 2002;23:872–94.

[256] Page J, Khadraoui F, Gomina M, Boutouil M. Influence of different surface treatments on the water absorption capacity of flax fibres: Rheology of fresh reinforced-mortars and mechanical properties in the hardened state. Constr Build Mater 2019;199:424–34. https://doi.org/10.1016/j.conbuildmat.2018.12.042.

[257] Poletanovic B, Dragas J, Ignjatovic I, Komljenovic M, Merta I. Physical and mechanical properties of hemp fibre reinforced alkali-activated fly ash and fly ash/slag mortars. Constr Build Mater 2020;259:119677. https://doi.org/10.1016/j.conbuildmat.2020.119677.

[258] Condren E, Pavía S. A comparative study of the moisture transfer properties and durability of PC and GGBS mortars. Int Conf Concr Platform M I Russell PA M Basheer Eds Queen's Univ Belfast 2007:469–78.

Appendices

This chapter will demonstrate all the data and images that are related to the research study done. Each Section will present the information related to its corresponding chapter.

Appendix: Chapter 3

Raw materials

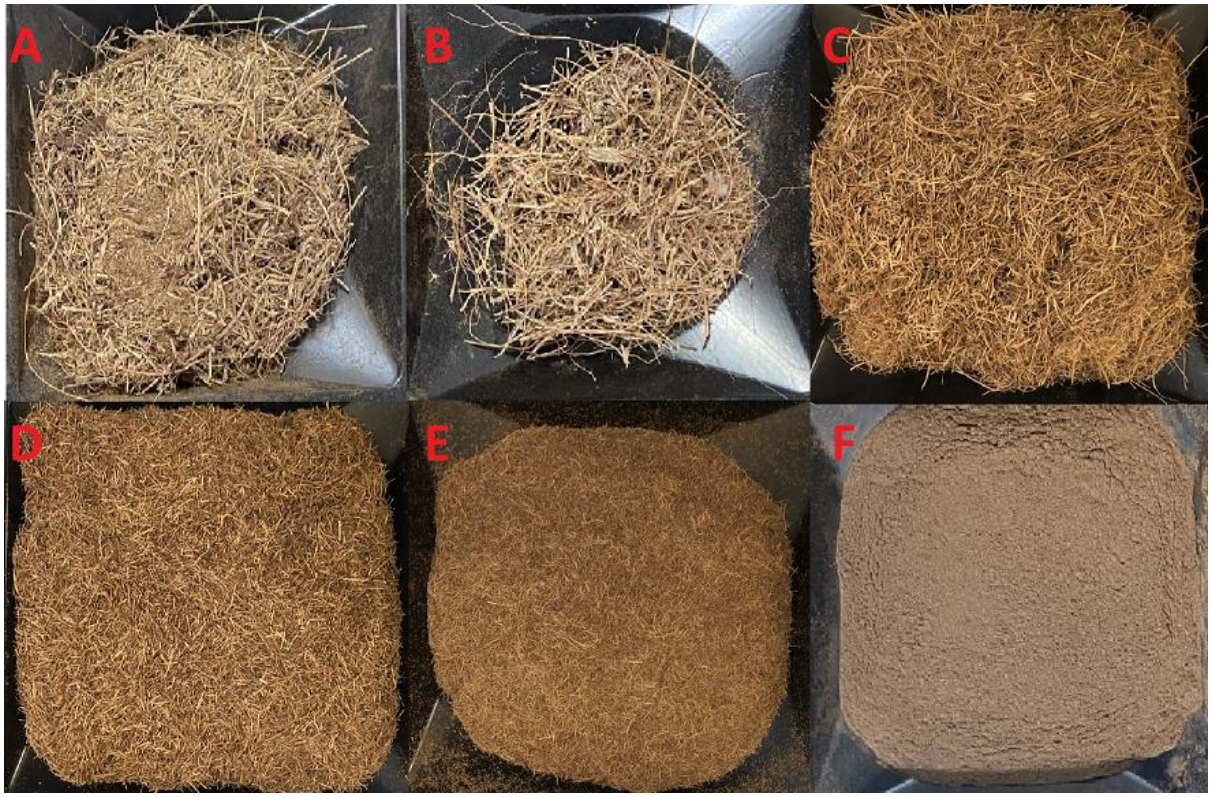

Figure 141 Shows different sieved size of DPF - A) Unsieved DPF, B) ≥1000 µm DPF, C) 500 - 1,000 µm DPF, D) 250 – 500 µm, E) 125 – 250 µm DPF, F) ≤125 µm DPF

Machinery and equipment

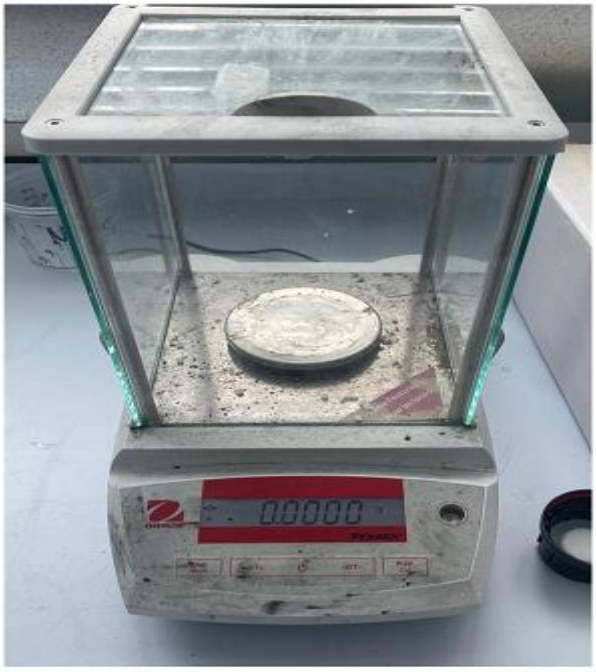

Figure 142 Digital measuring balance

Figure 143 Digital measuring balance

Figure 144 Polystyrene mould

Figure 145 Magnetic stirrer machine with heating plates

Figure 146 Oven

Figure 147 Sieving machine

Figure 148 Barbender Plastograph twin-screw mixer (N50EHT)

Figure 149 Retsch cutting mill (SM 100)

Figure 150 Kenwood mixer

Figure 151 Water bath for sample curing

Figure 152 Impact test machine

Figure 153 Instron 5967 machine tensile testing fitting

Figure 154 Instron 5967 flexural testing fitting

Figure 155 Instron 5588 machine compressive testing fitting

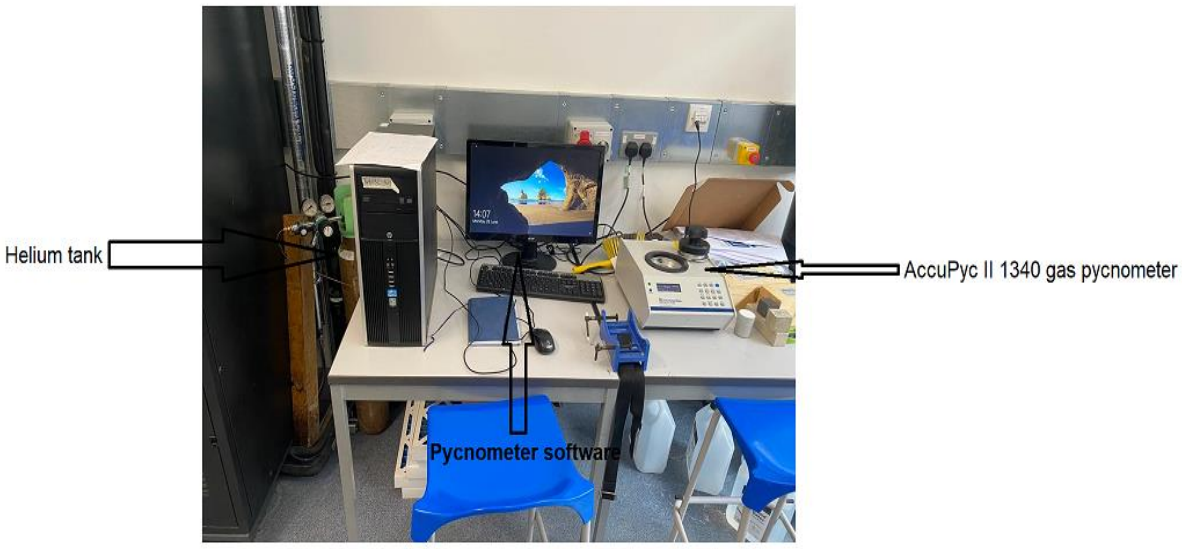

Figure 156 AccuPyc II 1340 gas pycnometer

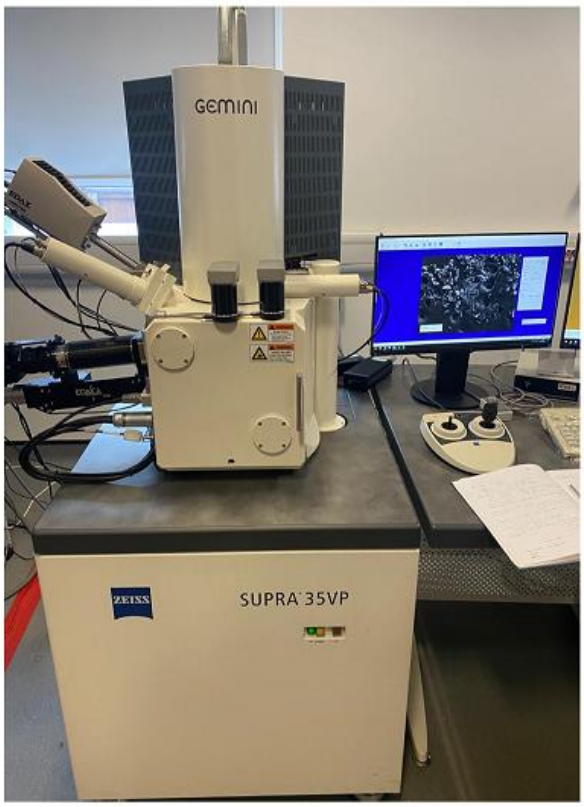

Figure 157 Supra 35VP - Scanning electron microscopy

Figure 158 Fourier transfer infrared

Figure 159 XRD

Appendix: Chapter 5

Table 60 Thickness swelling of DPF/RPVC composite

DPF loading content (wt.%)	Sieve size (μm)	Original Thickness (mm)			After 24 hrs thickness (mm)			After 48 hrs thickness (mm)			After 72 hrs thickness (mm)		
0	-	3.87	4.10	3.92	3.87	4.10	3.92	3.87	4.10	3.92	3.87	4.10	3.92
10	unsieved	5.750	5.870	6.070	5.790	5.880	6.070	5.79	5.88	6.07	5.79	5.88	6.07
	≤ 125	3.560	3.260	3.430	3.570	3.260	3.440	3.57	3.26	3.44	3.57	3.26	3.44
	125-250	6.140	6.490	6.300	6.200	6.490	6.310	6.2	6.49	6.31	6.2	6.49	6.31
	250-500	3.860	3.940	4.270	3.870	3.950	4.300	3.87	3.95	4.29	3.87	3.95	4.29
	500-1000	4.500	4.270	4.440	4.500	4.270	4.500	4.5	4.27	4.5	4.5	4.27	4.5
	≥ 1000	6.150	6.010	6.120	6.150	6.030	6.140	6.15	6.07	6.14	6.15	6.07	6.14
20	unsieved	5.590	5.680	5.710	5.620	5.680	5.750	5.62	5.68	5.75	5.62	5.68	5.75
	≤ 125	3.460	3.500	3.470	3.460	3.520	3.470	3.46	3.52	3.47	3.46	3.52	3.47
	125-250	6.460	6.110	6.350	6.490	6.120	6.390	6.49	6.12	6.39	6.49	6.12	6.39
	250-500	3.920	3.760	3.910	3.950	3.830	3.940	3.95	3.83	3.94	3.95	3.83	3.94
	500-1000	5.420	5.280	4.940	5.480	5.310	4.970	5.48	5.31	4.97	5.48	5.31	4.97
	≥ 1000	5.870	5.460	5.660	5.890	5.490	5.680	5.89	5.49	5.68	5.89	5.49	5.68
30	unsieved	5.620	5.560	5.410	5.660	5.560	5.490	5.66	5.55	5.49	5.66	5.55	5.49
	≤ 125	3.480	3.350	3.750	3.500	3.350	3.770	3.5	3.35	3.77	3.5	3.35	3.77
	125-250	5.690	5.780	5.770	5.730	5.830	5.850	5.73	5.83	5.85	5.73	5.83	5.85
	250-500	3.800	3.770	4.170	3.870	3.820	4.170	3.87	3.82	4.17	3.87	3.82	4.17
	500-1000	5.590	5.800	5.840	5.660	5.820	5.940	5.66	5.82	5.94	5.66	5.82	5.94
	≥ 1000	3.900	3.900	3.970	3.920	3.960	4.000	3.91	3.96	4.1	3.91	3.96	4.1
40	unsieved	6.060	6.040	5.480	6.180	6.150	5.530	6.18	6.15	5.53	6.18	6.15	5.53
	≤ 125	3.900	3.980	3.880	3.970	4.080	3.910	3.97	4.08	3.91	3.97	4.08	3.91
	125-250	6.230	6.220	6.140	6.320	6.290	6.220	6.31	6.29	6.22	6.31	6.29	6.22
	250-500	3.630	3.700	3.700	3.660	3.790	3.740	3.69	3.79	3.75	3.69	3.79	3.75
	500-1000	4.460	4.400	4.520	4.530	4.460	4.590	4.53	4.46	4.59	4.53	4.46	4.59

DPF loading content (wt.%)	Sieve size (μm)	Original Thickness (mm)			After 24 hrs thickness (mm)			After 48 hrs thickness (mm)			After 72 hrs thickness (mm)		
	≥ 1000	4.540	3.870	4.380	4.560	3.920	4.400	4.13	4.05	4.05	4.13	4.05	4.05

Table 61 Water absorption of DPF/RPVC composite after 24 and 48 hours

DPF loading content (wt.%)	Sieve size (μm)	Original weight (g)			After 24 hrs weight (g)			After 48 hrs weight (g)		
0	-	0.498	0.455	0.471	0.501	0.459	0.473	0.501	0.459	0.473
10	unsieved	0.783	0.746	0.811	0.800	0.765	0.831	0.803	0.768	0.831
	≤ 125	0.449	0.415	0.434	0.454	0.420	0.439	0.456	0.420	0.439
	125-250	0.716	0.703	0.758	0.729	0.721	0.769	0.732	0.721	0.769
	250-500	0.489	0.462	0.478	0.499	0.474	0.489	0.499	0.474	0.491
	500-1000	0.500	0.517	0.562	0.516	0.531	0.579	0.520	0.531	0.579
	≥ 1000	0.871	0.793	0.908	0.882	0.816	0.926	0.882	0.816	0.926
20	unsieved	0.663	0.733	0.673	0.692	0.765	0.703	0.696	0.767	0.708
	≤ 125	0.495	0.492	0.491	0.499	0.499	0.497	0.499	0.498	0.495
	125-250	0.730	0.681	0.723	0.753	0.701	0.749	0.753	0.704	0.754
	250-500	0.475	0.469	0.519	0.492	0.487	0.535	0.493	0.489	0.537
	500-1000	0.429	0.4586	0.466	0.4586	0.487	0.498	0.605	0.508	0.506
	≥ 1000	0.781	0.772	0.736	0.808	0.805	0.767	0.812	0.806	0.771
30	unsieved	0.718	0.696	0.659	0.753	0.735	0.699	0.762	0.746	0.706
	≤ 125	0.491	0.419	0.510	0.504	0.431	0.510	0.506	0.435	0.519
	125-250	0.712	0.755	0.718	0.780	0.759	0.721	0.794	0.759	0.733
	250-500	0.484	0.488	0.475	0.526	0.521	0.509	0.536	0.531	0.519
	500-1000	0.675	0.723	0.755	0.741	0.762	0.805	0.748	0.770	0.811
	≥ 1000	0.437	0.411	0.494	0.476	0.445	0.526	0.488	0.454	0.532
40	unsieved	0.734	0.684	0.673	0.789	0.735	0.728	0.804	0.749	0.739
	≤ 125	0.433	0.505	0.502	0.488	0.554	0.542	0.505	0.575	0.558

DPF loading content (wt.%)	Sieve size (μm)	Original weight (g)			After 24 hrs weight (g)			After 48 hrs weight (g)		
	125-250	0.636	0.636	0.588	0.687	0.698	0.667	0.703	0.721	0.689
	250-500	0.4280	0.4626	0.4640	0.4620	0.4875	0.4953	0.514	0.525	0.563
	500-1000	0.551	0.493	0.495	0.609	0.556	0.540	0.625	0.568	0.555
	≥ 1000	0.519	0.465	0.535	0.575	0.515	0.570	0.584	0.523	0.581

Table 62 Water absorption of DPF/RPVC composite after 72 and 96 hours

DPF loading content (wt.%)	Sieve size (μm)	Original weight (g)			After 72 hrs weight (g)			After 96 hrs weight (g)		
0	-	0.498	0.455	0.471	0.501	0.459	0.473	0.503	0.466	0.475
10	unsieved	0.449	0.415	0.434	0.803	0.768	0.831	0.811	0.781	0.843
	≤ 125	0.716	0.703	0.758	0.456	0.420	0.439	0.460	0.423	0.445
	125-250	0.489	0.462	0.478	0.732	0.721	0.769	0.743	0.736	0.775
	250-500	0.500	0.517	0.562	0.499	0.474	0.491	0.509	0.482	0.501
	500-1000	0.871	0.793	0.908	0.520	0.531	0.579	0.534	0.542	0.592
	≥ 1000	0.449	0.415	0.434	0.882	0.816	0.926	0.888	0.826	0.928
20	unsieved	0.663	0.733	0.673	0.697	0.775	0.709	0.712	0.786	0.713
	≤ 125	0.495	0.492	0.491	0.499	0.498	0.495	0.501	0.499	0.498
	125-250	0.730	0.681	0.723	0.756	0.708	0.757	0.770	0.717	0.777
	250-500	0.475	0.469	0.519	0.498	0.495	0.539	0.507	0.503	0.548
	500-1000	0.429	0.4586	0.466	0.611	0.525	0.512	0.638	0.548	0.541
	≥ 1000	0.781	0.772	0.736	0.817	0.816	0.774	0.826	0.820	0.785
30	unsieved	0.718	0.696	0.659	0.762	0.746	0.708	0.835	0.772	0.764
	≤ 125	0.491	0.419	0.510	0.506	0.435	0.519	0.540	0.606	0.529
	125-250	0.712	0.755	0.718	0.794	0.759	0.733	0.813	0.782	0.769
	250-500	0.484	0.488	0.475	0.536	0.532	0.527	0.537	0.550	0.587
	500-1000	0.675	0.723	0.755	0.748	0.770	0.811	0.763	0.793	0.829

DPF loading content (wt.%)	Sieve size (μm)	Original weight (g)			After 72 hrs weight (g)			After 96 hrs weight (g)		
	≥ 1000	0.437	0.411	0.494	0.492	0.457	0.534	0.513	0.486	0.552
40	unsieved	0.734	0.684	0.673	0.818	0.759	0.750	0.835	0.772	0.764
	≤ 125	0.433	0.505	0.502	0.522	0.591	0.572	0.540	0.606	0.592
	125-250	0.636	0.636	0.588	0.721	0.739	0.709	0.741	0.770	0.735
	250-500	0.4280	0.4626	0.4640	0.523	0.533	0.573	0.537	0.550	0.587
	500-1000	0.551	0.493	0.495	0.640	0.578	0.569	0.656	0.589	0.589
	≥ 1000	0.519	0.465	0.535	0.594	0.531	0.594	0.609	0.544	0.607

Table 63 Average flexural strength of DPF/RPVC composite

DPF loading content (wt.%)	Sieve size (μm)	Flexural stress (MPa)	Flexural stress S.D	Flexural Modulus	Flexural Modulus S.D
0	-	35.82	4.25	925.17	124.38
10	Unsieved	33.58	2.51	1,111.52	111.38
	≤ 125	27.60	1.63	941.75	162.60
	125 – 250	30.45	1.10	887.95	50.31
	250 – 500	28.08	1.93	944.82	159.96
	500 – 1,000	28.34	0.21	906.28	18.62
	≥ 1,000	20.41	1.13	542.76	112.60
20	Unsieved	28.16	1.28	1,192.34	60.32
	≤ 125	20.72	1.20	971.21	59.88
	125 – 250	30.89	3.53	980.24	133.16
	250 – 500	26.00	2.02	873.08	99.99
	500 – 1,000	26.82	2.67	1,242.15	150.17
	≥ 1,000	22.06	1.02	922.13	211.95
30	Unsieved	27.96	2.29	1,467.80	79.03
	≤ 125	23.41	2.10	1,206.49	222.37

DPF loading content (wt.%)	Sieve size (μm)	Flexural stress (MPa)	Flexural stress S.D	Flexural Modulus	Flexural Modulus S.D
	125 – 250	27.16	1.13		
	250 – 500	25.32	0.32	1,291.30	102.66
	500 – 1,000	22.92	1.35	1,139.75	103.06
	≥ 1,000	19.78	2.75	963.31	66.83
40	Unsieved	24.87	0.34	1,398.45	97.10
	≤ 125	12.41	1.54	1,393.10	235.32
	125 – 250	20.09	1.96	1,326.95	95.94
	250 – 500	19.37	0.87	1,156.75	131.07
	500 – 1,000	11.69	1.64	787.87	112.70
	≥ 1,000	23.32	2.52	1,347.97	82.82

Table 64 Average flexural strength of DPF/PLA composite

DPF loading content (wt.%)	Sieve size (μm)	Flexural stress (MPa)	Flexural stress S.D
0	-	58.36	3.87
10	Unsieved	57.22	2.04
	≤ 125	40.53	2.32
	125 – 250	47.42	2.87
	250 – 500	43.55	2.02
	500 – 1,000	54.16	1.85
	≥ 1,000	49.99	3.41
20	Unsieved	49.11	2.07
	≤ 125	34.72	3.54
	125 – 250	42.53	1.22
	250 – 500	36.41	1.87
	500 – 1,000	47.46	1.09

DPF loading content (wt.%)	Sieve size (µm)	Flexural stress (MPa)	Flexural stress S.D
	≥ 1,000	46.58	2.52
30	Unsieved	45.12	2.04
	≤ 125	28.63	2.64
	125 – 250	37.40	3.08
	250 – 500	32.63	1.88
	500 – 1,000	42.99	1.36
	≥ 1,000	42.18	1.22
40	Unsieved	41.88	1.43
	≤ 125	22.32	1.25
	125 – 250	32.20	1.34
	250 – 500	28.04	2.07
	500 – 1,000	27.52	2.11
	≥ 1,000	38.38	1.85

Table 65 Average tensile strength of DPF/RPVC composite

DPF loading content (wt.%)	Sieve size (µm)	Tensile stress (MPa)	Tensile stress S.D	Young's Modulus	Young's Modulus S.D
0	-	30.38	1.83	1,011.75	33.91
10	Unsieved	20.32	0.89	677.66	18.16
	≤ 125	25.12	1.04	827.79	69.41
	125 – 250	21.61	0.66	720.41	17.88
	250 – 500	16.69	0.90	620.96	31.63
	500 – 1,000	13.49	0.61	469.50	28.51
	≥ 1,000	19.49	1.55	579.21	66.04
20	Unsieved	16.08	0.40	632.22	18.70
	≤ 125	19.63	1.43	609.79	54.11

DPF loading content (wt.%)	Sieve size (μm)	Tensile stress (MPa)	Tensile stress S.D	Young's Modulus	Young's Modulus S.D
	125 – 250	17.23	0.74	653.22	77.60
	250 – 500	16.91	2.21	640.18	72.52
	500 – 1,000	12.94	0.45	536.95	21.00
	≥ 1,000	15.33	0.38	617.48	52.46
30	Unsieved	13.26	0.14	664.26	27.83
	≤ 125	15.18	0.33	602.06	77.29
	125 – 250	14.44	0.59	673.00	31.55
	250 – 500	16.27	0.39	764.00	88.73
	500 – 1,000	10.28	1.18	545.42	36.37
	≥ 1,000	12.53	0.56	643.07	33.01
40	Unsieved	12.63	0.89	692.81	20.25
	≤ 125	11.53	0.59	638.73	44.17
	125 – 250	12.90	0.82	649.71	26.49
	250 – 500	15.30	0.59	823.71	15.25
	500 – 1,000	8.83	0.60	468.90	34.07
	≥ 1,000	11.72	0.64	540.23	111.85

Table 66 Average tensile strength of DPF/PLA composite

DPF loading content (wt.%)	Sieve size (μm)	Tensile stress (MPa)	Tensile stress S.D
0	-	38.35	1.03
10	Unsieved	31.55	1.81
	≤ 125	28.08	1.41
	125 – 250	30.29	1.74
	250 – 500	20.70	1.52
	500 – 1,000	31.35	1.62

DPF loading content (wt.%)	Sieve size (µm)	Tensile stress (MPa)	Tensile stress S.D
	≥ 1,000	30.69	1.20
20	Unsieved	24.98	1.22
	≤ 125	24.64	1.66
	125 – 250	25.12	1.46
	250 – 500	22.80	1.33
	500 – 1,000	26.55	1.74
	≥ 1,000	24.22	1.44
30	Unsieved	22.78	1.78
	≤ 125	20.71	0.98
	125 – 250	22.48	0.85
	250 – 500	25.68	1.21
	500 – 1,000	23.24	1.18
	≥ 1,000	22.50	1.55
40	Unsieved	21.98	1.05
	≤ 125	17.70	1.33
	125 – 250	19.76	0.55
	250 – 500	23.11	0.94
	500 – 1,000	20.02	1.13
	≥ 1,000	21.57	1.32

Table 67 Average impact strength of DPF/RPVC composite

DPF loading content (wt.%)	Sieve size (µm)	Impact strength (KJ/m^2)	Impact strength S.D
0	-	13.77	1.56
10	Unsieved	8.05	0.36

	≤ 125	7.71	0.82
	125 – 250	7.73	0.63
	250 – 500	5.46	0.44
	500 – 1,000	4.69	0.52
	≥ 1,000	6.97	0.77
20	Unsieved	6.10	0.44
	≤ 125	5.71	0.50
	125 – 250	6.40	0.55
	250 – 500	4.86	0.61
	500 – 1,000	3.71	0.52
	≥ 1,000	3.31	0.45
30	Unsieved	4.95	0.33
	≤ 125	4.34	0.87
	125 – 250	5.71	0.55
	250 – 500	3.89	0.31
	500 – 1,000	3.14	0.99
	≥ 1,000	2.97	0.65
40	Unsieved	3.52	0.52
	≤ 125	3.03	0.27
	125 – 250	3.37	0.22
	250 – 500	3.31	0.41
	500 – 1,000	2.23	0.32
	≥ 1,000	2.51	0.84

Table 68Average impact strength of DPF/PLA composite

DPF loading content (wt.%)	**Sieve size (µm)**	**Impact strength (KJ/m^2)**	**Impact strength S.D**
0	-	31.03	2.41

10	Unsieved	10.52	1.31
	≤ 125	7.77	1.20
	125 – 250	10.06	1.15
	250 – 500	8.34	1.17
	500 – 1,000	7.71	0.57
	≥ 1,000	8.91	0.88
20	Unsieved	9.20	1.10
	≤ 125	6.51	0.95
	125 – 250	8.80	0.55
	250 – 500	7.66	0.77
	500 – 1,000	7.14	0.94
	≥ 1,000	8.23	1.23
30	Unsieved	8.54	0.92
	≤ 125	5.66	0.74
	125 – 250	8.11	0.62
	250 – 500	7.31	0.33
	500 – 1,000	5.49	1.08
	≥ 1,000	6.80	1.14
40	Unsieved	7.54	0.54
	≤ 125	4.34	0.56
	125 – 250	7.09	0.71
	250 – 500	6.80	0.62
	500 – 1,000	4.23	0.27
	≥ 1,000	5.77	0.81

Table 69 Decay resistance of the modified (DPF/RPVC) composite and control solid wood samples (Pinus sylvestris) against Tyromyces palustris and Irpex lacteus.

Blend Ratio	DPF diameter (μm)	WL% (Tyromyces palustris)	WL% (Irpex lacteus)
Control	N/A	30.01	28.26
Pure RPVC	N/A	0	0
90/10 RPVC/DPF	250 – 500	3.3	2.89
	≥1000	3.75	2.96
80/20 RPVC/DPF	250 – 500	4.02	3.95
	≥1000	4.12	4.01
70/30 RPVC/DPF	250 – 500	4.42	4.21
	≥1000	4.44	4.31
60/40 RPVC/DPF	250 – 500	5.66	5.14
	≥1000	5.72	5.12

Table 70 Decay resistance of the modified (DPF/PLA) composite and control solid wood samples (Pinus sylvestris) against Tyromyces palustris and Irpex lacteus.

Blend Ratio	DPF diameter (μm)	WL% (Tyromyces palustris)	WL% (Irpex lacteus)
Control	N/A	30.01	28.26
Pure PLA	N/A	0	0
90/10 PLA/DPF	250 – 500	2.84	2.58
	≥1000	2.67	2.58
80/20 PLA /DPF	250 – 500	3.6	3.68
	≥1000	3.36	3.37
70/30 PLA /DPF	250 – 500	3.94	3.68
	≥1000	3.75	3.74
60/40 PLA /DPF	250 – 500	5.38	5.26
	≥1000	5.61	5.46

Table 71 Disintegration results of DPF/RPVC composite

Blend Ratio	DPF diameter (μm)	WL%
Pure RPVC	N/A	0.00
90/10 RPVC/DPF	250 – 500	0.18
	≥1000	0.11
80/20 RPVC/DPF	250 – 500	0.22
	≥1000	0.32
70/30 RPVC/DPF	250 – 500	0.50
	≥1000	0.51
60/40 RPVC/DPF	250 – 500	0.31
	≥1000	0.48

Table 72 Disintegration results of DPF/PLA composite

Blend Ratio	DPF diameter (μm)	WL%
Pure PLA	N/A	29.7549

90/10 PLA/DPF	250 – 500	10.1914
	≥1000	10.459
80/20 PLA /DPF	250 – 500	9.26496
	≥1000	50.8519
70/30 PLA /DPF	250 – 500	21.9658
	≥1000	37.7049
60/40 PLA /DPF	250 – 500	27.8658
	≥1000	61.9357

Appendix: Chapter 6

Figure 160 DPF/PES casting

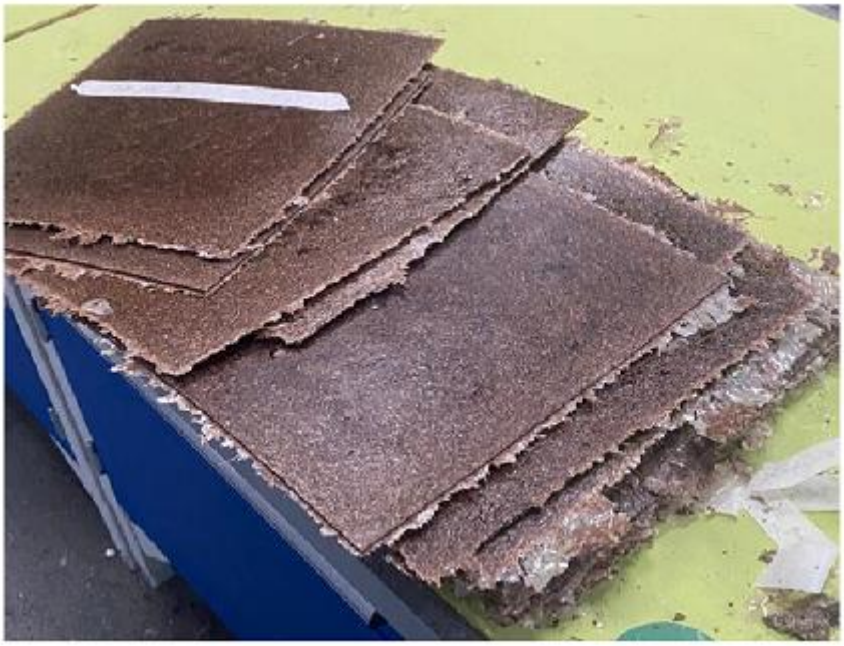

Figure 161 Hot pressed DPF/PES composites

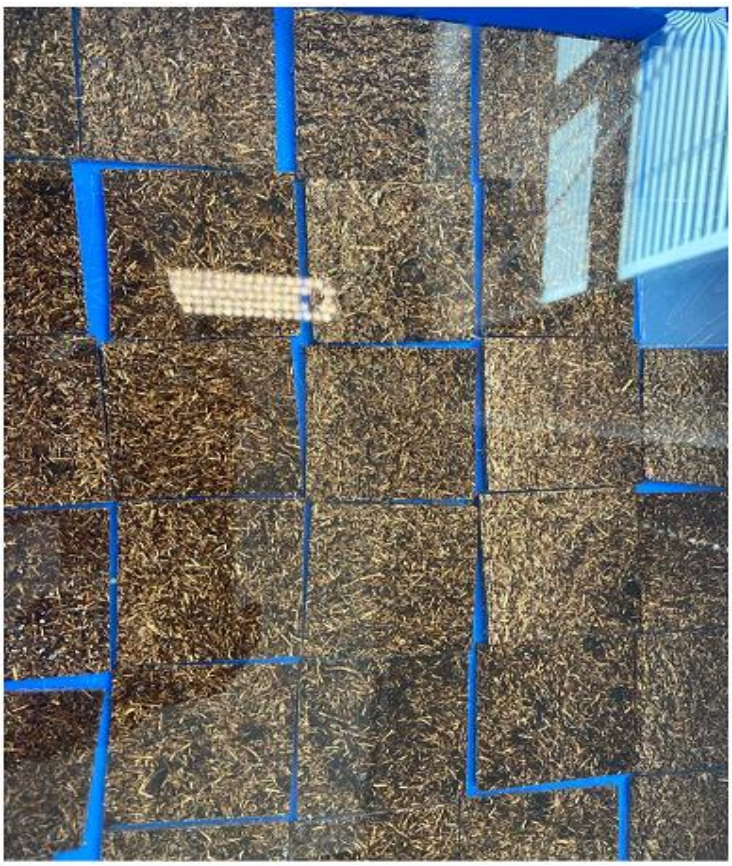

Figure 162 Thickness swelling and water absorption test for DPF/PES composites

Table 73 Average flexural strength of DPF/PES composites at different processing parameters

Processing Time (min)	Processing Temp. (ºC)	Processing Pressure (ton)	Flexural stress (MPa)	S.D	Flexural Modulus (MPa)	S.D
Pure PES			33.03	4.98	1512.32	90.92
3	90	10	17.77	2.51	703.37	110
	90	15	23.10	1.77	809.12	76.70
	90	20	18.46	1.54	780.60	85.11
	110	10	21.49	2.28	1897.53	110.01
	110	15	17.18	2.68	806.60	88.20
	110	20	19.36	0.69	1037.48	14.07
6	90	10	21.84	1.32	495.10	80.24
	90	15	20.13	1.47	759.99	35.79
	90	20	12.87	2.83	974.23	92.71
	110	10	20.06	1.75	1294.15	15.63
	110	15	17.68	2.42	1037.23	100.08
	110	20	13.18	0.21	402.45	62.88
9	90	10	14.45	0.60	562.43	6.70
	90	15	19.67	1.40	1284	100.53
	90	20	16.20	1.55	889.85	6911
	110	10	19.40	1.12	1420.95	23.72

	110	15	21.03	1.34	1625.98	2.3
	110	20	21.92	1.44	1714.27	77.88

Table 74 Average tensile strength of DPF/PES composites at different processing parameters

Processing Time (min)	**Processing Temp. (ºC)**	**Processing Pressure (ton)**	**Tensile stress (MPa)**	**S.D**	**Young's Modulus (MPa)**	**S.D**
Pure PES			13.56	0.21	1156	33.91
3	90	10	14.05	1.68	1198	69.41
	90	15	13.46	0.75	882	17.88
	90	20	11.22	0.45	1243	31.63
	110	10	14.70	0.91	1310	28.15
	110	15	14.98	1.55	1032	66.04
	110	20	11.70	0.61	913	18.16
6	90	10	14.34	0.72	953	54.11
	90	15	11.37	1.72	814	77.60
	90	20	7.14	0.34	909	72.52
	110	10	13.35	0.45	1180	21.02
	110	15	10.75	0.37	1050	52.46
	110	20	10.71	0.42	825	18.10
9	90	10	13.61	0.38	572	77.29
	90	15	6.22	0.45	643	31.55
	90	20	7.95	0.81	857	88.73
	110	10	17.03	0.95	1350	36.37
	110	15	10.43	0.88	810	33.01
	110	20	11.47	1.02	876	27.83

Table 75 Average impact strength of DPF/PES composites at different processing conditions

Processing Time (min)	**Processing Temp. (ºC)**	**Processing Pressure (ton)**	**Impact strength (KJ/m^2)**	**S.D**
Pure PES			1.87	0.16
3	90	10	1.98	0.18
	90	15	3.24	0.23
	90	20	2.67	0.21
	110	10	2.86	0.17
	110	15	2.57	0.21
	110	20	2.45	0.19
6	90	10	2.10	0.21
	90	15	2.67	0.14
	90	20	2.76	0.32
	110	10	3.71	0.18
	110	15	3.30	0.14

	110	20	3.15	0.16
9	90	10	2.57	0.22
	90	15	3.81	0.21
	90	20	3.14	0.14
	110	10	4.01	0.16
	110	15	3.54	0.15
	110	20	3.42	0.09

Appendix: Chapter 7

Table 76 Average flexural strength for different curing for untreated DPFCC (OPC)

DPF content (Wt.%)	DPF Length (mm)	7 d (Air cured)	S.D	7d (Water cured)	S.D	28 d (Air Cured)	S.D	28 d (Water cured)	S.D
0	0	4.12	0.25	5.12	0.28	4.32	0.52	7.31	0.57
1	10	3.21	0.29	5.78	0.33	5.74	0.34	8.82	0.37
2	10	4.44	0.17	6.59	0.19	7.04	0.21	9.30	0.23
3	10	4.19	0.13	6.39	0.15	6.17	0.20	9.25	0.22
1	20	3.62	0.19	6.37	0.22	5.09	0.22	9.20	0.24
2	20	3.17	0.21	5.37	0.24	5.03	0.34	8.02	0.37
3	20	3.98	0.13	6.14	0.15	6.86	0.21	8.18	0.23
1	30	3.75	0.22	5.91	0.25	5.76	0.29	8.15	0.32
2	30	3.49	0.38	5.84	0.44	5.22	0.29	8.13	0.32
3	30	3.12	0.29	4.39	0.33	3.07	0.23	7.80	0.25
1	40	4.06	0.48	5.50	0.55	6.75	0.24	8.10	0.26
2	40	3.87	0.36	4.54	0.41	5.21	0.25	6.75	0.28
3	40	3.35	0.19	4.12	0.22	4.66	0.30	6.18	0.33

Table 77 Average flexural strength for different curing conditions for untreated DPFCC (OPC/GGBS)

DPF content (Wt.%)	DPF Length (mm)	7 d (Air cured)	S.D	7d (Water cured)	S.D	28 d (Air Cured)	S.D	28 d (Water cured)	S.D
0	0	2.46	0.34	4.01	0.22	3.22	0.29	7.58	0.57
1	10	3.14	0.23	5.78	0.24	4.79	0.31	9.62	0.32
2	10	3.93	0.32	6.28	0.37	5.99	0.21	9.89	0.87
3	10	3.72	0.32	6.02	0.23	5.67	0.25	9.55	0.54
1	20	3.41	0.25	5.22	0.19	5.20	0.29	9.49	0.25
2	20	3.12	0.28	4.22	0.21	4.75	0.16	9.05	0.26
3	20	3.72	0.33	4.68	0.15	5.67	0.18	9.18	0.28

DPF content (Wt.%)	DPF Length (mm)	7 d (Air cured)	S.D	7d (Water cured)	S.D	28 d (Air Cured)	S.D	28 d (Water cured)	S.D
1	30	3.46	0.19	4.59	0.25	5.27	0.22	9.06	0.23
2	30	3.22	0.15	4.36	0.44	4.91	0.34	8.98	0.22
3	30	2.97	0.32	4.20	0.33	4.53	0.21	8.78	0.24
1	40	3.87	0.41	4.49	0.55	5.90	0.27	9.05	0.57
2	40	3.62	0.35	4.39	0.41	5.52	0.22	8.99	0.48
3	40	3.16	0.32	4.25	0.22	4.82	0.24	8.96	0.28

Table 78 Average flexural strength for different curing conditions for treated DPFCC (OPC)

DPF content (Wt.%)	DPF Length (mm)	7 d (Air cured)	S.D	7d (Water cured)	S.D	28 d (Air Cured)	S.D	28 d (Water cured)	S.D
0	0	4.12	0.25	5.12	0.28	4.32	0.52	7.31	0.57
1	10	5.63	0.28	5.88	0.32	6.12	0.40	9.61	0.44
2	10	6.30	0.76	6.78	0.87	7.95	0.59	10.05	0.65
3	10	6.14	0.47	6.71	0.54	7.61	0.32	10.02	0.35
1	20	5.90	0.22	6.66	0.25	6.87	0.38	9.97	0.42
2	20	5.24	0.23	5.51	0.26	5.87	0.50	8.74	0.55
3	20	6.18	0.24	6.49	0.28	7.33	0.37	9.10	0.41
1	30	5.89	0.20	6.21	0.23	6.82	0.20	8.98	0.22
2	30	5.73	0.19	5.87	0.22	6.29	0.22	8.92	0.24
3	30	4.56	0.21	4.88	0.24	5.33	0.34	8.05	0.37
1	40	5.94	0.50	6.05	0.57	6.87	0.21	9.08	0.23
2	40	5.53	0.42	5.88	0.48	6.23	0.17	8.59	0.19
3	40	5.16	0.24	5.32	0.28	5.78	0.19	8.23	0.21

Table 79 Average flexural strength for different curing conditions for treated DPFCC (OPC/GGBS)

DPF content (Wt.%)	DPF Length (mm)	7 d (Air cured)	S.D	7d (Water cured)	S.D	28 d (Air Cured)	S.D	28 d (Water cured)	S.D
0	0	2.46	0.34	4.01	0.22	3.22	0.29	7.58	0.57
1	10	4.51	0.35	5.97	0.37	6.09	0.16	10.88	0.64
2	10	5.23	0.26	7.20	0.23	7.06	0.18	11.91	0.86
3	10	4.67	0.31	7.02	0.22	6.30	0.22	11.23	0.51
1	20	4.52	0.21	6.87	0.24	6.10	0.34	10.47	0.42
2	20	4.22	0.25	4.49	0.37	5.70	0.35	9.11	0.55
3	20	4.65	0.29	5.72	0.23	6.28	0.26	9.86	0.41
1	30	4.51	0.16	5.59	0.32	6.09	0.31	9.52	0.28
2	30	4.33	0.18	5.10	0.32	5.85	0.21	9.37	0.33
3	30	3.89	0.22	4.35	0.25	5.25	0.25	9.10	0.19
1	40	4.52	0.34	5.02	0.26	6.10	0.22	9.28	0.15
2	40	4.33	0.21	4.94	0.28	5.85	0.24	9.31	0.22
3	40	4.18	0.27	4.87	0.33	5.64	0.37	9.26	0.24

Table 80 Average compressive strength for different curing conditions for untreated DPFCC (OPC)

DPF content (Wt.%)	DPF Length (mm)	7 d (Air cured)	S.D	7d (Water cured)	S.D	28 d (Air Cured)	S.D	28 d (Water cured)	S.D
0	0	16.89	1.45	26.30	1.20	27.45	1.66	34.60	1.44
1	10	13.36	1.22	26.97	1.11	16.61	1.41	34.88	0.99
2	10	22.37	0.98	28.14	1.45	27.84	1.24	35.82	0.88
3	10	21.15	1.54	27.72	1.22	27.66	1.67	35.66	0.98
1	20	19.6	1.33	27.40	0.98	25.06	1.41	35.54	1.20
2	20	11.21	1.66	26.79	1.20	15.98	1.11	30.55	1.20
3	20	21.07	1.41	27.11	1.66	22.66	1.45	31.02	1.20

DPF content (Wt.%)	DPF Length (mm)	7 d (Air cured)	S.D	7d (Water cured)	S.D	28 d (Air Cured)	S.D	28 d (Water cured)	S.D
1	30	18.96	1.35	26.33	1.41	21.13	1.20	30.76	1.11
2	30	14.89	1.67	25.10	1.35	17.33	1.66	30.62	1.45
3	30	9.66	1.41	25.87	1.66	14.29	1.41	27.61	1.22
1	40	19.77	1.35	26.40	1.41	20.44	1.54	28.54	1.44
2	40	13.88	1.20	22.15	1.35	18.95	1.33	26.33	0.99
3	40	13.21	1.11	19.80	1.20	16.34	1.08	25.98	0.88

Table 81 Average compressive strength for different curing conditions for untreated DPFCC (OPC/GGBS)

DPF content (Wt.%)	DPF Length (mm)	7 d (Air cured)	S.D	7d (Water cured)	S.D	28 d (Air Cured)	S.D	28 d (Water cured)	S.D
0	0	8.78	0.87	26.18	0.98	11.65	1.11	34.90	8.78
1	10	7.51	0.48	26.55	1.54	13.98	1.54	35.70	7.51
2	10	7.88	0.54	27.38	1.33	14.31	1.64	36.61	7.88
3	10	6.54	0.66	26.88	1.66	12.47	1.32	35.98	6.54
1	20	5.98	1.02	26.17	1.41	12.12	1.41	35.60	5.98
2	20	6.84	0.63	22.75	1.35	13.19	1.20	34.82	6.84
3	20	7.53	0.81	23.93	1.67	13.63	1.41	35.44	7.53
1	30	5.6	1.02	23.60	1.41	11.78	1.11	34.67	5.6
2	30	4.33	1.05	23.15	1.35	11.31	1.45	34.13	4.33
3	30	4.86	0.78	23.11	1.20	12.56	1.22	34.02	4.86
1	40	5.23	0.93	23.32	1.11	12.88	1.21	34.34	5.23
2	40	3.98	0.63	22.06	1.24	11.56	1.24	34.29	3.98
3	40	3.62	0.75	20.17	1.19	10.33	1.18	33.97	3.62

Table 82 Average compressive strength for different curing conditions for treated DPFCC (OPC)

DPF content (Wt.%)	DPF Length (mm)	7 d (Air cured)	S.D	7d (Water cured)	S.D	28 d (Air Cured)	S.D	28 d (Water cured)	S.D
0	0	16.89	1.45	26.30	1.2	27.45	1.66	34.60	1.44
1	10	14.2952	1.41	27.20	1.41	17.9388	1.41	39.72	1.11
2	10	23.9359	1.24	28.77	1.35	30.0672	1.54	41.30	1.45
3	10	22.6305	1.67	28.15	1.20	29.8728	1.33	40.82	1.22
1	20	20.972	1.41	28.13	1.45	27.0648	1.08	40.21	0.98
2	20	11.9947	1.35	27.25	1.22	17.2584	1.41	33.96	1.20
3	20	22.5449	1.35	27.62	0.98	24.4728	1.35	34.84	1.66
1	30	20.2872	1.20	27.40	1.20	22.8204	1.66	34.27	1.41
2	30	15.7834	1.11	27.29	1.66	18.7164	1.41	33.51	1.24
3	30	10.2396	1.22	26.41	1.41	15.4332	1.35	34.18	1.67
1	40	20.9562	0.98	27.25	1.54	22.0752	1.20	34.56	1.41
2	40	14.7128	1.20	25.74	1.33	20.466	1.33	31.22	1.35
3	40	14.0026	1.15	24.30	1.22	17.6472	1.53	29.23	1.20

Table 83 Average compressive strength for different curing conditions for treated DPFCC (OPC/GGBS)

DPF content (Wt.%)	DPF Length (mm)	7 d (Air cured)	S.D	7d (Water cured)	S.D	28 d (Air Cured)	S.D	28 d (Water cured)	S.D
0	0	8.78	0.87	26.18	0.98	11.65	1.11	34.90	1.20
1	10	8.56	0.99	28.42	1.31	15.43	1.34	42.06	1.66
2	10	8.98	1.02	29.62	1.29	17.41	1.52	45.71	1.41
3	10	7.46	0.84	29.24	1.22	16.55	1.44	42.67	1.54
1	20	6.82	0.76	29.06	1.11	15.92	0.99	41.65	1.33
2	20	7.80	0.55	26.74	1.54	14.88	0.88	35.27	1.08
3	20	8.58	1.10	27.02	1.33	15.97	1.20	36.22	1.44
1	30	6.48	0.48	26.01	1.66	15.21	1.64	36.02	0.99

DPF content (Wt.%)	DPF Length (mm)	7 d (Air cured)	S.D	7d (Water cured)	S.D	28 d (Air Cured)	S.D	28 d (Water cured)	S.D
2	30	5.01	0.64	25.72	1.41	14.12	1.32	35.94	0.88
3	30	5.63	0.45	25.06	1.35	13.11	1.41	35.46	0.98
1	40	6.06	0.34	25.62	1.67	14.28	1.20	36.01	1.20
2	40	4.61	1.03	24.95	1.41	13.74	1.41	35.76	1.20
3	40	4.19	1.07	24.38	1.20	13.22	1.33	35.61	1.20

Table 84 Water absorption % of untreated DPFCC (OPC/GGBS)

DPF content (Wt.%)	DPF Length (mm)	7 d (Air cured)	7d (Water cured)	28 d (Air Cured)	28 d (Water cured)
0	0	10.33	7.65	12.10	4.50
1	10	14.21	11.25	16.06	8.04
2	10	13.43	10.21	15.17	7.29
3	10	13.66	10.69	15.43	7.63
1	20	13.99	10.96	15.81	7.83
2	20	14.88	11.78	16.81	8.41
3	20	13.95	10.96	15.76	7.83
1	30	14.22	11.27	16.07	8.05
2	30	14.62	11.52	16.52	8.23
3	30	15.50	12.01	17.52	8.58
1	40	14.59	11.10	16.49	7.93
2	40	14.95	11.52	16.89	8.23
3	40	15.32	11.88	17.31	8.49

Table 85 Water absorption % of treated DPFCC (OPC/GGBS)

DPF content (Wt.%)	DPF Length (mm)	7 d (Air cured)	7d (Water cured)	28 d (Air Cured)	28 d (Water cured)
0	0	10.33	7.65	12.10	4.50
1	10	10.46	8.91	12.34	5.84
2	10	11.27	8.13	13.30	5.33
3	10	10.88	8.45	12.84	5.54
1	20	12.37	8.63	14.60	5.66
2	20	11.81	8.10	13.93	5.31
3	20	11.41	8.48	13.46	5.56
1	30	11.83	8.60	13.96	5.64
2	30	12.83	8.77	15.14	5.75
3	30	10.72	8.81	12.65	5.78
1	40	11.55	9.06	13.63	5.94
2	40	11.74	9.47	13.85	6.21
3	40	13.29	9.84	15.69	6.45